A Multi-objective Prediction and Optimisation Method for Additive Manufacturing Technology

Jimeng Yang

B.Eng.

Submitted in fulfilment of the requirements for the Degree of Doctor of Philosophy

School of Engineering

College of Science and Engineering

University of Glasgow

January 2020

ABSTRACT

Cleaner production in a sustainable and customised industrial environment has gradually become the focus of attention in industrial manufacturing. Additive manufacturing (AM) proposes a revolutionary paradigm for customised engineering design and manufacturing, attributed to its design freedom with limitless structural constraints. As an emerging manufacturing technology, most manufacturers and researchers are dedicated to the innovation of AM's manufacturing mechanism and the improvement of part quality. However, the understanding of this emerging manufacturing technology is not yet sufficient in the resource efficiency perspective, which includes three environmental dimensions, namely production time, electrical energy consumption and material usage.

In order to improve AM's resource efficiency, this thesis aims to provide a general modelling scheme to predict time, energy and material consumptions of the AM process, utilise meta-heuristic algorithms to optimise the process parameters of AM, and minimise the three consumptions (i.e. time, energy and material).

A hybrid data-driven and physics-based modelling method is proposed to build up the predictive models of AM's time, energy and material consumptions. To start with, all consumption-related components of the existing AM technologies are classified into five types of module: axis movement, material processing, material feeding, component heating and auxiliary components. Then, hybrid modelling is performed on each module to obtain the relationships between the consumptions and process parameters. In physics-based modelling, the time, distance of axis movement and amount of material usage are calculated from the computer numerical control (CNC) programming language (also named G-code). In data-driven modelling, the remaining parameters are measured through experiments. A power meter is used to measure the apparent power and time of each module under different process parameters. The relationships between the measured parameters and process parameters are derived through regression analysis methods. In addition, some parameters in the predictive models are affected by the characteristics of machine and material in a

practical manufacturing context. For example, the actual speed of axis movement is affected by the high loads of stepper motors during high-speed printing. To further improve the prediction accuracy, additional experiments are conducted to test the actual values of affected parameters. The nature of additional experiments is determined by the machine characteristics.

Meta-heuristics are developed to approximate the Pareto front of process parameters that consume the least time, energy and material. The predictive models are used as three objective functions to evaluate the performance of each solution of process parameters. Since the non-dominated sorting genetic algorithm (NSGA-II) has been widely used to solve optimisation problems with two or three objectives in industrial manufacturing, this study improves and applies NSGA-II to this optimisation problem. Experiments are designed to perform the optimisation under different combinations of optimisation parameters. A set of Pareto fronts is obtained. Hypervolume (HV) indicator is used to compare all obtained Pareto fronts before finally selecting the optimum solution sets of process parameters. In a practical manufacturing context, the optimisation result can provide guidance and a trend for selecting a feasible solution of process parameters.

To validate the effectiveness of the prediction and optimisation method, two case studies are conducted on two different types of fused deposition modelling (FDM) 3D printers. The predictive models of time, energy and material consumptions for each printer have been built by following the proposed prediction method. To improve the prediction accuracy, additional experiments are performed on both FDM 3D printers, including testing the actual speed of axis movement and the actual density of thermoplastic material. According to the prediction results and experimental results, the feasibility of prediction models has been proved, which achieves an acceptable prediction accuracy. The consideration of machine characteristic has also been proved to further improve the prediction accuracies.

The effectiveness of the optimisation method using NSGA-II are also verified in two case studies. To evaluate and compare the qualities of obtained Pareto fronts, the hypervolume (HV) indicator has been used as the response of each optimisation test. The non-dominated

solutions of the Pareto front that has the maximum HV indicator are the optimum solutions for the AM task. This result can provide guidance for setting a feasible combination of process parameters in the prefabrication stage. The optimal solutions of process parameters are compared with the default setting of process parameters. The comparison results prove that the consumptions of optimal solutions are significantly reduced. Furthermore, the significances of optimisation parameters (i.e. population size, number of generations, crossover probability and mutation probability) for the response are analysed by using the range analysis and analysis of variance (ANOVA) methods. According to the analysis results, the significances of optimisation parameters for the HV indicator are not found to be consistent in these two cases. Since the predictive models are customised, there is no general rule to recommend the setting of process parameters and optimisation parameters for general AM technologies.

The proposed prediction and optimisation methods provide a modular, customisable and flexible interface to personalise the predictive models, the optimisation objectives and the process parameter to be optimised. The method fully considers the characteristics of AM machine and material, process parameters, production environment, and customer demands. The use of manufacturing information provided by G-code significantly reduces the workload of the modelling process and achieves an acceptable prediction accuracy. Furthermore, the proposed method is unrestricted to any AM machine, task or complex structure of CAD design, and is also applicable to any other manufacturing technologies that fabricate through numerical control (NC) programming.

TABLE OF CONTENTS

LIST OF TABLES

Chapter 3

Chapter 4

Chapter 5

Chapter 6

Chapter 7

Chapter 8

LIST OF FIGURES

Chapter 1

Chapter 2

Chapter 3

Chapter 4

Chapter 5

Chapter 6

Chapter 7

Chapter 8

Chapter 9

ACKNOWLEDGEMENTS

AUTHOR'S DECLARATION

I declare that this dissertation is written by myself. Except for the explicit reference of the contributions of others, all the content in this dissertation is the result of my own work and has not been submitted for any other degree at the University of Glasgow or any other institutions. Part of the work presented in this thesis has been published in the following articles:

Yang, J., Chen, Y., Huang, W. and Li, Y. 2017. "Survey on artificial intelligence for additive manufacturing", *2017 23rd International Conference on Automation and Computing (ICAC)*, IEEE, pp. 1-6.

Yang, J. and Liu, Y. 2020. "Energy, time and material consumption modelling for fused deposition modelling process", *Procedia CIRP*, 90, pp. 510-515.

Working paper to be submitted:

Yang, J. and Liu, Y. 2020. "Predictive Modelling of Time, Energy and Material Consumptions for Additive Manufacturing", University of Glasgow. Unpublished.

Yang, J. and Liu, Y. 2020. "Framework of Multi-Objective Prediction and Optimisation for Additive Manufacturing", University of Glasgow. Unpublished.

Signature: …………………………………………

Jimeng Yang

December 2020

PUBLICATIONS

Conference Proceedings

Yang, J., Chen, Y., Kontis, K. and Li, Y. 2016. "Wind tunnel experiments of novel wing configurations for design and customisation in an industry 4.0 environment", *2016 10th International Conference on Software, Knowledge, Information Management & Applications (SKIMA)*, IEEE, pp. 92-97.

Yang, J., Chen, Y., Huang, W. and Li, Y. 2017. "Survey on artificial intelligence for additive manufacturing", *2017 23rd International Conference on Automation and Computing (ICAC)*, IEEE, pp. 1-6.

Yang, J. and Liu, Y. 2020. "Energy, time and material consumption modelling for fused deposition modelling process", *Procedia CIRP*, 90, pp. 510-515.

NOMENCLATURE

Chapter 4

Definition of conceptual predictive models

ρ Density of material

EM Finite set containing the apparent powers of all energy-consuming modules

TM Finite set containing the time consumptions of all time-consuming modules

I_n The nth decision variable in an n-dimensional vector $\mathbf{x}$ (also refers to the nth gene of a chromosome/individual)

m Number of consumption-related modules/components

n Number of decision variables; also refers to the process parameters in the multi-objective problem

P_i Apparent power of the ith module

t_i Time consumption of the ith module

E_{total} Total energy consumption

M_{total} Mass of total material consumption

t_{total} Total time consumption

V_{unit} Volume of material feeding amount for each displacement of axis movement

x   Vector of decision variables (also refers to a chromosome or individual representing a solution in NSGA-II)

Definition of the multi-objective problem for optimisation

$\mathcal{F}(\mathbf{x})$ Vector function of multiple objective functions

$\mathcal{F}_1(\mathbf{x})$ Objective function of time consumption

$\mathcal{F}_2(\mathbf{x})$ Objective function of energy consumption

$\mathcal{F}_3(\mathbf{x})$ Objective function of material consumption

I_r The rth decision variable in an n-dimensional vector **x** (also refers to the rth gene of a chromosome/individual)

$I_r{}^L$ Lower bound of the rth decision variable I_r

$I_r{}^U$ Upper bound of the rth decision variable I_r

X Finite set consisting of all feasible solutions

Methods used in hybrid prediction modelling

ΔX Component of displacement of axis movement in X direction

ΔY Component of displacement of axis movement in Y direction

ΔZ Layer thickness or displacement of axis movement in Z direction

F_{xy}	Speed of axis movement or rate of material feeding in X, Y directions
$F_{xy_{act}}$	Vector sum of the actual speeds of axis movement in X, Y directions
F_z	Speed of axis movement in Z direction
$F_{z_{act}}$	Actual speed of axis movement in Z direction
t_{xyz}	Time consumption of actual displacement for axis movement and material feeding
γ	Confidence level or the probability that the true parameter is in the estimated confidence bound
e	Number of variables
$f(x)$	Function of regression model
$f(x_s)$	Prediction value of the sth variable
p_1, p_2, p_3	Coefficients of an example fitted regression model
p_1^L	Lower bound of coefficient p_1
p_1^U	Upper bound of coefficient p_1
R^2	Statistical measure to evaluate the goodness of curve-fitting
S_{p_1}	Standard error of coefficient p_1
SS_{res}	Total sum of squares (TSS)
SS_{tot}	Residual sum of squares (RSS)

x_s	The sth variable among e number of variables
y_s	Observed value of the sth variable
$\bar{y}$	Average of all observed values

Methods used in multi-objective optimisation

λ	Lebesgue measure
$\lambda_w(H(A,R))$	Weighted Lebesgue measure bounded by the solution set A and the reference point R
A	Non-dominated solution set
$\mathcal{F}'_1(\mathbf{x})$	First normalised objective values of solution $\mathbf{x}$
$\mathcal{F}'_2(\mathbf{x})$	Second normalised objective values of solution $\mathbf{x}$
$\mathcal{F}'_3(\mathbf{x})$	Third normalised objective values of solution $\mathbf{x}$
Gen	Number of generations
$I_H(A)$	Hypervolume (HV) indicator of the non-dominated solutions $\mathbf{x} \in A$
$I_H^w(A)$	Weighted hypervolume (HV) indicator of the non-dominated solutions $\mathbf{x} \in A$ denotes the.
$L_{16}(4^4)$	Orthogonal table for four factors with four levels
N	Population size
n_{ns}	Total number of non-dominated solutions obtained from all searches

pc	Crossover probability
pm	Mutation probability
r_R	Coordinates $(r_R,\ r_R)$ of the reference point R
$w(z)$	Weight function used to configure the importance of each solution point $z \in H(A, R)$

Methods used in experimental validation

DF_p	Degrees of freedom of each factor
DF_e	Residual degrees of freedom
ER_i	Experiment results (i.e. the actual time, energy, mateiral consumptions) of the ith AM task
$F - value$	A test statistic to determine whether the factor is associated with the response
MAPE	Mean absolute percent error
MS_p	Mean squares of the pth factor
MS_e	Residual mean square
n_{level}	Number of levels of each factor
n_{test}	Number of experimental tests
PR_i	Prediction results (i.e. the predicted time, energy, mateiral consumptions) of the ith AM task
$\bar{R}$	Mean response of all tests
R_p^i	Response of the ith level of the pth factor in each test

$\overline{\sum R_p^i}$	Mean response of the ith level of the pth factor in all relative tests
SS_e	Residual sum of square
SS_p	Sum of squares of the pth factor
SS_t	Total sum of squares

Chapter 5

Predictive model of time consumption

ΔT_h^b	Temperature difference from the current temperature $T_{h_0}^b$ to the target temperature T_h^b of the bth module of component heating
ΔT_{mp}^a	Temperature difference from the current temperature $T_{mp_0}^a$ to the target temperature T_{mp}^a of the ath module of material processing
H	Height of printed 3D object
LN	Layer number of an AM task
LT	Layer thickness
t_{axis}	Time consumption of axis movement
t_{feed}^c	Time consumption of material feeding between two adjacent layers
t_h^b	Time consumption of the bth module of component heating

t_{layer}	Time consumption of material feeding per layer
t_{mf}^c	Time consumption of the cth module of material feeding
t_{mp}^a	Time consumption of the ath module of material processing
t_{others}	Time consumption of the module of auxiliary components
t_{xyz}^0	Intermittent time during axis movement
T_h^b	Target temperature of the bth module of component heating
$T_{h_0}^b$	Current temperature of the bth module of component heating
T_{mp}^a	Target temperature of the ath module of material processing
$T_{mp_0}^a$	Current temperature of the ath module of material processing
u	Number of material processing modules
v	Number of component heating modules
w	Number of material feeding modules

Predictive model of energy consumption

E_{axis}	Energy consumption of axis movement
E_h	Energy consumption of component heating
E_{mf}	Energy consumption of material feeding
E_{mp}	Energy consumption of material processing

E_{others} Energy consumption of the module of auxiliary components

P_0 Apparent power of start-up mode

P_{axis} Apparent power of axis movement

P_h^b Apparent power of initial heating of the bth module of component heating

$P_{h_{hp}}^b$ Apparent power of heat preservation of the bth module of component heating

P_{mf}^c Apparent power of the cth module of material feeding

P_{mp}^a Apparent power of initial heating of the ath module of material processing

$P_{mp_{hp}}^a$ Apparent power of heat preservation of the ath module of material processing

P_s Apparent power of standby mode

Predictive model of material consumption

$\emptyset$ Diameter of polylactic acid (PLA) filament material in fused deposition modelling (FDM) technology;

Diameter of laser, electron bean or print head in direct energy deposition (DED), powder bed fusion (PBF), binder-jetting (BJ), sheet lamination and polymerisation technologies

ℓ_E Length of deposited material in each displacement of axis movement in FDM technology;

Distance of axis movement in each displacement in direct energy deposition (DED), powder bed fusion (PBF), binder-jetting (BJ), sheet lamination and polymerisation technologies

V_{avg} Average volume of liquid material supplied per unit displacement of axis movement in material jetting (MJ) technology

Additional experiments to improve prediction accuracy

ρ_{act} Actual density of material

F_x Speed of axis movement or rate of material feeding in X direction

F_y Speed of axis movement or rate of material feeding in Y direction

$F_{x_{act}}$ Actual speed of axis movement in X direction

$F_{y_{act}}$ Actual speed of axis movement in Y direction

$V_{unit_{act}}$ Actual volume of material feeding amount for each displacement of axis movement

Chapter 6

η_c Probability density index of simulated binary crossover (SBX) operator

η_m Probability density index of polynomial mutation (PLM) operator

β_c	Spread factor of SBX operator
β_c^0	An arbitrary point within the range of β_c
β_m	Spread factor of PLM operator
c_1	Genes (or variables) of offspring for crossover
c_2	Genes (or variables) of offspring for crossover
c_3	Genes (or variables) of offspring for mutation
$c(\beta_c)$	Probability density function of SBX operator
$\mathcal{D}[\mathbf{x}_p]_{distance}$	Crowding distance of individual $\mathbf{x}_p$
$\mathcal{F}_{Obj}{}^{max}$	The maximum objective value of the Obj^{th} objective function
$\mathcal{F}_{Obj}{}^{min}$	The minimum objective value of the Obj^{th} objective function
$\mathcal{F}_{Obj}(\mathbf{x}_p)$	Objective value of individual $\mathbf{x}_p$ for the Obj^{th} objective
ID	Infill density
I_n^N	The nth gene/variable on the Nth chromosome/individual in the initialised population
L_α	The αth level of non-dominated front
LT_1	Layer thickness variable of offspring for crossover
LT_2	Layer thickness variable of offspring for crossover
LT_3	Layer thickness variable of offspring for mutation

$LT_1{}'$	Layer thickness variable of parents for crossover
$LT_2{}'$	Layer thickness variable of parents for crossover
$LT_3{}'$	Layer thickness variable of parents for mutation
$\mathcal{L}_{\mathbf{x}_p}$	Dominance counter of individual $\mathbf{x}_p$
$\mathcal{L}_{\mathbf{x}_q}$	Dominance counter of individual $\mathbf{x}_q$
M	Number of objectives to be optimised
N	Population size
Obj	The Obj^{th} objective among M objectives
$O(MN^2)$	Computational complexity of NSGA-II optimisation
p_1	Genes (or variables) of parents for crossover
p_2	Genes (or variables) of parents for crossover
p_3	Genes (or variables) of parents for mutation
P_k	Parent population in the kth iteration of NSGA-II optimisation
Q_k	Offspring population in the kth iteration of NSGA-II optimisation
$\mathcal{R}_{\mathbf{x}_p}$	Non-domination rank level of individual $\mathbf{x}_p$
$\mathcal{R}_{\mathbf{x}_q}$	Non-domination rank level of individual $\mathbf{x}_q$
$S_{\mathbf{x}_p}$	A set of solutions dominated by individual $\mathbf{x}_p$

$S_{\mathbf{x}_q}$	A set of solutions dominated by individual $\mathbf{x}_q$
u_c	A random number between 0 and 1 used to determine the value of spread factor β_c at each SBX operation
u_m	A random number between 0 and 1 used to determine the value of spread factor β_m at each PLM operation
$\mathbf{x}_p$	A random individual or solution belonging to the current population
$\mathbf{x}_q$	A random individual or solution belonging to the current population
$\mathbf{x}_t$	A random individual or solution belonging to the current population

Chapter 7

Experimental setup

ρ_{H_2O}	Water density under current room temperature T
W_{air}	Mass of material sample in air
W_{water}	Mass of material sample in water

Predictive model of ANYCUBIC i3 Mega FDM 3D printer

E^1_{cycle}	Energy consumption per cycle of heat preservation of build platform/bed

l_e	Cumulative extruded length of polylactic acid (PLA) filament material
r	Diameter of polylactic acid (PLA) filament material
T	Room temperature during the experiment on testing the actual material density

Predictive model of Monoprice MP Mini Delta FDM 3D printer

q	Total number of G-code commands to instruct the AM machine to print the first layer in X, Y directions
$t^1_{mp_{hp\_first}}$	Time of heat preservation of nozzle hotend for the material deposition of the first layer
$t^1_{mp_{hp\_rest}}$	Time of heat preservation of nozzle hotend for the material deposition of the layers, excluding the first layer
t_{trans}	Transition time between the initial heating and heat preservation of nozzle hotend

Chapter 8

F_{xy_m}	Speed of axis movement with material feeding in X, Y directions
F_{xy_n}	Speed of axis movement without material feeding in X, Y directions

Chapter 9

A	Rotary angle in additional axis X_A

B   Tilt angle in additional axis Y_B

X_A Additional axis for axis movement

Y_B Additional axis for axis movement

ABBREVIATIONS

AC	Alternating current
AM	Additive manufacturing
ANNs	Artificial neural networks
ANOVA	Analysis of variance
BJ	Binder jetting
CAD	Computer-aided design
CAM	Computer-aided manufacturing
CNC	Computer numerical control
DED	Direct energy deposition
EBM	Electron beam melting
FDM	Fused deposition modelling
GA	Genetic algorithm
HM	Hybrid manufacturing
HPC	High-performance computing
HSM	High-speed milling
HV	Hypervolume
LOM	Laminated object manufacturing

MAPE	Mean absolute percent error
ME	Material extrusion
MJ	Material jetting
MOGA	Multi-objective genetic algorithm
NC	Numerical control
NSGA-II	Non-dominated sorting genetic algorithm II
PBF	Powder bed fusion
PC	Personal computer
PLA	Polylactic acid
PLM	Polynomial mutation
PSO	Particle swarm optimisation
RSS	Residual sum of squares
SBX	Simulated binary crossover
SLA	Stereolithography
SLS	Selective laser sintering
SLM	Selective laser melting
SM	Subtractive manufacturing
STL	Standard triangle language

TSP	Travelling salesman problem
TSS	Total sum of squares
UV	Ultraviolet
WS	Workstation
3D	Three-dimensional
3DP	3D printing

CHAPTER 1   INTRODUCTION

1.1. Background and motivation

Additive manufacturing (AM), also called 3D printing (3DP), is a revolutionary manufacturing technology derived from rapid prototyping (Yang and Liu, 2020). AM fabricates three-dimensional (3D) models through a material deposition process layer by layer (Yang et al., 2017; Huang et al., 2016). A general AM process consists of three stages: prefabrication, printing and post-processing. In the prefabrication stage, a computer-aided design (CAD) in standard triangle language (STL) format is, first, imported into computer-aided manufacturing (CAM) software, also known as slicer software (Jiang et al., 2019). After the setting of process parameters in CAM, the 3D model is sliced into multiple layers. The toolpath on each layer is programmed as the computer numerical control (CNC) programming language, also named G-code commands. In the printing stage, the AM machine fabricates the material by executing the G-code commands line by line. The material is deposited on the desired toolpaths to form the 3D object (Jiang and Ma, 2020). In the post-processing stage, some AM technologies need to post-process the printed object, such as removing the supporting material, surface finishing and part reprocessing, etc. (Mueller, 2012).

Compared with subtractive manufacturing (SM), the thin-skin and lightweight production without additional requirements of dies, moulds and tools is the major highlight of AM technology (Kellens et al., 2017). Due to its layer-by-layer nature, AM realises the easier and faster manufacturing of parts with complex geometries, integrated assemblies and multifunctions (Ford and Despeisse, 2016; Jiang and Ma, 2020). Such a production mode is adaptable for mass customisation to produce highly differentiated products on demand (Huang et al., 2016).

With the increasing demand in recent decades for customised production, AM has found an important role in numerous domains, including aviation, architecture, chemicals,

machinery, medicine, food, education and social culture, due to its limitless structural constraints (Frazier, 2014). With the continuous innovation of this technology, AM has expanded into various branches with different types of material-feeding and material-processing mechanisms. Kellens et al. (2017) investigated existing AM technologies available on the market. These technologies are classified within seven categories: material extrusion (ME), direct energy deposition (DED), powder bed fusion (PBF), binder jetting (BJ), material jetting (MJ), sheet lamination and polymerisation. At present, several manufacturers are committed to the development of AM's manufacturing mechanism and supporting software, in order to provide an easy-to-use and customised production environment (Yang and Liu, 2020). Several studies are focusing on improving the quality and mechanical properties of manufactured components, from the advanced commercial rapid prototypers to the open-source 3D printers (Tymrak et al., 2014). Nevertheless, this emerging technology still displays weaknesses in three perspectives of resource efficiency, namely time efficiency, energy efficiency and material efficiency. Each perspective needs to be concerned for the following reasons.

From the time efficiency perspective, Chen et al. (2015) compared the process productivities of selective laser sintering (SLS), as a typical AM technology, and injection moulding, as a traditional manufacturing technology. According to the experimental results, due to the unique manufacturing mechanism of material deposition, SLS requires a much longer manufacturing time than the injection moulding to fabricate the same parts. The tool travelling, component heating and material deposition processes are the major factors that increase the time requirement of AM (Bhuvanesh and Sathiya, 2020). The researchers also stated that, although a high printing speed (e.g. 50 kg of material produced per hour) can accelerate the AM process, this negatively impacts the surface finishing with decreased resolution, and increases the power demands and occurrences of structural defects. Therefore, the problem of how to find a balance between improving time efficiency and also satisfying other demands is still to be addressed.

From the energy efficiency perspective, Watson and Taminger (2018) presented a decision-support model to compare the feasibility of additive manufacturing (AM) and

subtractive manufacturing (SM), based on energy consumption during production. They stated that the key discriminating variable is the volume fraction of solid material contained in the boundary envelope, since the consumed energy of a specific part is determined by the volume of material to be added or subtracted. According to the comparison results, AM was found to be less energy efficient in producing a part with a large volume fraction or a higher ratio of support structure. Kellens et al. (2017) also stated that AM is more beneficial for the production of very small batch sizes, lightweight parts and part remanufacturing. However, some of the existing AM technologies need post-processing of the printed objects, since AM is unable to produce parts with equivalent dimensional tolerances and surface quality. Therefore, the development of an effective, high-precision prediction to estimate and reduce AM's energy consumption is still to be addressed.

From the material efficiency perspective, both AM and traditional manufacturing technologies face the problem of material waste due to their manufacturing mechanisms (Newman et al., 2015). Material waste in the subtractive manufacturing (SM) process is generated by removing the excess from the raw material to obtain the geometry of the desired part. However, material waste in the AM process is caused by the production of a support structure in order to realise the construction of complex structures. To improve the material efficiency, most research has focused on integrating the AM and SM processes, which aims to exploit their respective advantages and avoid their deficiencies. Thus, an innovative production mode has been developed, named hybrid manufacturing (HM). However, the method of using multiple manufacturing technologies is still challenging for the manufacturers with limited manufacturing resources. For the production using single manufacturing technology, an efficient, high-precision prediction and optimisation method can reduce material waste and material consumption. The related research for AM is still to be addressed.

Research on the prediction and optimisation of time, energy and material consumptions mainly draws on SM technologies, such as cutting, drilling, turning and milling processes. Computer numerical control (CNC) milling is the typical technology, which has been applied in over 75.7% manufacturing businesses in the UK and over 67.4% manufacturing

businesses in the US (Swamidass and Winch, 2002). Based on G-code, it fabricates through the collaborative use of multiple tools to remove material from a solid workpiece and thereby form the desired geometry. Compared with AM, the popularity of SM is attributed to its excellent dimensional accuracy, cost efficiency and mechanical strength of manufactured products (Aramcharoen and Mativenga, 2014). Thus, the existing methods to reduce the time, energy and material consumptions of SM are relatively comprehensive. For AM, as an emerging manufacturing technology, the related research is still scarce at present. Most slicer software on the market can only provide an approximate prediction of time consumption of an AM process. The approximation only considers the time spent on material deposition based on the part volume, however, neglects the impact of process parameters, machine setup time, component warm-up time, production environment, etc. At present, there is still a lack of slicer software that can provide an accurate prediction of AM's time, energy and material consumptions, and also recommend the most suitable process parameters for the manufacturers in terms of the CAD design, machine characteristics, production environment and customer demands.

In practical manufacturing context, an efficient and accurate prediction of AM's time, energy and material consumptions can significantly improve the resource efficiency and reduce the resource waste. Therefore, approaches to predict and optimise the above three indicators need to be developed, which will benefit not only AM industries but also any other manufacturing technology that fabricates by using CNC programming.

1.2. Research objectives

The main goal of this thesis is to develop a prediction and multi-objective optimisation method to estimate and reduce time, energy and material consumptions for AM technologies. These three consumptions are selected as the objectives to be predicted and optimised for the following reasons.

Firstly, cleaner production has become the major goal in manufacturing industry. The improvements in energy, production and material efficiencies not only reduce manufacturing

costs but also deliver a number of environmental benefits, such as tackling climate change, and reducing material waste pollution and carbon emissions (Zhang et al., 2019). An efficient prediction and optimisation of AM's time, energy and material consumptions can significantly improve the resource efficiency, especially for the mass production and mass customisation.

Secondly, the existing slicer software on the market cannot provide a high-precision prediction of resource consumptions. Most software can only simulate the material deposition process and provide an approximate prediction of material deposition time. It is lack of consideration of the entire AM cycle and the impacts of process parameters, machine characteristics, production environment on the actual total consumptions.

Thirdly, a general and systematic prediction and optimisation approach with regard to time, energy and material consumptions for all existing AM technologies has not yet been proposed in research to date. Most of the current research is focused on a single AM technology, or a single objective to be predicted or optimised. The lack of a more fundamental approach is a significant gap to be addressed.

In this research, the prediction modelling of three consumptions is performed with consideration of the process parameters, coding rules and machine characteristics. These factors are considered for the following reasons. Due to the particularities of each AM machine, CAD designs produced by different machines will eventually produce different G-code files, and have different time, energy and material consumptions. This is because the coding rules, components and operation mechanisms of the different machines are completely different. Therefore, in order to achieve an accurate prediction, a hybrid modelling method is proposed, in which the physics-based modelling fully uses the manufacturing information provided by G-code to calculate the time of axis movement and amount of material feeding; the data-driven modelling calculate the remaining parameters in the predictive models through the experimental measurements of machine characteristics. The obtained predictive models continue to be used in the process of multi-objective optimisation. Since different process parameters produce different G-code, which effects the

parameters in the predictive models, the entire process – from inputting the process parameters into CAM to the generation of G-code – is embedded in the fitness calculation of each solution of process parameters. The consequence of this is that the optimisation results are more convincing.

The major focus of this research work is to improve the AM technologies from a resource efficiency perspective. From other perspectives, AM still faces weaknesses regarding the improvement of part quality, which is mainly affected by the build orientation, layer thickness and microstructure of solidified AM material (Bayraktar et al., 2016). An effective prediction and optimisation method of AM's part quality is important, however, this will be another scope to be developed.

1.3. Research contributions

The contributions of this research work are summarised as two parts: the contributions of hybrid modelling method for AM's consumption prediction, the contributions of multi-objective optimisation method for reducing AM's consumptions. Details of each part are discussed in the following sections.

1.3.1. Contributions of hybrid modelling for predicting additive manufacturing time, energy and material consumptions

One of the main contributions to this thesis is the hybrid modelling method based on G-code and experimental measurements. Details of this contribution are described as follows.

Firstly, the module classification divides all consumption-related components of the existing AM technologies into five types of modules: axis movement, material processing, component heating, material feeding and auxiliary components. Since general AM technologies perform material deposition through the coordinated operation of multiple components, the module classification based on the function of each component can provide

a general and clear understanding of how the AM machine works, which components participate in the AM process and consume time, energy and material. Based on the classified components, it will be easier to perform the modelling of each module based on its functions.

Secondly, a Gantt chart is formulated to display the running sequences, power profiles, and corresponding G-code commands of all modules participating in an AM process. Since the operation of each module is instructed by its corresponding G-code command, the power profiles and running sequences of all modules are related and determined by the G-code commands. This method aims to clearly reflects two information: 1). the running sequences of all modules; 2). the overlaps of running time of parallel modules. Above information also provide clear guidance for the modelling of total time, energy and material consumptions.

Thirdly, the manufacturing information in G-code is sufficiently used in the physics-based modelling. Since every G-code file can provide detailed manufacturing information including the amount of material feeding, toolpath and speeds of axis movement, this information can be used to calculate the time of axis movement and the amount of material usage. This method has been shown to achieve a good precision of prediction and also reduces the workload of experiments in data-driven modelling.

Fourthly, additional experiments are conducted to test some parameters in the predictive models that are affected by the machine characteristics in a practical manufacturing context; for example, the occurrence of a motor being out of step due to the high loads of high-speed axis movement and high-rate material feeding, which causes the axis movement module to fail to reach the target speed. Therefore, additional experiments are conducted to test the actual speed of axis movement. Note that the factors affecting the prediction accuracy are determined by the machine characteristics. Although this step takes more time to conduct the additional experiments, it fully considers the machine characteristics in a practical manufacturing context and has been validated in case studies to achieve better prediction accuracy.

Finally, the prediction method based on G-code can be extended to subtractive manufacturing (SM) process. Since G-code is used as a universal computer numerical control (CNC) programming language in both AM and SM technologies, the proposed modelling and optimisation method is expected to be further improved as the foundation to general manufacturing technologies that fabricates by using CNC programming.

1.3.2. Contributions of multi-objective optimisation

Due to the wide application in sophisticated optimisation problems, meta-heuristics algorithms are applied in the multi-objective optimisation process to search for solutions of process parameters related to the near-optimal approximate Pareto front (Liu, 2014). The consumptions of time, energy and material are used as objective functions to be minimised, while the process parameters are used as decision variables during the optimisation process.

One contribution of the optimisation method is that the optimisation process embeds the inputting of process parameters into computer-aided manufacturing (CAM) for the generation of G-code, as shown in **Figure 1.1**. Since different process parameters produce different G-code, every new solution of process parameters has its unique G-code and unique predictive models of time, energy and material consumptions. This optimisation method can produce more convincing optimisation results, i.e., the solutions on the near-optimal approximate Pareto front, which are closer to the actual optimal solutions.
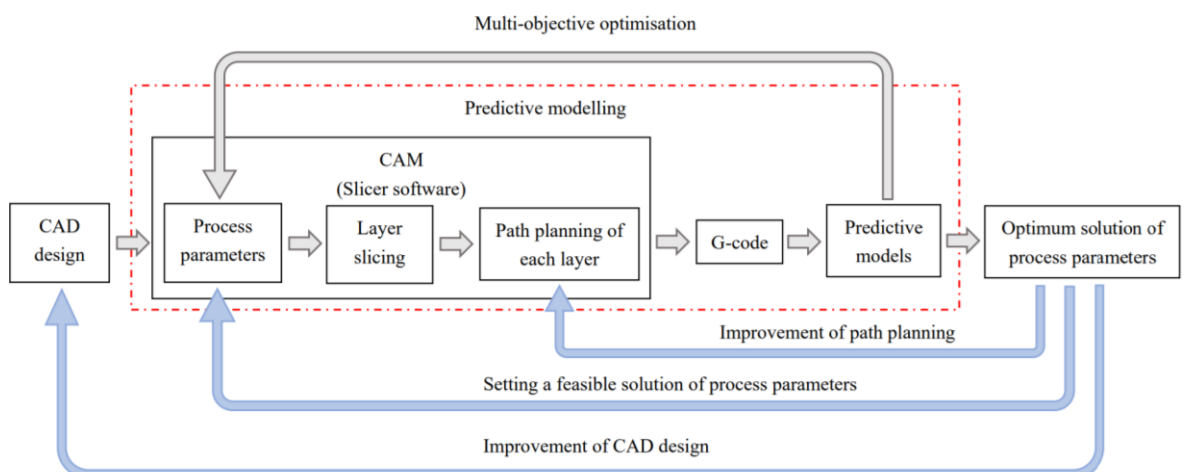
Figure 1.1: Contributions of multi-objective optimisation

Another contribution is that the optimum solution set of process parameters with the minimum time, energy and material consumptions provides guidance to the setting of process parameters in CAM.

Furthermore, referring to the predicted consumptions of the optimal solutions, additional works can be potentially extended to further reduce the consumptions from two aspects (as shown in **Figure 1.1**): 1). the improvement of design structure; 2). the improvement of path planning in G-code. Several studies have proposed the related path planning schemes to minimise the traveling distances of axis movement. Those schemes are reviewed in the next chapter. This study mainly focuses on the foundational work of prediction and optimisation of AM's time, energy and material consumptions. How to integrate the above-mentioned expandable works into this PhD research will continue to be developed in future.

1.4. Outline of thesis

The organisation of this thesis is as follows. Chapter 2 conducts an in-depth literature review of the existing research in three perspectives: the improvement of AM's time, energy and material efficiencies. The state-of-the-art prediction and optimisation methods for reducing time, energy and material consumptions for the AM process are summarised. Since most of the AM research has evolved from research into improving subtractive manufacturing (SM) technologies, this thesis also provides a literature review of the latter in the same area. Based on the literature review, research gaps are clarified, which motivates the work in this thesis.

Chapter 3 proposes the framework of prediction and multi-objective optimisation for AM technologies. To begin, all consumption-related components of the existing AM technologies are summarised. Based on their functions, the components are classified into five modules: axis movement, material processing, component heating, material feeding and auxiliary components. Then, hybrid modelling is performed on each module based on the manufacturing information in G-code and experimental measurements. Considering that some parameters are affected by the machine characteristics, additional experiments are

performed to test the actual values of those parameters in order to improve the prediction accuracy. After the consumption modelling, the multi-objective problem is defined. Meta-heuristics are applied to find solutions related to the near-optimal approximate Pareto front (Liu, 2014). Three predictive models of time, energy and material consumptions are used as three objective functions to calculate the fitness of each solution. The basic steps of the optimisation process are introduced in this chapter.

Based on the framework in Chapter 3, Chapter 4 introduces the methods that have been applied in this research work. A hypothesis is made that the proposed prediction and optimisation method is effective in the prediction and minimisation of AM time, energy and material consumptions. The prototypes of the predictive models and the optimisation problem are defined in this chapter. Then, the methods used in the hybrid modelling are introduced, including the calculation based on G-code, and curve-fitting tool used for regression analysis. The methods used in multi-objective optimisation are also introduced, including the basic workflow of non-dominated sorting genetic algorithm II (NSGA-II), Taguchi design of experiments used to perform the optimisation tests, and hypervolume indicator used to evaluate the obtained Pareto fronts. In addition, the methods used in experimental validation are introduced, including the calculation of prediction accuracy, range analysis and analysis of variance (ANOVA) used to evaluate the significances of optimisation parameters to the optimisation results.

Chapter 5 describes the details of the predictive models of time, energy and material consumptions for each module. In physics-based modelling, the time of axis movement and amount of material feeding are obtained from the manufacturing information in G-code. In data-driven modelling, experiments are conducted to derive the functional relationships between the measured power, time of each module and its related process parameters. The parameters affected by the machine characteristics (e.g. the actual speed of axis movement, the actual material density, etc.) are measured through additional experiments. Finally, all parameters in the predictive models are summarised as three types: parameters calculated from G-code, parameters obtained through experiments, and parameters whose values are decided by the running sequences of five modules. In the final section of this chapter, the

application indication of how to apply the prediction method to a new AM system is presented.

Chapter 6 presents the application of meta-heuristics in this multi-objective optimisation problem. As part of this, NSGA-II has been widely used to solve optimisation problems, with two or three objectives in the area of industrial manufacturing. This study improves this algorithm to search for the optimum solution of process parameters that results in the minimum consumptions. Since the process parameters are used as decision variables to be optimised, and all process parameters belong to the range of real number, the real-coded genetic algorithm (GA) is applied. The binary tournament selection, simulated binary crossover (SBX) operator and polynomial mutation (PLM) operator are applied to produce new generations of candidate solutions. The basic steps of the optimisation process are described in this chapter. Experiments are designed to perform the optimisation under different parameters, including population size, number of generations, crossover probability and mutation probability. Each combination of optimisation parameters produces one Pareto front. Based on the experimental results, the hypervolume (HV) indicator is applied to evaluate the performance of each Pareto front before finally determining the optimum front. In the final section of this chapter, the application indication of how to apply the optimisation method to a new AM system is presented.

Chapter 7 applies the proposed prediction method to two fused deposition modelling (FDM) 3D printers. Based on the modelling method described in Chapter 5, the predictive models of time, energy and material consumptions of two FDM printers are established. To improve the prediction accuracy, additional experiments are conducted to measure the actual values of some parameters, including the actual speed of axis movement and actual density of polylactic acid (PLA) filament material.

Chapter 8 presents the prediction and optimisation results for the two FDM printers. Each printer has been assigned to print two AM tasks under different process parameters. A comparison is made between the predicted consumptions and the measured consumptions. The prediction accuracies are calculated by using mean absolute percent error (MAPE). According to the MAPE results, the prediction method is proved to achieve an acceptable prediction accuracy. Furthermore, the NSGA-II algorithm is applied to search for the optimal

Pareto fronts of process parameters for another AM task printed by two FDM printers. The Taguchi robust design method is applied to design the experiments of optimisation tests under different optimisation parameters (i.e. population size, number of generations, crossover probability and mutation probability). Each test produces one Pareto front. The front that has the maximum HV indicator contains the optimum solutions for the AM task. The optimal solutions have been proved to significantly reduce the consumptions compared with the default setting of process parameters. Moreover, the range analysis and analysis of variance (ANOVA) are applied to evaluate the significances of optimisation parameters for the HV indicator. The analyses results indicate that significances of optimisation parameters depend on the predictive models and machine characteristics.

Chapter 9 summarises this PhD research and proposes future research work, which includes improvement of material consumption prediction, acceleration and deceleration of axis movement, multi-task parallel manufacturing, experimental validations on the same AM machines and other AM technologies, additional optimisation tests under large optimisation parameters, prediction and optimisation of additional objectives, real-time consumption modelling and updating of predictive models.

CHAPTER 2   LITERATURE REVIEW

2.1. Introduction

The goal of this study is to develop an innovative method for predicting and optimising time, energy and material consumptions of additive manufacturing (AM) processes. The selected objectives are based on the current focus around the development of AM technologies. To clearly identify the knowledge gaps that have not been resolved by previous research, this chapter conducts a literature review to explore the research area of improving time, energy and material efficiencies for AM technologies. Based on the review, it is found that most methods are evolved from research work for improving subtractive manufacturing (SM) resource efficiency. Since both AM and SM technologies fabricates through computer numerical control (CNC) programming, the related prediction and optimisation methods for SM technologies are also reviewed in this thesis, aiming to explore and analyse the deficiencies of the existing methods for general CNC manufacturing technologies.

In this chapter, the existing modelling methods to predict time, energy and material consumptions are reviewed on the parameter-based level, unit-based level and state-based level. The applications of optimisation techniques to improve AM and SM technologies are also reviewed, in which the optimised objectives include path planning, production planning, process parameters and consumption-related factors. Based on the review, current knowledge gaps are clearly identified and thus motivate this research.

2.2. Improvement of time efficiency for additive manufacturing and subtractive manufacturing technologies

As an emerging technology, AM has been found to possess a potential advantage of rapid prototyping compared with conventional SM technologies (Pei et al., 2013; Arora et al., 2020). By offering the freedom to design complex structures, AM has been widely used in

mass customisation on demand without additional tooling and setup, which has a significant impact on the supply chain performance (Walter et al., 2004; Arora et al., 2020; Yılmaz, 2020). For instance, Mueller and Kochan (1999) emphasised this statement through several applications of laminated object manufacturing (LOM), which is a common branch of sheet lamination technology. The review highlighted the remarkable suitability of LOM as a rapid patternmaking tool with high robustness in several domains, including moulding and plastics processing, foundries, medicine, ceramics, architecture and civil engineering. During the recent COVID-19 pandemic, AM is also playing an important role in producing healthcare facilities and medical equipment. Arora et al. (2020) summarised the use of AM at short notice, for items such as ventilators, face shields, swabs for COVID-19 testing, antimicrobial polymers, oxygen valves and 3D-printed lung models for surgical use. This demonstrates the increasing adoption of AM in the rapid production of customised designs.

Although AM is exceptional for mass customisation, it still possesses certain weaknesses compared with SM in mass production. Bhuvanesh and Sathiya (2020) stated that the tool travelling, component heating and material deposition processes are the major factors hindering AM from being popularised. For instance, fused deposition modelling (FDM) technology constructs 3D objects through the extrusion of a thermoplastic filament. The limited print speed can significantly increase the time consumption, especially with the fabrication of large volumes. However, a high rate of material feeding (e.g. 50 kg/h) can affect surface finishing due to the decreased resolution, increase the energy consumption, and lead to occurrences of the stepper motor being out of step and insufficient melting of material (Wu et al., 2020; Bhuvanesh and Sathiya, 2020). Regarding the conflicts between multiple objectives, the core issue to be addressed is to search for the optimal balance between time efficiency and other demands, such as energy consumption, part quality, etc. This requires an effective prediction modelling and optimisation method that can optimise time efficiency together with other objectives.

In the following sections, the state of the art regarding improving AM's time efficiency is reviewed and summarised (see **Figure 2.1)**. The research mainly focuses on two perspectives: prediction methods for time consumption and optimisation methods to reduce time consumption. The prediction methods mainly include the modelling based on part volume,

process parameters and machine working states. The optimisation methods include the optimisations of path planning and production planning. In addition, since several methods are evolved from research work for improving SM's time efficiency, the related prediction and optimisation methods for SM technologies are also reviewed, as summarised in **Figure 2.2**. The prediction methods mainly include the modelling based on material removal rate, G-code and machine characteristics. The optimisation methods include the optimisation of path planning and production planning. Details of each method are reviewed in the following sections.

Flow of AM process

| Import CAD design | Setting of process parameters | Path planning | Production planning | Printing |
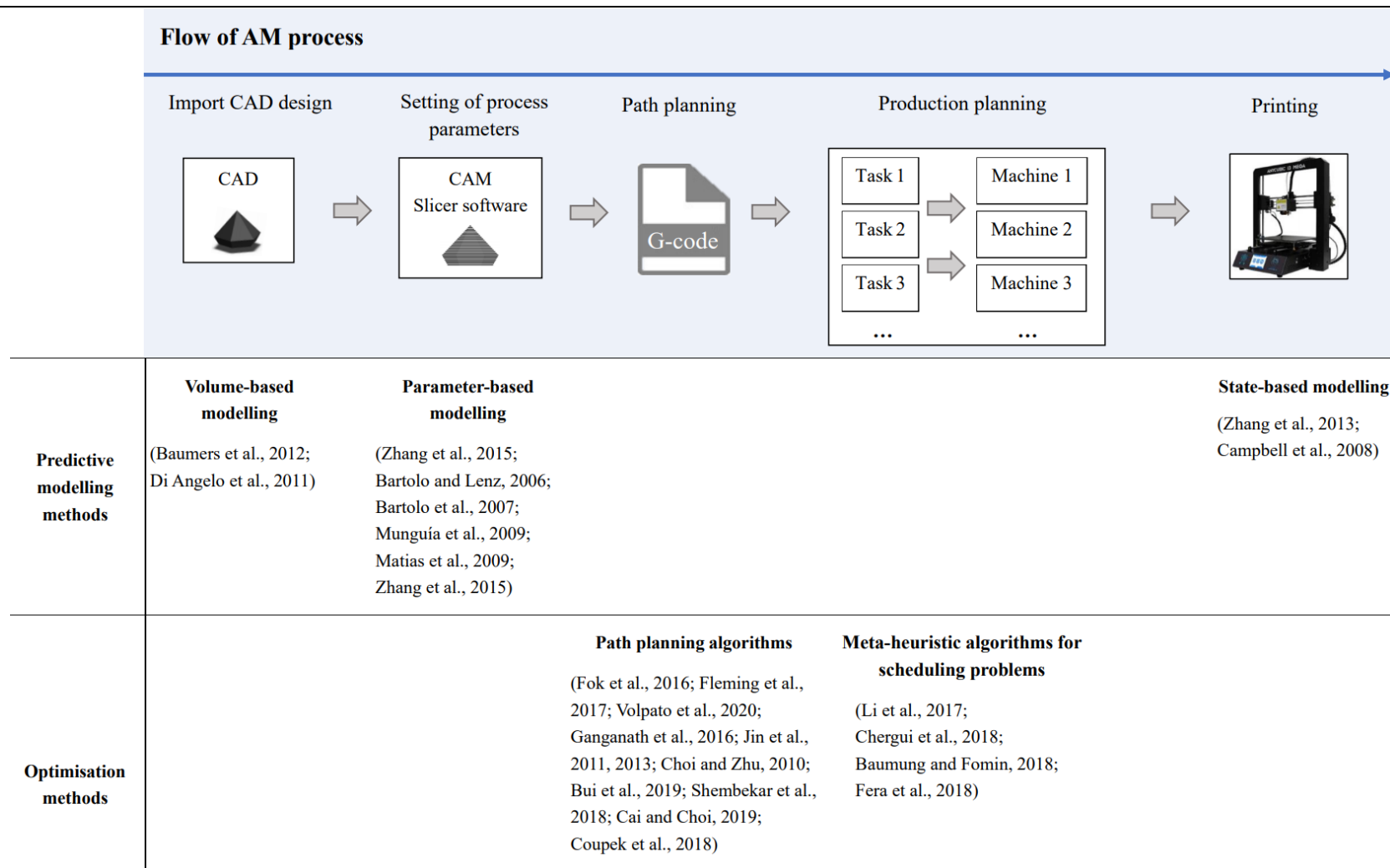
Figure 2.1: Existing research into improving time efficiency of AM technologies

Flow of SM process

Import CAD design → Setting of process parameters → Path planning → Production planning → Machining

CAD → CAM → G-code → (Task 1 → Machine 1, Task 2 → Machine 2, Task 3 → Machine 3, …)

Predictive modelling methods		**Modelling based on material removal rate** (Ou-Yang and Lin, 1997; Jung, 2002; Faassen et al., 2003; Hbaieb et al., 2011)	**Modelling based on G-code and machine characteristics** (Coelho et al., 2010; Liu et al., 2013)
Optimisation methods		**Path planning algorithms** (Balabokhin and Tarbutton, 2017)	**Programming tools and platforms for scheduling problems** (Kumar et al., 2014; Wdowik et al.. 2018)

Figure 2.2: Existing research into improving time efficiency of SM technologies

2.2.1. Research into prediction approaches for time consumption in additive manufacturing technologies

The methods for estimating and modelling the time consumption of AM processes can be classified into three categories: state-based modelling, volume-based modelling and parameter-based modelling. State-based modelling is carried out in terms of machine characteristics. This method divides the manufacturing process into different working states. The time consumptions of one or more working states are modelled based on machine characteristics; for example, the running sequences of components. Volume-based modelling is carried out based on the design geometry; for example, the contour area of the printed layer, or the volume of the printed object. Parameter-based modelling is carried out in terms of process parameters set in the slicer software. This method aims to derive the functional relationships between the time consumption and consumption-related process parameters through experiments. The following three sub-sections respectively review the existing research on the above three types of modelling methods.

2.2.1.1. State-based modelling of time consumption for additive manufacturing technologies

With respect to state-based modelling, Zhang and Bernard (2013) developed an analytical modelling method to predict the time consumption of selective laser sintering (SLS) technology, which is a branch of powder bed fusion (PBF) technology. The method considered the consumption-related factors from the state of machine preparation to the end of the AM task. Since SLS fabricates by consolidating powder material on each layer, a beam deflection system is used to selectively scan the contour areas (Kruth et al. 2003; 2005). Thus, Zhang and Bernard (2013) divided the SLS process into three stages: material feeding by the powder roller, material processing by the laser beam and axis movement in Z direction to switch to the construction of the next layer. Nevertheless, the proposed method was only suitable for SLS due to its unique operating mechanism, in which (a) the build time of each layer was modelled based on the laser scanning rate and part volume, (b) the time spent on

material feeding was modelled based on the feeding rate of the roller, and (c) the movement time in Z direction was modelled based on the movement speed and part height. For other AM technologies, Campbell et al. (2008) utilised volumetric shapes to estimate the time consumption of stereolithography (SLA) technology, which is a common branch of polymerisation technology. SLA fabricates by using an ultraviolet (UV) laser to selectively cure the photosensitive resin (Zhou et al., 2000). Thus, the SLA process was divided into two stages: material processing by using a UV laser and axis movement in Z direction to construct the new layer. A time estimator was built to calculate the average scanning time of the laser per unit contour area on each layer (Campbell et al., 2008), which achieved a rapid estimation of the build time. This method was also limited to SLA technology, in which only two major components, i.e., UV laser and stepper motors for axis movement in Z direction, participate in the manufacturing process.

Note that the above methods mainly focused on a single type of AM technology. Since different AM technologies have different components and manufacturing mechanisms, the division of working states is dependent on the type and characteristics of the AM machine. A general prediction method is still to be addressed for estimating the time consumptions of general AM technologies.

2.2.1.2. Volume-based modelling of time consumption for additive manufacturing technologies

With respect to volume-based modelling, Baumers et al. (2012) demonstrated a generic modelling method to predict AM's time consumption based on part volume and layer numbers. The average build time per unit contour area on each layer was obtained through experimental measurements. Di Angelo and Di Stefano (2011) used artificial neural networks (ANNs) to develop an estimator of the build time of the contour area, which can be applied to various types of AM technologies, including fused deposition modelling (FDM), selective laser sintering (SLS), stereolithography (SLA), laminated object manufacturing (LOM), material jetting (MJ) and electron beam melting (EBM). The contour area was separated into two parts: the toolpath loops and the hatching distance between two

adjacent segments of toolpath. Thus, the build time was modelled based on the average toolpath length per unit area. ANNs were developed from the known case base, using sufficient training samples.

Compared with state-based modelling, volume-based modelling can be more widely used in various AM technologies as it is based on the volume of a printed object. However, the execution of a predefined toolpath is the core working principle of computer numerical control (CNC) manufacturing technologies. Most studies have over-simplified the toolpaths on each layer and calculate the total time consumption by using the average time consumption per unit area or volume. Despite achieving the fast prediction of time consumption, the impacts of process parameters on the toolpath planning and layer slicing should also be considered in the prediction modelling. Besides, the above methods only modelled the build time of sliced layers but ignored the time consumptions of other manufacturing stages; for example, the time spent on component heating, nozzle calibration, etc.

2.2.1.3. Parameter-based modelling of time consumption for additive manufacturing technologies

With respect to parameter-based modelling, it is challenging for current research to develop an accurate predictive model without inputting a large quantity of data, including part geometry, machine characteristics, manufacturing details and production planning (Zhang et al., 2015). For instance, Bartolo and Lenz (2006), Bartolo (2007) and Matias et al. (2009) proposed analytical and thermo-kinetic modelling methods to simulate the material processing mechanism (i.e. photo-initiated curing reaction) of SLA technology. The thermo-kinetic model was built to quantify the impacts of material properties and process parameters on the time consumption for completing the cure of one resin layer. The process parameters included layer thickness, ultraviolet (UV) light intensity and resin composition. The proposed method was limited to the SLA technology, since it mainly focused on the fundamental physical and chemical phenomena that determined the behaviour of thermoset materials in light-initiated curing applications.

Munguía et al. (2009) developed a time estimator using ANNs to model the time consumption of selective laser sintering (SLS) technology. Machine learning was applied to train and simulate the consumption model from a sufficient case base of more than 130 models. Three consumption-related parameters were considered, including part height, part volume and bounding box. Zhang et al. (2015) demonstrated a predictive and adaptive modelling method using Grey Theory. With the assistance of experiments, the method utilised a Bayesian form to simulate the unknown functional relationships between the time consumption of AM processes and consumption-related factors, including process parameters, part volume, support volume and production planning. Since a large quantity of data inputs can increase the complexity of the modelling process, the above parameter-based modelling methods generally select the most important process parameters and information from the CAD design that affect the time consumption and production planning. In fact, since the programming of G-code is determined by the setting of process parameters through slicer software, the variations in any process parameter will change the planning of the toolpath, and therefore effect the final time consumption. Hence, all process parameters set in the slicer software should be considered in the modelling process to further improve the prediction accuracy.

2.2.2. Research into optimisation approaches to reduce time consumption of additive manufacturing technologies

The optimisation of AM technology is another way to improve time efficiency. Some research has been devoted to optimising the AM system itself to achieve a better G-code program; for example, by adjusting the coding rules for path planning. Other research has focused on optimising the production planning of multiple AM tasks to reduce time consumption or meet other demands. The following two sub-sections respectively review the existing optimisation methods from the above two perspectives.

2.2.2.1. Optimisation of path planning for additive manufacturing technologies

Fok et al. (2016) developed a toolpath optimiser using the Christofides algorithm. The algorithm simulates the path planning of each layer as the 'travelling salesman problem' (TSP), which aims to minimise the travelling distance of axis movement, thereby reducing the time consumption. Fleming et al. (2017) proposed a path planning strategy using the greedy algorithm to simulate the TSP. The greedy algorithm is an intuitive algorithm commonly used in optimisation problem. It aims to search for the optimal solution at each step of the TSP and reduce the travelling distance between adjacent space-filling curves and layers. Similarly, Volpato et al. (2020) proposed a path planning method for material extrusion (ME) technology, which combined the greedy algorithm and the 2-opt heuristics algorithm (also called the nearest insertion). The distance of axis movement was mapped and reduced, and thus also reduced the build time. Ganganath et al. (2016) further improved the path planning method by using triangular and trapezoidal velocity profiles for ME technology. The Christofides and k-opt heuristics algorithms were applied to the conventional TSP to obtain the most time-efficient trajectories of axis movement. Jin et al. (2011; 2013) used closed non-uniform rational B-spline curves to represent the contours on each layer, and proposed an adaptive toolpath generation algorithm to minimise the build time and maximise the surface quality. The algorithm planned the contour toolpath for the boundary of each layer and the zigzag toolpath for the internal area of each contour.

The above-mentioned path planning methods for single-head AM technologies can be further extended to multi-head AM technologies, since the collaboration of multiple printer nozzles to fabricate the different parts of a single object can significantly reduce the build time. Choi and Zhu (2010) demonstrated a path planning method for the decoupled motion of multiple nozzles. The toolpath of each nozzle was programmed independently, and the potential collisions were detected through a dynamic priority scheme. By comparing the movement speeds of two nozzles that conflicted each other, the one with a higher priority (at a higher speed) was instructed to continue the movement, while the other one with a lower priority was paused until the potential collision had passed. Bui et al. (2019) proposed a path

planning method for multi-head material extrusion (ME) technology. By integrating a tabu search with novel collision detection and resolution algorithms, the planner yielded a collision-free toolpath for the cooperation of multiple nozzles. Shembekar et al. (2018), Cai and Choi (2019) also developed similar collision-free path planning methods for instructing the movement of multiple nozzles and robotic arms. Furthermore, Coupek et al. (2018) proposed a path planning strategy for multi-axis movement in AM processes. The planning considered the adaption of build orientation and used integrated building blocks to replace the infill structure, which avoided the material usage of a support structure, and thus also saved build time.

The methods on the level of path planning have been well explored in ME technology with a single nozzle, multiple nozzles or robotic arms. These methods are expected to be extended to other types of additive manufacturing (AM) and subtractive manufacturing (SM) technologies that fabricates by following the computer numerical control (CNC) programmed toolpaths. Besides, the variations of process parameters may also affect the layer slicing and path planning in prefabrication stage. Thus, apart from artificially improving the path planning, the optimisation of process parameters is another way to shorten the build time spent on the axis movement, however, the related methods in this area are still scarce.

2.2.2.2. Optimisation of production planning for additive manufacturing technologies

Due to the high processing costs of AM technologies, efficient production planning and scheduling of AM tasks can significantly reduce time consumption and operational costs. Li et al. (2017) defined a production planning problem and proposed a mathematical model to minimise the build time and operation costs of selective laser melting (SLM) technology, which is a common branch of powder bed fusion (PBF) technology. The build time and operation costs were modelled based on the machine set-up time, maximum build space, part volume and geometry. Meanwhile, two heuristic procedures were developed, namely 'best-fit' and 'adapted best-fit', to search for the optimal solution for the allocations of tasks and machines. Chergui et al. (2018) defined a planning, nesting and scheduling problem solved

by a heuristic approach, which aimed to search for the optimal production planning of mass customisation in the AM process. A mathematical model of production time was built based on job due time, maximum build space, part volume and geometry. Fera et al. (2018) improved and applied genetic algorithm to the job scheduling for a single SLM machine. The optimisation models of build time and operation costs were built in a similar way, based on job due time, maximum build space, part volume and geometry. Through experimental validations, the proposed heuristics in above studies have been validated to obtain the optimal allocations and effectively shortened the production time of multiple AM tasks. Furthermore, Baumung and Fomin (2018) utilised a nesting algorithm to estimate the combinability of multiple CAD designs for scheduling the AM production process. The built time per design is directly obtained from the CuraEngine slicer software, which calculates the built time based on part volume. Based on the build time of each AM task and the available AM machines, an optimisation model was built to represent the utilisation of time-oriented build space.

It is found that most of the existing research mainly focus on optimising production planning in an ideal manufacturing environment, since the time modelling of printing process is only based on the part volume. In fact, the variations of process parameters have a great impact on the toolpath planning and layer slicing, thereby effect the actual time consumption of each AM task. These impacts cannot be reflected in the volume-based modelling methods. Besides, due to the unique manufacturing mechanism, same part volume printed on different machines may consume different built time. Thus, the entire AM cycle and machine characteristics should also be considered; for example, the machine set-up time, the running sequences and time of machine components, etc.

2.2.3. Research into prediction and optimisation approaches for time consumption of subtractive manufacturing technologies

As an emerging manufacturing technology, the research on improving AM's time efficiency is relatively insufficient compared with the research on subtractive manufacturing (SM)

technologies. Both types follow the computer numerical control (CNC) commands to manufacture through material accumulation or material removal. The difference is that the time efficiency of SM is determined by cutting tool performance and machining parameters. High-speed milling (HSM) is one of the most representative technologies, which was first applied in aerospace engineering, and then the die and mould industry (Dewes and Aspinwall, 1997). With respect to the cutting tool performance, the speed of HSM was found to be closely related to the type of cutting tool. Corduan et al. (2003) stated that carbide and high-speed steel tools might cause complex changes of wear mechanism (e.g. adhesion, abrasion, corrosion, diffusion and fatigue) due to the unique mechanical and chemical properties of the tool material. Meanwhile, the regenerative chatter also affected the material removal rate and surface finish, which accelerated tool wear and reduced part quality (Burwell, 1957). With respect to the machining parameters, there have been several experimental studies conducted on ultra-HSM of dies and moulds in order to establish the impact of parameter variations on dimensional accuracy, tool life, tool failure and surface finish. According to the experimental results, it was found that the material removal rate in HSM was better and more stable, with a greater tool life, an acceptable surface finish, and a lower production time and costs (Elbestawi et al., 1997; Dewes and Aspinwall, 1997). Several studies have dedicated to proposing effective models to express the relationship between machining parameters and various demands (such as tool performance, tool life, surface finish, production time and costs, etc.), and to find the optimal solution of machining parameters to balance these demands. Due to the similarities between SM and AM, that both fabricates through computer numerical control (CNC) programming, the review in following sections is to derive inspirations from the relevant prediction and optimisation methods for SM technologies.

2.2.3.1. Prediction of time consumption for subtractive manufacturing technologies

Ou-Yang and Lin (1997) stated that the machining time of subtractive manufacturing (SM) processes was determined by the material removal volume. Some estimation methods were proposed to model the machining time based on material removal volume and material removal rates (Ou-Yang and Lin, 1997; Jung, 2002). Faassen et al. (2003) modelled the

functional relationship between machining parameters and chatter boundaries to improve the time efficiency of the HSM process. Experiments were conducted to test machine dynamics and material properties at different spindle speeds, which aimed to identify the maximum spindle speed within the chatter boundaries. Hbaieb et al. (2011) developed a similar model to calculate the machining time at different material removal rates.

Apart from the prediction methods only based on material removal rates, various other methods further improved the estimations with a consideration of numerical control (NC) programs and machine characteristics. Coelho et al. (2010) proposed a practical method for estimating the machining time of a CNC milling process. It was stated that most commercial CAM software simply predict the machining time by dividing the toolpath length by the programmed material removal rate. In fact, due to the limitations of the machine capacity and CNC, the material removal rate is not always constant, thus this time estimate is different from the actual machining time. A global performance feature, named machine response time, was characterised based on the machine capacity at high milling speeds. According to the experimental results, it was found that the actual machining time was dependent on the machine characteristics: the longer machine response time resulted in a larger difference between actual and predicted milling times. Furthermore, Liu et al. (2013) proposed a feature-based estimation method to predict the machining time for a CNC milling process. The method modelled the machining time by fully considering the part geometry, process plan, toolpaths in NC programs and machine characteristics. Experiment results validated the feasibility of the proposed estimation method, with a better prediction accuracy compared with the time estimation from commercial CAM software.

The prediction of time consumption for SM technologies has evolved from the modelling based on material removal rate to the modelling based on NC programs and machine characteristics. This integrated modelling method is also what the prediction methods of AM technology need to learn from. For instance, in a general AM process, the actual speed of nozzle motion is not always as constant as the expected printing speed predefined in slicer software, resulting in the deviation between the actual printing time and the time estimate in slicer software. In practical cases, the actual speed depends on the performance of stepper motors used for driving the nozzle motions on multiple axes, and the travelling distance of

nozzle depends on the programmed toolpaths. Therefore, an effective prediction considering the impact of machine characteristics and numerical control (NC) programs is also required for AM technologies.

2.2.3.2. Optimisation of production planning and path planning for subtractive manufacturing technologies

Kumar et al. (2014) stated that path planning and production planning have vital roles in improving the delivery performance of CNC manufacturing technology. With respect to the optimisation of production planning, a planning method using Single-Minute Exchange of Die and Overall Equipment Effectiveness techniques was carried out to reduce setup time and CNC machining time in an impeller manufacturing plant. The two techniques both effectively schedule the available resources, which achieved a 47% reduction in setup time and 14.6% improvement in the delivery performance. Wdowik et al. (2018) improved the existing programming tools and platforms for CNC milling, incorporating them as a simple and transparent programming interface which could be customised. In the prefabrication stage, an analytical estimation of CAD design was conducted to analyse the most appropriate machining tools, machining parameters to coordinate measuring machines and programming platform. The machining parameters include tool specifications, machining strategy, feed rate, cutting layer and velocity. Through the NC programs, the milling information was programmed in G-code format to instruct the machining operation and coordinate measurement. With respect to the optimisation of path planning, Balabokhin and Tarbutton (2017) developed a novel path planning algorithm to program a contour-parallel and iso-scallop toolpath in a CNC milling process, which aimed to shorten the toolpath and milling time. The method transferred the milling surface from a triangular mesh to voxel-based depth maps, where the start points on the milling boundary were selected to plan the subsequent toolpath. Other cutting points were selected from start points at the maximum material removal rate within the tolerance limit. The path planning was repeated until the milling of the whole area was completed.

Compared with SM, the optimisation methods for improving AM's time efficiency mainly focus on the optimal planning of two perspectives: toolpaths, machine and task allocation, as summarised in **Figure 2.2**. The method of reducing AM's time consumption through the optimisation of process parameters has yet been well explored. From the perspective of the entire AM process, the setting of process parameters in prefabrication stage determines the subsequent layer slicing, numerical control (NC) programming of G-code, and thus effect the total time consumption. Therefore, referring to the research into SM, an effective time modelling and optimisation method integrated with process parameters, G-code in NC programs and machine characteristics is still to be addressed for AM.

2.3. Improvement of energy efficiency for additive manufacturing and subtractive manufacturing technologies

Energy sustainability is the major goal in the manufacturing industry, which aims to reduce carbon dioxide emissions from the use of electrical energy (Jeswiet et al., 2008.). Watson and Taminger (2018) compared the energy consumptions between subtractive manufacturing (SM) and additive manufacturing (AM) technologies. A decision-support model was developed, using the volume fraction to estimate the feasibilities of both technologies. The results indicated that AM is less energy efficient when fabricating an object with a higher ratio of the support structure. Yoon et al. (2014) performed another comparison between various manufacturing technologies, including bulk forming, subtractive manufacturing (SM) and selective laser sintering (SLS) processes. It was found that SLS was comparatively more energy consuming, when including the entire manufacturing cycle – from machine setup to post-processing – in the calculation (Chua and Leong, 2014, Ford and Despeisse, 2016, Peng and Sun, 2017). Since material processing or heating is synchronous with axis movement in general AM technologies, the energy spent on a component's heating represents a large proportion of the total energy consumption. According to statistics by Sreenivasan and Bourell (2010) regarding SLS, it was found that approximately 40% of the total electrical energy usage is for material processing/heating, 25% is for axis movement, and the rest is for material feeding and other uses.

In the following sections, the state of the art in terms of improving AM's energy efficiency is reviewed. As summarised in **Figure 2.3**, the research mainly focuses on two perspectives: prediction methods for energy consumption and optimisation methods to minimise energy consumption in the AM process. The prediction methods include the energy modelling based on part volume, process parameters, machine working states and machine components. The optimisation methods include the optimisation of process parameters to minimise energy consumption. Similarly, the related prediction and optimisation methods of SM are also reviewed. As summarised in **Figure 2.4**, the prediction methods mainly include the energy modelling based on machining parameters, NC programs, machine working states and machine components. The optimisation methods mainly focus on optimising machining parameters and production planning. Details of each method are reviewed in the following sections.

Flow of AM process

Import CAD design	Setting of process parameters	Path planning	Production planning	Printing

CAD → CAM Slicer software → G-code → | Task 1 → Machine 1 | Task 2 → Machine 2 | Task 3 → Machine 3 ... ... | → Printing

Predictive modelling methods	**Volume-based modelling** (Luo et al., 1999; Sreenivasan and Bourell, 2010; Watson and Taminger, 2018; Peng et al., 2016, 2017)	**Modelling based on process parameters and design geometry** (Qin et al., 2020)	**State-based modelling** (Balogun et al., 2014; Peng et al., 2016; Peng and Sun, 2017; Baumers et al., 2011) **Unit-based modelling** (Meteyer et al., 2014)
Optimisation methods		**Meta-heuristic algorithms for optimising process parameters** (Griffiths et al., 2016; Hao et al., 2010; Qin et al., 2020)	

Figure 2.3: Existing research into improving energy efficiency of AM technologies

Figure 2.4: Existing research into improving energy efficiency of SM technologies

2.3.1. Research into prediction approaches for energy consumption of additive manufacturing technologies

The most recent research on predicting AM's energy consumption can be classified into three categories: volume-based modelling, unit-based modelling and state-based modelling. Volume-based modelling uses measurements of average power per unit volume or mass of material. Unit-based modelling refers to the sub-modelling of each energy-consuming component in the AM machine. State-based modelling refers to the classification of the entire AM cycle into different states. Some studies have integrated one or two of the above modelling methods for estimating energy consumption. The related research is summarised as follows.

2.3.1.1. Volume-based modelling for additive manufacturing technologies

Luo et al. (1999) modelled the energy consumption of fused deposition modelling (FDM), selective laser sintering (SLS) and stereolithography (SLA) by measuring the power rate per process productivity, in which the process productivity was calculated as the average mass of solidified material per unit time. Sreenivasan and Bourell (2010) used a similar method to measure the mean power consumption per process productivity of SLS technology. Watson and Taminger (2018) also used a similar method to model the average energy consumption per unit volume of material.

Predictions based on material volume provides a fast and simplified modelling method. Nevertheless, the CAD design consuming the same material volume fabricated under different process parameters or by different AM machines will produce different G-code and energy consumptions. The simple volume-based modelling cannot reflect the impact of process parameters and machine characteristics on the energy consumption. A more detailed prediction model considering the above impacts is required.

2.3.1.2. Unit-based modelling for additive manufacturing technologies

Meteyer et al. (2014) demonstrated a modelling method to predict the energy consumption of a binder jetting (BJ) process on the unit-process level. The method divided the BJ machine into multiple energy-consuming components, including infra-red heater, curing oven, print head, roller, sinter part and others. Experiments were performed to measure the power and mean time of each component. However, the proposed modelling method was limited to BJ technology. Due to the unique mechanism of BJ machine, the toolpath of inkjet nozzle is similar to the nozzle of desktop 2D printer, which selectively deposits droplets of binder on the powder material when passing over the build platform. Thus, the toolpath of axis movement and the time spent on each layer's printing are constant, which can be directly measured through experiments. To propose a prediction method for general AM technologies, the energy modelling only based on experimental measurement is not enough. For most AM technologies, the toolpaths of axis movement are not constant, but are programmed in terms of the process parameters, part geometry, and specific coding rules of the slicer software.

2.3.1.3. State-based modelling for additive manufacturing technologies

Baumers et al. (2011) developed a classification system by dividing the energy usage of selective laser sintering (SLS) into different states: the energy consumed by the construction of all layers in X and Y directions, the energy consumed by the axis movement in Z direction, and the energy consumed by the machine during warm-up. To calculate the printing time, the design geometry was divided into multiple voxels, and the total time consumption for the material deposition was approximated by the average time of each voxel. The energy of each layer's construction was modelled as the summation of energy consumed by depositing each voxel. Balogun et al. (2014) presented a generic modelling method to estimate the energy consumed in a layered manufacturing process. The performances of three FDM machines were benchmarked under different working states, including start-up, warm-up, ready and build. The power requirement of each state was measured to formulate the consumption model, where the time spent on material deposition was calculated through the

part volume and the measurement of average deposited volume per second. Another study by Peng (2016), Peng and Sun (2017) classified the AM process into four working states: material heating, axis movement, material feeding and idle state. The energy consumption of each state was modelled directly through the volume of material usage and the average power per unit volume. On the basis of volume-based energy modelling methods, the above state-based modelling methods divide the entire AM process into multiple working states, which further refine the predictive model by considering the components functions and the running sequences of all energy-consuming components. However, for the modelling of printing state, the methods estimate the energy only based on the part volume without considering the impacts of process parameters on the toolpath planning and layer slicing.

To further improve the prediction accuracy, Qin et al. (2017) proposed an Internet of Things framework to estimate AM's energy consumption. The real-time raw data was firstly collected from the AM machine, including component temperatures, component powers, operating duration, etc. Based on the process parameters and design information, the data features were analysed by data analytical technologies, and then uploaded to the cloud database. The cloud integrated all relevant data used for discovering the energy consumption knowledge of the AM machine, including energy consumption status, behaviour and prediction information. This proposed framework presented the basic workflow of energy consumption estimation. Nevertheless, the specific data analysis methods and algorithms have not been elaborated. In the work published later that year, Qin et al. (2018) proposed a data-driven modelling method to exploit the energy consumption information using clustering and deep learning techniques. The data collected from AM machine, including process operations, design geometry, manufacturing environment and material condition, was processed through a clustering based merged neural network. The target value to be predicted was the energy consumption per unit part weight, which was calculated by measuring the energy consumption of each machine working state. Through the sensing and collecting data from practical AM process, the experimental results validated the merits of model performance. Nevertheless, the data of toolpaths in G-code file are not fully used as inputs of merged neural network, resulting in a large amount of experimental work for measuring the printing time. For general manufacturing technologies, the programmed

toolpaths significantly influence the construction time and therefore also affect the energy consumption during design construction. An effective physics-based modelling of printing time through the toolpaths of printer nozzle can avoid the time measurements based on part volume. However, the related modelling methods are still absent to date.

2.3.2. Research into optimisation approaches to reduce energy consumption of additive manufacturing technologies

Griffiths et al. (2016) utilised a Taguchi design of experiments method to optimise AM process parameters for a desired output response between part weight, scrap weight, production time and energy consumption. The optimisation was performed on four process parameters: build orientation, infill density, shell number and layer thickness. According to the experimental results, the main effects of the adopted parameters were emphasised on the energy consumption and other demands. A lower layer thickness was found to consume lower energy. Another research activity conducted by Hao et al. (2010) optimised the process parameters, internal lightweight structures and reaction temperatures to improve the AM time efficiency and reduce energy consumption through in-situ thermite material reaction. Qin et al. (2020) utilised the deep learning-driven particle swarm optimisation (PSO) to optimise AM's energy consumption based on the real-time collected design-relevant data. On the basis of design-relevant data analytics approach proposed by Qin et al. (2018), the energy consumption knowledge in the design-relevant features was used to formulate the predictive model. The deep learning PSO was applied to search for the optimum design-relevant features, including part-design features and process-planning features, to provide guidance of design revise and process parameter settings to reduce the energy consumption.

Compared with conventional manufacturing, it is challenging to obtain a general rule for optimising AM energy consumption due to the specificity of different types of AM technologies. Most studies have focused on investigating the influence of major process parameters on energy demands through experimental tests. In order to build up a precision model for optimisation, each AM system need to be tested with respect to the relationship

between energy consumption and consumption-related factors. How to reduce the number of experiments while providing an effective prediction and optimization method is still to be addressed.

2.3.3. Research into prediction and optimisation approaches for energy consumption of subtractive manufacturing technologies

The related research into prediction and optimisation approaches for improving subtractive manufacturing (SM) energy efficiency is also reviewed in this section. The existing prediction methods mainly focus on the energy modelling based on four perspectives: machine working states, machine components, machining parameters and G-code in numerical control (NC) programs. The optimisation methods mainly focus on optimising machining parameters and production planning to reduce the energy consumption. Each method is reviewed as follows.

2.3.3.1. Prediction methods for energy consumption of subtractive manufacturing technologies

Based on the review, the existing prediction modelling methods of SM technologies are summarised into four categories: state-based, unit-based, parameter-based and code-based. State-based modelling divides the entire SM cycle into multiple states based on the machine operations. Unit-based modelling divides the milling machine into multiple components based on their manufacturing functions. Parameter-based modelling relates to the functional relationships between energy consumption and the consumption-related machining parameters. Code-based modelling uses manufacturing information in G-code provided by the NC programs.

Gutowski et al. (2006) initially proposed a fundamental model on the state-based level to calculate the energy consumption of a computer numerical control (CNC) milling process. The model divided the manufacturing process into two states: the "ready-to-work" state at a constant power and the machining state at variable power. The energy consumed in each

state was modelling based on measured power, material removal rate and time consumption. Rajemi and Mativenga (2010) proposed the predictive model to minimise energy consumption, with a consideration of the milling process as well as the states of machine setup and tool changing. With the evolution of SM technology, multifunctional machines for the production of complex structures are being developed, accompanied by upgrades in energy modelling methods. Several studies integrated state-based modelling and unit-based modelling to improve and refine the prediction model to make it more realistic in a practical manufacturing context. The machining process was further refined into various machine operating states, such as start-up, standby (also named idle), machining with or without spindle acceleration or deceleration, and rotating with or without cutting. Meanwhile, the milling system was divided into multiple machine tool functional modules, such as the servos for manipulating the machinery, spindle for axis movement, rotated carousel and coolant devices (Kordonowy, 2002).

Combined with state-based modelling, a modular modelling method can be implemented for each unit, based on the measured power and the scheduling of machine operations. For instance, Dietmair and Verl (2009a) demonstrated a unit-based and state-based modelling method to predict the energy consumption of a CNC milling machine. The machine components were divided into multiple modules, including machining, coolant, spindle, drives, hydraulics and cabinet. Each module was scheduled on a corresponding machining state, including chipping, spindle cooling, spindle rotation, axis movement, emergency stop, machine run-up and off. Calvanese et al. (2013) developed an analytical model to estimate the energy consumptions of main machine components, including spindle, axis, chillers, tool change system, auxiliaries, etc. The manufacturing process was divided into different working states, including start-up state, standby state, machining state, tool wear, tool changing, and axis movement at various cutting speeds and feed rates. The total energy demand was modelled as the sum of the power demands of each considered component during different machine working state (Kong et al., 2011).

The research into unit-based and state-based modelling for SM technologies fully consider the entire SM cycle from the machine set-up to the end of milling process. On this basis, parameter-based modelling has been proposed to further improve the prediction accuracy,

since the variations in machining parameters determine the numerical control (NC) programs and machine operations, and thereby influence the prediction of energy consumption. Diaz et al. (2011) emphasised the impact of material removal rate on energy demand in the CNC milling process. They stated that an increased rate of material removal significantly shortened the machining time, but this led to increased loads on the spindle and axis movements with a higher power demand. Thus, a function expressing the characteristics of energy consumption of a machine tool was modelled at various material removal rates. Liu et al. (2015) demonstrated a hybrid model to estimate energy consumption in a slot milling process under various settings of cutting parameters and cutting force profiles. The cutting power at the tool tip was modelled under different cutting forces and the total power was modelled based on the measured cutting powers under different parameters, including depth of cut, spindle speed, and feed rate.

The above prediction methods are mainly based on experiment data to carry out data-driven modelling of the manufacturing system. To reduce the workload of experiments, several studies fully use the numerical control (NC) commands in prediction modelling. He et al. (2012) proposed a novel modelling scheme at the unit-based level to estimate the correlations between component powers and machining parameters. The time consumption of each machining operation was calculated from G-code information, including the coordinates and speed of axis movement, speed of spindle motion, material removal rate, etc. Avram and Xirouchakis (2011) proposed a unit-based and state-based modelling method to estimate the energy consumed by a machine tool system, in which the cutting power, spindle and feed axes power in in steady-state and transient state, and auxiliary component power were mainly considered. The time consumption of machining operations was calculated by processing the corresponding NC commands, which covered the cutter location data, length of each toolpath segment, spindle speeds and feed rates. Aramcharoen and Mativenga (2014) further improved the modelling scheme on both the unit-based and state-based levels. They combined the machining parameters and toolpaths provided by G-code with energy consumption in different processing states. Thus, a consumption model was built based on the running sequence of each component or unit, including machine start-up and setup, spindle rotation, tool cutting, tool changing, material feeding and coolant pumping. Since

the operation of each state and each unit followed G-code commands, their time consumptions were directly calculated from G-code. The researchers also stated that the manufacturing information in G-code and the modelling on both unit-based and state-based levels are expected to be applied in the prediction of AM energy consumption. From the afore-mentioned reviews, it is found that the related research on code-based modelling for AM technologies is still blank. Most methods are purely based on a large number of experiments to build up the data-driven model.

2.3.3.2. Optimisation approaches to reduce energy consumption of subtractive manufacturing technologies

To maximise energy efficiency, a feasible optimisation tool can be selected to search for the optimum production planning and optimum solution set of machining parameters. With respect to the optimisation of machining parameters, Deng et al. (2020) proposed a carbon utilisation efficiency model based on the characteristics of machining flow and material removal mechanism in a milling process. A multi-objective optimisation method using a particle swarm optimisation (PSO) algorithm was implemented to search for the optimum machining parameters with the minimum time and energy consumptions. Four main machining parameters were considered to be optimised, including spindle speed, feed speed, milling width and milling depth.

   With respect to the optimisation of production planning, Wang et al. (2018) demonstrated a hybrid modelling approach based on the Standard for Exchange of Product model data numerical control, which is an official standard that provides the contributing factors effecting energy consumption in machining process. A multi-objective optimisation problem was defined, wherein a set of preliminary machining schemes were generated in terms of energy demand information and rules. With the assistance of an ant colony optimisation technique, the optimal combination of operations, strategies, machining parameters, machine tools and cutting tools was selected from the preliminary machining schemes to maximise energy efficiency. Dietmair and Verl (2009b) presented a number of examples to illustrate how the model was applied in a real-time, strategic and tactical decision-making

process, to obtain the optimal resource allocation and minimise the energy consumption. A study by Rajemi et al. (2010) proposed an energy footprint model of turning and milling processes, wherein the critical parameters included the power of machine setup and start-up mode, time consumption of tool changing, energy footprint and velocity of tool cutting. The model was used to search for the optimum tool life and cutting conditions for machining, with the minimum energy requirements. A direct search method was applied to optimise tool life and corresponding machining parameters, including depth of cut, feed and velocity.

Through the review of optimisation methods for improving AM and SM energy efficiency, it is found that the machining parameters or process parameters to be optimised are limited to a few important parameters. Due to the diversity of manufacturing mechanisms, the significance of each machining parameter to the total energy consumption is uncertain. To deliver convincing optimisation results, it is necessary to optimise all consumption-related parameters in energy modelling. In addition, the use of precise prediction accompanied with the optimisation of machining parameters is a feasible way to improve the energy efficiency of both AM and SM. Although there is no general rule for predicting and optimising energy consumption, power and time measurements of each consumption-related component are inevitable. From the review of code-based modelling of SM's energy consumption, the manufacturing information in G-code can be fully used to calculate the time consumption of machining process. This method can be also extended in the consumption modelling of AM process, since AM technologies also fabricated by following the numerical control (NC) commands in G-code.

2.4. Improvement of material efficiency for additive manufacturing and subtractive manufacturing technologies

Material saving is challenging in both additive manufacturing (AM) and subtractive manufacturing (SM) technologies due to their special manufacturing mechanisms (Newman et al., 2015). In SM processes, material waste inevitably occurs during production by material removal, but this process allows high-precision production through the milling

process. In AM processes, the design with a higher proportion of support structure consumes a large amount of material, but this process provides the freedom to construct complex structures. Therefore, the application of individual manufacturing technology is often constrained by its production capabilities, such as the failure to fabricate complex structures, inability to use certain materials or a large amount of material waste (Newman et al., 2015; Zhu et al., 2013a). In order to improve efficiency, several studies have integrated multiple SM and AM processes to apply their respective advantages and overcome the drawbacks (i.e. hybrid manufacturing (HM) process).

In the following sections, research on production planning in HM processes for improving material efficiency is reviewed. Furthermore, research on optimising the factors that affect the material efficiency of AM technologies are also reviewed. As summarised in **Figure 2.5**, the research mainly focuses on two perspectives: prediction methods for material consumption and optimisation methods to minimise material consumption in the AM process. The research of prediction modelling was based on layer thickness. The optimisation methods include the optimisation of build orientation, path planning and production planning. Details of each method are reviewed as follows.

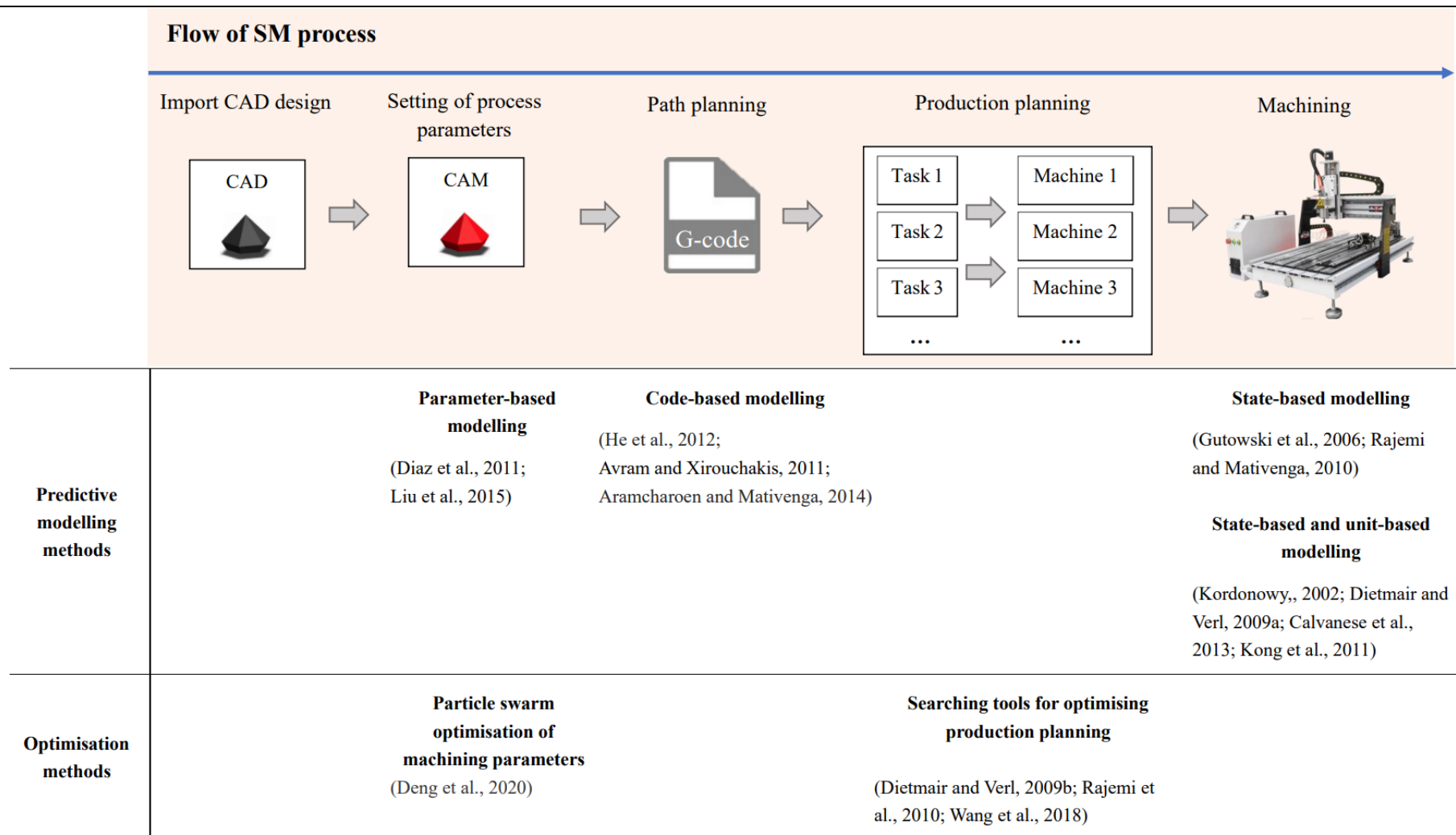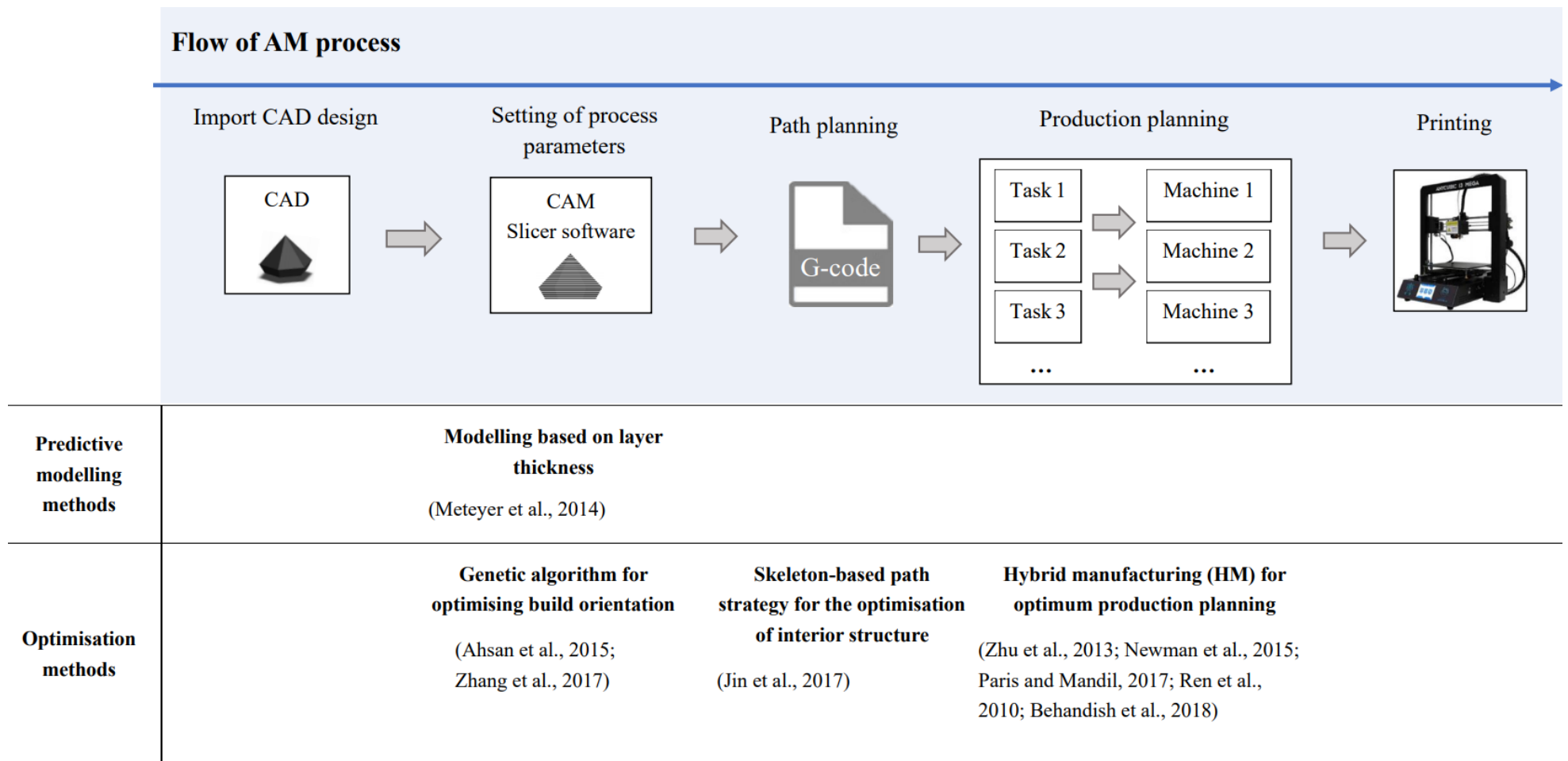Figure 2.5: Existing research into improving material efficiency of AM technologies

2.4.1. Research into process planning to reduce material consumption of hybrid manufacturing technology

HM technology has been widely applied in industrial manufacturing in recent years. It integrates multiple types of manufacturing processes or technologies to capitalise on and consolidate the advantages of each individual process, while also minimising their disadvantages (Newman et al., 2015). A feasible process planning of various additive manufacturing (AM) and subtractive manufacturing (SM) technologies can significantly reduce material waste. For instance, Zhu et al. (2013b) proposed a process planning algorithm entitled iAtractive to plan and schedule the additive, subtractive and inspection processes for a given CAD design. By dividing the design into multiple parts, three factors were analysed on each part, namely process capability, production time and material usage. Then, iAtractive implemented part-specific process planning to minimise the manufacturing constraints of complex geometries. This algorithm was further improved by Newman et al. (2015). Additional factors were defined as inputs to iAtractive (including process planning knowledge, geometry constraints and remanufacturing information of the existing part/raw material) to maximise the material efficiency and recycling of material waste for the next production. Le et al. (2017) developed a lifecycle method to evaluate the feasibility of remanufacturing existing parts/raw material in a hybrid manufacturing (HM) process. The process planning was based on the geometry constraints, available resources and machine characteristics. Ren et al. (2010) developed an integrated strategy to realise the automatic process planning of computer numerical control (CNC) machining and selective laser sintering (SLS). The method separated the CAD design into multiple parts with non-uniform layer thicknesses and toolpaths. Behandish et al. (2018) proposed a similar systematic computational algorithm to automate the process planning. The optimal solution set of machining parameters was obtained to maximise the time efficiency, and minimise the production costs and material consumptions.

Based on the above, HM is found to be an efficient production mode for large-scale production enterprises to save materials. For the manufacturers such as individual users, it is challenging to integrate multiple AM and SM manufacturing processes due to the limited

manufacturing resources and capacities. For the manufacturing process performed by a single technology, it is still necessary to improve the existing manufacturing technology to reduce material consumption.

2.4.2. Research into optimisation of factors affecting material efficiency of additive manufacturing technologies

An effective prediction method of material usage is necessary for the improvement of material efficiency. A study by Meteyer et al. (2014) estimated the average material consumption of binder jetting (BJ) technology through experimental tests. Except for the metal powder, the liquid binder and cleaner used for bonding powders and the washing system were also estimated based on layer thickness and layer numbers. It was found that part geometry is the major factor that determines the material efficiency in an AM process. Yoon et al. (2014) stated that AM is outperformed in small-size production by conventional manufacturing technologies. This is because the poor recycling rate of AM is the bottleneck of AM development, especially for designs with a large proportion of support structures. This weakness is magnified when the time and energy consumed by the construction and post-processing of support material increase with the part volume (Watson and Taminger, 2018).

Several studies have focused on the optimisation of part geometry and process parameters through computer-aided manufacturing (CAM) to minimise AM material consumption. The build orientation and interior structure (or infill density) are the two main factors that affect the amount of material consumed by the support and internal structures. Regarding build orientation, Ahsan et al. (2015) investigated the impact of this on AM material saving through experimental tests. They stated that the toolpath and the number of contour areas on each layer varied with build orientation, and excessive contours could increase the construction time and surface quality defects. Therefore, Zhang et al. (2017) developed a feature-based optimisation algorithm to seek the optimal build orientation of multi-part construction. A finite set of alternative orientations for every single part was generated within the constraint of product quality. A genetic algorithm (GA) was applied to search for the

optimal orientation with the minimum build time and material usage among each finite set. Regarding the interior structure or infill density, Jin et al. (2017) developed a skeleton-based path strategy to minimise the interior volume of solid parts, which was based on the supporting angle, contour area and layer thickness.

Based on the above, research on the prediction of AM's material consumption is still scarce. Many commercial slicer software can provide estimates of material usage based on the part geometry in the prefabrication stage. However, the estimation is lack of accuracy since the impact of machine and material characteristics is not considered, for example, the insufficient melting and extrusion of thermoplastic material in fused deposition modelling (FDM) process. Besides, note that even if the same design structure is adopted, the different combinations of process parameters will yield different G-code, in which the commands used for instructing the machine to deposit material will be also different, resulting in different material consumption. Thus, it is vital to develop a precise and general modelling method based on the process parameters, and characteristics of the machine and material. Furthermore, the existing methods of optimising material consumption mainly optimise the major process parameters, such as build orientation and infill density. Considering the impact of each process parameters on the final consumption, the scope of optimisation should be expanded to all process parameters.

2.5. Knowledge gaps

Based on the review of existing research, the knowledge gaps are identified in this section. From the consumption modelling perspective, several studies have simplified the toolpath on each layer in the area and volume calculation. This prediction method of time consumption without considering the impacts of process parameter variations on the layer slicing and path planning results in a limited prediction accuracy. To further improve the prediction accuracy, the consumption modelling should consider all related process parameters, machine characteristics, and resources spent throughout the entire AM cycle. Besides, there is still a lack of prediction method associated with the path planning in CAM,

which reduces the workload of experimental measurements, and allows the predictive model to be expandable to the resource modelling for general manufacturing process using computer numerical control (CNC) programming. Furthermore, due to the diversity of AM mechanisms, most of the proposed modelling methods only focus on a single type of AM technology. A general prediction method is needed to achieve accurate prediction of general AM systems.

From the multi-objective optimisation perspective, most studies have optimised only a few important process parameters (e.g. build orientation, infill density) to minimise as single objective from time, energy or material consumptions. In fact, all process parameters that can be personalised in CAM determine the corresponding G-code together with the programming process and the final consumptions. From the existing studies, there is still a lack of general multi-objective optimisation method, in which the inputs contain all process parameters for constructing the CAD design, and the outputs are no longer restricted to a single objective.

Based on the above, a general prediction and multi-objective optimisation method is still required to predict and minimise time, energy and material consumptions of the AM process. To achieve an effective prediction of a specific AM task, the consumption modelling needs fully consider the related process parameters, characteristics of AM machine and material, production environment, and customer demands. To minimise the resource consumptions, the optimisation is supposed to provide the optimal solution of all related process parameters in prefabrication stage.

2.6. Summary

This chapter introduces the major focuses for improving AM technologies, and provides a literature review on the area of prediction and optimisation of time, energy and material consumptions of AM technologies. Since some AM research has evolved from the existing

research into SM technologies, the related work for improving SM technologies is also reviewed.

Based on the preceding review of the literature, knowledge gaps have been identified to motivate the research work in this thesis and provide evidence of its contribution. The aim of this current work is to propose a general prediction and multi-objective optimisation scheme, to predict and minimise time, energy and material consumptions of the AM process. In the next chapter, the framework of the proposed methodology will be introduced.

CHAPTER 3   FRAMEWORK OF PREDICTION AND MULTI-OBJECTIVE OPTIMISATION FOR ADDITIVE MANUFACTURING TECHNOLOGIES

3.1. Introduction

The framework of prediction and multi-objective optimisation of time, energy and material consumptions for additive manufacturing (AM) technologies is described in this chapter. In order to provide a general prediction method, all energy-consuming components of the existing AM technologies on the market are investigated. Based on their manufacturing functions, the components are classified into five types of modules: axis movement, material processing, component heating, material feeding and auxiliary components. To clearly illustrate the running sequences of five types of modules, their power profiles integrated with the corresponding G-code commands are displayed in the form of a Gantt chart. Then, the hybrid data-driven modelling and physics-based modelling are performed, which aims to establish the models of time, energy and material consumptions related to the process parameters for each module. In physics-based modelling, the time and distance of axis movement with actual displacements, and the amount of material feeding are directly calculated from G-code. In data-driven modelling, the functional relationships between the consumptions and process parameters of the remaining modules are obtained from experiment data. The experiments mainly include: the apparent powers of all modules, the time consumptions of material processing module and component heating module, and the temperatures of modules to be heated.

In addition, some AM technologies, such as fused deposition modelling (FDM), might experience a motor out-of-step problem in the actual production environment, which causes the failure of axis movement speed and material feeding rate to reach their targets. Moreover, the quoted density of some AM materials also deviates from the actual density. Thus, in order

to reduce the impact of above-mentioned similar machine characteristics on prediction accuracy, the proposed framework is upgraded with additional experiments to obtain the relationships between the actual and expected axis movement speeds, material feeding rates and material densities. The models of those parameters can replace the original parameters in the predictive models.

Finally, meta-heuristics are applied to approximate the optimal combination of process parameters that consume the least time, energy and material. The predictive models of time, energy and material consumptions are used as the objective functions to calculate the fitness of each combination of process parameters. Since different process parameters produce different G-code and predictive models, the process from the generation of G-code through slicer software to the consumption prediction is embedded in the fitness calculation. Details of the proposed framework is described in the following sections.

3.2. Classifications of consumption-related modules
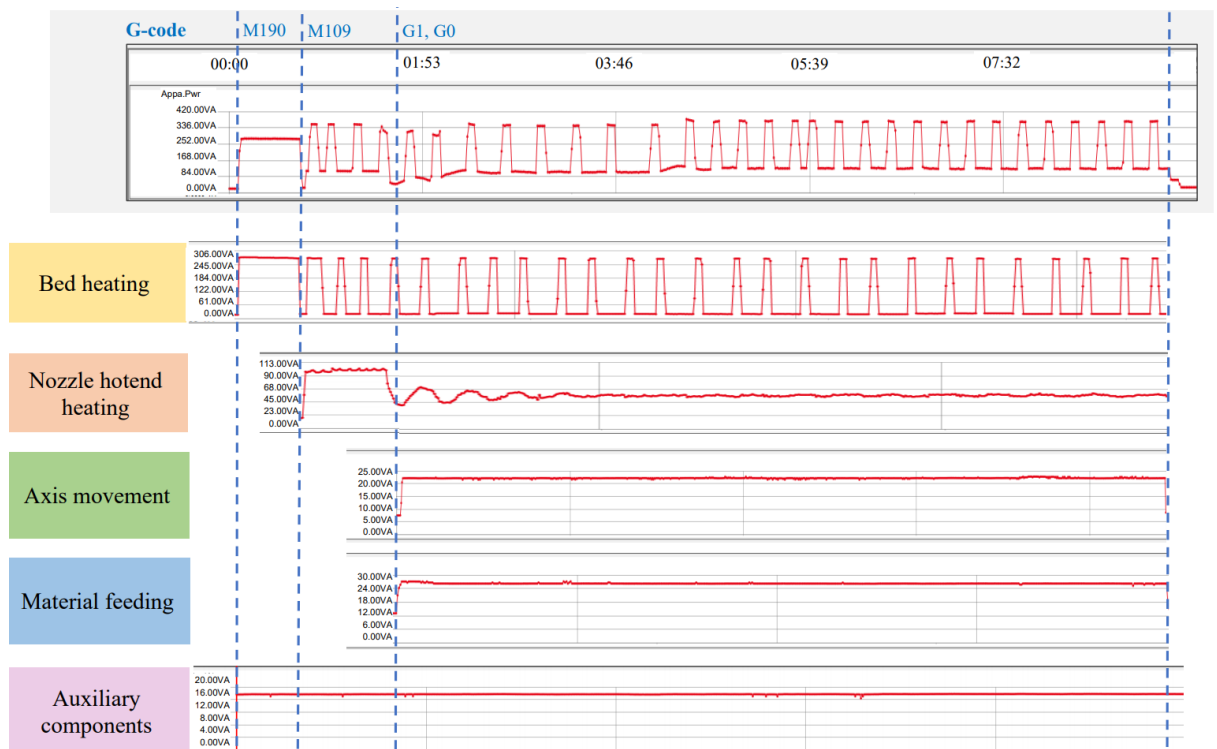
Figure 3.1: Power profiles of a general AM task printed by a typical FDM 3D printer

At the beginning of this study, a typical fused deposition modelling (FDM) 3D printer was tested by using a power analyser. The aims is to figure out how the various components of a typical AM machine cooperate to accomplish an AM task. **Figure 3.1** presents the power profiles of the printer and its energy-consuming components participating in the AM process. The first plot in the grey box indicates the total power profile of the whole printer. The remaining five plots indicate the power profile of each component. In details, the bed heating refers to the heating of the build platform, which is done to make the base of the printed object firmly adhere to the build platform. Nozzle hotend heating refers to the heating of the hotend component located inside the nozzle, which involves melting the polylactic acid (PLA) filament material from solid to liquid. Axis movement refers to the movement of the printer nozzle. Material feeding refers to the extrusion and deposition of melted PLA material. The auxiliary components refer to those used for monitoring and controlling the machine status.

Note that the running sequences of above components are decided by the machine characteristics and the coding rules of slicer software for the AM machine. In this example, according to the instructions of G-code commands, the bed heating first starts at the beginning of an AM task, and then followed by the heating of nozzle hotend. After both components reach their target temperatures, the axis movement and material feeding begin to construct the physical object. The auxiliary components remain in running state throughout the entire AM process. In addition, **Figure 3.1** is also a representative case that illustrates the running power of general AM technologies. From this figure, two points are concluded:

- Firstly, the total power profile is a combination of the power profiles of all the components.

- Secondly, the time when each component starts to run strictly follows the instruction of the G-code command.

AM technology	Material form	Material type	Time, energy, material consumptions related components of each module				
			Material processing	**Component heating**	**Material feeding**	**Axis movement**	**Auxiliary components**
Material Extrusion	Wire	Polymers	Nozzle heater / hotend	Build platform / bed	Wire feeder / extruder	XYZ axes Cartesian system	Display unit
	+	Thermoplastics	+	+	+	Delta system (3 parallel stepper motors)	User interface and connectivity
		Ceramics				Polar system (radial and angular coordinates)	Cooling system
		Concrete				Multi axis robotic arm	Temperature sensor
		+				+	
Binder Jetting	Powder	Metals	Inkjet nozzles (liquid binder)	+	Powder roller / recoater	XY axes gantry system	
	+	Polymers			New powder stock	Build platform / bed	
		Ceramics	+		Overflow bin	+	
		+			+		
Material Jetting	Liquid	Photopolymers	Ultraviolet light	Build platform / bed	Build material feeder	XY axes gantry system	
		Metals		Material container	Support material feeder+	Build platform / bed	
		Wax	+			+	
	+	+		+	+		
Direct Energy Deposition	Wire	Metals	Laser	+	Wire feeder	XYZ axes gantry system	
	Powder	Polymers	Electron beam		Powder feeder	Multi axis robotic arm	
		Ceramics	Electric arc			X/Y/Z tables	
			Plasma		+	Rotary table	+
	+	+	+			Tilt-rotate trunnion	
						+	
Powder Bed Fusion	Powder	Metals	Laser	+	Powder roller / recoater	Laser scanner / XY plotter	
	+	Polymers	Electron beam		Powder supply platform	Build platform / bed	
		+	Thermal print head		Overflow bin	+	
			+		+		
Sheet lamination	Sheet	Paper	Laser	Heated roller	Material supply roller / spool	Laser scanner / XY plotter	
	+	Plastic sheets	+	+	+	Build platform / bed	
		Metal sheets				+	
		Fibre composites					
		+					
Polymerisation	Liquid	Resin photopolymer	Ultraviolet light	+	+	Laser scanner / XY plotter	
	+	+	Laser			Build platform / bed	
			+			+	
+	+	+	+	+	+	+	

Figure 3.2: Module classifications of consumption-related components of current AM technologies on the market

Based on the above, it can be known that an AM system constructs a 3D object through the collaboration of various components with their unique functions. Thus, this study has classified all consumption-related components of AM technologies commonly used on the market into five types of modules. As shown in **Figure 3.2**, the module types are material processing, component heating, material feeding, axis movement and auxiliary components. The classification is based on the specific manufacturing function of each component, which is described as follows.

- The material processing module is to continuously process or heat the material to prepare it for deposition. For example, the nozzle hotend of a fused deposition modelling (FDM) machine is heated to melt the thermoplastic filament from a solid state to a liquid state. The ultraviolet (UV) light of material jetting (MJ) and polymerisation machines is to cure the photopolymer from a liquid state to a solid state.

- The axis movement module is to move the material processing module by following the predefined toolpath in G-code. For example, the XY axes gantry system of a binder jetting (BJ) machine is to drive the inkjet nozzle to the target coordinate in X and Y directions, while the build platform is to drive the inkjet nozzle to the next layer in Z direction.

- The material feeding module is to feed a specific amount of processed material on the target coordinates. The running of this module is usually accompanied by material processing to construct the 3D object. For example, the material feeding driven by the powder feeder of a direct energy deposition (DED) machine is synchronised with the heating of laser. This is to ensure that the metal powder is melted from solid to liquid and then deposited on the platform.

- The component heating module – as the name suggests – is to heat the components used to support the object construction. For example, heating of the build platform/bed of material extrusion (ME) and material jetting (MJ) machines is performed to ensure that the material at the bottom of the printed part does not

completely cool and instead adheres firmly to the platform. Similarly, the heating material container of a MJ machine ensures that material such as photopolymer and wax remain in a liquid state. The heated roller of a sheet lamination machine is used to apply pressure and activate the adhesive on the film to achieve the bonding of the two layers.

● The auxiliary components module plays an auxiliary role in supporting the manufacturing process, such as monitoring and controlling the machine status. The components in this module always keep running, irrespective of whether the AM machine is in a standby state or printing state. For example, the display unit is used to show the machine status; the user interface and connectivity provide a means to control the machine operation in a wired or wireless manner; the cooling system accompanies the manufacturing process to reduce the machine temperature; and the temperature sensor is used to monitor the temperature of components being heated.

Note that some components may have more than two functions. For example, the build platform of a material jetting (MJ) machine is not only used to drive the movement of ultraviolet (UV) light in Z direction, but it is also heated to ensure that the deposited material adheres firmly to the platform. In this case, the component should be defined as two modules: axis movement module, and component heating module. Each module has only one function. This is to facilitate prediction modelling of the resource consumed by each function when the component performs multiple functions.

To propose a general modelling method for long-term use, the module classification in **Figure 3.2** can be used as the database to be updated and supplemented with the continuous development and innovation of AM technologies. For a novel AM technology, the energy-consuming components can be classified into different modules based on their functions, and the information of each module can be added to the blank area marked with a "+" sign in the database. If encountering a component with a new function, an additional new module can be defined to record the information of this component.
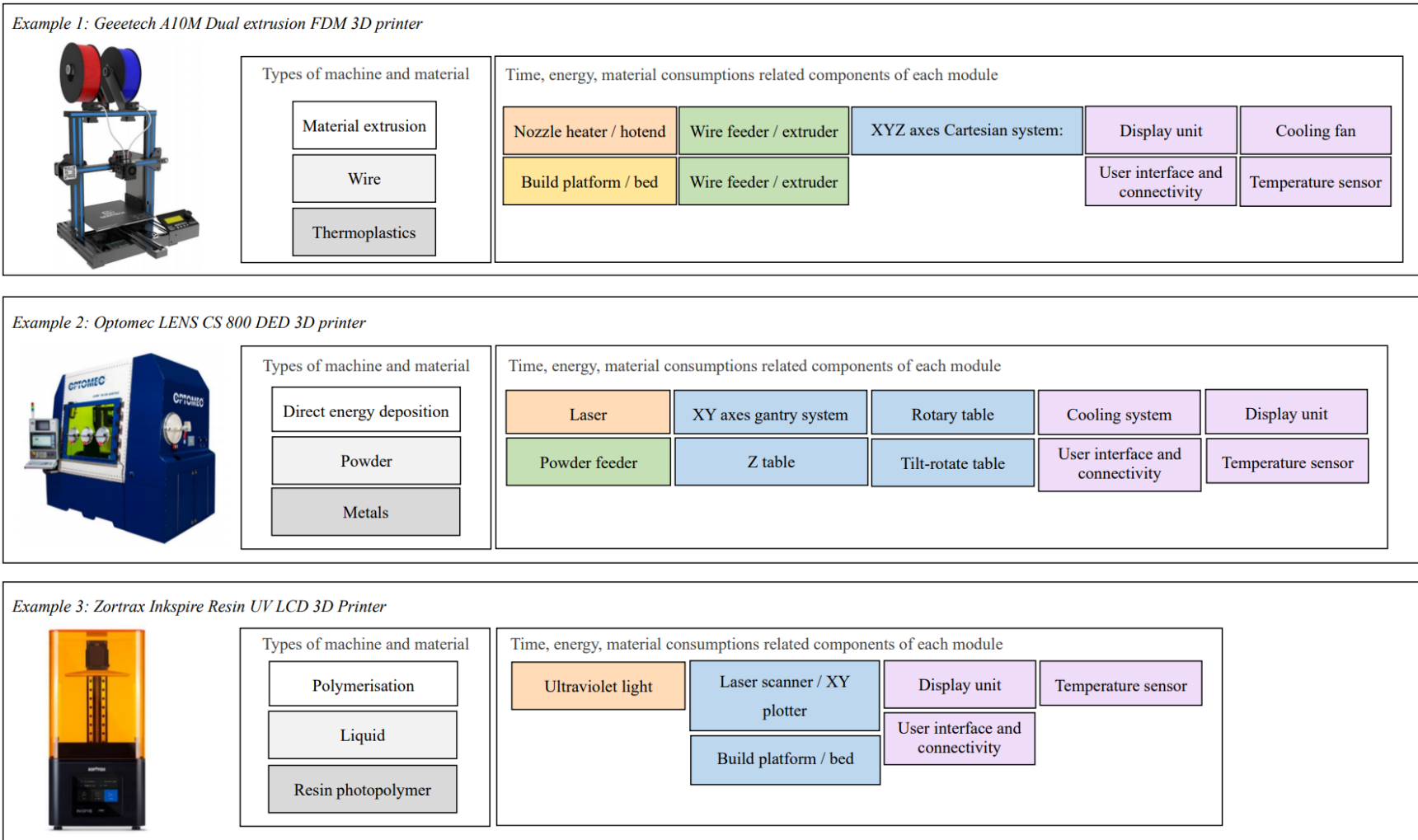
Figure 3.3: Examples of consumption-related modules of three different AM machines

Based on the above, **Figure 3.3** presents three different AM machines as examples to illustrate the module classification according to the database in **Figure 3.2**. The first example is the Geeetech A10M dual extrusion fused deposition modelling (FDM) 3D printer, which uses a dual-material extrusion system to produce 3D objects. Specifically, the printer allows switching between two extruders that provide two different types of thermoplastics. The same as general FDM 3D printers, each extruder deposits material melted by the nozzle heater/hotend on the heated build platform/bed, accompanied by the axis movement driven by an XYZ-axes Cartesian system. Other components running in the standby state also participate in the manufacturing process to control and monitor the machine status. Therefore, the consumption modelling selects nine modules from the database: two material extruders, nozzle heater, build platform, Cartesian system, display unit, user interface and connectivity, cooling system and temperature sensor.

The second example is the Optomec LENS CS 800 direct energy deposition (DED) printer. During the AM process, a powder feeder sprays the metal powders melted by a laser or electron beam to produce 3D objects, accompanied by axis movement driven by a combination of an XY-axes gantry system and Z table. This AM machine also provides an interchangeable rotary table and tilt-rotate trunnion to realise the 4-axis and 5-axis movements. These components are instructed by the corresponding toolpaths on multi-axes in G-code programming. Therefore, 10 modules are selected to form the predictive models: laser, powder feeder, XY-axes gantry system, Z table, rotary table, tilt-rotate trunnion, cooling system, user interface and connectivity, display unit and temperature sensor.

The third example is the Zortrax Inkspire Resin ultraviolet (UV) LCD 3D printer, which uses polymerisation technology to produce 3D objects. During the AM process, the resin photopolymer is solidified by the scanning of a UV beam emitted from the laser scanner/XY plotter, accompanied by axis movement driven by these two components in X and Y directions and the build platform/bed in Z direction. Therefore, there are six

modules selected for the modelling: UV light, laser scanner/XY plotter, build platform/bed, user interface and connectivity, display unit and temperature sensor.

After the module classification for a specific AM machine, the power profile of an AM process performed by the machine can be measured and used to formulate a Gannt chart, in which the time node of each power variation corresponds to the start time of each module operation. The start time is determined by the G-code commands. Thus, a Gannt chart as shown in **Figure 3.4** is generated to clearly identify the running sequences of all modules, and their correspondences to G-code commands and power profiles. In addition, this chart can intuitively reflect the overlap of multiple module operations on the time axis. This can facilitate the subsequent prediction modelling, and the design of experiments to measure the time consumption and apparent power of each module.
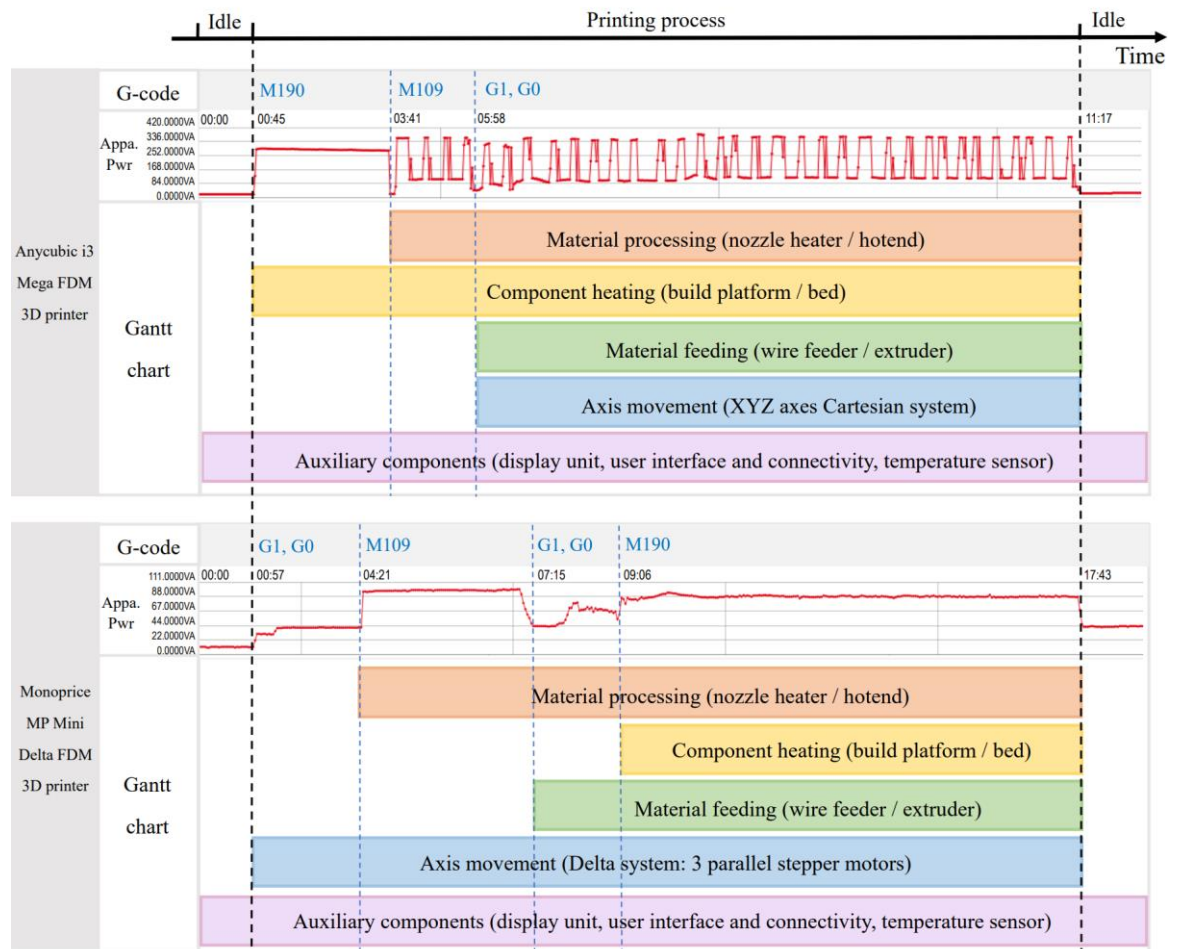
Figure 3.4: Examples of the correspondence diagrams between modules, G-code commands and power profiles

Two examples of fused deposition modelling (FDM) 3D printers are presented. As shown in **Figure 3.4**, each module is distributed along the time axis as a Gantt chart by following the G-code commands. For both machines, the module of auxiliary components are running and consuming energy during the entire AM process. These components comprise the display unit, temperature sensor, and user interface and connectivity. However, the running sequences of other modules are completely different. For the ANYCUBIC i3 Mega 3D printer, the heating of the build platform/bed takes precedence over the nozzle heating. Once both components reach the target temperatures, the heating powers are stabilised to maintain constant temperatures. Then, the wire feeder and the XYZ-axes Cartesian system start running to construct the 3D object. For the Monoprice MP Mini Delta 3D printer, the difference is that the calibration of the central coordinates is required at the beginning of each AM task. Thus, the delta system of axis movement runs first, from the task starting until the task ends. After the calibration, the nozzle is heated to the target temperature and then the wire feeder begins to deposit the first layer of material. After completing the first layer, the build platform/bed is heated to ensure that the printed object adheres firmly to the build platform.

The above two examples demonstrate the specificity of AM machines and the importance of G-code in this study. Details of the prediction and multi-objective optimisation for the two machines will be discussed as case studies in **Chapter 7** and **Chapter 8**. In the following sections, the consumption modelling procedures and the multi-objective optimisation procedures will be introduced to illustrate the proposed framework.

3.3. Framework of prediction and multi-objective optimisation
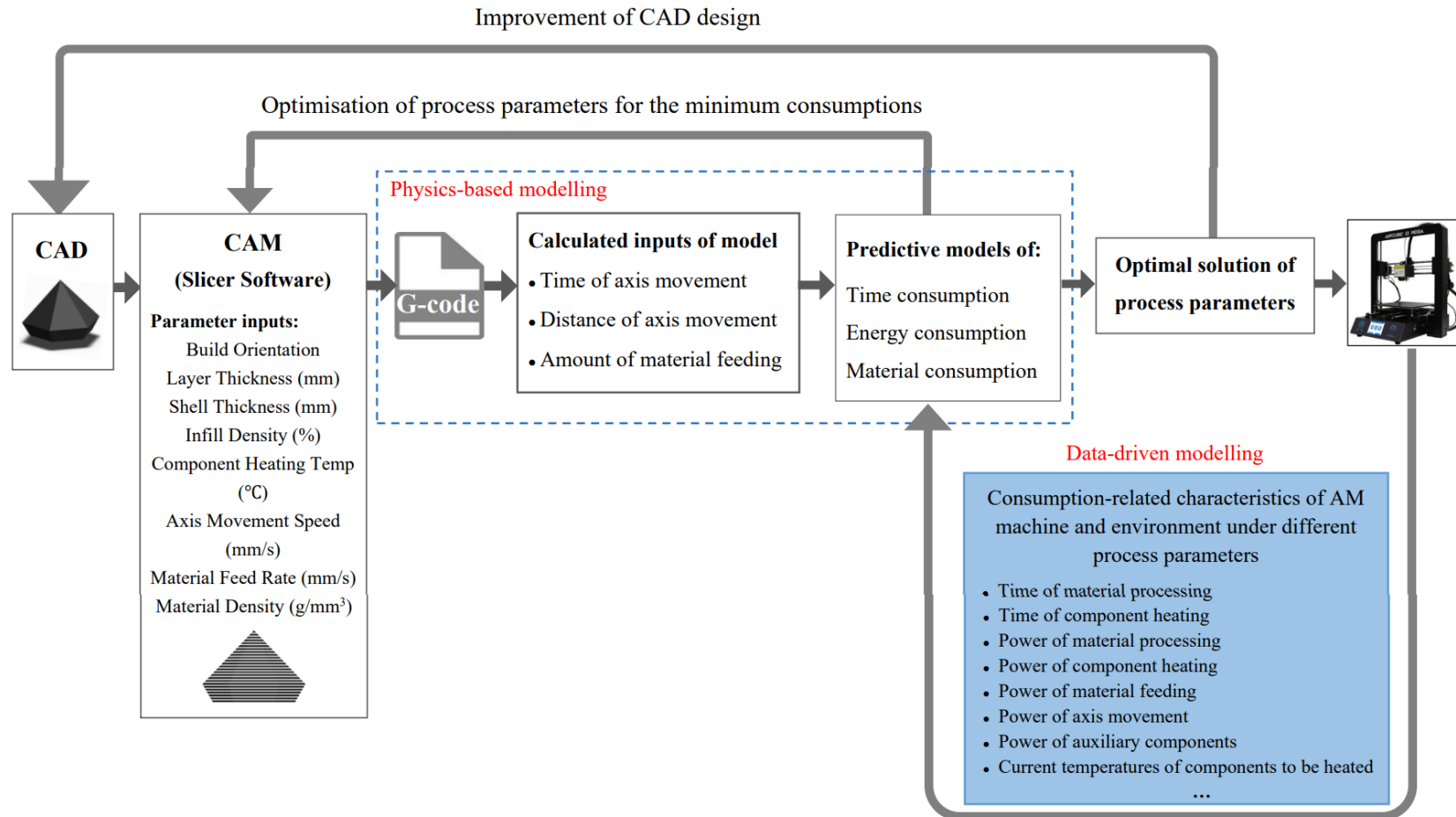
Figure 3.5: Framework of prediction modelling and multi-objective optimisation for AM's time, energy and material consumptions

The framework of the proposed method is presented in **Figure 3.5**. To begin, a CAD design in standard triangle language (STL) format is imported into CAM (i.e. slicer software) to slice the 3D prototype into multiple layers (Yang et al., 2017). The slicer software provides an interface to personalise the process parameters according to the machine characteristics and customer demands. After the setting of process parameters, the slicer software encodes the printing information of each layer into G-code commands through computer numerical control (CNC) programming. The information is used to instruct the machine operation during the AM process. Then, for each module, the conceptual models of time, energy and material consumptions are built as the functions of process parameters. The functional relationships are derived in two ways: through physics-based modelling and data-driven modelling.

In physics-based modelling, the data in G-code is processed to calculate three parameters of the models: the time, distance of axis movement with actual displacements and the amount of material feeding. In data-driven modelling, besides the above parameters calculated from G-code, the relationships between other parameters and process parameters are unknown and can only be obtained from experiments. The experiments consist of three parts: the time measurements of the material processing module and component heating module, the power measurements of all five modules and the current temperatures of components to be heated. All the above time consumptions and power are measured under different combinations of process parameters. After the experiments, the functional relationships between these parameters and the process parameters are derived by using regression analysis method. Polynomial regression is applied to curve-fit the functional relationships (i.e. to calculate the coefficient of the functions).

When the predictive models are obtained, a multi-objective optimisation technique is applied to optimise the process parameters and minimise the time, energy and material consumptions of the current AM task. The optimisation results provide guidance to select a feasible solution set of process parameters and improve the structure of the CAD design. In the following sub-section, details of each step in the proposed framework are described.

3.3.1. Physics-based modelling based on G-code

Physics-based modelling based on G-code is one of the main contributions of this study, since a CAD design can produce different G-code for different AM machines and different slicer software. **Figure 3.6** presents an example of a CAD design manufactured by two different machines. Each machine has two supporting sets of slicer software. By importing the design in standard triangle language (STL) format into two sets of slicer software, this enables the generation of two G-code files for each AM machine based on its specific coding rules. Thus, four AM tasks with unique G-code files are generated. Each G-code file contains different commands to instruct the AM machines. The time, energy and material consumptions of these four tasks will also be different.
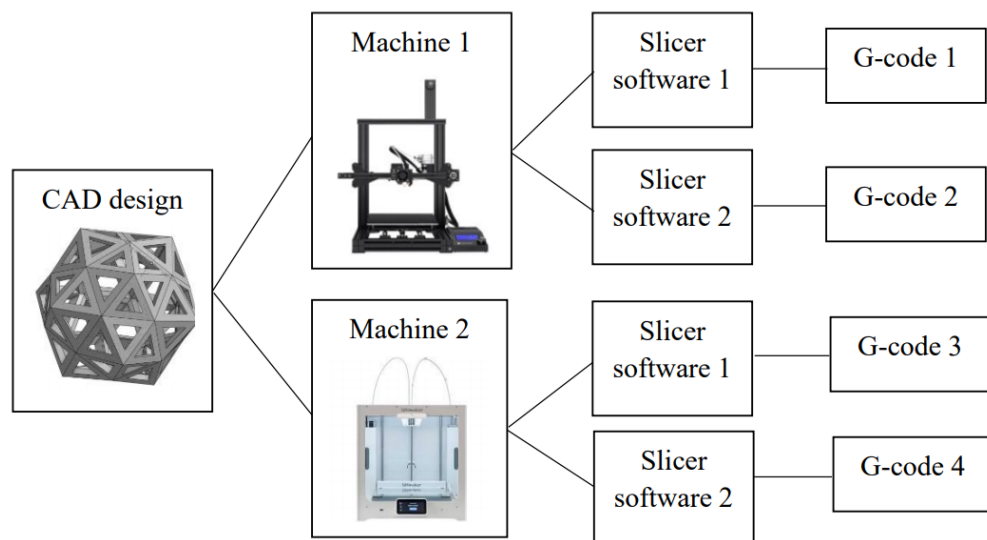
Figure 3.6: G-code generation by different slicer software for different AM machines

The main types of G-code commands are summarised in **Table 3.1**. These commands provide the AM machine with the target temperature of component heating, the accurate coordinates and corresponding speeds of axis movements, and the rate and amount of material feeding. For instance, a command starting with the letter "F" denotes the target speed of axis movement or the target rate of material feeding. A command starting with "G1" or "G0" denotes the commencement of axis movement or material feeding. A command starting with "X", "Y" or "Z" denotes the target coordinate of axis movement in the X, Y or

Z direction. Commands starting with "M104" or "M140" denote the setting of target temperatures for the heating material processing module and the component heating module. Commands starting with "M109" or "M190" indicate to begin the heating of the above two modules.

Table 3.1: Instructions of typical G-code commands in the AM process (Smid, 2003; 2010)

Module type	G-code command	Meaning	Unit
Axis movement	G1, G0	Begin axis movement	
	G28	Home all axes back to the initial coordinates	
	Fnnn	Rate of material feeding/speed of axis movement	*mm/min*
	Xnnn	Target X coordinate of axis movement	*mm*
	Ynnn	Target Y coordinate of axis movement	*mm*
	Znnn	Target Z coordinate of axis movement	*mm*
Material feeding	Ennn	Consumed amount of material feeding	*mm*
	G92 E0	Reset the consumed amount of material feeding	
Material processing/ heating	M104 Snnn	Set the target temperature of the material processing component	
	M109 Snnn	Begin heating the material processing component to the target temperature nnn°C	
Component heating	M140 Snnn	Set the target temperatures of components	
	M190 Snnn	Begin heating component to the target temperature nnn°C	
Auxiliary components	G4 Snnn	Pause the machine for nnn seconds	
	M106	Turn the cooling fan on	
	M107	Turn the cooling fan off	
	M84	Disable the idle hold of axis movement and material feeding components	
Example of a G-code command			
G1 F9600 X119.483 Y151.786 E24.523		Axis movement to the target coordinate (X119.483, Y151.786) at a rate of 9600 *mm/min* for material feeding and the current consumed amount of material feeding is 24.523 *mm*	

```
G92 E0                              ; Reset the amount of mateiral feeding to 0

M104 S205                           ; Set the temperature of material processing module to 205℃

M109 S205                           ; Start heating the material processing module to 205℃

G0 F9000 X-8.536 Y10.408 Z0.263     ; Move the nozzle to the target coordinate at a speed of 9000mm/min

G1 F3000 X10.704 Y9.942 E0.62524    ; Move the nozzle to the target coordinate with material feeding at a

G1 X10.108 Y10.165 E0.64959         rate of 3000mm/min

G1 X9.488 Y10.312 E0.67397          ; Continue the axis movement and material feeding at the last speed

G1 X8.638 Y10.385 E0.70662          (3000mm/min)

G1 X-7.842 Y10.408 E1.33731

G0 F2700 X-8.536 Y10.408

G0 F9000 X-8.537 Y10.058

G1 F2400 E1.36387

G1 F3000 X-9.15 Y10.019 E1.38738

G1 X-9.753 Y9.9 E1.4109

…

M140 S60                            ; Set the temperature of component heating module to 60℃

M190 S60                            ; Start heating component heating module to 60℃

G0 X-3.083 Y-1.001 Z0.413           ; Continue the axis movement and material feeding

G1 F2400 E61.40787

G1 F3000 X-2.946 Y-1.018 E61.41088

G1 X-2.837 Y-1.02 E61.41326

G1 X-2.837 Y-.99

G1 X-2.837 Y-.968

G1 X-2.837 Y-.85 E61.41471

G1 X-2.837 Y-.806 E61.41513

G1 X-2.837 Y-.782 E61.41526         ; The total amount of material feeding in the current AM task is
                                      61.41526mm
```

Figure 3.7: G-code commands of a typical AM task

The G-code commands of a typical AM task are shown in **Figure 3.7**. According to the main types of G-code commands listed in **Table 3.1**, "G92 E0" indicates that the amount of material is reset back to zero at the beginning of the AM task. "M104 S205" and "M109 S205" indicate that the components of the material processing module are set and heated to the target temperature of 205℃. "M140 S60" and "M190 S60" indicate that the components

of the component heating module are set and heated to the target temperature of 60℃. The G-code commands can provide three types of important information in the prediction modelling: 1). the running sequences of machine components; 2). the coordinates and speeds of axis movement. 3). the amount of material feeding.

The running sequences of machine components are determined by the coding rules of slicer software. Since the AM machine executes G-code commands line by line, the machine will execute the next command after the current command is completed. For example, when the components of the material processing module are heated in the middle of the printing process, the axis movement module will be paused until the heated components reach the target temperature. During this period, the axis movement module will still be in running status at the previous power level. Thus, the time consumption of the axis movement module consists of two parts: the time spent on actual displacements with or without material feeding and the time spent on waiting for other components to finish running. In this study, we define the latter period of time as the 'interval time'. According to the Gannt chart, the interval time is equal to the time spent on other components running.

The coordinates, speeds of axis movement and the amount of material feeding can be processed for the physics-modelling of two modules: axis movement and material feeding. Three parameters of the predictive models are calculated, namely the time and distance of axis movement with actual displacements, and the amount of material feeding. The detailed calculation methods of above three parameters are described in next chapter.

3.3.2. Data-driven modelling based on experiments

Apart from the parameters calculated from G-code, the relationships between other parameters and process parameters are unknown because they cannot be calculated from G-code. For example, for the heating of material processing module and component heating module, G-code only provides the commands "M140" and "M104" to instruct the AM machine to start heating the components, but it does not provide the time consumption and

power of this heating process. Therefore, data-driven modelling is applied to obtain the functional relationships between the remaining parameters and process parameters through experiments.

Table 3.2 lists the modules that need to be tested through experiments. Power measurements are conducted to test the apparent powers of all five modules under different related process parameters. Time measurements are conducted to test the setup time or heating time of the material processing module and component heating module under different process parameters. For the axis movement module, the time consumption of axis movement with actual displacements is calculated from G-code, while the interval time is determined by the running sequences and time consumptions of other modules. For other four types of modules, their time consumptions are also determined by the running sequences and time consumptions of all modules. In addition, the current temperatures of the components to be heated in the material processing module and component heating module are also recorded at the beginning of each AM task. Since general AM technologies have sensors to monitor the temperatures of components being heated, the current temperatures of these components can be directly recorded from the AM machine.

Table 3.2: List of modules to be tested through experiments

Modules	Related process parameters	Apparent powers	Setup time / heating time	Current temperature
Axis movement	Speed of axis movement	✓		
Material feeding	Rate of material feeding	✓		
Material processing	Target temperature	✓	✓	✓
Component heating	Target temperature	✓	✓	✓
Auxiliary components	None	✓		

The apparent power is the combination of active power and reactive power. The former refers to the real electrical resistance power consumed by the alternating current (AC) power,

which is converted into thermal and mechanical energy during the AM process. The latter refers to the inductive and capacitive power consumed by the AC power passing through the inductive and capacitive components to build up the magnetic and electrical files (El-Habrouk et al., 2000). The above two types of power both consume electrical energy in actual production. Therefore, this study selects to use the apparent power to build up the energy consumption model.
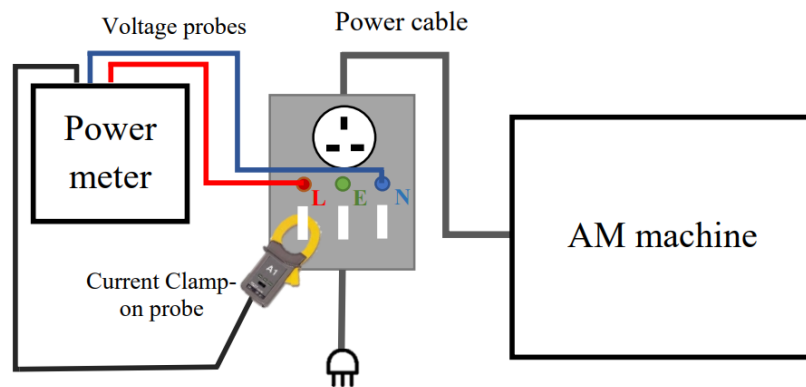
Figure 3.8: Circuit connection of power and time measurements by using a power meter

The circuit connection for the measurements of apparent power and time consumptions is displayed in **Figure 3.8**. To avoid disassembling the AM machine, a circuit box has been designed to separate the power cable of the AM machine into three wires: neutral, live and earth. This aims to conduct the power and time measurements only through the power cord without disassembling the AM machine. Two voltage probes are connected with the neutral and live wires to form a parallel circuit, which are used to measure the voltage of the AM machine. The current clamp-on probe is an electrical device with jaws, which is used to read the magnitude of AC flowing through a conductor (Gregorec Jr et al., 2006). In this study, the current clamp-on probe is used to measure the AC flowing through the live wire of the AM machine. Since general power meters have functions of measuring both time and apparent power, the time consumptions and apparent powers of the modules listed in **Table 3.2** are directly measured by following the circuit connection in **Figure 3.8**.

To test the time and apparent power of each single module, G-code commands can be manually designed to instruct the AM machine to run the modules individually. **Section**

3.3.1 provides a detailed explanation of the G-code commands. The G-code commands used to instruct each individual module are summarised in **Table 3.3**. During the experiments, measurements are conducted under different settings of process parameters in these G-code commands. The process parameters include the speed of axis movement, rate of material feeding, and target temperatures of the material processing module and component heating module.

Table 3.3: G-code commands for the time and power measurements of each single module

Module	G-code command	Meaning
Axis movement	G1 Fnnn Xmmm Ymmm	Move the printer nozzle to the target coordinate (Xmmm, Ymmm) in X, Y directions at a speed of nnn
	G1 Fmmm Znnn	Move the printer nozzle to the target coordinate (Zmmm) in Z direction at a speed of nnn
Material feeding	G1 Fmmm Ennn	Feed material with an amount of nnn at a rate of mmm
Material processing	M104 Snnn M109 Snnn	Set the target temperature nnn of the material processing module and then heat the module to the target temperature
Component heating	M140 Snnn M190 Snnn	Set the target temperature nnn of the component heating module and then heat the module to the target temperature
Auxiliary components	None	This module keeps running throughout the entire AM task without the need for G-code commands

Based on the experimental results, the functional relationships between the measured results and process parameters can be derived with the assistance of a curve-fitting tool. Curve-fitting is the process of generating the curve of a mathematical function with the best fit, based on a series of data points (Sandra, 1994). Regression analysis is used to curve-fit

the functional relationships and calculate the coefficient of functions. There are various regression analysis methods, such as linear, polynomial, Poisson, ride, lasso, logistic, elastic net, etc. (Liang and Zeger, 1993). In statistics, polynomial regression is a common form of regression analysis used to model the relationship between independent variables and dependent variables as a multi-degree polynomial. Thus, polynomial regression is selected as the tools to curve-fit the above relationships.

Above two sections mainly introduce the basic flow of prediction modelling according to the proposed framework. The definition of predictive models and the methods used in the prediction modelling will be introduced in next chapter. Details of the modelling procedures for each module will be discussed in Chapter 5.

3.3.3. Multi-objective optimisation

The prediction is followed by multi-objective optimisation. Since meta-heuristic algorithms have been widely applied for solving sophisticated optimisation problems, a suitable optimisation technique can be selected from the existing meta-heuristic algorithms to solve the multi-objective problem in this study. According to Abdel-Basset et al. (2018) and Crespo-Cano et al. (2019), the major algorithms include genetic algorithm (GA), particle swarm optimisation (PSO), clonal selection, chemical reaction optimisation, evolution strategies, harmony search, teaching–learning-based optimisation, Tabu search and variable neighbourhood search.

The basic flowchart of meta-heuristic algorithms applied in this study is presented in **Figure 3.9**. To start with, initial populations containing random solutions of process parameters are generated. Then, each solution is imported into the slicer software to generate the corresponding G-code file. Based on the G-code information and predictive models, the time, energy and material consumptions of each solution are predicted. Then, based on the rules of selection or guided search in different algorithms, the elite solutions are retained. After that, a new generation of candidate solutions is obtained through exploitation or

exploration steps (Abdel-Basset et al., 2018). This new generation and the retained solutions will continue to be imported into the slicer software for the next iteration of the optimisation process. The iteration will be stopped when the stopping criterion is satisfied. The optimal solution set of process parameters related to the near-optimal approximate Pareto front is finally obtained at the end of this optimisation process. To evaluate the performance of optimisation algorithm, hypervolume (HV) indicator is used to compare the optimal solutions obtained from multiple tests. The solution set with the maximum HV indicator can be compared with the default solution to validate the merit of optimisation method.
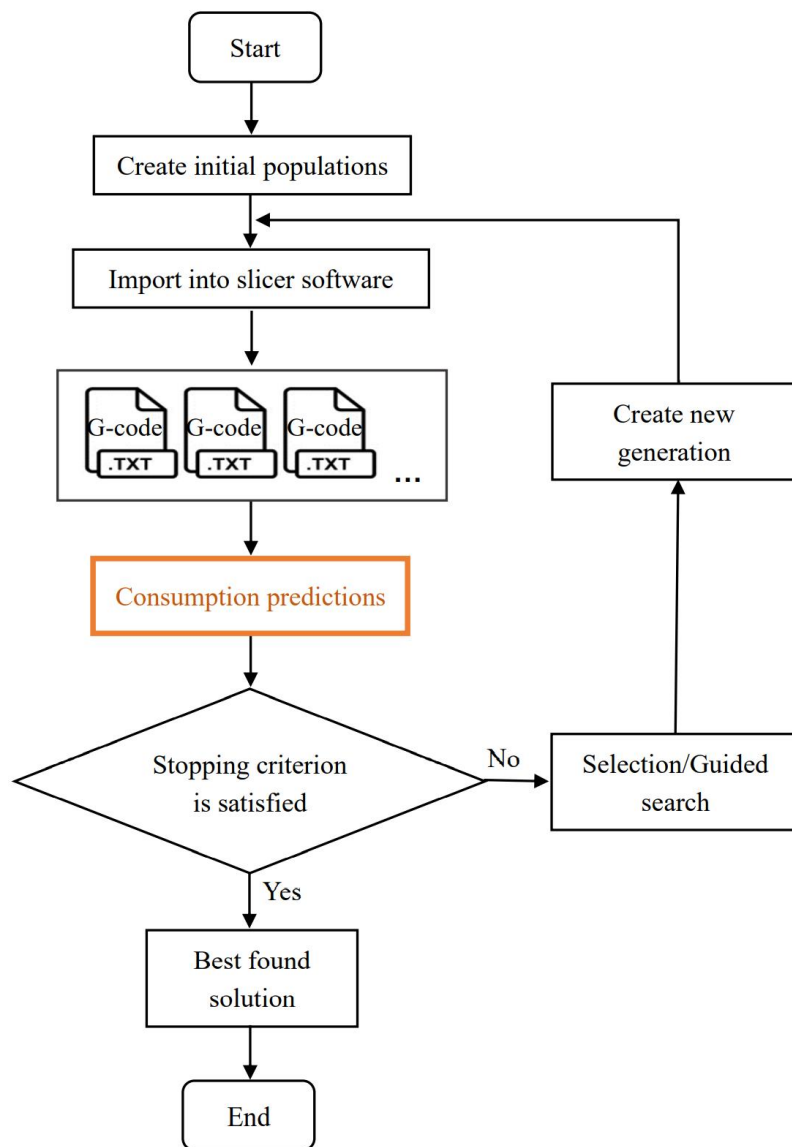
Figure 3.9: Flowchart of general meta-heuristics (Deb and Goyal, 1996; Crespo-Cano et al., 2019)
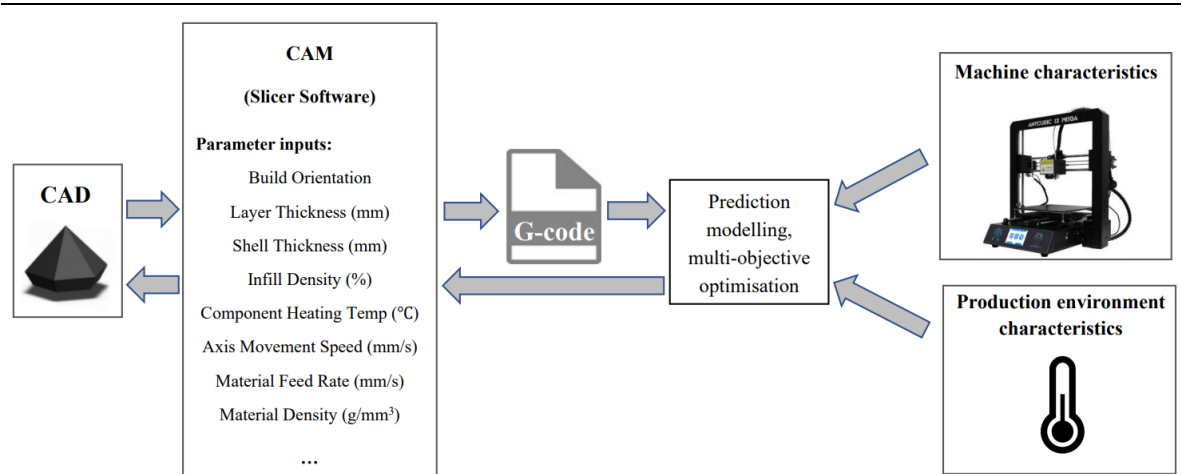
Figure 3.10: Two-way feedback bridge between practical production and CAM

Based on the above, reductions of AM's time, energy and material consumptions can be achieved through two ways: optimisation of the CAM process parameters and improvement of the CAD design. As shown in **Figure 3.10**, one of the main contributions of this study is to establish a two-way feedback bridge between practical production and CAD design. At the start, the experimental results of the machine characteristics and production environment are fed back to build up the prediction models. At the same time, the G-code of the CAD design generated by CAM provides the manufacturing information to accomplish the prediction modelling. After obtaining the predictive models, the multi-objective optimisation is performed. The best solution set of process parameters can finally be fed back to CAM and CAD. In CAM, the optimisation result provides guidance or a trend for selecting a feasible solution of process parameters. In CAD, the optimisation result provides guidance for improving the design structure.

3.4. Additional experiments for improving the framework of prediction

In a practical manufacturing context, some parameters in the predictive models are affected by the characteristics of the machine and the material. For example, motor out-of-step commonly occurs during the fused deposition modelling (FDM) process. It is caused by the high loads and insufficient torques of stepper motors during high-speed axis movement and

high-rate material feeding, which leads to the axis movement module and material feeding module failing to reach the specified speeds and rates. To improve the prediction accuracy, additional experiments are conducted to test the actual speed of axis movement and actual rate of material feeding. As shown in **Figure 3.11**, the measured speeds and rates are used to replace the speeds and rates provided by G-code in the predictive models. In addition, the proposed material consumption model uses the quoted density of the polylactic acid (PLA) filament material. To improve the prediction accuracy, the actual material density can also be measured through experiments to replace this quoted density.
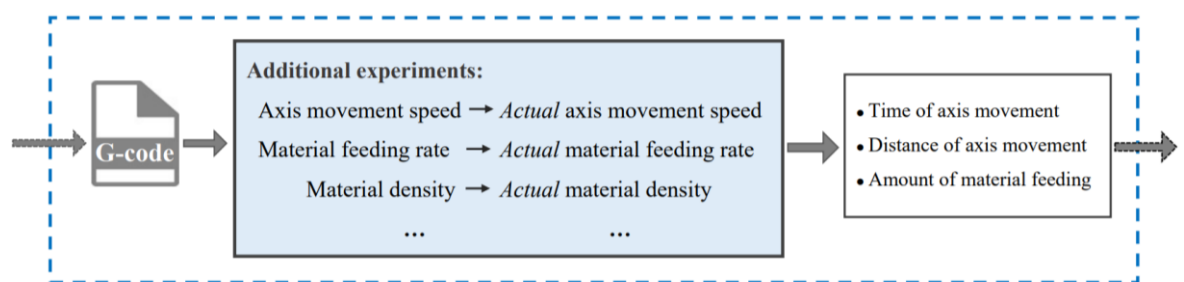
Figure 3.11: Schematic of additional experiments for improving the framework of consumption prediction (e.g. FDM technology)

By replacing the expected values with actual values, the predictive models are updated and continue towards the subsequent optimisation. The parameters that need to be additionally measured are determined by the characteristics of the AM machine and material.

3.5. Summary

This chapter introduces the framework of prediction and multi-objective optimisation of AM's time, energy and material consumptions. The classification of consumption-related modules, hybrid modelling of each module, consideration of machine characteristics and multi-objective optimisation are the main contributions of this study. Details of each contribution is explained as follows.

Firstly, the module classification divides the machine components into five types: axis movement, material processing, component heating, material feeding and auxiliary

components. The running sequences and power profiles of the five modules correspond to G-code commands, which provide clear guidance for the prediction of time, energy and material consumptions.

Secondly, hybrid modelling consists of two parts: physics-based modelling based on G-code and data-driven modelling based on experiments. The former makes full use of manufacturing information provided by G-code to calculate three essential parameters in the models: time, distance of axis movement with actual displacement and the amount of material feeding. For other parameters that cannot be calculated from G-code, experiments are conducted to test the relationships between these parameters and process parameters. Compared with traditional modelling methods, physics-based modelling based on G-code not only provides a precise prediction but also reduces the workload as it requires fewer experiments. Meanwhile, the entire process – from importing process parameters into CAM to the prediction of consumptions – is embedded into the optimisation process. This is because every new solution of process parameters has its own unique predictive model, as its G-code is unique. Thus, instead of providing a fixed predictive model, the proposed method has developed customisable modelling method with a consideration of process parameters, machine characteristics and environmental characteristics.

Thirdly, in a practical manufacturing context, the values of certain parameters in the predictive models are affected by the characteristics of machine and material. Thus, additional experiments are conducted to test the relationships between the actual and expected values of affected parameters. The model of each parameter is used to replace the original parameter in the predictive models. This step fully considers the machine performance and improves the prediction accuracy.

Finally, meta-heuristic algorithms are applied to search for the most feasible solution set of process parameters to minimise time, energy and material consumptions. The main procedures of the optimisation are also presented. Different from a traditional optimisation process, the modelling process from inputting process parameters into CAM to the generation of G-code, and then from the processing of G-code data to the prediction of the

three consumptions, is entirely embedded in the optimisation process. This method of integrating prediction with the optimisation process realises the customised modelling and optimisation with accurate prediction and optimisation results.

This chapter only introduces the framework of consumption modelling and optimisation. The methodology used to realise this research work is presented in the next chapter.

CHAPTER 4   METHODOLOGY

4.1. Introduction

This chapter introduces the methodology of proposed research work. At first, the hypothesis is identified that the proposed prediction and optimisation method can be effectively used to predict and minimise the resource consumption for general AM technologies. Then, the prototypes of predictive models are defined in terms of classified modules. Based on the Gannt chart of all modules, the model of total time consumption is built by the union of the time consumption of each module. The total energy consumption is the sum of the integral of the apparent power over the time consumption of each module. The total material consumption is calculated through the amount of material feeding provided by G-code. Besides, the multi-objective problem to be optimised is also defined. The process parameters are defined as decision variables, and the predictive models of time, energy and material consumptions are defined as objective functions.

After the definitions of predictive models and optimisation problem, the methods applied in hybrid prediction modelling are introduced in this chapter. In physics-based modelling, the G-code calculation method used to predict the axis movement time and material feeding amount is described. In data-driven modelling, the regression analysis method used to process the experiment data is described. In addition, a feasible optimisation technique is selected to search for the optimal solution set of process parameters that fabricates by using the minimum consumptions. Since the non-dominated sorting genetic algorithm (NSGA-II) has been widely used to solve optimisation problems with two or three objectives in industrial manufacturing, this study applies NSGA-II to this optimisation problem. The basic workflow of NSGA-II algorithm and the Taguchi design of experiments are described to perform optimisation tests under different combinations of optimisation parameters. The performance measures using hypervolume (HV) indicator are also described to compare all obtained Pareto fronts and select the optimum solution sets of process parameters.

At last, the methods used in experimental validation is presented to prove the hypothesis that proposed method is effective in solving the consumption prediction and optimisation problem for real-world AM machines. The methods used to calculate prediction accuracies and evaluate the significance of optimisation parameters for the HV indicator are described in this chapter.

4.2. Hypothesis of research work

To start with the research work, a hypothesis has been made that the proposed prediction and multi-objective optimisation method can realise an effective prediction and minimisation of time, energy and material consumptions for general AM technologies. Details of the hypothesis are as follows.

● The hybrid modelling method can achieve an efficient prediction of AM's recourse consumptions, and the additional experiments for testing the model parameters effected by machine characteristics can improve and achieve an acceptable prediction accuracy.

● The multi-objective optimisation method using NSGA-II algorithm can effectively minimise the resource consumptions of an AM process, and provide a feasible solution of process parameters to guide the parameter settings.

● Since this research aims to lay the foundation for resource prediction and optimisation for general AM technologies, the proposed method is currently based on the assumption that the machine is intact and operate normally.

4.3. Definition of conceptual predictive models

This section describes the conceptual models of AM's time, energy and material consumptions, which can be used as general models for all AM technologies. For specific cases, the models of each module should be further expanded and refined, based on the machine characteristics.

4.3.1. Conceptual predictive model of time consumption
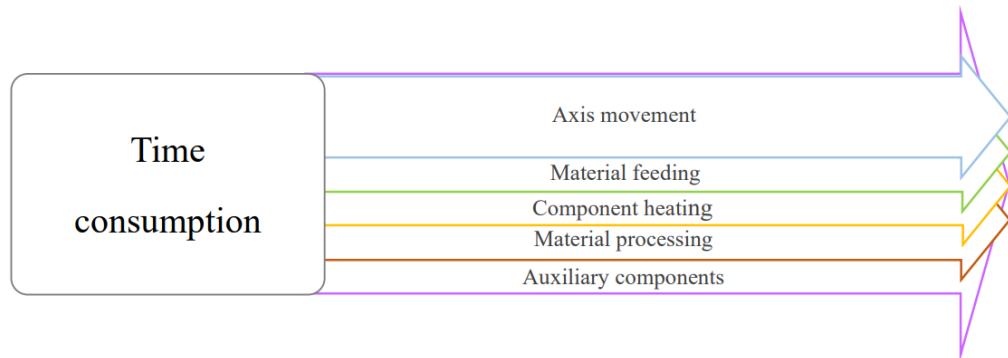
Figure 4.1: Time flows into five types of time-consuming modules

This section introduces the conceptual modelling to predict time consumption in the AM process. **Figure 4.1** presents the flows of total time consumption into five modules. In this study, the following notation applies:

- TM denotes the finite set that contains the time consumptions of all time-consuming modules, shown in **Equation (4.1)**.

$$TM = \{t_i\}_{i=1}^{m} \tag{4.1}$$

- m denotes the total number of time-consuming modules.

- t_i denotes the total time consumption of the ith module, which is modelled as a function of the process parameters in **Equation (4.2)**.

$$t_i = f_i(\mathbf{x}) \tag{4.2}$$

- $\mathbf{x}$ denotes a finite set containing all process parameters, in which n denotes the total number of process parameter and I_n is the nth process parameter in this finite set $\mathbf{x}$, as shown in **Equation (4.3)**.

$$\mathbf{x} = [I_1, I_2, \ldots, I_n]^T \tag{4.3}$$

- Referring to the running sequences of modules, and since overlap exists between the time consumptions of the five types of modules, the total time consumption t_{total} of the entire AM process is modelled as the union of time consumed by each module, as expressed in **Equation (4.4)**. Due to the different mechanisms of different AM systems, this conceptual model is supposed to be refined in terms of the running sequences of machine modules.

$$t_{total} = \bigcup_{i=1}^{m} t_i \tag{4.4}$$

4.3.2. Conceptual predictive model of energy consumption
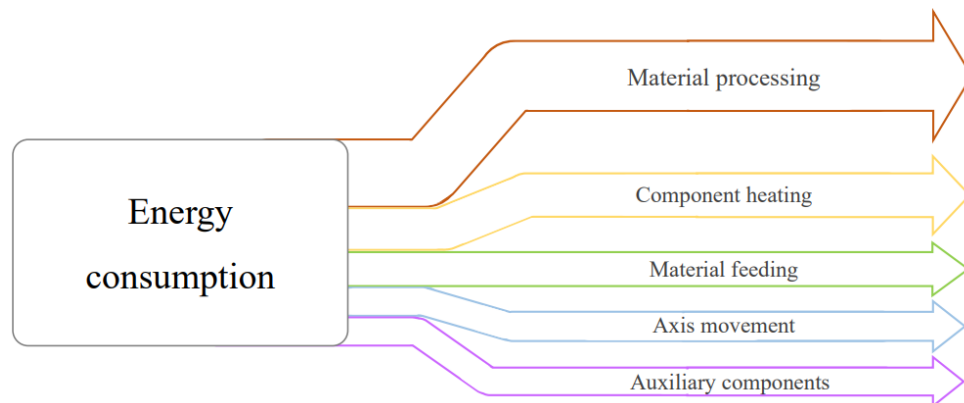
Figure 4.2: Energy flows into five types of energy-consuming modules

After the conceptual modelling of time consumption described above, this section continues with the conceptual modelling of energy consumption in the AM process. **Figure 4.2** presents the energy flows into five modules. The energy consumption of each module is independent and has no intersections with other modules. In this study, the following notation applies:

- *EM* denotes the finite set that contains the apparent powers of all energy-consuming modules, as shown in **Equation (4.5)**.

$$EM = \{P_i\}_{i=1}^{m} \tag{4.5}$$

- m denotes the total number of time-consuming modules.

- P_i denotes the apparent power of the ith module, which is modelled as a function of process parameters $\mathbf{x}$ in **Equation (4.6)**.

$$P_i = g_i(\mathbf{x}) \tag{4.6}$$

- As expressed in **Equation (4.7)**, the total energy consumption E_{total} is modelled as the sum of energy consumed by each module, which is calculated as the integral of apparent power P_i over its total time consumption t_i.

$$E_{total} = \sum_{i=1}^{m} \int_0^{t_i} P_i \, dt \tag{4.7}$$

The last section provides the conceptual modelling of time consumption t_i for each module. Thus, the time consumption models can be directly imported into **Equation (4.7)**. Besides, the apparent powers of all five modules cannot be obtained from G-code. Thus, the relationships between the apparent powers and process parameters $\mathbf{x}$ can only be derived from experiments. These experiments are designed to test the apparent power of each module under different process parameters. Based on the experimental results, polynomial regression is applied to curve-fit the above functional relationships (i.e. to calculate the coefficient values in the functions).

4.3.3. Conceptual predictive model of material consumption

This section introduces the conceptual modelling to predict material consumption in the AM process. The amount of material usage is provided by the G-code commands beginning with the letter "E". Thus, the total material consumption M_{total} in the AM process can be directly modelled based on the G-code. Generally, the consumed amount indicated by G-code is in units of length or volume. However, in the subsequent experimental validation of the case studies, the mass of the printed object needs to be measured to calculate the

prediction accuracy. Therefore, this study uses mass as the unit to model the total material consumption M_{total}, which is equal to the product of the material density ρ and the cumulative volume $\sum V_{unit}$ of material feeding, as expressed in **Equation (4.8)**.

$$M_{total} = \rho \cdot \sum V_{unit} \qquad (4.8)$$

4.4. Definition of the multi-objective problem for optimisation

After the conceptual modelling in the previous section, three predictive models of time, energy and material consumptions for general AM technologies are obtained and used as objective functions for the multi-objective optimisation. This section introduces the definition of the multi-objective problem. Since the purpose of this study is to reduce time, energy and material consumptions of the AM process, the problem can be set as the minimisation of three objective functions, defined as follows:

$$minimise\ \mathcal{F}(\mathbf{x}) = \ [\mathcal{F}_1(\mathbf{x}), \mathcal{F}_2(\mathbf{x}), \mathcal{F}_3(\mathbf{x})]^T \quad \mathbf{x} \in X^n \qquad (4.9)$$

$$\mathcal{F}_1(\mathbf{x}) = T_{total} \qquad (4.10)$$

$$\mathcal{F}_2(\mathbf{x}) = E_{total} \qquad (4.11)$$

$$\mathcal{F}_3(\mathbf{x}) = M_{total} \qquad (4.12)$$

$$\mathbf{x} = [I_1, I_2, \dots, I_n]^T \qquad (4.13)$$

$$Subject\ to: \quad I_r^{\ L} \leq I_r \leq I_r^{\ U} \qquad r = 1, 2, \dots, n \qquad (4.14)$$

In this study, the three objectives are treated with the same weights. In the above equations, $\mathcal{F}(\mathbf{x})$ is the vector function to be minimised. Its three elements respectively represent the three objective functions of time, energy and material consumptions T_{total}, E_{total}, M_{total} which are designated as $\mathcal{F}_1(\mathbf{x})$, $\mathcal{F}_2(\mathbf{x})$ and $\mathcal{F}_3(\mathbf{x})$. X is defined as the finite set consisting

of all candidate solutions, wherein each solution $\mathbf{x}$ indicates a n-dimensional vector consisting of n number of decision variables. Each decision variable represents one type of process parameter for AM. The constraint (I_r^L and I_r^U) of each decision variable I_r is determined by the properties and production capacity of the AM machine.

Table 4.1: Example of constraints of three decision variables/process parameters for a general FDM 3D printer

Decision variables/process parameters I_r		Upper limit I_r^U	Lower limit I_r^L	Constraints
I_1	Target temperature of component heating module	I_1^U: the highest temperature of the component heating module	I_1^L: the current room temperature	$25°C \leq I_1 \leq 65°C$
I_2	Speed of axis movement	I_2^U: the highest speed of axis movement	I_2^L: the lowest speed of axis movement	$300mm/min \leq I_2 \leq 9000mm/min$
I_3	Target temperature of material processing module	I_3^U: the highest temperature of the material processing module	I_3^L: the melting point of the material	$160°C \leq I_3 \leq 250°C$

An example of three decision variables for a general fused deposition modelling (FDM) 3D printer is presented in **Table 4.1**. The example has three process parameters (i.e. $n = 3$) to be optimised, namely the target temperature I_1 of component heating, the speed I_2 of axis movement and the target temperature I_3 of material processing. According to the characteristics of the FDM machine, the upper limit I_1^U of I_1 is defined as the highest temperature the component heating module can be heated to, while the lower limit I_1^L is defined as the current room temperature. The upper limit I_2^U and lower limit I_2^L of I_2 are respectively defined as the highest and lowest speeds of axis movement. Similarly, the upper limit I_3^U of I_3 is defined the highest temperature that the material processing module can be heated to, while the lower limit I_3^L is defined as the melting point of the material. In this way, the optimisation can finally find a vector of decision variables that not only optimises the three consumptions but also satisfies the constraints or achievable ranges of all variables (Chiandussi et al., 2012; Osyczka and Kundu, 1995).

4.5. Methods used in hybrid prediction modelling

This section introduces the methods used in prediction modelling of AM's time, energy and material consumptions. Based on the module classification, the consumptions of each module are modelled as functions of the process parameters. The relationships between the consumptions and process parameters are derived through two ways: physics-based modelling and data-driven modelling. Physics-based modelling processes the data in G-code to calculate the time, distance of axis movement with actual displacements and amount of material feeding. Data-driven modelling obtains the remaining parameters through experiments. According to experiment data, regression analysis is applied to derive the relationships between these parameters and process parameters.

4.5.1. Calculation based on G-code in physics-based modelling

G-code provides detailed manufacturing information, including the coordinates of axis movement, amount of material feeding, and variations in axis movement speed and material feeding rate. Thus, the time consumptions of axis movement with actual displacements can be obtained from G-code through physics-based modelling. Since the axis movement in X, Y, Z directions is commonly used in the existing AM technologies, this study mainly focuses on the time modelling of axis movement in X, Y, Z directions. The modelling of multi-axis movement is similar to the above method, which is discussed in **Section 9.2.5** as future work.

G-code commands:
$P_0 \rightarrow P_1$: G1 F_{xy_1} $X_1 Y_1 E_1$
$P_1 \rightarrow P_2$: G1 F_{xy_2} $X_2 Y_2$
$Layer_1 \rightarrow Layer_2$: G1 F_z Z

$P_1 (X_1, Y_1)$
$P_2 (X_2, Y_2)$
$(0,0,0)$
$P_0 (X_0, Y_0)$

$Layer_2$
$Layer_1$
$Layer_0$
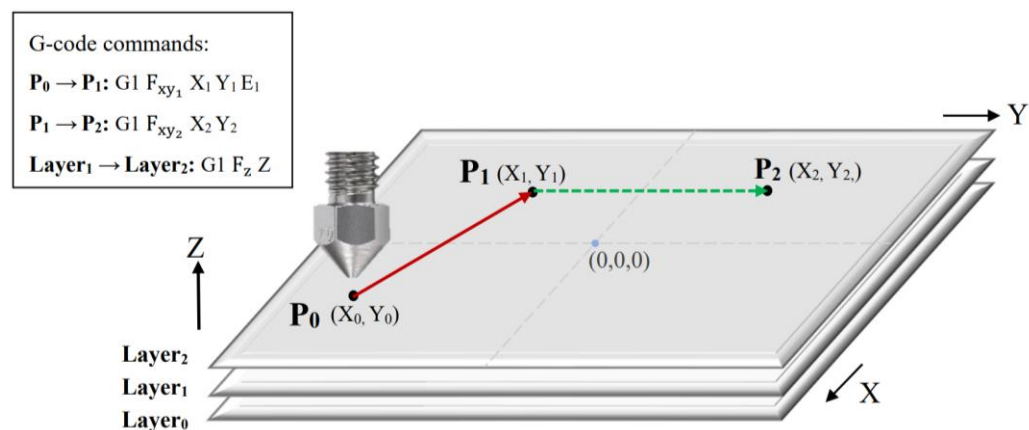
Figure 4.3: Example toolpaths in X, Y, Z directions based on G-code commands

Figure 4.3 presents an example schematic of axis movement with actual displacement in X, Y, Z directions. By following the G-code commands, the nozzle of the AM machine firstly moves from P_0 (X_0, Y_0) to P_1 (X_1, Y_1) with material feeding at a speed or rate of F_{xy_1}, and then moves to P_2 (X_2, Y_2) without material feeding at a speed of F_{xy_2}. The movement from Layer$_1$ to Layer$_2$ at a speed of F_z is for the layer construction in Z direction. The above three displacements represent the three typical movements in X, Y, Z directions in an AM process, for which the total consumption t_{xyz} can be calculated as the accumulation of the average time spent on each displacement. As expressed in **Equation (4.15)**, ΔX and ΔY respectively denote the components of each displacement in X, Y directions, and F_{xy} denotes the corresponding speed of axis movement or rate of material feeding. ΔZ denotes both the displacement in Z direction and the layer thickness, and F_z denotes its corresponding speed.

$$t_{xyz} = \sum \frac{\sqrt{\Delta X^2 + \Delta Y^2}}{F_{xy}} + \sum \frac{\Delta Z}{F_z} \tag{4.15}$$

In addition, motor out-of-step commonly occurs during high-speed printing in general AM technologies, which leads to the axis movement failing to reach the target speed. Thus, additional experiments are conducted to test the actual speeds $F_{xy_{act}}$ and $F_{z_{act}}$ of axis movement in X, Y, Z directions. By replacing the speeds F_{xy} and F_z provided by G-code with the actual speeds $F_{xy_{act}}$ and $F_{z_{act}}$, the time consumption t_{xyz} of axis movement with actual displacement is expressed as **Equation (4.16)**.

$$t_{xyz} = \sum \frac{\sqrt{\Delta X^2 + \Delta Y^2}}{F_{xy_{act}}} + \sum \frac{\Delta Z}{F_{z_{act}}} \tag{4.16}$$

4.5.2. Curve-fitting tool for regression analysis and R-square calculation in data-driven modelling

The consumptions of some modules cannot be calculated from G-code, as relationships with process parameters can only be derived from experiments. As mentioned in Section **3.3.2**, experiments should be conducted to test the apparent powers of all five modules under different related process parameters and the setup time or heating time of the material processing module and component heating module under different process parameters. Then, polynomial regression is applied to curve-fit the above functional relationships (i.e. to calculate the coefficient value in the functions) based on experimental results. Referring to Jenkins and Quintana-Ascencio (2020), the recommended sample size for regressions should be more than 25 data points. It indicates that each of the above indicators can be measured under 25 different related process parameters.

Based on experimental data, this study utilises Curve Fitting Toolbox™ in MATLAB to apply the least squares method and provide the polynomial functions for fitting curves (Kraaikamp and Meester, 2005; Curve Fitting Toolbox, 2020). According to guidance provided by Polynomial Curve Fitting (2020), the selection of degree for the polynomial functions is based on the confidence bound. In statistics, the confidence bound, also named confidence interval, is an estimate computed from the statistical calculation of the observed data. It provides a range of plausible values for the unknown coefficient of the regression model. Besides, the bound is associated with the confidence level (i.e. the confident or probability that the true parameter value is in the estimated bound) (Kraaikamp and Meester, 2005). A higher level of confidence results in a wider confidence bound. In general terms, the default value of confidence level in regression analysis is 0.95. It indicates that there is 95% probability that the true parameter is in the estimated confidence bound.

Referring to Kraaikamp and Meester (2005), the calculation of confidence bound is summarised as **Equation (4. 17)** to **Equation (4. 20)**. An example of quadratic polynomial is presented to illustrate the calculation process. Note that p_1 is an estimated coefficient of

the second order model term. The confidence bound of p_1 is expressed as **Equation (4. 18)**, wherein p_1^L and p_1^U denote the end points of the confidence bound, γ denotes the confidence level or the probability that the true parameter is in the estimated confidence bound. The values of two end points are calculated as **Equation (4. 19)** and **Equation (4. 20)**, wherein S_{p_1} denotes the standard error of coefficient p_1. c is a number from the standard normal distribution. As shown in **Figure 4.4**, the value of c is determined by the confidence level according to the Z-score table. For example, the value of c is 1.96 for a confidence level of 95%.

$$f(x) = p_1 x^2 + p_2 x + p_3 \qquad (4.\ 17)$$

$$\Pr(p_1^L < p_1 < p_1^U) = \gamma \qquad (4.\ 18)$$

$$p_1^L = p_1 - cS_{p_1} \qquad (4.\ 19)$$

$$p_1^U = p_1 + cS_{p_1} \qquad (4.\ 20)$$
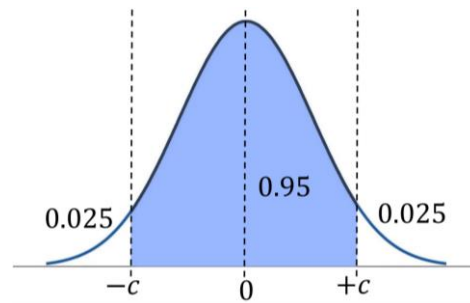
Figure 4.4: Standard normal distribution of constant c

The confidence bounds of the estimated coefficients determine the accuracy of regression model and also the selection of degree for the polynomial functions. **Figure 4.5** presents an example of how to select a suitable polynomial degree according to the confidence bound. By using the Curve Fitting Toolbox™ in MATLAB, a set of data points generates multiple options of polynomial functions. When the coefficient's bound in the highest order model term crosses zero, it cannot be sure whether this coefficient is different from zero. It indicates

that the census data is overfitted and the degree of polynomial curve is higher than needed for an accurate fit. Thus, the solution is to select as low a degree as possible for an accurate fit (Polynomial Curve Fitting, 2020). In the following case studies, the selection of polynomial degree during the curve-fitting of experiment data is based on this method.

$f(x) = p_1 x + p_2$

Coefficients (with 95% confidence bounds):

$p_1 = 0.2834$ $(0.2606, 0.3062)$

$p_2 = 10.29$ $(7.244, 13.33)$

$f(x) = p_1 x^2 + p_2 x + p_3$

Coefficients (with 95% confidence bounds):

$p_1 = -0.00005768$ $(-0.0007005, 0.0005852)$

$p_2 = 0.2973$ $(0.14, 0.4547)$

$p_3 = 9.597$ $(1.171, 18.02)$

Figure 4.5: Schematic of R-square calculation

To evaluate the performance of the curve-fitting results, this study uses R-square (R^2) as a statistical measure to evaluate the goodness of fit (Draper and Smith, 1998). As expressed in **Equation (4. 21)**, R^2 is calculated as the proportion of variance of a dependent variable, in which SS_{res} denotes the total sum of squares (TSS) and SS_{tot} denotes the residual sum of squares (RSS). The values of the TSS and RSS are calculated through **Equation (4. 22)** and **Equation (4. 23)**. $f(x)$ refers to a fitted regression model. The number of variables is defined as e. The observed value of the sth variable x_s is defined as y_s and its corresponding prediction value is defined as $f(x_s)$. $\bar{y}$ denotes the average of all observed values. In the following sections, all curve-fitting results are evaluated using R^2. When the value of R^2 is closer to 1, it indicates that the measured data is closer to the fitted regression line.

$$R^2 = 1 - \frac{SS_{res}}{SS_{tot}} \tag{4. 21}$$

$$SS_{res} = \sum_{s=1}^{e}(y_s - f(x_s))^2 \tag{4. 22}$$

$$SS_{tot} = \sum_{s=1}^{e}(y_s - \bar{y})^2 \tag{4. 23}$$

4.6. Methods used in multi-objective optimisation

In this study, time, energy and material consumptions are defined as the three objectives to be minimised in this multi-objective problem. A suitable optimisation technique should be selected based on the number of objectives to be optimised. Since non-dominated sorting genetic algorithm II (NSGA-II) is known to be an effective optimisation technique for solving a multi-objective problem with two or three objectives, it has been chosen to search for the optimal solution set of process parameters to minimise the above consumptions. This section introduces the methods used to solve the optimisation problem in this study, including the basic workflow of NSGA-II algorithm, the design of experiments for performing NSGA-II optimisation test, and hypervolume (HV) indicator used to evaluate the performance of NSGA-II algorithm.

4.6.1. Non-dominated sorting genetic algorithm II

Non-dominated sorting genetic algorithm II (NSGA-II) is one of the most popular multi-objective optimisation techniques used to optimise machining parameters under three conflicting machining operation objectives. Compared with other multi-objective optimisation techniques, such as the strength Pareto evolutionary algorithm, multi-objective genetic algorithm (MOGA) and Pareto-archived evolution strategy, NSGA-II is advanced with two innovative characteristics: fast non-dominated sorting and fast crowding distance ranking (Deb et al., 2002; Yusoff et al., 2011). It also enables a faster computation with $O(MN^2)$ complexity, in which M denotes the number of objectives and N denotes the population size (Curry and Dagli, 2014). According to (Deb et al., 2002), the NSGA-II algorithm can be classified into eight steps: population initialisation, non-dominated sorting, crowding distance ranking, elitism, selection, mutation, crossover and recombination. The basic flow of NSGA-II applied in general optimisation problems is presented in **Figure 4.6** and summarised as follows.
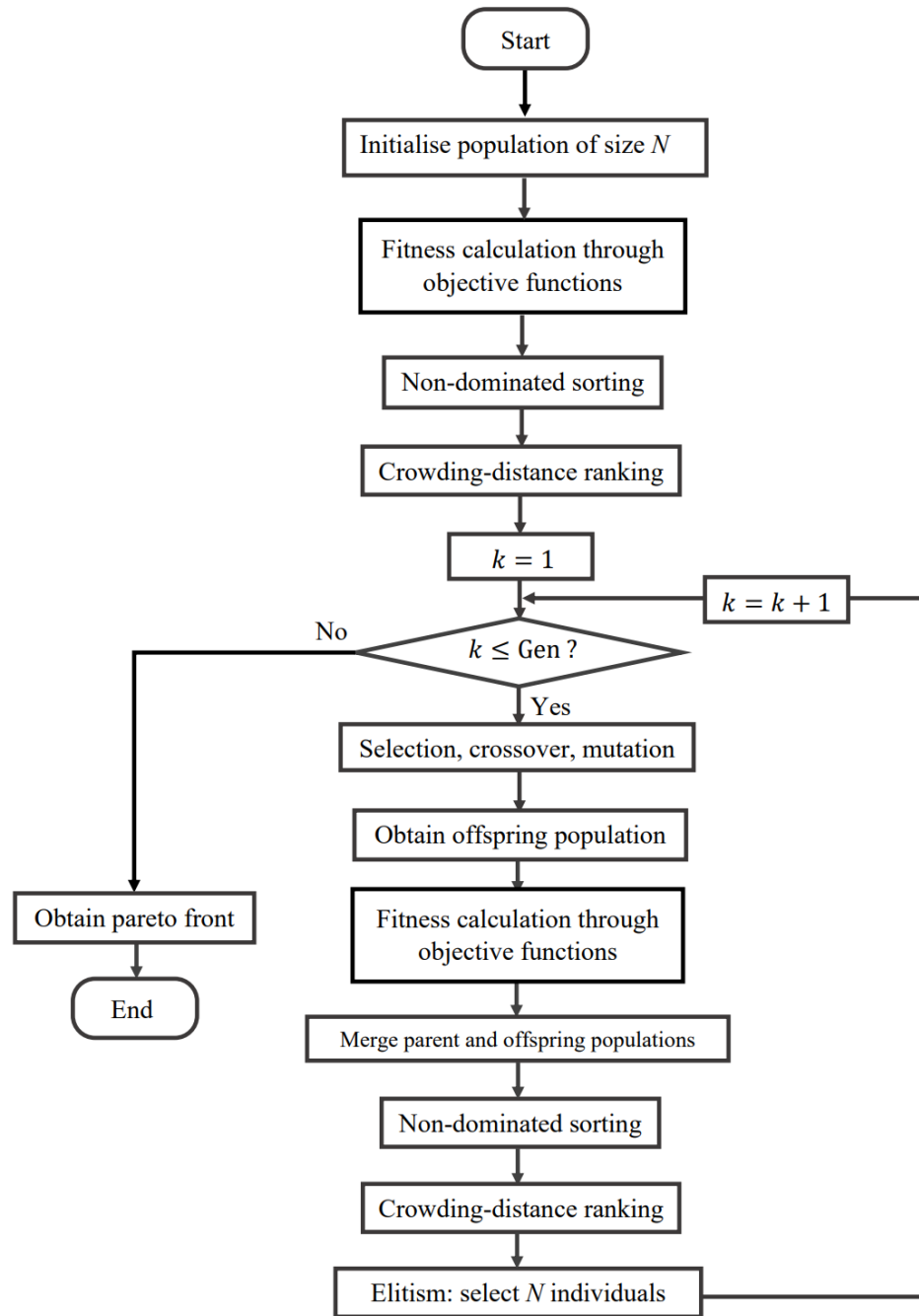
Figure 4.6: Flowchart of NSGA-II algorithm (Lin et al., 2019)

As shown in **Figure 4.6**, a random set of individuals or solutions is generated to form the initialised population of size N. The fitness of each individual is evaluated through objective functions. Based on the fitness values, all individuals are sorted and the one that that is superior to other individuals (i.e., the one is not dominated by any other individual) is ranked as the lowest level. The remaining individuals are also ranked one by one. by following the principle of non-dominated sorting. For the ranking of individuals with the same sorted level, their crowding distances are calculated. The individuals with larger crowding distances are

ranked as the lower levels, since a large crowding distance results in a better diversity in the population (Khan and Baig, 2015). Then, the parents are selected from the current population. The criterion of this selection process is also based on the rank and crowding distance of each individual (Deb et al., 2002). An individual is selected as a parent when its rank is lower than the other. However, if the ranks of both individuals are same, the one with a larger crowding distance will be selected as the parent (Khan and Baig, 2015). After the selection, the parents are used to generate offspring through the crossover operator and mutation operator. The above parent generation and offspring generation form the new generation, which begins to be imported into the iteration of optimisation.

Note that the process of iteration is different after the initial generation. First, the individuals in the combined population of size *2N* are sorted through non-dominated sorting and crowd distance ranking. Then, the elite *N* individuals are remained based on their non-dominated levels. For the individuals belonging to the same non-dominated set, the individuals with higher crowding distances are retained, while the rest are eliminated. After that, the parents are selected from the elite population of size *N*. The selected parents are used to generate offspring through the crossover operator and mutation operator. The above parent generation and offspring generation form the next generation, which continues to be imported into the next iteration of non-dominated sorting, crowd distance ranking, elitism, selection, crossover and mutation. The iteration stops when the number of generations Gen is reached (i.e. $k = Gen$). A Pareto front containing the optimum solution is finally obtained.

This section only introduces the basic workflow of original NSGA-II algorithm. Details of adjusting and applying the algorithm to solve the optimisation problem in this study will be discussed in **Chapter 6**.

4.6.2. Taguchi design of experiments for NSGA-II optimisation

Experiments are designed to implement the non-dominated sorting genetic algorithm II (NSGA-II) algorithm at different settings of the optimisation parameters. The aim is to

evaluate the influence of optimisation parameters on the optimisation results, and compare the pareto fronts obtained from optimisation tests under different optimisation parameters. The optimisation parameters are also called the optimisation factors, including the population size N, number of generations Gen, crossover probability pc and mutation probability pm. The population size N refers to the number of individuals that always tends to a stable value during the optimisation process. The number of generations Gen refers to the maximum generation that optimisation finally reaches. The crossover probability pc refers to the probability that an individual in parent population produces offspring through the crossover operator. The mutation probability pm refers to the probability that an individual in parent population produces offspring through the mutation operator.

There are various methods for the design of experiments in the area of industrial manufacturing, such as full factorial design, fractional factorial design, optimal design, mixture design, Taguchi robust design, screening design and response surface design (Carlson, 2001; Gunst and Mason, 2009). Taguchi robust design and full factorial design have been widely used in experiments related to genetic algorithm (GA) optimisation. Note that the computational time increases with the increasing of population size N and number of generation Gen. In the case of large values of those two parameters (e.g., $N = 40, Gen = 200$), the computational time of a general personal computer (i.e., Dell Optiplex 7040) can be as long as 42 days in this study. Thus, due to the limitation of computing resources, a full factorial design for all possible combinations far exceeds our computational capability. For example, if each factor has three levels, there will be 81 tests of optimisations to be performed. Therefore, considering the scale of the experiments, Taguchi robust design – also called orthogonal design – is an efficient method to estimate the main effects and interactions of the representative test points in this study. Compared with full factorial design, an orthogonal design can greatly reduce the number of experiments through the rational and scientific application of orthogonal tables (Hao and Wang, 2014).

An orthogonal table is designed by following two principles (Lee et al., 2013): 1) the number of each level in a single factor is equal, which means that each level has the same probability of participating in the experiments and excludes the interference from other

levels; and 2) any possible pair of levels across two arbitrary factors has the same number of occurrences. This is to ensure that the test points are evenly distributed in terms of the complete combination of attributes and levels.

There are many existing orthogonal tables available in Taguchi robust design. Considering the computational capabilities of our computing resources, the $L_{16}(4^4)$ orthogonal table is applied to design experiments of NSGA-II optimisation. It indicates that there are four factors being considered, and each factor is defined to have four levels. As shown in **Table 4.2**, the four factors respectively refer to the four optimisation parameters, including population size N, number of generations *Gen*, crossover probability *pc* and mutation probability *pm.* The values of four levels of each factor are determined by the computational capabilities of existing computing resources, and are also within the range of values commonly used in NSGA-II optimisation.

Table 4.2: Levels of NSGA-II optimisation parameters

	Factor	Symbol	Levels			
1	Population size	N	$N1$	$N2$	$N3$	$N4$
2	Number of generations	*Gen*	*Gen*1	*Gen*2	*Gen*3	*Gen*4
3	Crossover probability	*pc*	*pc*1	*pc*2	*pc*3	*pc*4
4	Mutation probability	*pm*	*pm*1	*pm*2	*pm*3	*pm*4

According to the level numbers and factor numbers, the $L_{16}(4^4)$ orthogonal table is designed by following the above two principles. As shown in **Table 4.3**, 16 optimisation tests should be performed under different combinations of optimisation parameters. The levels of each parameter are evenly distributed in the table. Each level has four times to participate in the optimisation test. The output of each test is defined as the response of the corresponding parameter combination.

Table 4.3: Orthogonal table for the experiments of NSGA-II optimisation

Test No.	Factor levels			
	Population size	Number of generations	Probability of crossover	Probability of mutation
	N	*Gen*	*pc*	*pm*
1	*N*1	*Gen*1	*pc*1	*pm*1
2	*N*1	*Gen*2	*pc*2	*pm*2
3	*N*1	*Gen*3	*pc*3	*pm*3
4	*N*1	*Gen*4	*pc*4	*pm*4
5	*N*2	*Gen*1	*pc*2	*pm*3
6	*N*2	*Gen*2	*pc*1	*pm*4
7	*N*2	*Gen*3	*pc*4	*pm*1
8	*N*2	*Gen*4	*pc*3	*pm*2
9	*N*3	*Gen*1	*pc*3	*pm*4
10	*N*3	*Gen*2	*pc*4	*pm*3
11	*N*3	*Gen*3	*pc*1	*pm*2
12	*N*3	*Gen*4	*pc*2	*pm*1
13	*N*4	*Gen*1	*pc*4	*pm*2
14	*N*4	*Gen*2	*pc*3	*pm*1
15	*N*4	*Gen*3	*pc*2	*pm*4
16	*N*4	*Gen*4	*pc*1	*pm*3

Each optimisation test will produce one Pareto front. To evaluate and compare the performances of all obtained Pareto fronts, the hypervolume (HV) indicator $I_H(A)$ is applied to quantify the qualities of all fronts. In this study, the response of each optimisation test is defined as its corresponding HV indicator. The calculation method of HV indicator is discussed in the following section.

4.6.3. Performance measures of near-optimal approximate Pareto fronts by using hypervolume indicator

There are two criteria for evaluating the near-optimal approximate pareto front: the convergence of non-dominated solutions to the Pareto-optimal set, and the diversity or the spreading extent of non-dominated solutions (Deb et al., 2002). To compare the pareto fronts

obtained from optimisation tests, the above two criteria of non-dominated sorting genetic algorithm II (NSGA-II) can be quantified by using the hypervolume (HV) indicator. This section introduces the method of calculating HV indicator to evaluate and compare the solutions of obtained pareto fronts.

The HV indicator is a set measure to evaluate the quality of a solution set by transforming the multi-objective problem into a single-objective problem. In more detail, it is used to calculate the maximum volume of objective subspace dominated by the overall optimisation set of solutions under consideration (Zitzler and Thiele, 1998; Zitzler et al., 2007). **Figure 4.7** presents an example of the HV calculation in a two-objective optimisation problem. A reference point R is needed to calculate the area or volume of the region in the target space enclosed by the reference point and the non-dominated solutions.

The position of the reference point is necessary as it determines the HV result and the optimal solution set from different searches. Regarding this issue, Ishibuchi et al. (2017) discussed the specification of the reference point for a fair comparison. Firstly, the objective space is normalised by defining the ideal point and the nadir point as (0, 0) and (1, 1), respectively (Deb et al., 2009). Secondly, to ensure that all solutions are uniformly distributed inside the area of HV and have similar contributions, the coordinates (r_R, r_R) of the reference point R should be defined as in **Equation (4. 24)**. n_{ns} denotes the total number of non-dominated solutions obtained from all searches (Ishibuchi et al., 2017).

$$r_R = 1 + \frac{1}{n_{ns}-1} \tag{4. 24}$$

In this study, the specification of the reference point in the three-objective problem is similar to the two-objective problem. **Figure 4.8** presents an example of non-dominated solutions in a three-dimensional coordinate, in which three normalised objectives $\mathcal{F}_1'$, $\mathcal{F}_2'$ and $\mathcal{F}_3'$ respectively denote the time, energy and material consumptions in the AM process. The objective space is normalised by defining the ideal point and the nadir point as (0, 0, 0) and (1, 1, 1), respectively. The coordinates of the reference point should be (r_R, r_R, r_R). For

example, there are five non-dominated solutions obtained from a search of NSGA-II optimisation. The reference set $R \subset R^3$ should be defined as (1.25, 1.25, 1.25), according to **Equation (4. 24)**.
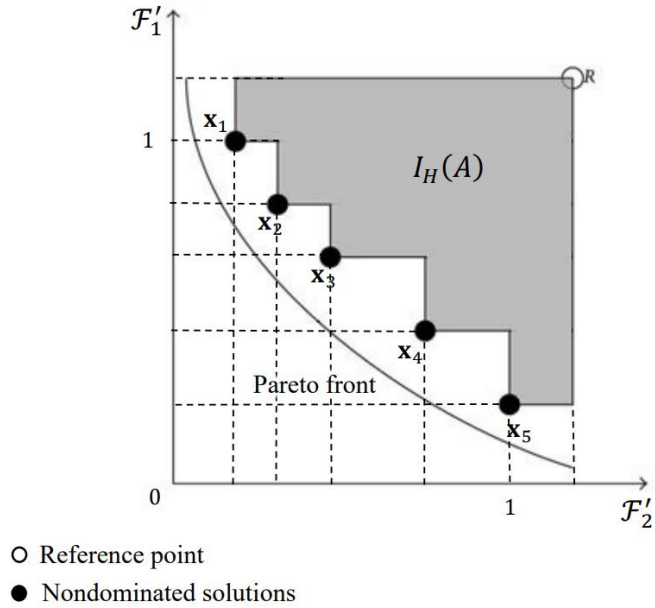
Figure 4.7: Example of HV indicator in two-objective optimisation problem
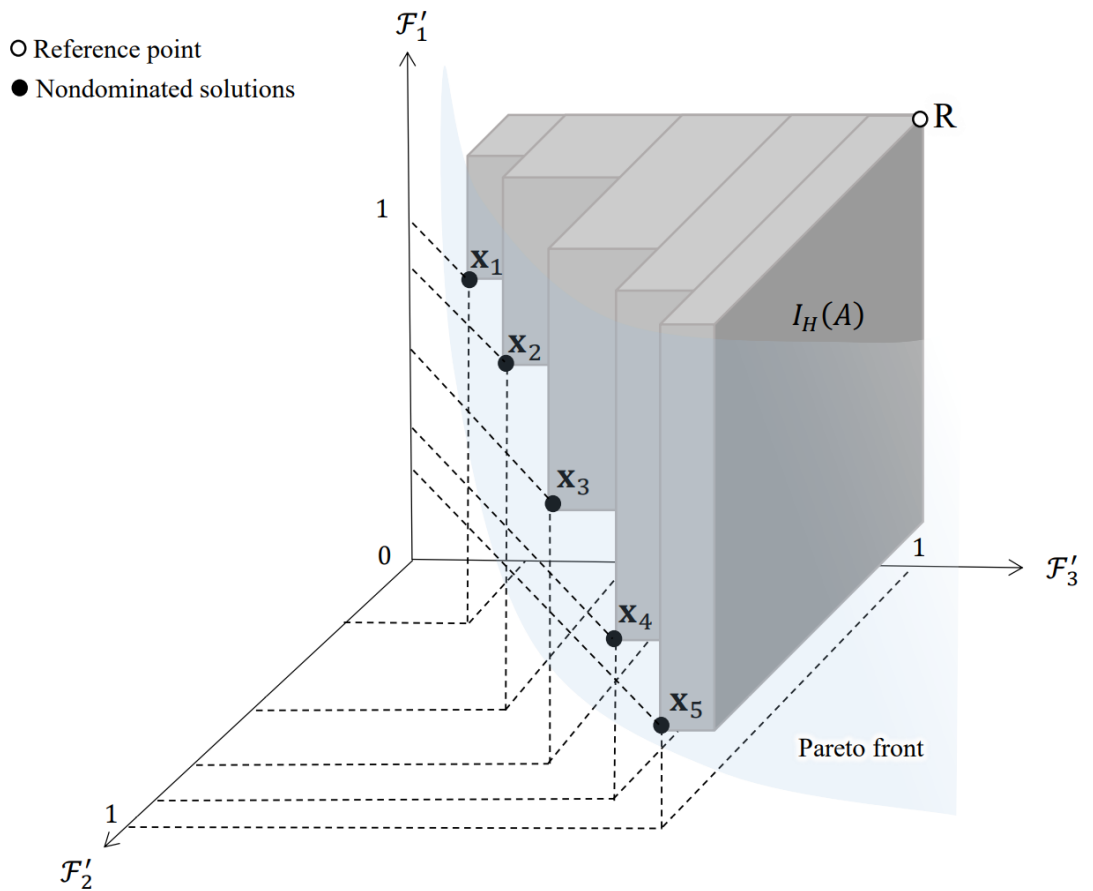
Figure 4.8: Example of HV indicator in three-objective optimisation problem

After the objective normalisation and selection of the reference point, the HV indicator $I_H(A)$ can be calculated by the union of HV of all non-dominated solutions $\mathbf{x} \in A$ (Brockhoff et al., 2008), as expressed in **Equation (4. 25)**. Note that λ denotes the Lebesgue measure of the solution set A, while $\mathcal{F}'_1(\mathbf{x})$, $\mathcal{F}'_2(\mathbf{x})$, $\mathcal{F}'_3(\mathbf{x})$ indicate three normalised consumptions of each solution $\mathbf{x}$. The coordinates of the reference point R are defined as (r_R, r_R, r_R) in three dimensions and the coordinate value is determined by the total number of non-dominated solutions. $[\mathcal{F}'_1(\mathbf{x}), r_R] \times [\mathcal{F}'_2(\mathbf{x}), r_R] \times [\mathcal{F}'_3(\mathbf{x}), r_R]$ refers to the three-dimensional hypercubic of the domain dominated by solution $\mathbf{x}$. This hypercubic is also bounded by the reference point R.

$$I_H(A) = \lambda(\cup_{\mathbf{x}\in A}[\mathcal{F}'_1(\mathbf{x}), r_R] \times [\mathcal{F}'_2(\mathbf{x}), r_R] \times [\mathcal{F}'_3(\mathbf{x}), r_R]) \qquad (4.\,25)$$

Note that the three objectives are treated with the same weights in this study. Thus, the HV indicator in **Equation (4. 25)** can be directly used in this optimisation problem. For the optimisation of three objectives with different weights, the weighted HV indicator $I_H^w(A)$ evolved from HV indicator $I_H(A)$ can be used, as expressed in **Equation (4. 26)** and **Equation (4. 27)**. $\lambda_w(H(A, R))$ denotes the weighted Lebesgue measure bounded by the solution set A and the reference point R. The weight function $w(z)$ is used to configure the importance of each solution point $z \in H(A, R)$ in this area (Brockhoff et al., 2013).

$$I_H^w(A) = \lambda_w\big(H(A, R)\big) = \int_{z\in H(A,\ R)} w(z)dz \qquad (4.\,26)$$

$$H(A, R) = \cup_{\mathbf{x}\in A}[\mathcal{F}'_1(\mathbf{x}), r_R] \times [\mathcal{F}'_2(\mathbf{x}), r_R] \times [\mathcal{F}'_3(\mathbf{x}), r_R] \qquad (4.\,27)$$

Based on the above, a higher value of HV indicator means that the solution of process parameters has a higher convergence and dispersion; that is, there is a better performance of the solution (Zitzler et al., 2007; Auger et al., 2009). Finally, the optimum solutions are used as guidance for manufacturers to select the feasible process parameters in prefabrication stage.

4.7. Methods used in experimental validation

This section introduces the methods used to analyse the prediction results and optimisation results of practical AM processes. The aim is to validate the hypothesis proposed at the beginning of this chapter, i.e., the proposed method can realise an effective prediction and optimisation of AM resource consumptions. For the analysis of prediction results, the mean absolute percent error (MAPE) is used as a statistical measure to evaluate the prediction accuracy of predictive models for an AM machine. For the analysis of optimisation results, the methods of range analysis and ANOVA are used to compare and quantify the significance of optimisation parameters on the HV indicator. Details of each analysis method are described in the following sub-sections.

4.7.1. Calculation of prediction accuracy

Mean absolute percent error (MAPE) is an effective statistical measure commonly used to calculate the prediction accuracy of a forecasting method. It is calculated as the average of the absolute percent errors in all experimental tests, as expressed in **Equation (4. 28)**. n_{test} denotes the number of experimental tests. ER_i and PR_i respectively denote the actual value and the forecast value of the ith test (De Myttenaere et al., 2016).

$$\text{MAPE} = \frac{1}{n_{test}} \sum_{i=1}^{n_{test}} \left| \frac{ER_i - PR_i}{ER_i} \right| \tag{4. 28}$$

This study uses MAPE to calculates the prediction accuracy of predictive models for an AM machine. n_{test} denotes the number of experimental tests on the AM machine. ER_i and PR_i respectively denote the actual consumption and the predicted consumption of the ith test. $\frac{ER_i - PR_i}{ER_i}$ denotes the prediction accuracy of consumption of the ith test. When $\frac{ER_i - PR_i}{ER_i} < 0$, the predicted consumption is higher than the actual consumption. When $\frac{ER_i - PR_i}{ER_i} = 0$, the predicted consumption is consistent with the actual consumption. When $\frac{ER_i - PR_i}{ER_i} > 0$, the predicted consumption is lower than the actual consumption.

4.7.2. Range analysis method

Range analysis is an effective and intuitive result analysis method for Taguchi experiments. In static designs, the method calculates a separate mean for each factor level in order to compare the significant contributions of factors for the related response. Meanwhile, the most dominant factor and the optimal levels can be intuitively displayed from the main effect plots (Li et al., 2016).

Table 4.4 gives a typical response table to illustrate the range analysis method. R denotes the response of each experimental test. In this study, the response R represents the hypervolume (HV) indicator obtained from each optimisation test. At first, the mean response of each level for each factor is calculated from experimental results. Then, the difference (i.e. Delta) between the highest and lowest mean responses (i.e. $\overline{\sum R}_{max}$ and $\overline{\sum R}_{min}$) for each factor is calculated. Finally, the main effects of all factors can be plotted and ranked from high to low based on the Delta values.

Table 4.4: Response table for evaluating the main effects of factors for the related response

Levels	Calculation methods	Factors			
		Factor 01	Factor 02	Factor 03	...
1	$\overline{\sum R^1}$				
2	$\overline{\sum R^2}$				
3	$\overline{\sum R^3}$				
...	...				
Delta	$\overline{\sum R}_{max} - \overline{\sum R}_{min}$				
Rank					

4.7.3. Analysis of variance method

Based on the results from range analysis, the analysis of variance (ANOVA) method is applied to further identify the contribution and significance of a factor for the response (Barzegari and Rodrigue, 2009). It is a widely used statistical technique for the interpretation of experimental works.

Table 4.5: ANOVA table for evaluating the significances of factors for the related response

Factors	Degree of freedom	Sums of squares	Mean squares	F-Value	P-Value
	DF	SS_p	MS_p		
Factor 01					
Factor 02					
Factor 03					
...					
Error		SS_e	MS_e		
Total		SS_t			

Table 4.5 gives an example ANOVA table, which includes all the indicators used to quantify the significances of all factors. The indicators include total sum of squares SS_t, sum of squares SS_p, mean squares MS_p, degree of freedom DF, residual sum of the squares SS_e, residual mean squares MS_e, F-value and P-value. The calculation of each indicator is summarised as follows.

The total sum of squares SS_t quantifies the total variation of all observed responses from the mean response. As expressed in **Equation (4. 29)**, SS_t is calculated as the sum of all squared differences between the observed responses and the total mean response of all tests. n_{test} denotes the number of experimental tests and R denotes the response of each test.

$$SS_t = \sum R^2 - \frac{(\sum R)^2}{n_{test}} \qquad (4. 29)$$

The sum of squares SS_p refers to the variation or deviation of the pth factor from the mean response, as shown in **Equation (4. 30)**. n_{level} denotes the number of levels of each

factor. $\overline{\sum R_p^i}$ denotes the mean response of the ith level of the pth factor. $\bar{R}$ denotes the mean response of all tests. In this study, each factor is defined to have four levels (i.e. $n_{level} = 4$).

$$SS_p = n_{level} \sum_{i=1}^{n_{level}} (\overline{\sum R_p^i} - \bar{R})^2 \qquad (4.30)$$

The mean squares MS_p of the pth factor is obtained by dividing the sum of squares SS_p by the degrees of freedom DF. It represents the influence of this factor on the variations of response. As expressed in **Equation (4. 31)** and **Equation (4. 32)**, the degrees of freedom DF_p is calculated as the number of levels for the factor minus one.

$$DF_p = n_{level} - 1 \qquad (4.31)$$

$$MS_p = \frac{SS_p}{DF_p} \qquad (4.32)$$

Since the ANOVA is used to examine the polynomial relationship between the factors and response, the amount of error between the data points and the regression model can be quantified through the residual sum of the squares SS_e. It is a measure of the response deviations that the regression model is unable to explain. Referring to Gandhi et al. (2011), SS_e is calculated as the difference between the total sum of squares SS_t and the sum of squares SS_p of all factors, as expressed in **Equation (4. 33)**. A small SS_e indicates a good fit of the data points to the regression model. Furthermore, the residual mean squares MS_e is obtained by dividing the residual sum of the squares SS_e by its corresponding degrees of freedom DF_e, as shown in **Equation (4. 34)**. DF_e is calculated as the difference between the total degrees of freedom DF_t and the degrees of freedom DF_p of all factors, as expressed in **Equation (4. 35)**.

$$SS_e = SS_t - \sum SS_p \qquad (4.33)$$

$$MS_e = \frac{SS_e}{DF_e} \qquad (4.34)$$

$$DF_e = DF_t - \sum DF_p \qquad (4.35)$$

Based on the above, the significance of each factor can be quantified by using the F-value and P-value. The F-value is a test statistic to determine whether the factor is associated with the response. It is calculated as the ratio of the mean squares MS_p and the residual mean square MS_e, as expressed in **Equation (4. 36)**. A large F-value indicates that the factor is significant for the response.

$$F - \text{value} = \frac{MS_p}{MS_e} \tag{4. 36}$$

The F-value is used to calculate the P-value, which aims to finally quantify the statistical significance of a factor. Referring to Bower (2007), the P-value is a measure that indicates the probability of the evidence against the null hypothesis (i.e. the factor is not significant for the response). The probability (i.e. P-value) is based on an F-distribution that assumes the null hypothesis is true. According to F-Distribution Tables (2020), a significance level is firstly defined to determine whether this null hypothesis holds. Usually, the significant level is specified as 0.05. It indicates that the risk of this null hypothesis is 5% and the analysis is carried out 95% level of confidence (Pattanaika et al., 2018).

Based on the F-Distribution table with a significance level of 0.05, the corresponding critical value 9.2766 is obtained for the F-distribution with 3 degree of freedom in the numerator (i.e. mean squares MS_p) and 3 degrees of freedom in the denominator (i.e. residual mean square MS_e). According to the F-distribution in **Figure 4.9**, the factor with an F-value higher than the critical value, or a P-value less than the significant level indicates a strong evidence against the null hypothesis. It also indicates that the factor has a significant contribution on the response.
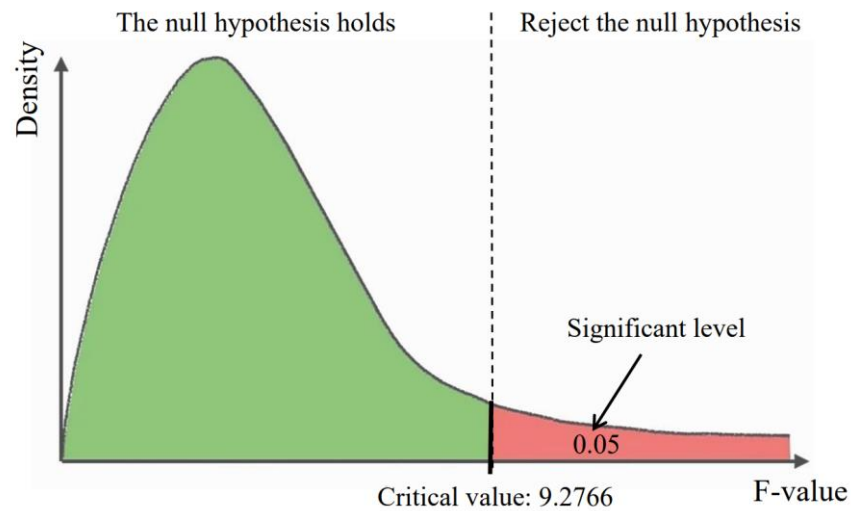
Figure 4.9: F-distribution with 3 degrees of freedom in the numerator and 3 degrees of freedom in the denominator

In this study, experiments are designed to test the NSGA-II optimisation process under different optimisation parameters. Since different combinations of optimisation parameters produce different Pareto fronts, it is necessary to figure out which optimisation parameter has a significant contribution on the hypervolume (HV) indicator of Pareto front. Therefore, the range analysis and ANOVA are applied to case studies to evaluate, rank and quantify the significance of each optimisation parameter.

4.8. Summary

In this chapter, the hypothesis of this research work is firstly identified. Then, the conceptual predictive models of AM's time, energy and material consumptions are defined based on the classified modules. The methods applied to the hybrid prediction modelling are introduced, including the G-code calculation in physics-based modelling and the regression analysis in data-driven modelling. In addition, the basic workflow of NSGA-II algorithm used in multi-objective optimisation is introduced. Taguchi design of experiments is applied to perform NSGA-II optimisation tests under different combinations of optimisation parameters. To evaluate the pareto fronts obtained from optimisation tests, the method of performance measures using hypervolume (HV) indicator is introduced. At last, the methods used in

experimental validation are introduced, including the calculation of mean absolute percent error (MAPE), range analysis and analysis of variance (ANOVA).

Since this chapter only introduces the methods used to implement the proposed research work, the consumption modelling on each module will be described in detail in the next chapter. Chapter 6 will introduce the detailed description and application of NSGA-II algorithm.

CHAPTER 5   PREDICTIVE MODELS OF TIME, ENERGY AND MATERIAL CONSUMPTIONS FOR ADDITIVE MANUFACTURING TECHNOLOGIES

5.1. Introduction

The goal in this chapter is to present the detailed modelling procedures of time, energy and material consumptions in the AM process. Based on the proposed framework in last chapter, all consumption-related components are classified into five types of modules, namely axis movement, material processing, component heating, material feeding and auxiliary components. Details of the prediction modelling of each module are described in this chapter.

To begin, different working states of each module are defined based on the power profiles. The axis movement module has two working states: the axis movement state with actual displacements and the standby state waiting for completion of other modules' operations. The material processing module and component heating module both have two working states: the initial heating state for heating the module to the target temperature and the heat preservation state for maintaining the module at the target temperature. The material feeding module has two working states: the material feeding state with an actual feeding amount and the standby state waiting for the next feeding operation. The auxiliary components module has one working state: the continuous monitoring and control of the machine status.

Next, the predictive models of time, energy and material consumptions of each working state are built as the functions of process parameters. In physics-based modelling, three parameters are calculated directly from G-code: the time, distance of axis movement with actual displacements and the amount of material feeding. For other parameters, data-driven

modelling is performed on each working state of the five modules. Experiments are conducted to measure the time consumption and apparent power of each state under different process parameters. The functional relationships between the measured results and process parameters are derived through polynomial regression method. In addition, factors affecting the prediction accuracy, such as the occurrence of motor out-of-step, and the deviation between actual material density and quoted material density, are also considered in this study. Thus, additional experiments are conducted, such as measurement of the actual axis movement speed, the actual material feeding rate and the actual material density. The experimental contents are determined by the characteristics of machine and material.

To clearly understand the structures of predictive models, all parameters constituting the models are classified into three types: 1). parameters to be calculated from G-code; 2). parameters to be obtained from experiments; 3). parameters whose values are determined by the running sequences and resource consumptions of the five modules through the Gannt chart. In this chapter, different AM technologies are used as examples to illustrate the modelling process.

The hybrid modelling method is one of the contributions of this research work. Firstly, the module classification divides all consumption-related components of general AM technologies into five types, each with different working states according to its function. This method of modularising different AM systems provides a clear, customisable and general modelling environment for the subsequent consumption modelling of each module. Secondly, physics-based modelling based on G-code makes a sufficient use of manufacturing information in G-code, which enables an effective prediction and also reduces the workload of data-driven modelling through experiments. Finally, the additional experiments fully consider the characteristics of each machine and material. According to the experimental validations, this step has been shown to produce a significant improvement in prediction accuracy. Details of the modelling process are described in the following sections.

5.2. Definitions of different working states for each module
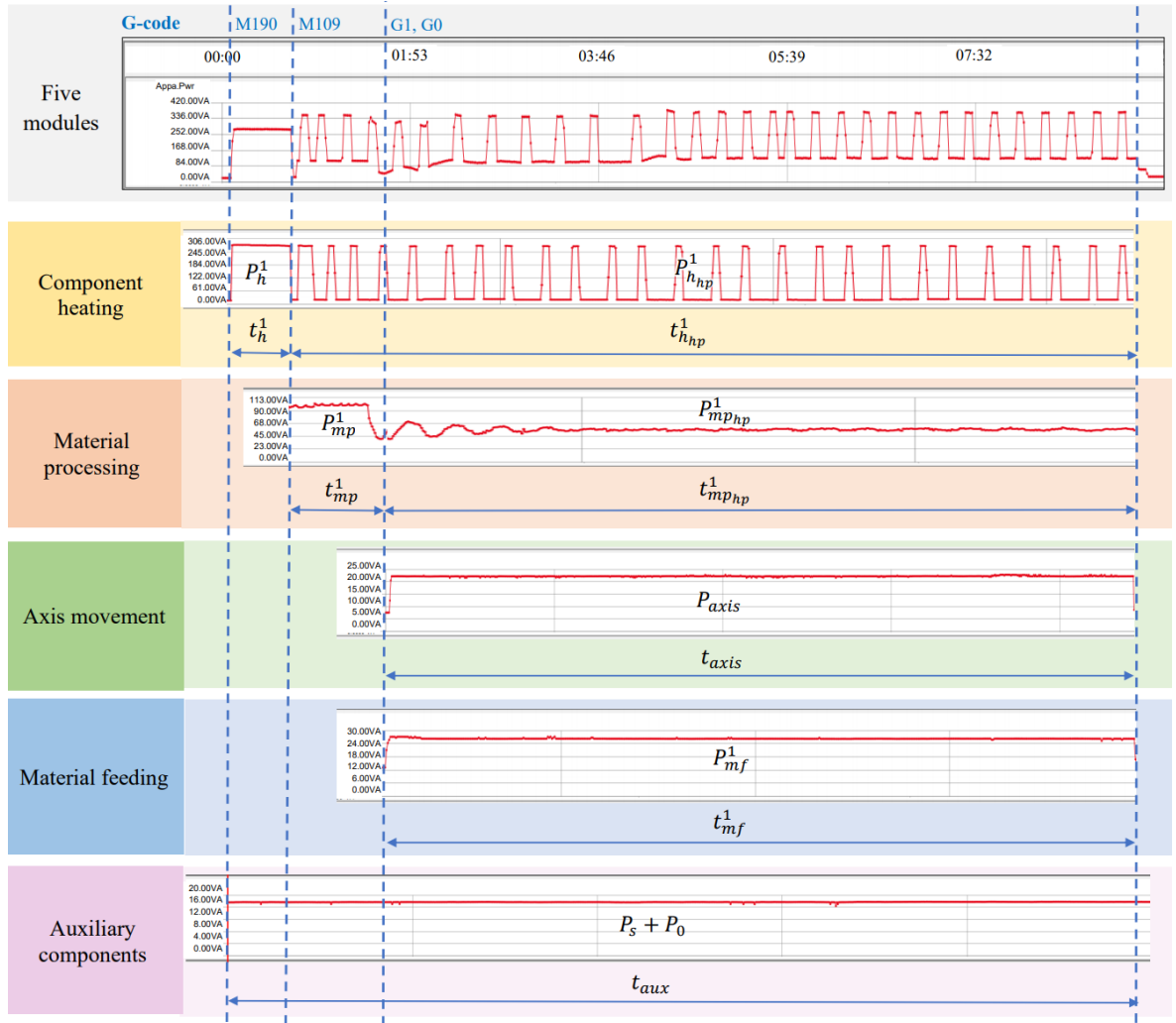
Figure 5.1: Example of running time and apparent powers of five types of modules in a general AM process

Referring to the module classification in **Section 3.2**, all consumption-related components are classified into five types: axis movement, material processing, material feeding, component heating and auxiliary components. This section defines the different working states of each module. **Figure 5.1** presents a representative example of power profiles for a general AM machine. In this example, there are five modules and each one represents a component. Three regular patterns can be concluded from this figure. Firstly, all modules that need to be heated contain two stages: the initial heating state for heating the module to the target temperature and the heat preservation state for maintaining the module at the target temperature until the end of the AM task. Secondly, the auxiliary components module only

has one working state; that is, the continuous monitoring and control of the machine status throughout the entire AM process. Thirdly, once the two modules of axis movement and material feeding start to run according to the G-code instructions, they will continue in a running status in the subsequent process until the end of the AM task, regardless of whether other modules are running during the middle of this process. Based on the above, the working states of each module are defined as follows.

The axis movement module has two working states: the axis movement state with actual displacements and the standby state waiting for completion of other modules' operations. The time spent on the former state can be directly calculated from G-code, since G-code provides the detailed coordinates and speeds to instruct the motions of axis movement module. The time spent on the latter state is defined as the 'interval time'. During this interval time, the motion of axis movement module is interrupted to wait for completion of other modules' operations. In general, as shown in **Figure 5.1**, the apparent powers of these two states are the same, which are both defined as P_{axis}. The total time consumption of the axis movement module is defined as t_{axis}. This is the sum of the time consumption t_{xyz} of axis movement with actual displacements and the interval time t_{xyz}^0. In this study, t_{xyz} can be calculated from G-code, while t_{xyz}^0 is determined by the running sequences and time consumptions of the other four modules.

The material feeding module also has two working states: the material feeding state with an actual feeding amount and the standby state waiting for the next feeding operation. According to **Figure 5.1**, the apparent powers of these two states are the same, which are both defined as P_{mf}^1. The total time consumption of the axis movement module is defined as t_{mf}^1. For general AM technologies, t_{mf}^1 is equal to the total time consumption t_{xyz} of the axis movement module, since these two modules run simultaneously to deposit material on the toolpaths.

The material processing module and component heating module both need to be heated for general AM machines. The heating of the material processing module is to turn the material from solid to liquid. The heating of the component heating module is to warm up the components, such as the build platform and heated roller, to support the manufacturing process, as discussed in **Section 3.2**. Thus, these two modules both have two working states: the initial heating state for heating the module to the target temperature and the heat preservation state for maintaining the module at the target temperature. According to **Figure 5.1**, the apparent power and time consumptions of the initial heating state for the material processing module are defined as P_{mp}^1 and t_{mp}^1, while the apparent power and time consumptions of the initial heating state for the component heating module are defined as P_h^1 and t_h^1. The apparent power and time consumptions of the heat preservation state for the material processing module are defined as $P_{mp_{hp}}^1$ and $t_{mp_{hp}}^1$, while the apparent power and time consumptions of the heat preservation state for the component heating module are defined as $P_{h_{hp}}^1$ and $t_{h_{hp}}^1$.

The auxiliary components can be classified into two types. The first type is the components that monitor and control the machine status during the printing process, such as the display unit, temperature sensor, and user interface and connectivity. These components keep running even when the machine is in standby mode. The apparent power of this standby mode is defined as standby power P_s. The second type is the components that are used to support the printing process, such as the cooling system. When an AM task starts, the second type of components start to run and the power increases from standby power P_s to a higher level to start up the machine. This increased power difference is defined as start-up power P_0. Thus, as shown in **Figure 5.1**, the total power of the auxiliary components is calculated as the sum of standby power P_s and start-up power P_0. Based on the above, the entire module of auxiliary components has only one working state: the continuous monitoring and control of the machine status. Thus, the time consumption t_{aux} of the auxiliary components module is equal to the total time consumption t_{total} of the entire AM task. Since t_{aux} and t_{total} are unknown, their values are determined by the running sequences and time consumptions of the other four modules.

5.3. Predictive model of time consumption

This section presents the predictive model of time consumption in the AM process. Based on the definitions of different working states for each module, the time consumptions of all working states of the five modules in the existing AM technologies are summarised in **Table 5.1**.

Table 5.1: Time consumptions of different working states for each module of the existing AM technologies

Modules	Working states	Time consumptions	AM technologies	
Axis movement	Axis movement with actual displacements	t_{xyz}	Material extrusion (ME); Binder jetting (BJ) Material jetting (MJ); Direct energy deposition (DED) Powder bed fusion (PBF); Sheet lamination Polymerisation	
	Standby	t_{xyz}^0		
Material processing	Initial heating	t_{mp}^a		
	Heat preservation	$t_{mp_{hp}}^a$		
Auxiliary components	Monitoring and control of machine status	t_{aux}		
Component heating	Initial heating	t_h^b	Material extrusion (ME) Material jetting (MJ) Sheet lamination	
	Heat preservation	$t_{h_{hp}}^b$		
Material feeding	Material feeding with an actual feeding amount	t_{mf}^c	**Material feeding synchronised with axis movement**	**Material feeding not synchronised with axis movement**
			Material extrusion (ME) Material jetting (MJ) Direct energy deposition (DED) Polymerisation	Binder jetting (BJ) Powder bed fusion (PBF) Sheet lamination
	Standby			

The axis movement modules of all general AM technologies have two working states: the axis movement state with actual displacements and the standby state waiting for completion

of other modules' operations. The material processing modules also have two working states: the initial heating state and the heat preservation state. However, the auxiliary components modules of all existing technologies have only one working state: the monitoring and control of the machine status. The predictive models of time consumptions for all the above modules can be applied to all general AM technologies.

The component heating module has two working states: the initial heating state for heating the module to the target temperature and the heat preservation state for maintaining the module at the target temperature. Different from the aforementioned three other modules, the component heating module only participates in the AM processes of material extrusion (ME), material jetting (MJ) and sheet lamination, and therefore there is no such module for other AM technologies.

The material feeding module has two working states: the material feeding state with an actual feeding amount and the standby state waiting for the next feeding operation. Moreover, this module has two types of operation system for the existing AM technologies, as summarised in **Table 5.1** One type of operation system refers to the material feeding that is synchronised with axis movement in X, Y directions, for example, material extrusion (ME), material jetting (MJ), direct energy deposition (DED) and polymerisation technologies. **Figure 5.2** presents an example of material feeding in a DED process. When the printer nozzle needs to deposit material on a specific toolpath, the module runs in the material feeding state with an actual feeding amount. When the printer nozzle moves without depositing material, the module runs in the standby state to wait for the next G-code command to feed material.

The other type of operation system refers to the material feeding that is not synchronised with axis movement, for example, binder jetting (BJ), powder bed fusion (PBF) and sheet lamination technologies. The material is supplied between the construction of two adjacent layers. **Figure 5.3** presents an example of material feeding in a PBF process. When a PBF machine finishes the printing of one layer, the powder supply platform moves to the height of the next layer. Then, the powder for the next layer is transported from the powder stock

to the build platform by using a powder roller/recoater. In this case, when the AM machine needs to construct a new layer, the module runs in the material feeding state with an actual feeding amount. For the rest of the time, the module runs in the standby state to wait for the material feeding of the next layer.
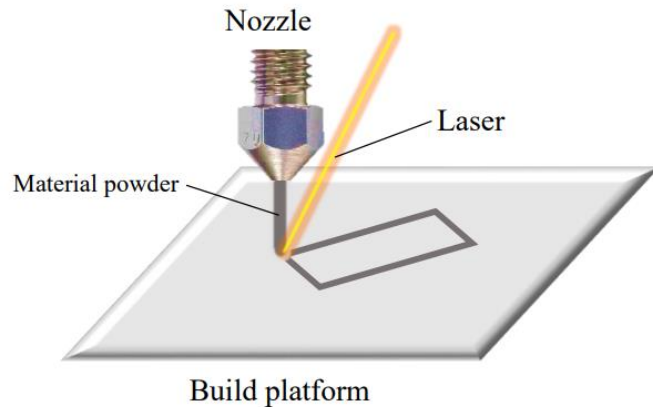
Figure 5.2: Example of material feeding synchronised with axis movement in a DED process
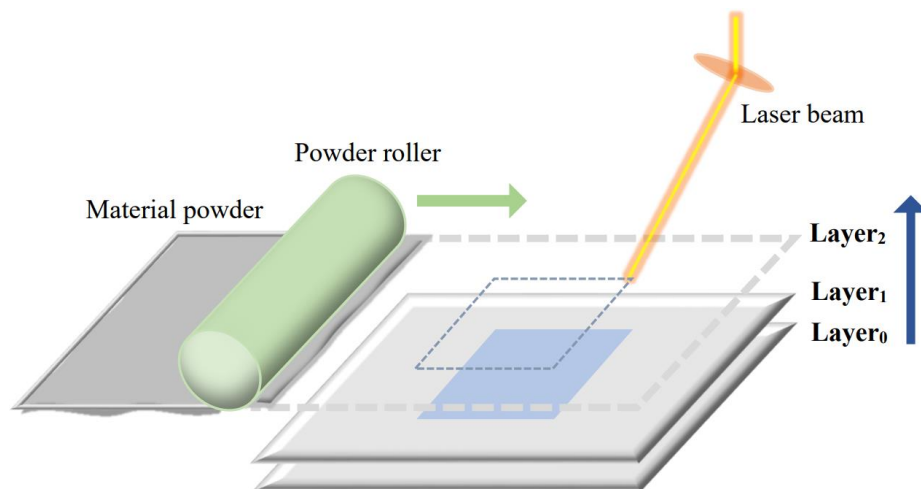
Figure 5.3: Example of material feeding between the construction of two adjacent layers in a PBF process

Based on the above, the material feeding module is always in one of the two working states and runs accompanied by axis movement. From the beginning of axis movement to the end of material deposition, the total time consumption t_{mf}^c of the material feeding module in two working states is equal to the time consumption of axis movement during the material deposition process.

5.3.1. Time consumption of axis movement

In this section, the predictive model of time consumption for the axis movement module is presented. According to the working states defined in last section, the total time consumption of the axis movement module has two parts: the time t_{xyz} spent on the axis movement with actual displacements and the interval time t_{xyz}^0 spent in a standby state.
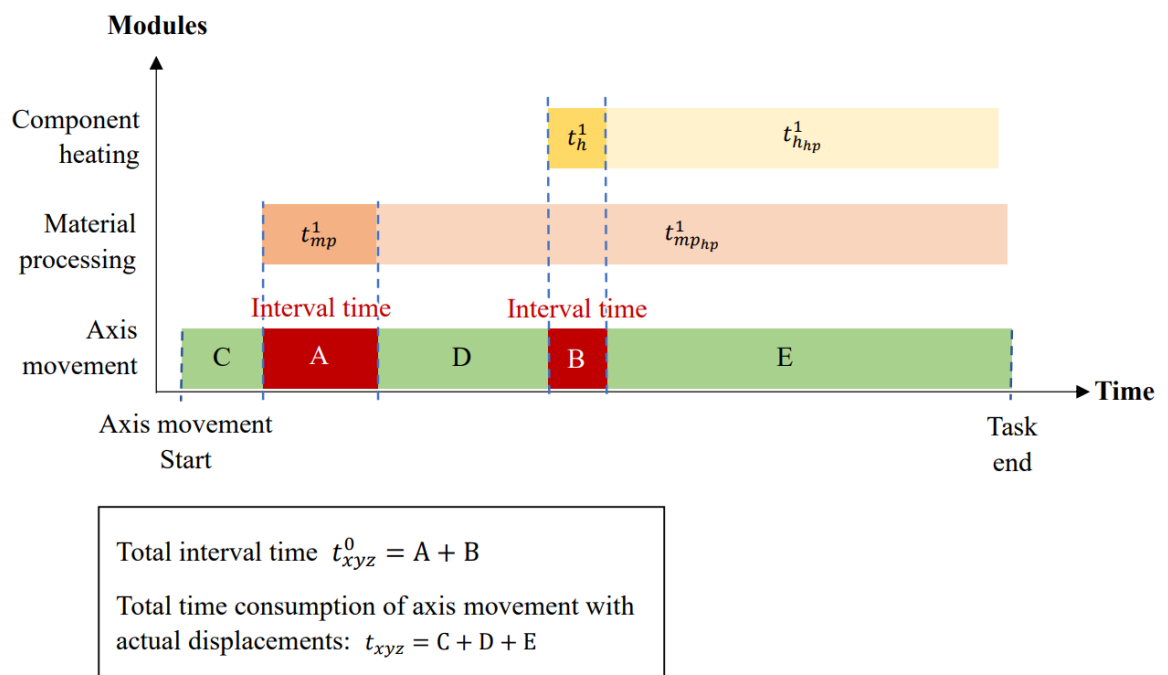
Figure 5.4: Interval time between axis movement with actual displacements

Figure 5.4 presents an example Gantt chart of the axis movement module to clearly illustrate the two working states. When there are other modules starting to run during axis movement, such as material processing and component heating, the axis movement module will be switched to standby mode and wait for the other modules to reach the target temperatures. When the target temperature is reached, it means that the G-code command line that commands this heating action has been successfully executed. Then, the axis movement module will be switched back to the state of axis movement with actual displacement, and the heated components will continue to be in the state of heat preservation until the end of the current AM process. Referring to **Section 3.3.1**, the time t_{xyz}^0 spent during this waiting period is named the 'interval time', with a value determined by the

running sequences and time consumptions of the other modules. The time consumption t_{xyz} of axis movement with actual displacements can be calculated from G-code, which is modelled as $t_{xyz} = \sum \frac{\sqrt{\Delta X^2 + \Delta Y^2}}{F_{xy}} + \sum \frac{\Delta Z}{F_z}$.

Based on the above, the total time consumption of the axis movement module is calculated as the sum of time consumption t_{xyz} with actual displacement and the interval time t_{xyz}^0, as expressed in **Equation (5.1)**. If no interruption occurs during the process of material deposition, there will be no interval time and the value of t_{xyz}^0 will be zero (i.e. $t_{xyz}^0 = 0$).

$$t_{axis} = t_{xyz} + t_{xyz}^0 \tag{5.1}$$

5.3.2. Time consumption of material processing

This section describes the predictive model of time consumption for the material processing module. In general AM technologies, materials need to be pre-processed before deposition, with heating being the major processing method. For example, a nozzle heater, electron beam, laser and ultraviolet (UV) light are all material processing modules used to melt materials from a solid to a liquid. Such a processing method usually takes a certain amount of time to reach the melting point of the material. In this study, the number of material processing modules is defined as u. Each module has two working states: the initial heating state and the heat preservation state. In the initial heating state, the consumed time of the ath module is defined as t_{mp}^a. Through observations from experiments, the initial heating time t_{mp}^a is related to the temperature difference ΔT_{mp}^a between the target temperature T_{mp}^a and the current temperature $T_{mp_0}^a$ of the module. Thus, t_{mp}^a is modelled as a function of ΔT_{mp}^a, as expressed in **Equation (5.2)** and **Equation (5.3)**.

$$t_{mp}^a = f(\Delta T_{mp}^a) \tag{5.2}$$

$$\Delta T_{mp}^a = T_{mp}^a - T_{mp_0}^a \tag{5.3}$$

To obtain the functional relationship in **Equation (5.2)**, experiments are conducted to measure the time consumptions t_{mp}^a under different temperature differences ΔT_{mp}^a. As shown in **Table 5.2**, the target temperature T_{mp}^a in the G-code commands of "M104 ST_{mp}^a" and "M109 ST_{mp}^a" is manually assigned with different values. The value of T_{mp}^a is set within the range from the melting point of the material to the maximum temperature that the material processing module can be heated to. The value of the current temperature $T_{mp_0}^a$ is set within the range from the current room temperature to the maximum temperature of the module. Then, the defined G-code commands are used to instruct the heating of the material processing module from the current temperature $T_{mp_0}^a$ to the target temperature T_{mp}^a. During the experiments, a power meter is used to measure the initial heating time t_{mp}^a.

Based on the experimental results, polynomial regression method is applied to curve-fit the functional relationship between the initial heating time t_{mp}^a and temperature difference ΔT_{mp}^a. Thus, the coefficient in **Equation (5.2)** is finally obtained.

Table 5.2: Information for measuring the time consumptions of the material processing module under different process parameters

Time consumption	Related parameters		Parameter ranges	
			Lower bound	Upper bound
t_{mp}^a	Current temperature	$T_{mp_0}^a$	Current room temperature	Maximum temperature of material processing module
	Target temperature	T_{mp}^a	Melting point of material	Maximum temperature of material processing module
G-code commands	M104 S(T_{mp}^a) : Set the target temperature T_{mp}^a of material processing module M109 S(T_{mp}^a) : Heat the module to the target temperature T_{mp}^a			

After the initial heating, the material processing module is switched to the heat preservation state. This process is parallel to the operation of other modules until the end of the AM task. In this study, the time spent on this process is defined as the heat preservation

time $t^a_{mp_{hp}}$, whose value is determined by the running sequences and time consumptions of other modules.

5.3.3. Time consumption of component heating

This section describes the predictive model of time consumption for the component heating module. These modules also need to be heated to support the AM process, such as the build platform in material extrusion (ME) and material jetting (MJ) technologies, the heated roller in sheet lamination technology, etc. In this study, the number of component heating modules is defined as v. Each module has two working states: the initial heating state for heating the module to the target temperature and the heat preservation state for maintaining the module at the target temperature. In the state of initial heating, the consumed time of the bth module is defined as t^b_h. This initial heating time t^b_h is related to the temperature difference ΔT^b_h between the target temperature T^b_h and the current temperature $T^b_{h_0}$ of the module. Thus, the consumed time t^b_h of the bth module is also modelled as a function of the temperature difference ΔT^b_h, as expressed in **Equation (5.4)** and **Equation (5.5)**.

$$t^b_h = f(\Delta T^b_h) \tag{5.4}$$

$$\Delta T^b_h = T^b_h - T^b_{h_0} \tag{5.5}$$

To obtain the functional relationship in **Equation (5.4)**, experiments are conducted to measure the time consumptions t^b_h under various temperature differences ΔT^b_h. As shown in **Table 5.3**, the target temperature T^b_h in the G-code commands of "M140 ST^b_h" and "M190 ST^b_h" is manually assigned with different values. The values of $T^b_{h_0}$ and T^b_h are both set within the range from the current room temperature to the maximum temperature of the component heating module. Then, the defined G-code commands are used to instruct the heating of the component heating module from the current temperature $T^b_{h_0}$ to the target

temperature T_h^b. During the experiments, a power meter is used to measure the initial heating time t_h^b.

Based on the experimental results, polynomial regression method is applied to curve-fit the functional relationship between the initial heating time t_h^b and temperature difference ΔT_h^b. Thus, the coefficient in **Equation (5.4)** is finally obtained.

Table 5.3: Information for measuring the time consumptions of the component heating module under different process parameters

Time consumption	Related parameters		Parameter ranges	
			Lower bound	Upper bound
t_h^b	Current temperature	$T_{h_0}^b$	Current room temperature	Maximum temperature of component heating module
	Target temperature	T_h^b	Current room temperature	Maximum temperature of component heating module
G-code commands	M140 S(T_h^b) : Set the target temperature T_h^b of component heating module M190 S(T_h^b) : Heat the module to the target temperature T_h^b			

After the initial heating, the component heating module is then switched to the heat preservation state. This process is parallel to the operation of other modules until the end of the AM task. In this study, the time spent on this process is defined as the heat preservation time $t_{h_{hp}}^b$, whose value is also determined by the running sequences and time consumptions of other modules.

5.3.4. Time consumption of material feeding

This section describes the predictive model of time consumption for the material feeding module. In the study, the number of material feeding modules is defined as w. Each module has two working states: the material feeding state with an actual feeding amount and the standby state waiting for the next feeding operation. Through observations from experiments

on real-world AM systems, it is found that the module is always in one of the two working states accompanied by axis movement. Therefore, the total time consumption t_{mf}^c of the cth material feeding module is equal to the total time consumption t_{axis} of the axis movement module. Referring to **Equation (5.1)**, the predictive model is expressed as follow.

$$t_{mf}^c = t_{axis} = t_{xyz} + t_{xyz}^0 \tag{5.6}$$

Furthermore, the material feeding module has two types of operating system, as shown in **Figure 5.2** and **Figure 5.3**. The first type is applied in material extrusion (ME), material jetting (MJ), direct energy deposition (DED) and polymerisation technologies. In these AM technologies, the material feeding module runs synchronously with the axis movement module. There is no need for both modules to spend extra time waiting for material supply.

The second type of operating system is applied in other AM technologies, including binder jetting (BJ), powder bed fusion (PBF) and sheet lamination technologies. In these AM technologies, material is supplied between the construction of two adjacent layers. Thus, the axis movement module needs extra time t_{feed}^c to wait for the material to be transported from the powder stock to the build platform. This extra time t_{feed}^c belongs to the interval time t_{xyz}^0 when the axis movement module is in a standby state, as expressed in **Equation (5.7)**. The value of this time consumption t_{feed}^c is calculated as shown in **Equation (5.8)**, where t_{layer} denotes the time consumption of material feeding per layer. LN denotes the total number of layers in the current AM task. This is calculated as the height H of the printed design divided by the layer thickness LT, as shown in **Equation (5.9)**.

$$t_{feed}^c \in t_{xyz}^0 \tag{5.7}$$

$$t_{feed}^c = t_{layer} \cdot LN \tag{5.8}$$

$$LN = \frac{H}{LT} \tag{5.9}$$

Based on the above, the time consumption t_{feed}^c is related to three parameters: the height of the printed design H, the layer thickness LT and the time of material feeding per layer t_{layer}. The height of the printed design H is determined by the design geometry and build orientation. The layer thickness LT is one of the process parameters, which can be configured in slicer software in the prefabrication stage. The time of material feeding per layer t_{layer} needs to be measured through experiments, as listed in **Table 5.4**. It is a fixed constant with a value determined by the characteristics of the material feeding module (e.g. the moving speed of the powder roller, recoater, etc.).

Table 5.4: Information for measuring the time consumptions of the material processing module

Time consumption	Related parameter	
t_{feed}^c	Time of material feeding per layer	t_{layer}

This study mainly focuses on the consumption prediction of fused deposition modelling (FDM) technology, which is a common branch of ME technology. The material feeding modules in the FDM process run synchronously with the axis movement modules. Thus, there is no need to calculate material feeding time t_{feed}^c for FDM systems. For other AM technologies that feed material between the construction of two adjacent layers, experiments need to be conducted to measure the time t_{layer} of material feeding per layer.

5.3.5. Time consumption of auxiliary components

This section describes the time consumption modelling for the module of auxiliary components. Different from the above modules, the auxiliary components have only one working state throughout the entire AM process: the continuous monitoring and control of the machine status. Thus, the total time consumption t_{aux} is equal to the total time consumption t_{total} of the AM task, as expressed in **Equation (5.10)**. The value of t_{aux} is determined by the running sequences and time consumptions of the other four modules.

$$t_{aux} = t_{total} \tag{5.10}$$

Above all, the total time consumption t_{total} of the entire AM process is refined by integrating **Equation (5.1)** to **Equation (5.10)**. According to the Gannt chart of all modules, there exist overlaps of running time in a general AM process. Therefore, the total time consumption t_{total} is modelled as the union of the time consumed by all five types of modules, as expressed in **Equation (5.16)**. The time consumption of each type of module is defined from **Equation (5.11)** to **Equation (5.15)**. t_{axis} denotes the running time of all axis movement modules. t_{mp} and $t_{mp_{hp}}$ denote the running time of all material processing modules in initial heating state and heat preservation state. t_h and $t_{h_{hp}}$ denote the running time of all component heating modules in initial heating state and heat preservation state. t_{mf} denotes the running time of all material feeding modules. t_{aux} denotes the running time of the module of auxiliary components.

$$t_{mp}=\bigcup_{a=1}^{u} t_{mp}^{a} \tag{5.11}$$

$$t_{mp_{hp}}=\bigcup_{a=1}^{u} t_{mp_{hp}}^{a} \tag{5.12}$$

$$t_{h}=\bigcup_{b=1}^{v} t_{h}^{b} \tag{5.13}$$

$$t_{h_{hp}}=\bigcup_{b=1}^{v} t_{h_{hp}}^{b} \tag{5.14}$$

$$t_{mf} = \bigcup_{c=1}^{w} t_{mf}^{c} \tag{5.15}$$

$$t_{total} = t_{axis} \cup t_{mp} \cup t_{mp_{hp}} \cup t_{h} \cup t_{h_{hp}} \cup t_{mf} \cup t_{aux} \tag{5.16}$$

Note that **Equation (5.16)** is a general predictive model of AM's time consumption. In the modelling of a specific AM machine, the model should be adjusted based on the number and running sequences of machine components.

5.4. Predictive model of energy consumption

This section establishes the predictive model of energy consumption in the AM process. Based on the definitions of different working states in **Section 5.2**, the apparent powers of all working states for the five modules in the existing AM technologies are defined in **Table 5.5**. The related parameters that determine the apparent power of each working state are also defined.

The axis movement module has two working states: the axis movement state with actual displacements and the standby state waiting for completion of other modules' operations. According to observations of experiments, the module runs with stable apparent power in both working states. Thus, the power of the axis movement module is defined as P_{axis}. Based on its corresponding G-code commands (as listed in **Table 5.5**), the speed F_{xy} of axis movement in X, Y directions and the speed F_z in Z direction are the related parameters that affect the value of apparent power P_{axis}. Therefore, the apparent power P_{axis} is modelled as a function of axis movement speeds F_{xy} and F_z in X, Y, Z directions. This predictive model is adoptable across all general AM technologies.

The modules of material processing and component heating both have two working states: the initial heating state and the heat preservation state. In the initial heating state, the apparent powers of material processing and component heating are respectively defined as P_{mp}^a, P_h^b. In the heat preservation state, the apparent powers of two modules are defined as $P_{mp_{hp}}^a$, $P_{h_{hp}}^b$. Based on the G-code commands (as listed in **Table 5.5**), above apparent powers of these two modules are related to their target temperatures T_{mp}^a, T_h^b. Therefore, the apparent power of each state is modelled as a function of target temperature. For the material processing module, the predictive model is adoptable across all general AM technologies. For the component heating module, the predictive model is only adoptable for material extrusion (ME), material jetting (MJ) and sheet lamination technologies, because there is no such module in other AM technologies.

The material feeding module has two working states: the material feeding state with an actual feeding amount and the standby state waiting for the next feeding operation. According to observations of experiments, the module runs with stable apparent power in both working states. In this study, the power is defined as P_{mf}^c. For some AM technologies including ME, MJ, direct energy deposition (DED) and polymerisation, the material feeding is synchronised with axis movement. According to its corresponding G-code command in **Table 5.5**, the apparent power P_{mf}^c is related to the rate F_{xy} of material feeding. Thus, P_{mf}^c is modelled as a function of F_{xy}. For other AM technologies including binder jetting (BJ), powder bed fusion (PBF) and sheet lamination technologies, the material feeding is between the construction of two adjacent layers. The apparent power P_{mf}^c of material feeding is a fixed constant, since its related parameter (i.e. the time consumption of material feeding t_{layer} for one layer) is a fixed constant.

The auxiliary components module has only one working state: the monitoring and control of the machine status. The module remains in this working state with stable apparent power throughout the entire AM process. Its apparent power is defined as P_{aux}, which is a fixed constant and has no related parameters.

The energy consumption modelling needs two important elements: time consumption and apparent power. The time consumptions of the five modules directly use the time models from the last section. The apparent powers of the five modules need to be measured through experiments. In the following sections, the energy consumption of each module is modelled based on **Table 5.5**. Experimental measurements of each module are also presented.

Table 5.5: Apparent powers of different working states for each module of the existing AM technologies (G-Code – Reprap, 2020)

Modules	Working states	G-code commands	Powers	Related parameters	AM technologies
Axis movement	Axis movement with actual displacements	G1 F(F_{xy}) Xnnn Ynnn G1 F(F_z) Znnn	P_{axis}	F_{xy}, F_z	Material extrusion (ME) Material jetting (MJ) Direct energy deposition (DED) Polymerisation Binder jetting (BJ) Powder bed fusion (PBF) Sheet lamination
	Standby	None			
Material processing	Initial heating	M104 S(T_{mp}^a) M109 S(T_{mp}^a)	P_{mp}^a	T_{mp}^a	Material extrusion (ME) Material jetting (MJ) Direct energy deposition (DED) Polymerisation Binder jetting (BJ) Powder bed fusion (PBF) Sheet lamination
	Heat preservation	None	$P_{mp_{hp}}^a$	T_{mp}^a	
Component heating	Initial heating	M140 S(T_h^b) M190 S(T_h^b)	P_h^b	T_h^b	Material extrusion (ME) Material jetting (MJ) Sheet lamination

	Heat preservation	None	$P_{h_{hp}}^b$	T_h^b		
Material feeding	Material feeding with actual feeding amount	G1 F(F_{xy}) Xnnn Ynnn Emmm	P_{mf}^c	F_{xy}	**Material feeding synchronised with axis movement**	Material extrusion (ME) Material jetting (MJ) Direct energy deposition (DED) Polymerisation
	Standby	None		t_{layer}	**Material feeding synchronised with axis movement**	Binder jetting (BJ) Powder bed fusion (PBF) Sheet lamination
Auxiliary components	Monitoring and control of machine status	None	P_{aux}	None	Material extrusion (ME) Material jetting (MJ) Direct energy deposition (DED) Polymerisation Binder jetting (BJ) Powder bed fusion (PBF) Sheet lamination	

5.4.1. Energy consumption of axis movement

This section presents the energy consumption modelling for the axis movement module. The module has two working states: the axis movement state with actual displacements and the standby state. During the printing process, the module remains running with stable apparent power in both working states. For example, **Figure 5.5** presents a typical axis movement module using a Cartesian system in fused deposition modelling (FDM) processing. The system is driven by three stepper motors. Each motor is responsible for the axis movement in each direction. When the nozzle moves only in X, Y directions, the motor in Z direction remains in the standby state with stable apparent power to wait for the next operation. Therefore, the total apparent power P_{axis} of the axis movement module is the sum of apparent powers of all stepper motors in the module.
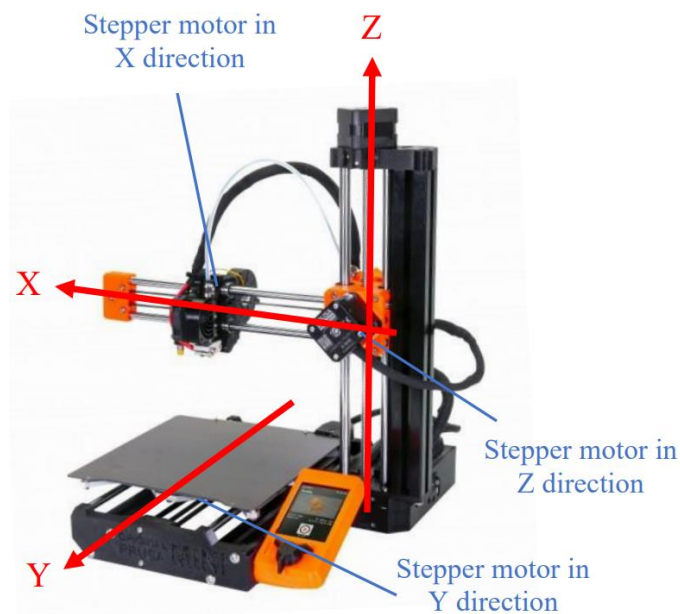
Figure 5.5: Three stepper motors in a Cartesian system of Original Prusa MINI+ FDM printer (MINI+, 2020)

According to the G-code command to instruct the axis movement module in **Table 5.6**, the apparent power P_{axis} of this module is related to its speed F_{xy} in X, Y directions and speed F_z in Z direction. Thus, P_{axis} is modelled as a function of F_{xy} and F_z, as expressed in **Equation (5.17)**. To calculate the functional relationship, experiments are conducted to test the apparent powers P_{axis} of axis movement at different speeds F_{xy}, F_z. As shown in

Table 5.6, the speeds F_{xy} and F_z in G-code commands "G1 F_{xy} Xnnn Ynnn" and "G1 F_z Znnn" are manually assigned with different values. The value of each speed is set within the range that the module can achieve. Then, the defined G-code commands are used to instruct the axis movement module to move at different speeds. During the experiments, a power meter is used to measure the apparent power of the module. Based on the experimental results, the functional relationship in **Equation (5.17)** is derived by using regression analysis methods. In this study, polynomial regression is applied to calculate the coefficient in this function.

$$P_{axis} = f\left(F_{xy}, F_z\right) \tag{5.17}$$

Table 5.6: Information for measuring the apparent powers of the axis movement module in X, Y, Z directions under different process parameters (G-Code – Reprap, 2020)

Apparent power	Related parameters		Parameter ranges	
			Lower bound	Upper bound
P_{axis}	Speed of axis movement in X, Y directions	F_{xy}	Lowest speed of axis movement module in X, Y directions	Highest speed of axis movement module in X, Y directions
	Speed of axis movement in Z direction	F_z	Lowest speed of axis movement module in Z direction	Highest speed of axis movement module in Z direction
G-code commands		G1 F_{xy} Xnnn Ynnn : Nozzle moves to the target coordinate (Xnnn, Ynnn) at a speed of F_{xy} G1 F_z Znnn : Nozzle moves to the target coordinate (Znnn) at a speed of F_z		

Based on the above, the total energy consumption E_{axis} of the axis movement module is modelled as the integral of power P_{axis} over its time consumption t_{axis}, as expressed in **Equation (5.18)**.

$$E_{axis} = \int_0^{t_{axis}} P_{axis}\, dt \tag{5.18}$$

5.4.2. Energy consumption of material processing

This section presents the energy consumption modelling for the material processing module. The module has two working states: the initial heating state and the heat preservation state. The following modelling is carried out for these two stages.

In this study, the number of material processing modules is defined as u. The apparent power of the ath module in the initial heating state is defined as P_{mp}^{a}, while the apparent power in the heat preservation state is defined as $P_{mp_{hp}}^{a}$. According to the G-code command to instruct the material processing module in **Table 5.7**, the apparent powers P_{mp}^{a} and $P_{mp_{hp}}^{a}$ are both related to the target temperature T_{mp}^{a} of this module. Thus, P_{mp}^{a} and $P_{mp_{hp}}^{a}$ are respectively modelled as the functions of T_{mp}^{a}, as shown in **Equation (5.19)** and **Equation (5.20)**. To obtain the functional relationships in the two equations, a power meter is used to measure the apparent powers P_{mp}^{a}, $P_{mp_{hp}}^{a}$ of the material feeding module under different target temperatures T_{mp}^{a}. As shown in **Table 5.7**, the target temperature T_{mp}^{a} in the G-code commands "M104 ST_{mp}^{a}" and "M109 S T_{mp}^{a}" is manually assigned with different values. The value of the target temperature T_{mp}^{a} is set within the range from the melting point of the material to the maximum temperature that the module can be heated to. Then, the defined G-code commands are used to instruct the heating of the material processing module to different target temperatures T_{mp}^{a}.

Based on the experimental results, polynomial regression method is applied to curve-fit the functional relationships (i.e. to calculate the coefficients in **Equation (5.19)** and **Equation (5.20)**).

$$P_{mp}^{a} = f(T_{mp}^{a}) \tag{5.19}$$

$$P_{mp_{hp}}^{a} = f(T_{mp}^{a}) \tag{5.20}$$

Table 5.7: Information for measuring the apparent powers of the material processing module under different process parameters

Apparent power		Related parameters		Parameter ranges	
				Lower bound	Upper bound
Initial heating	P_{mp}^a	Target temperature	T_{mp}^a	Melting point of material	Maximum temperature of material processing module
Heat preservation	$P_{mp_{hp}}^a$				
G-code commands		M104 S(T_{mp}^a) : Set the target temperature T_{mp}^a of material processing module M109 S(T_{mp}^a) : Heat the module to the target temperature T_{mp}^a			

Based on the above, the total energy consumption E_{mp} of the material processing is modelled as the sum of the time-integral of power of all modules, as expressed in **Equation (5.21)**.

$$E_{mp} = \sum_{a=1}^{u}(\int_0^{t_{mp}^a} P_{mp}^a \, dt + \int_0^{t_{mp_{hp}}^a} P_{mp_{hp}}^a \, dt) \tag{5.21}$$

5.4.3. Energy consumption of component heating

In this section, the energy consumption modelling for the component heating module is presented. The module has two working states: the initial heating state and the heat preservation state. The following modelling is carried out for these two stages.

In this study, the number of component heating modules is defined as v. The apparent power of the bth module in the initial heating state is defined as P_h^b, while the apparent power in the heat preservation state is defined as $P_{h_{hp}}^b$. According to the G-code command to instruct the module heating in **Table 5.8**, the apparent powers P_h^b and $P_{h_{hp}}^b$ are both related to the target temperature T_h^b of this module. Therefore, P_h^b and $P_{h_{hp}}^b$ are respectively modelled as the functions of T_h^b, as expressed in **Equation (5.22)** and **Equation**

(5.23). To obtain the functional relationships in the two equations, a power meter is used to measure the apparent powers P_h^b, $P_{h_{hp}}^b$ of the component heating module under different target temperatures T_h^b. The target temperature T_h^b in the G-code commands "M140 ST_h^b" and "M190 S T_h^b" is manually assigned with different values. The value of T_h^b is set within the range from current room temperature to the maximum temperature that the module can be heated to. Then, the defined G-code commands are used to instruct the heating of module to different target temperatures T_h^b.

$$P_h^b = f(T_h^b) \tag{5.22}$$

$$P_{h_{hp}}^b = f(T_h^b) \tag{5.23}$$

Table 5.8: Information for measuring the apparent powers of the component heating module under different process parameters

Apparent power		Related parameters		Parameter ranges	
				Lower bound	Upper bound
Initial heating	P_h^b	Target temperature	T_h^b	Current room temperature	Maximum temperature of component heating module
Heat preservation	$P_{h_{hp}}^b$				
G-code commands		M140 S(T_h^b) : Set the target temperature T_h^b of component heating module M190 S(T_h^b) : Heat the module to the target temperature T_h^b			

Based on the experimental results, polynomial regression method is applied to calculate the coefficients in **Equation (5.22)** and **Equation (5.23)**. The total energy consumption E_h of the component heating is modelled as the sum of the time-integral of power of all modules, as expressed in **Equation (5.24)**.

$$E_h = \sum_{b=1}^{v} \left(\int_0^{t_h^b} P_h^b \, dt + \int_0^{t_{h_{hp}}^b} P_{h_{hp}}^b \, dt \right) \tag{5.24}$$

5.4.4. Energy consumption of material feeding

In this section, the energy consumption modelling for the material feeding module is presented. The module has two working states: the material feeding state with an actual feeding amount and the standby state to wait for the next feeding operation. In both working states, the module remains running with stable power so as to be ready for supplying material at any time. In this study, the number of material feeding modules is defined as w. The apparent power of the cth module is defined as P_{mf}^c. As discussed in **Section 5.3**, the material feeding module has two types of feeding operations. The modelling of each type is described as follows.

The first type of feeding operation is mainly applied in material extrusion (ME), material jetting (MJ), direct energy deposition (DED) and polymerisation technologies. In these AM technologies, the material feeding module runs synchronously with the axis movement module. According to the G-code command for material feeding in **Table 5.9**, the apparent power P_{mf}^c of this task is related to the feeding rate F_{xy} in X, Y directions. Thus, P_{mf}^c is modelled as a function of F_{xy}, as expressed in **Equation (5.25)**.

$$P_{mf}^c = f(F_{xy}) \tag{5.25}$$

To obtain the functional relationship, a power meter is used to measure the apparent powers P_{mf}^c of material feeding at different feeding rates F_{xy}. The feeding rate F_{xy} in the G-code command "G1 F_{xy} Xnnn Ynnn Emmm" is manually assigned with different values. The value of F_{xy} is set within the range from the lowest feeding rate to the highest feeding rate of the material feeding module. Then, the defined G-code command is used to instruct the module to feed the material at different rates F_{xy}. Based on the experimental results, polynomial regression method is applied to model the functional relationship in **Equation (5.25)**. Thus, the coefficient in this function is finally obtained.

The second type of feeding operation is mainly applied in binder jetting (BJ), powder bed fusion (PBF) and sheet lamination technologies, as discussed in **Section 5.3**. In the material feeding state with an actual feeding amount, the module supplies material between the construction of two adjacent layers. In the standby state, the module is maintained at the previous power level to wait for the material feeding of the next layer. Thus, the apparent power P_{mf}^c of the material feeding module and its related parameter (i.e. the time consumption of material feeding t_{layer} for one layer) are fixed constants. In these AM technologies, the apparent power P_{mf}^c can be measured by using a power meter.

Based on the above, the total energy consumption E_{mf} of material feeding is modelled as the sum of the time-integral of power of all modules, as expressed in **Equation (5.26)**.

$$E_{mf} = \sum_{c=1}^{w} \int_0^{t_{mf}^c} P_{mf}^c dt \qquad (5.26)$$

Table 5.9: Information for measuring the apparent powers of the material feeding module under different process parameters (G-Code – Reprap, 2020)

Apparent power	Related parameters		Parameter ranges		Applied AM technologies
			Lower bound	Upper bound	Material extrusion (ME),
P_{mf}^c	Rate of material feeding in X, Y directions	F_{xy}	Lowest speed of material feeding module in X, Y directions	Highest speed of material feeding module in X, Y directions	Material jetting (MJ), Direct energy deposition (DED), Polymerisation
	Time consumption of material feeding for one layer	t_{layer}	Fixed constant		Binder jetting (BJ), Powder bed fusion (PBF) Sheet lamination
G-code commands	G1 F(F_{xy}) Xnnn Ynnn Emmm : Nozzle moves to the target coordinate (Xnnn, Ynnn) with material feeding. The total amount of material feeding is mmm. The rate of material feeding or the speed of axis movement is F_{xy}.				

5.4.5. Energy consumption of auxiliary components

This section presents the energy consumption modelling for the auxiliary components module. As discussed in **Section 5.2**, the auxiliary components are classified as two types based on their functions. Details of each type are described as follows.

The first type is a component used to monitor and control the machine status during the printing process, such as the display unit, temperature sensor, and user interface and connectivity. These components keep running even when the machine is in standby mode. According to experimental results, the components maintain a stable apparent power P_s no matter whether they are in standby mode or operating throughout the manufacturing process.

The second type is a component used to support the AM process, such as the cooling system. When an AM task begins, these components start running until the end of the task. Meanwhile, the apparent power increases from standby power P_s to a higher level to start up the machine. This mode is defined as the start-up mode in this study. This increased power difference is defined as the start-up power P_0.

Based on the above, the auxiliary components run throughout the entire AM task. A power meter is used to measure the total apparent power (i.e. $P_s + P_0$) before or after the printing process. The total time consumption t_{aux} of this module is equal to the total time consumption t_{total} of the entire AM process. Therefore, the total energy consumption E_{aux} of the auxiliary components is modelled as the product of total apparent power and total time consumption t_{total}, as expressed in **Equation (5.27)**. The value of t_{total} is determined by the running sequences and time consumptions of the other four modules.

$$E_{aux} = (P_s + P_0)t_{total} \tag{5.27}$$

Above all, the total energy consumption E_{total} of the entire AM process is refined. By integrating **Equation (5.17)** to **Equation (5.27)**, E_{total} is modelled as the sum of the energy consumed by all five types of modules, as expressed in **Equation (5.28)**.

$$E_{total} = E_{axis} + E_{mp} + E_h + E_{mf} + E_{aux} \tag{5.28}$$

5.5. Predictive model of material consumption

The total material consumption can be directly modelled from the calculation of G-code. Thus, the conceptual model of **Equation (4.8)** in **Section 4.3.3** is used as the final predictive model. Due to different materials being used in different AM technologies, the volume calculation of total material usage (i.e. $\sum V_{unit}$) depends on the particular type and state of material. The volume calculation of each type of AM technology is described as follows.

Fused deposition modelling (FDM) is a common branch of material extrusion (ME) technology. The material most commonly used in FDM technology is polylactic acid (PLA) thermoplastic filament. As shown in **Figure 5.6**, the amount of material usage is in millimetres of length, which is provided by the G-code command beginning with the letter "E". As discussed in the conceptual model of **Equation (4.8)**, V_{unit} denotes the volume of material consumption in each displacement of axis movement. In the FDM process, the value of V_{unit} is calculated through **Equation (5.29)**, in which $\emptyset$ denotes the diameter of material filament and ℓ_E denotes the length of supplied material filament in each displacement of axis movement.

$$V_{unit} = \ell_E \pi \frac{\emptyset^2}{4} \tag{5.29}$$
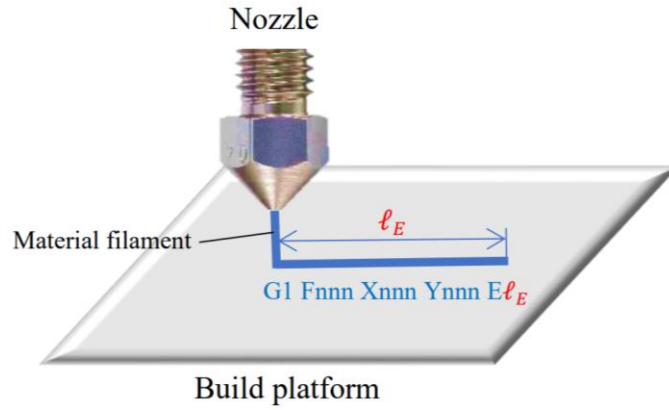
Figure 5.6: Volume calculation of material consumption in FDM technology

The material most commonly used in powder bed fusion (PBF) technology is metal powder. As shown in **Figure 5.7**, the powders are firstly supplied on the new layer. Then, the laser or thermal print head runs, accompanied by the axis movement, to solidify the powder on the predefined toolpaths. In this case, the consumption of solidified powder is calculated through **Equation (5.30)**, where V_{unit} denotes the volume of solidified powder in each displacement of axis movement, $\emptyset$ denotes the diameter of the laser or thermal print head, LT denotes the layer thickness and ℓ_E denotes the distance of axis movement in each displacement.

$$V_{unit} = \emptyset \cdot LT \cdot \ell_E \tag{5.30}$$
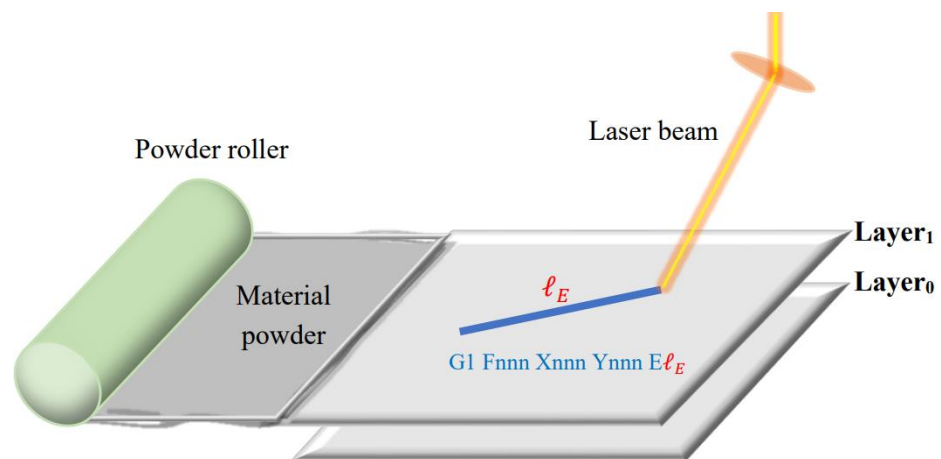
Figure 5.7: Volume calculation of material consumption in PBF technology

The material most commonly used in direct energy deposition (DED) technology is metal powder. As shown in **Figure 5.8**, the material feeding is synchronous with axis movement

in X, Y directions. During the printing process, the powders are sprayed onto the build platform through the powder feeder and melted by the laser or electron beam. In this case, the consumption of solidified powder is also calculated through **Equation (5.30)**, where V_{unit} denotes the volume of solidified powder in each displacement of axis movement, $\emptyset$ denotes the diameter of the laser or thermal print head, LT denotes the layer thickness and ℓ_E denotes the distance of axis movement in each displacement.
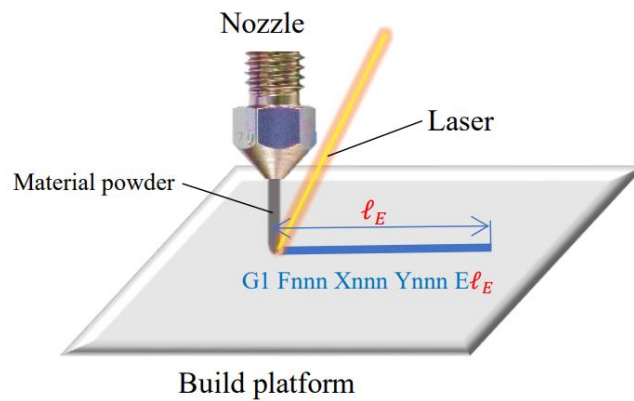
Figure 5.8: Volume calculation of material consumption in DED technology

Similar to powder bed fusion (PBF) and direct energy deposition (DED) technologies, both sheet lamination and polymerisation technologies use lasers to solidify material on the predefined toolpaths of each layer. Therefore, the volume calculations for these two AM technologies also use the same method in **Equation (5.30)**.

Material jetting (MJ) technology fabricates by jetting liquid material onto the build platform. As shown in **Figure 5.9**, there are multiple print heads located on the jetting head. All print heads are extremely small and can provide resolutions up to 16 microns (Treatstock, 2020). During the printing process, the material droplets are selectively jetted from the print heads onto the desired area, using a thermal or piezoelectric method (Yap et al., 2017). Then, the materials are cured by ultraviolet (UV) light to form the 3D object. Since the material feeding is synchronous with axis movement in X, Y directions, V_{unit} is defined as the volume of supplied liquid per displacement per print head. The value of V_{unit} is calculated as shown in **Equation (5.31)**, where V_{avg} denotes the average volume of liquid supplied per unit displacement and ℓ_E denotes the distance of axis movement in each displacement.

Based on the above, the total volume $\sum V_{unit}$ of material consumption is the sum of all print heads' material consumed across all displacements.

$$V_{unit} = V_{avg} \cdot \ell_E \qquad (5.31)$$
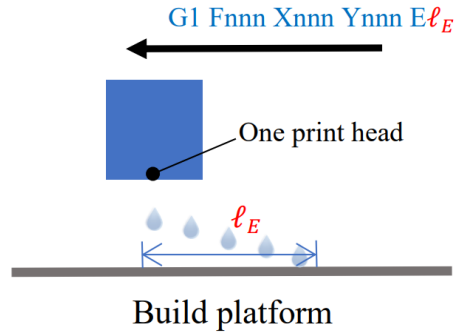
Figure 5.9: Volume calculation of material consumption in MJ technology

Binder jetting (BJ) technology uses a similar method to MJ. As shown in **Figure 5.10**, BJ fabricates by selectively jetting liquid binder to the layered powders by following the predefined toolpaths. Since the material feeding is synchronous with axis movement in X, Y directions, V_{unit} is defined as the volume of bonded powders in each displacement of axis movement. The value of V_{unit} is also calculated by using **Equation (5.30)**. In this case, $\emptyset$ denotes the diameter of the print head, LT denotes the layer thickness and ℓ_E denotes the distance of axis movement in each displacement. Based on the above, the total volume $\sum V_{unit}$ of material consumption is the sum of all print heads' material consumed across all displacements.
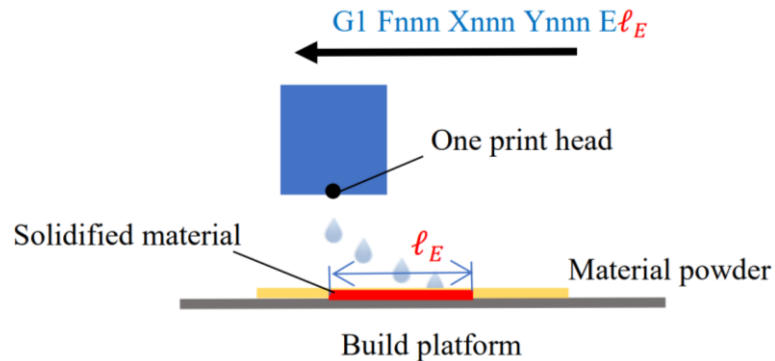
Figure 5.10: Volume calculation of material consumption in BJ technology

Table 5.10: Related parameters in the predictive model of material consumption for different AM technologies

AM technologies	Material forms	Related parameters			Predictive models
Material extrusion (ME)	Wire	$\emptyset$	ℓ_E		$V_{unit} = \ell_E \pi \dfrac{\emptyset^2}{4}$
		Diameter of material filament	Length of deposited material in each displacement of axis movement		
Powder bed fusion (PBF)	Powder	$\emptyset$	ℓ_E	LT	$V_{unit} = \emptyset \cdot LT \cdot \ell_E$
		Diameter of laser or thermal print head	Distance of axis movement in each displacement	Layer thickness	
Direct energy deposition (DED)	Powder	Diameter of laser of electron beam	Distance of axis movement in each displacement	Layer thickness	
Sheet lamination	Sheet	Diameter of laser	Distance of axis movement in each displacement	Layer thickness	
Polymerisation	Liquid	Diameter of laser	Distance of axis movement in each displacement	Layer thickness	
Binder jetting (BJ)	Powders	Diameter of print head	Distance of axis movement in each displacement	Layer thickness	
Material jetting (MJ)	Liquid	ℓ_E	V_{avg}		$V_{unit} = V_{avg} \cdot \ell_E$
		Distance of axis movement in each displacement	Average volume of liquid material supplied per unit displacement		

Based on the above, **Table 5.10** summarises all related parameters to calculate the material consumptions in different AM technologies. For each AM technology, the corresponding calculation equation of V_{unit} is substituted into the conceptual model in **Equation (4.8)**. The total mass of material consumption can finally be calculated through the product of the material density ρ and the cumulative volume $\sum V_{unit}$ of material feeding. The material density ρ in **Equation (4.8)** uses the quoted density of the material. For some materials where the density is unknown, a density meter is applied to measure the actual value of this parameter.

5.6. Experimental measurements of parameters in the predictive models

The previous sections introduce the detailed modelling procedures for predicting time, energy and material consumptions. In this section, the parameters in the predictive models are summarised in the format of tree diagrams. To clearly illustrate the diagrams, fused deposition modelling (FDM) and powder bed fusion (PBF) technologies are used as two examples to list all parameters that form the predictive models. To begin, the manufacturing flows of the two AM technologies are displayed and introduced. Then, the parameters are classified into three types: parameters calculated from G-code, parameters obtained from experiments, and parameters determined by the running sequences and time consumptions of the five modules. Based on the classification of parameters, it can clearly be seen which parameters need to be measured under different related process parameters.

Figure 5.11 displays the manufacturing flow of FDM technology. At the start, material is treated through the material processing module (i.e. nozzle heater or hotend). Then, the construction of the first layer begins through axis movement and material feeding in X, Y directions. Once the material deposition on the current layer is completed, the nozzle moves to the height of the next layer through axis movement in Z direction. Then, the construction of a new layer is commenced. The AM process is completed when all layers are printed.

During the AM process, other modules – including component heating and auxiliary components – also participate in the printing. Their running sequences are determined by the machine characteristics.
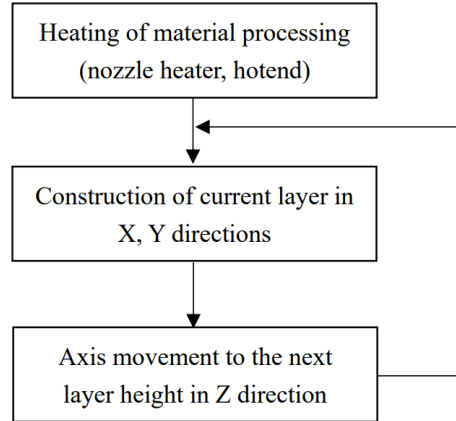
Figure 5.11: Manufacturing flow of FDM technology
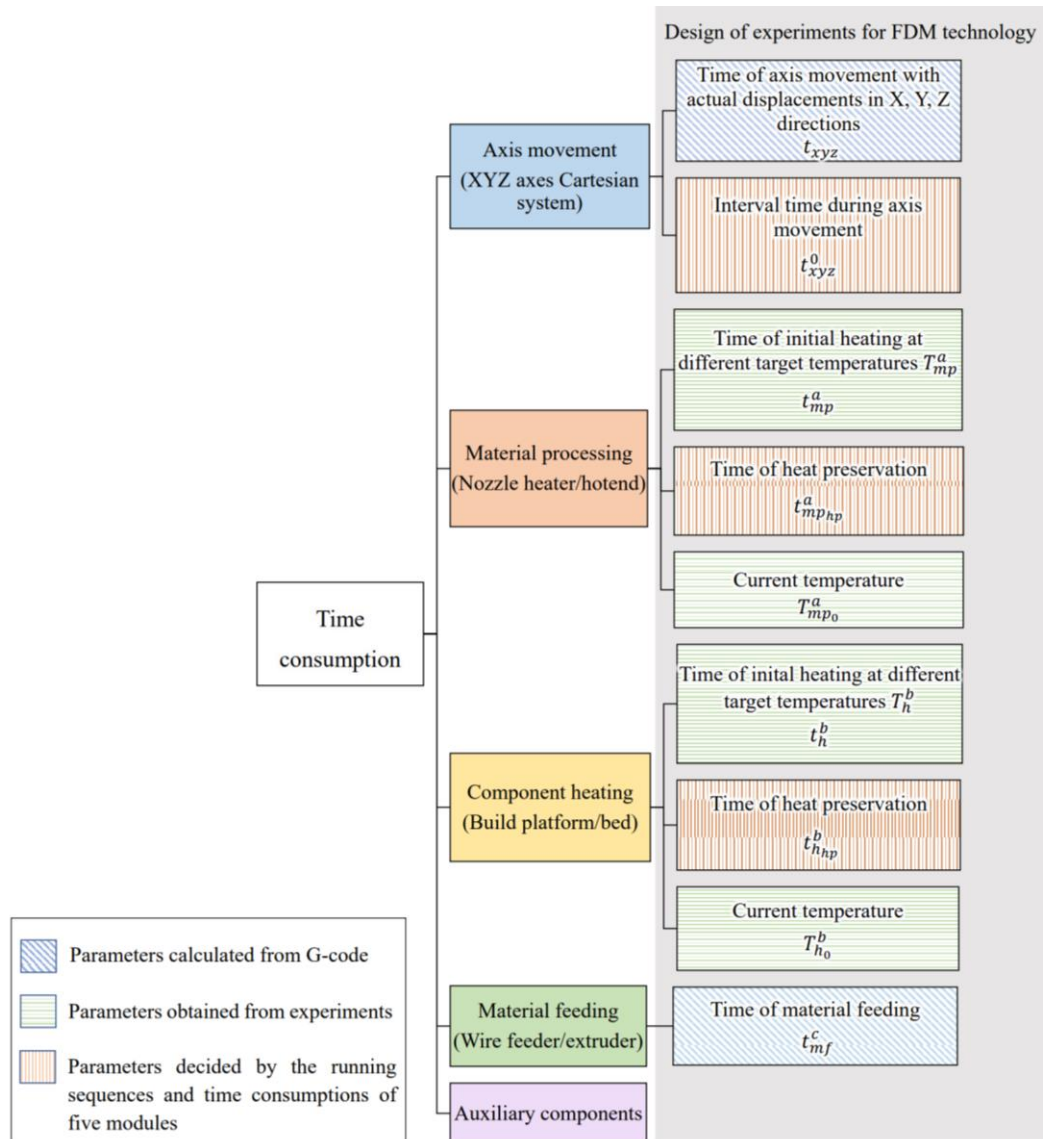
Figure 5.12: Three types of parameters for the time modelling of FDM technology
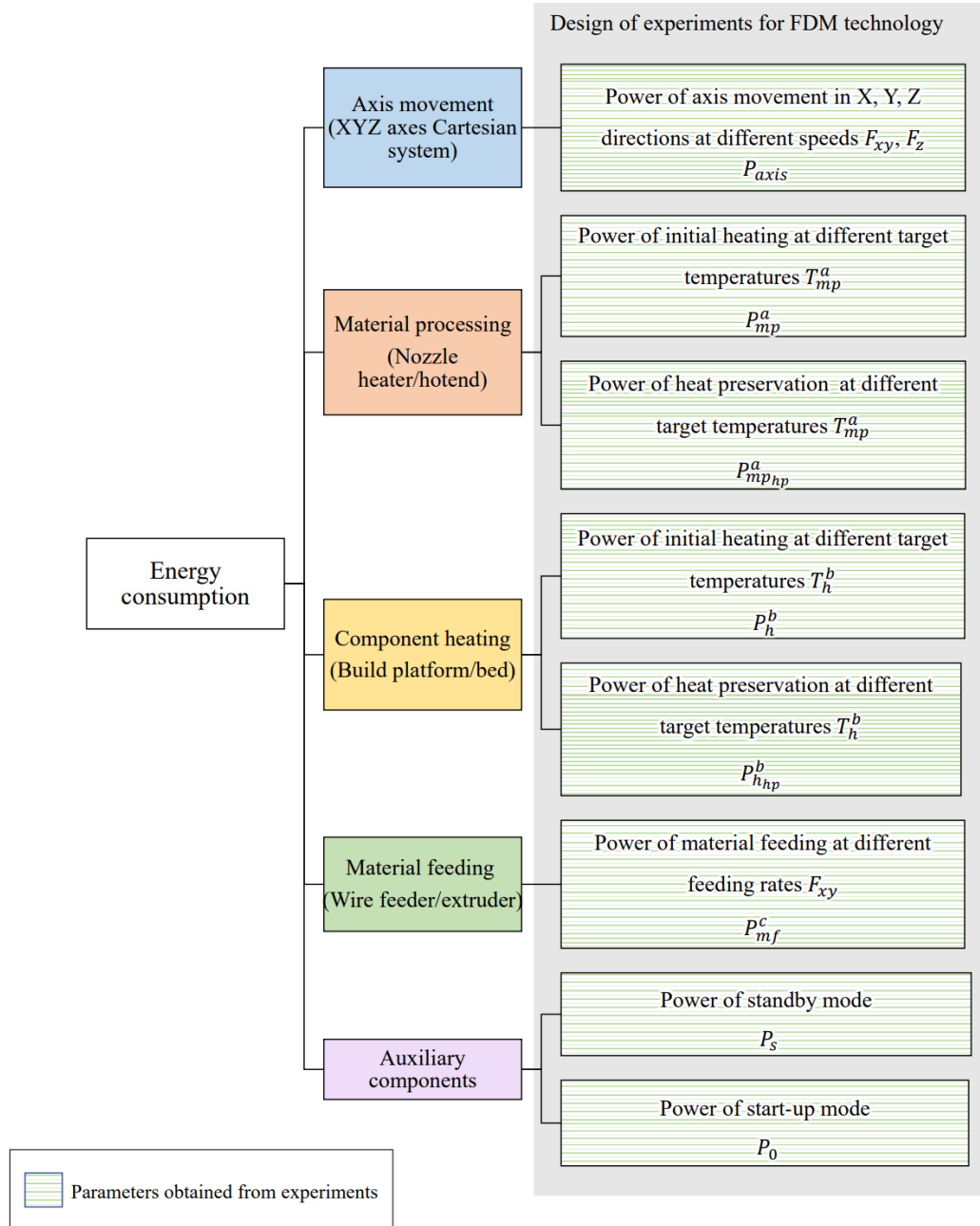
Figure 5.13: Three types of parameters for the energy modelling of FDM technology
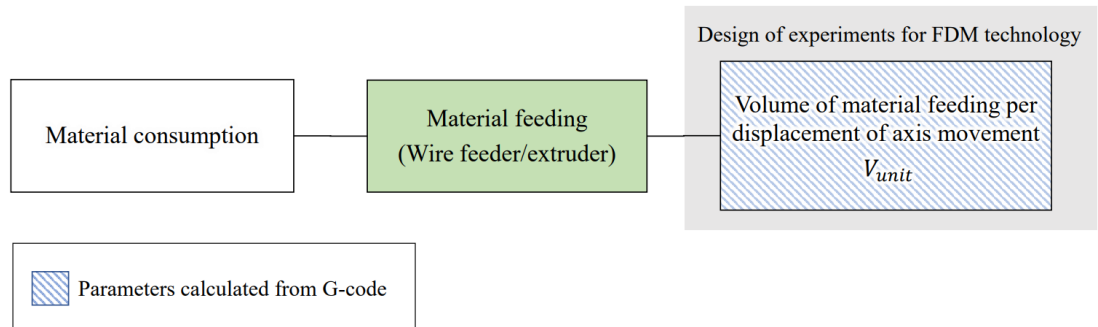
Figure 5.14: Three types of parameters for the consumed material modelling of FDM technology

As shown in **Figure 5.12** to **Figure 5.14**, three types of parameters are needed to form the predictive models of FDM technology. The first type is a parameter in blue diagonal stripes that is directly calculated from G-code. The second type is a parameter in green horizontal stripes that is measured through experiments. The third type is a parameter in red vertical stripes that is dependent on the running sequences and time consumptions of other modules.

In details, the first type of parameter to be calculated from G-code includes three parts: the time t_{xyz} of axis movement with actual displacements, the time t_{mf}^c of material feeding and the volume V_{unit} of material feeding per displacement of axis movement. The second type of parameter is derived from experimental measurements. **Table 5.11** lists all parameters to be measured under different related process parameters. Note that the standby power P_s, start-up power P_0 of auxiliary components, and current temperatures $T_{mp_0}^a$ and $T_{h_0}^b$ of the material processing module and component heating module are all fixed constants without any related process parameters. Furthermore, other parameters in **Table 5.11** are measured under different values of their related process parameters. All of the time and apparent powers to be measured for this FDM technology are tested by using a power meter. All current temperatures to be measured are recorded directly through the display unit of the AM machine, since all general AM machines have temperature sensors to monitor the heated components. The third type of parameter is dependent on the running sequences and time consumptions of the five modules. These parameters are modelled based on the Gantt chart of the five modules. The parameters include the interval time t_{xyz}^0 during axis movement, and the heat preservation time $t_{mp_{hp}}^a$ and $t_{h_{hp}}^b$ of the material processing module and component heating module.

Table 5.11: Parameters to be measured through experiments under different related process parameters for FDM technology

Module	Parameters	Meanings	Related process parameters	Meanings
Material processing	t_{mp}^a	Initial heating time	T_{mp}^a	Target temperature
	P_{mp}^a	Apparent power of initial heating		
	$P_{mp_{hp}}^a$	Apparent power of heat preservation		
	$T_{mp_0}^a$	Current temperature	None	None
Component heating	t_h^b	Initial heating time	T_h^b	Target temperature
	P_h^b	Apparent power of initial heating		
	$P_{h_{hp}}^b$	Apparent power of heat preservation		
	$T_{h_0}^b$	Current temperature	None	None
Axis movement	P_{axis}	Apparent power of axis movement	F_{xy}, F_z	Speed of axis movement in X, Y, Z directions
Material feeding	P_{mf}^c	Apparent power of material feeding	F_{xy}	Speed of axis movement in X, Y directions
Auxiliary components	P_s	Standby power	None	None
	P_0	Start-up power	None	None

Figure 5.15 displays the working flow of powder bed fusion (PBF) technology. First, the laser in the material processing module is heated to the target temperature. Then, the powder for the first layer is supplied to the build platform by the material feeding module (i.e. powder roller or recoater). Next, the construction of the first layer begins through axis movement in X, Y directions. The powder is solidified by the laser. Once the material deposition on the current layer is completed, the build platform moves down to the height of the next layer through the axis movement module in Z direction. The material feeding and construction of the new layer are then continued. The AM process is completed when all layers all printed. During this AM process, auxiliary components also participate in the entire printing process. Different from FDM technology, the material feeding and axis movement of PBF technology are carried out separately during the AM process. Additionally, there is no component heating module in PBF technology. Thus, there are only four types of modules involved in

the PBF process, namely axis movement, material feeding, material processing and auxiliary components.
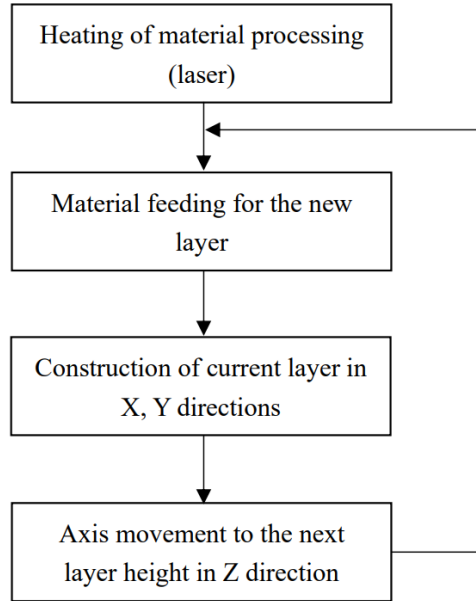
Figure 5.15: Manufacturing flow of PBF technology
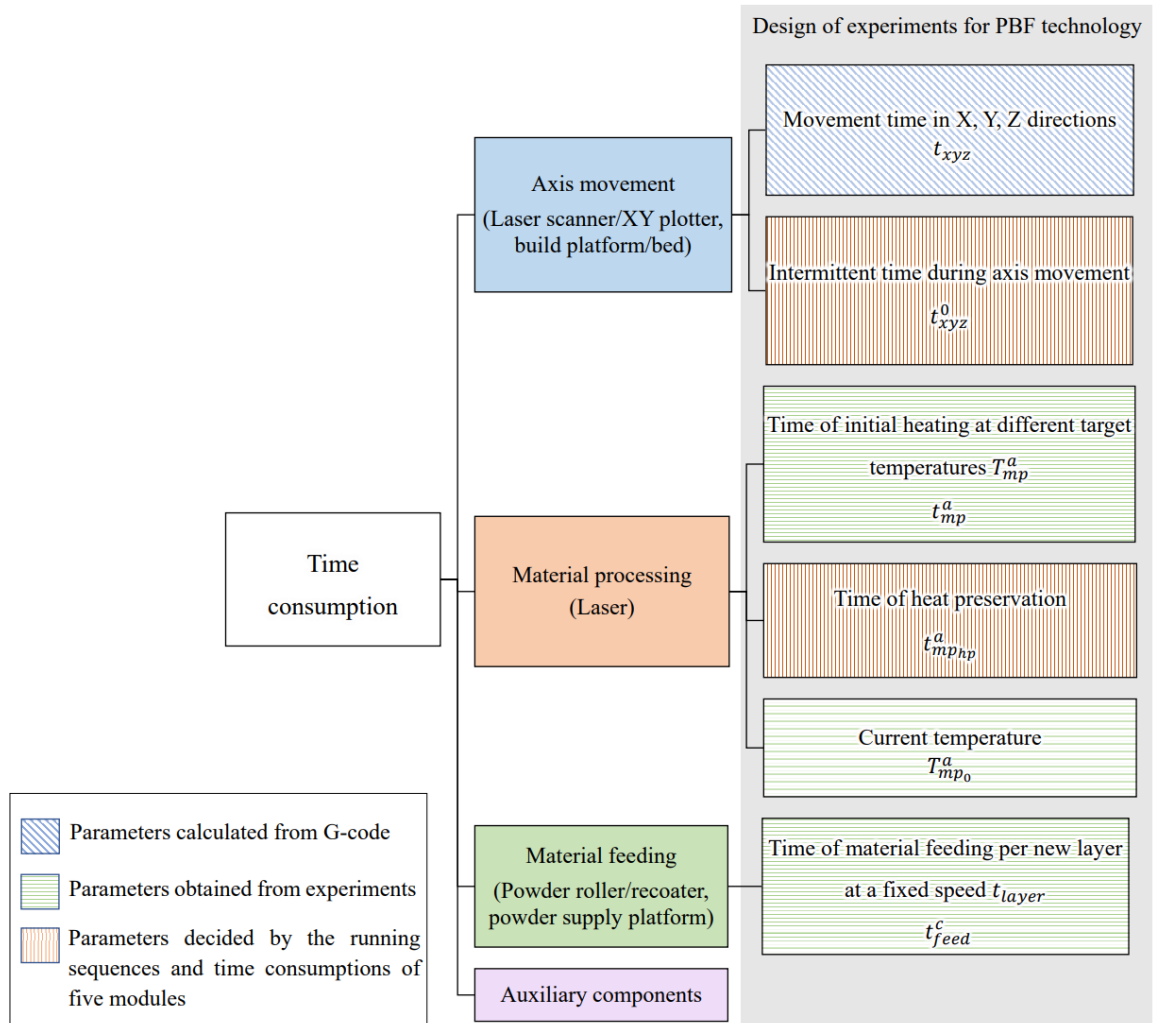
Figure 5.16: Three types of parameters for the time modelling of PBF technology
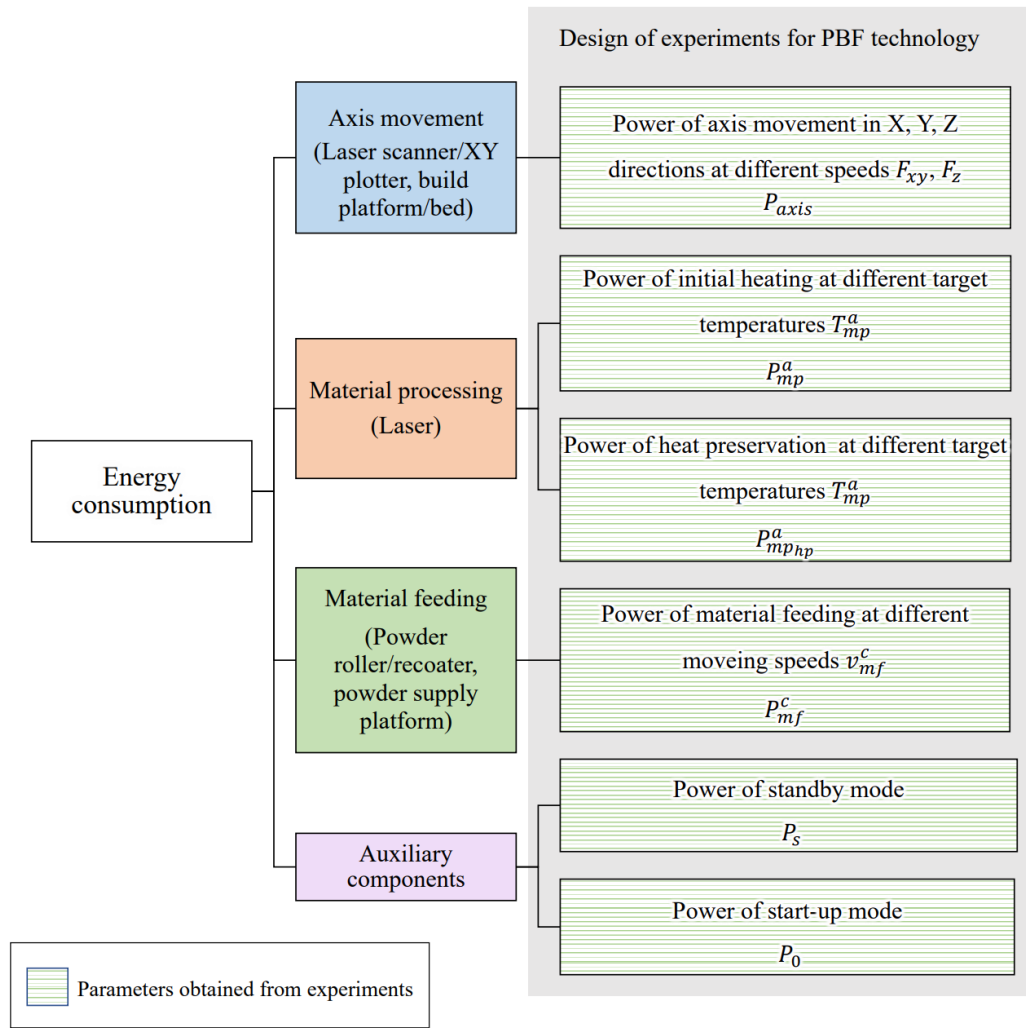
Figure 5.17: Three types of parameters for the energy modelling of PBF technology
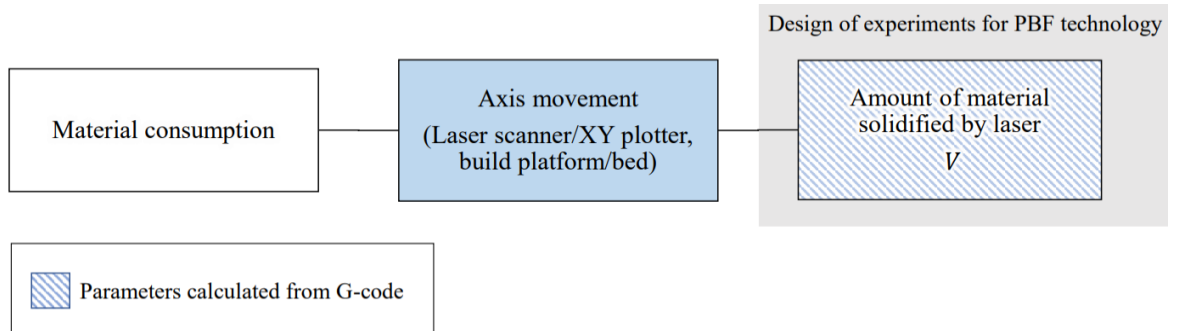
Figure 5.18: Three types of parameters for the material modelling of PBF technology

Figure 5.16 to **Figure 5.18** present three types of parameters in the predictive models of PBF technology. In details, the first type of parameter can be obtained from G-code and comprises three parts: the time consumption t_{xyz} of axis movement with actual

displacements in X, Y, Z directions, the time consumption t_{mf}^c of material feeding and the volume V_{unit} of solidified powder in each displacement of axis movement.

The second type of parameter is derived from experimental measurements. **Table 5.12** lists all parameters to be measured under different related process parameters. As discussed in **Section 5.3.4**, the material feeding module needs extra time t_{feed}^c to transport the material from the powder stock to the build platform. During this time, the axis movement module is in a standby state to wait for the completion of material feeding. This period of time belongs to the interval time of axis movement. According to $t_{feed}^c = t_{layer} \cdot LN$ in **Equation (5.8)**, the time consumption t_{layer} of material feeding per layer should be measured through experiments in order to calculate the total time t_{feed}^c of material feeding for new layers. Furthermore, the current temperature $T_{mp_0}^a$ of the material processing module, and the standby power P_s and start-up power P_0 of auxiliary components are all fixed constants without any related process parameters. Moreover, other parameters in **Table 5.12** are measured under different values of their related process parameters. All the time and apparent powers to be measured for this PBF technology are tested by using a power meter. All current temperatures to be measured are recorded directly through the display unit of the AM machine.

The third type of parameter is dependent on the running sequences and time consumptions of the five modules. In PBF technology, this parameter includes two parts: the interval time t_{xyz}^0 during axis movement and the heat preservation time $t_{mp_{hp}}^a$ of the material processing module.

Table 5.12: Parameters to be measured through experiments under different related process parameters for PBF technology

Module	Parameters	Meanings	Related process parameters	Meanings
Material processing	t_{mp}^a	Initial heating time	T_{mp}^a	Target temperature
	P_{mp}^a	Apparent power of initial heating		
	$P_{mp_{hp}}^a$	Apparent power of heat preservation		
	$T_{mp_0}^a$	Current temperature	None	None
Axis movement	P_{axis}	Apparent power of axis movement	F_{xy}, F_z	Speed of axis movement in X, Y, Z directions
Material feeding	t_{feed}^c	Time of material feeding for new layers	t_{layer}	Time of material feeding per new layer
	P_{mf}^c	Apparent power of material feeding	F_{xy}	Speed of axis movement in X, Y directions
Auxiliary components	P_s	Standby power	None	None
	P_0	Start-up power	None	None

The above two examples illustrate three types of parameters that form the predictive models of different AM technologies. The parameters to be measured through experiments are determined by the machine characteristics. Based on the experiments, polynomial regression method is applied to curve-fit the functional relationships between the measured parameters and their related process parameters. The coefficients in these functions are finally obtained to form the predictive models.

5.7. Additional experiments to improve prediction accuracy

The previous section discusses the design of experiments for consumption modelling. This section presents the additional experiments for testing the actual values of certain parameters in the predictive models in order to improve the prediction accuracy. In a practical manufacturing context, some parameters in the predictive models are affected by the characteristics of the particular machine and material. For example, motor out-of-step is caused by the high loads and insufficient torques of stepper motors during high-speed axis

movement and high-rate material feeding. The occurrence of motor out-of-step leads to the axis movement module and material feeding module failing to reach the specified movement speeds and feeding rates. Therefore, to improve the prediction accuracy, additional experiments are conducted to test the actual speed of axis movement and actual rate of material feeding.

Except for the above example, there are other similar factors that lead to deviations between the parameter values and the actual values. Thus, the purpose of additional experiments is to reduce the impact of these deviations on the accuracy of the predictive models. For AM machines with superior performance, or in the case of limited experimental resources and time, it is unnecessary to spend extra time on additional experiments. Based on the characteristics of different AM technologies, details of additional experiments are described below. Similar to the previous section, fused deposition modelling (FDM) and powder bed fusion (PBF) technologies as used again as two examples for illustration purposes.

Figure 5.19 presents three common factors affecting the performance of an FDM 3D printer. The running of the X, Y, Z axes in a Cartesian system is driven by three stepper motors in X, Y, Z directions. Each motor is responsible for the axis movement in one direction. Through experiments on an ANYCUBIC i3 Mega FDM 3D printer and Monoprice Mini Delta three-linear slider FDM 3D printer, it was observed that a speed of axis movement above 3000*mm/min* can cause the overloading and out-of-step of the stepper motors. In addition, the material feeding module is driven by another stepper motor and the high-speed feeding of the polylactic acid (PLA) filament can also cause motor out-of-step. This is because the material cannot be melted in time when the feeding rate exceeds 6000*mm/min*, resulting in an insufficient supply of material for each displacement.
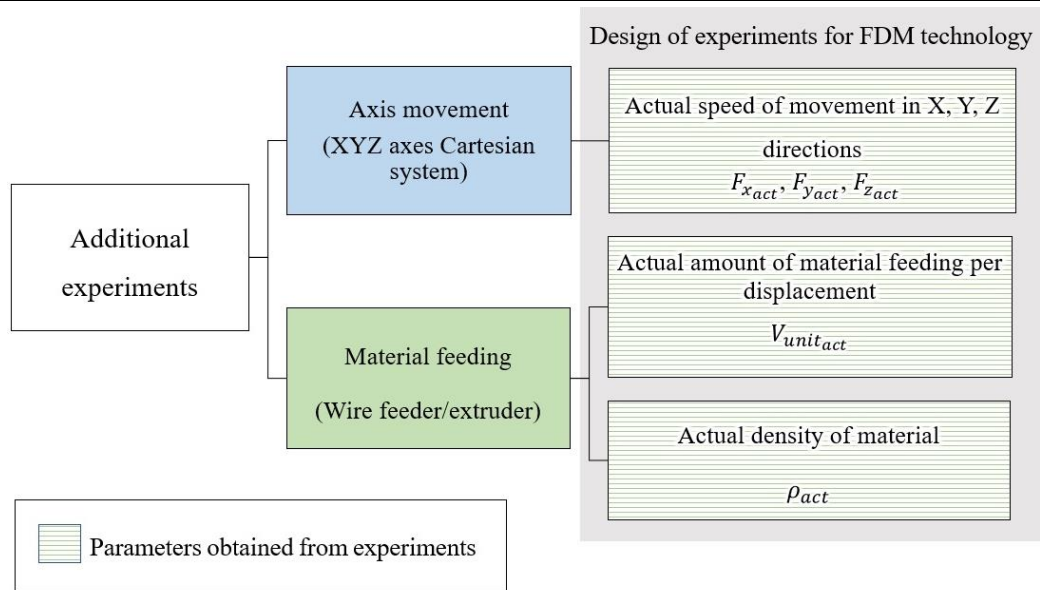
Figure 5.19: Additional experiments on FDM technology

Therefore, additional experiments are conducted to measure the actual movement speeds $F_{x_{act}}$, $F_{y_{act}}$, $F_{z_{act}}$ in X, Y, Z directions. Their functional relationships with the expected speeds F_x, F_y, F_z are modelled from **Equation (5.32)** to **Equation (5.34)**. The coefficients in these functions are obtained by using polynomial regression method.

$$F_{x_{act}} = f(F_x) \tag{5.32}$$

$$F_{y_{act}} = f(F_y) \tag{5.33}$$

$$F_{z_{act}} = f(F_z) \tag{5.34}$$

Based on the above, the actual resultant velocity $F_{xy_{act}}$ is calculated as the vector sum of the actual speeds $F_{x_{act}}$, $F_{y_{act}}$ in X, Y directions, as expressed in **Equation (5.35)**. Both actual speeds $F_{xy_{act}}$ and $F_{z_{act}}$ are used to replace the expected speeds F_{xy} and F_z in **Equation (4.16)**.

$$F_{xy_{act}} = \sqrt{F_{x_{act}}^2 + F_{y_{act}}^2} \tag{5.35}$$

In addition, motor out-of-step commonly occurs during high-rate material feeding in general AM technologies. To improve the prediction accuracy, additional experiments are conducted to measure the actual amount $V_{unit_{act}}$ of material feeding per displacement of axis movement. The measured results can be used to replace the expected amount V_{unit} of material feeding provided by G-code. Furthermore, the actual density ρ_{act} of material is also measured to replace the quoted density ρ. The improved conceptual model of material consumption is expressed as **Equation (5.36)**.

$$M_{total} = \rho_{act} \cdot \sum V_{unit_{act}} \qquad (5.36)$$

Similar to FDM, there are two factors affecting the performance of powder bed fusion (PBF) technology: the out-of-step of stepper motors caused by high-speed axis movement and the actual density of material, as shown in **Figure 5.20**. Since the powder is supplied by the powder roller, there is no motor out-of-step occurring during the material feeding. Therefore, the same experiments are conducted to calculate the coefficients between the actual speeds $F_{x_{act}}$, $F_{y_{act}}$, $F_{z_{act}}$ and the expected speeds F_x, F_y, F_z. The actual material density ρ_{act} is also measured.
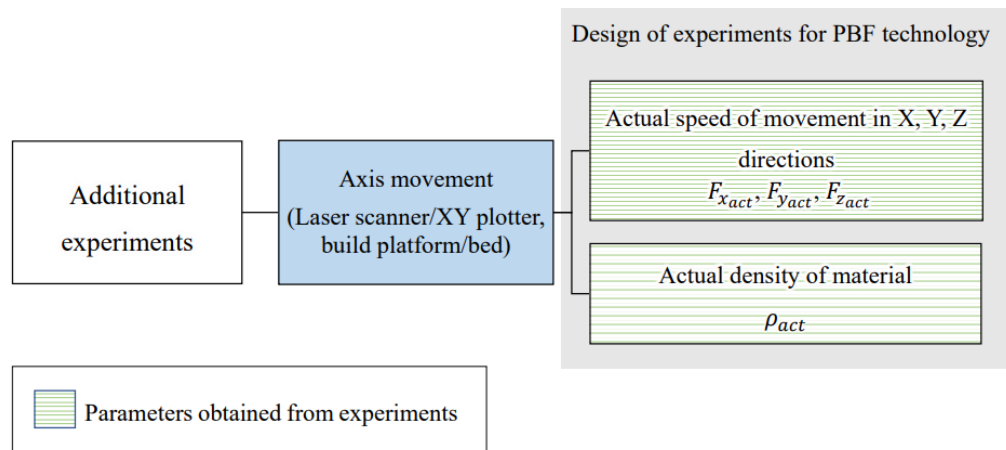
Figure 5.20: Additional experiments on PBF technology

The results measured above are used to replace the original parameters in the predictive models. The additional experiments conducted in this step are based on the prediction

accuracy of the original models, machine performance and customer demands. During the process of data-driven modelling, this step requires more time and a greater number of experiments to improve the prediction accuracy.

5.8. Application indication of prediction modelling

The previous sections present the details of prediction modelling of AM time, energy and material consumptions. This section summarises the previous contents and provides a concise indication of applying the prediction modelling method to real-world AM systems.

Module classification
- Classify the energy-consuming components into five types of modules based on their functions.

Power and time tests of AM system
- Record the power profies of a complete AM process and five modules individually.
- Classify the working states of each module.
- Mark the starting point of each module on the power plot of the complete AM process based on G-code commands.
- Formulate the Gannt chart: correspond the power plot of each module to its starting point on the time axis.

Generate prototype of predictive models
- Based on the Gannt chart, identify the parameters that need to be obtained to formulate the predictive models.
- Formulate the tree diagram: classify the parameters into three types:
  - 1).parameters to be calculated from G-code;
  - 2) parameters to be obtained from experiments;
  - 3). parameters that are decided by the running sequences and time consumptions of five modules

Hybrid modelling to obtain model parameters
- Physics-based modelling: calculate the first type of parameters based on G-code.
- Data-driven modelling: perform experiments on testing the second type of parameters and collect experimental data. For the parameters related to process parameters, obtain its function expressed by the process parameters through regression analysis method.
- Based on the Gannt chart, derive the third type of paramters.
- Finally, formulate the predictive models of time, energy and material consumptions

Figure 5.21: Basic workflow of prediction modelling of AM time, energy and material consumptions

The basic workflow of the prediction modelling of a new AM machine is summarised in **Figure 5.21**. At the beginning, which type of AM technology the current machine belongs to needs to be clarified. Referring to the table of module classification in **Figure 3.2**, all energy-consuming components of the AM machine should be identified and classified into five types of modules based their functions.

The second step is to figure out the manufacturing mechanism of the AM machine, i.e., the running sequences of modules, and the working states of each module. The aim is to formulate a Gannt chart that can intuitively reflect the operating rules of this AM machine. In this step, six power profiles need to be recorded and generated by using a power meter.

- At first, five modules are commanded to run separately to record the power profile of each module, as shown in **Figure 5.22**. Based on the manufacturing function, the working states of each module can be observed and classified. For example, when the material processing module is started to heat up to the specified temperature, it can be observed through the machine display that the module has two working states, namely initial heating and heat preservation. In initial heating state, the module is heated from the current temperature to the target temperature. In the heat preservation state, the module is maintained at the target temperature. It can also be observed from the power profile that the power curves in two states are completely different.

- In addition, the power profile of a general AM task printed by the AM machine needs to be recorded. Once the AM process starts, the power curve is gradually generated along the time axis, as shown in **Figure 5.22**. As each module is started up and running by following G-code commands, its starting point needs to be manually marked on the power profile. When the AM process is finished, the Gannt chart can be formulated by corresponding the power profiles of five modules to their starting points on the power profile of the AM task.
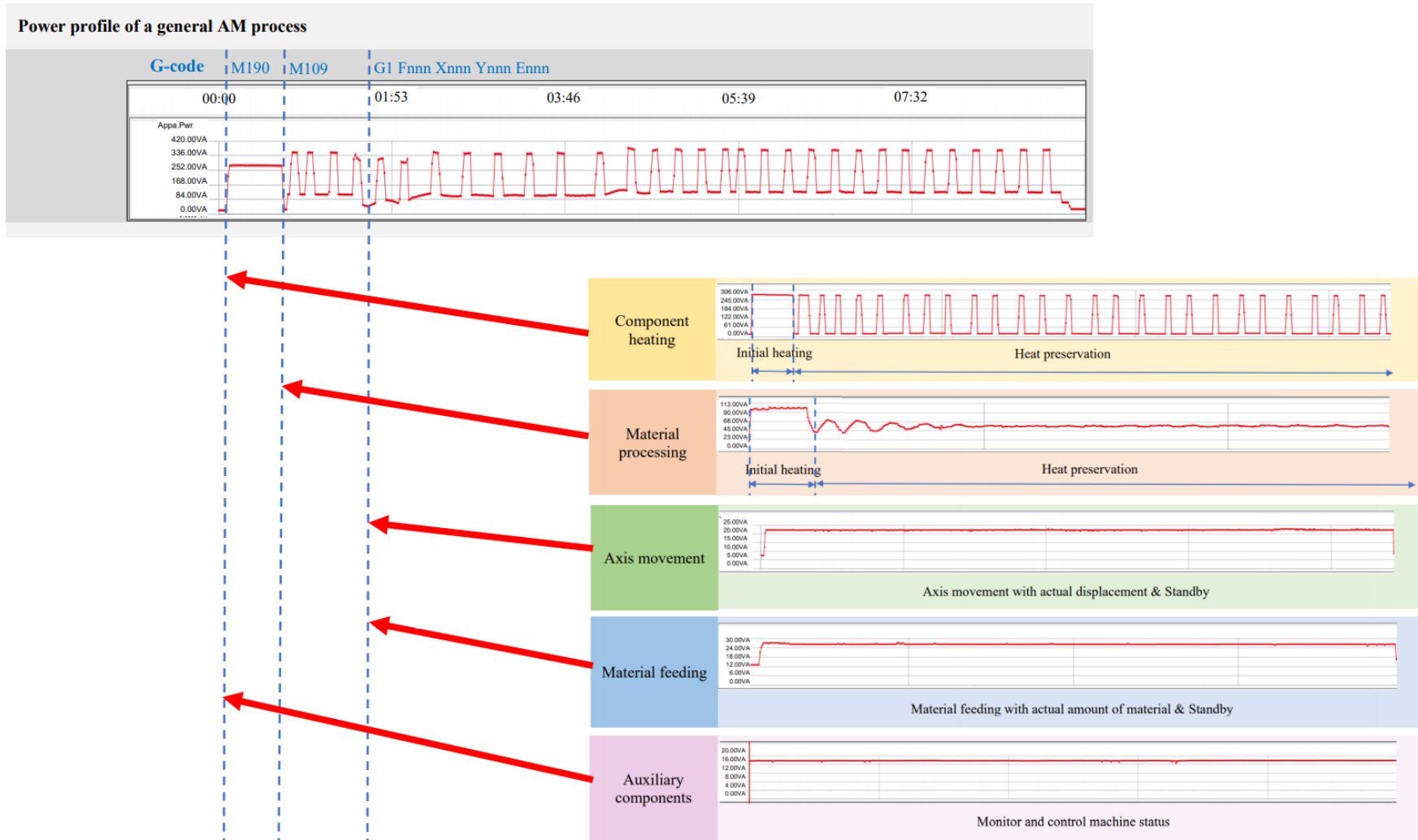
Figure 5.22: Instruction of the power profile of each module corresponding to the starting point on the power profile of an AM process

The third step is to identify the parameters that formulate the predictive models. The previous sections have defined the predictive models for general AM technologies. The parameters in the predictive models can be classified into three types:

1). The first type refers to the parameters to be calculated from G-code, including the time of axis movement with actual displacements, and the amount of material feeding;

2). The second type refers to the parameters to be obtained through experiments, including the apparent powers of all modules, the initial heating time and current temperatures of modules to be heated;

3). The third type refers to the remaining parameters decided by the running sequences and time consumptions of the five modules based on the Gannt chart.

Above parameters can be summarised to formulate the tree diagram as discussed in previous sections. The tree diagram can clearly show all the parameters needed to build the predictive models and their types.

The final step is to obtain the models of above parameters through hybrid-modelling method. In physics-based modelling, the first type of parameters can be directly calculated from G-code. In data-driven modelling, the second type of parameters can be obtained through experiments under different process parameters. Regression analysis method is applied to process the experimental data and derive the functional relationships between measured parameters and their related process parameters. Based on the Gannt chart, the third type of parameters can be modelled as the functions of other parameters. For example, the time consumption t_{aux} of auxiliary components is equal to the total time consumption of other four modules. Once obtain the models of all parameters, the predictive models of AM time, energy and material consumptions can be finally formulated.

From the practical applications of proposed modelling method, it is found that the predictive models of some specific modules need to be adjusted according to machine

characteristics. In order to facilitate the consumption modelling of general AM technologies, the following points are summarised to be noticed in a practical manufacturing context.

- Firstly, the proposed method has assumed that some parameters in the models are related to the process parameters. For example, since the material processing module processes raw material by being heated to a specified temperature, the target temperature T_{mp}^a is the only process parameter that determines the energy consumption of this module. Thus, in **Section 5.4.2**, we assume that the apparent powers P_{mp}^a and $P_{mp_{hp}}^a$ of material processing in initial heating state and heat preservation state are the functions of the target temperature T_{mp}^a. However, due to the machine particularity, it is possible that the measured power is constant and is irrelated with the process parameter. In this case, the model of such parameters needs to be adjusted according to the experimental results.

- Secondly, the additional experiments are optional and determined by machine characteristics and customer demands. For example, the stepper motors of some AM machines lose steps during the material deposition process, which results in the deviation between the actual speed and the expected speed of axis movement. In this case, the experimental measurements can be added to obtain the relationship between the actual speed and the expected speed. Nota that the purpose of additional experiments is to improve the prediction accuracy of the predictive models for some AM machines that have deviations between the ideal and actual values of some model parameters. For AM machines with superior performance, or in the case of limited experimental resources and time, there is no need to spend extra time on additional experiments.

5.9. Summary

The conceptual predictive models proposed in **Chapter 4** are refined in this chapter. Detailed modelling principles and procedures of each module are presented in this chapter. To begin,

the different working states of each module are defined. Then, the time, energy and material consumptions of each working state are modelled as functions of related process parameters. All of the parameters that form the predictive models are summarised as three types: parameters calculated from G-code, parameters obtained from experiments, and parameters determined by the running sequences and time consumptions of the five modules. In more detail, the time consumption of axis movement with actual displacements and the amount of material feeding are directly modelled from G-code. Experiments are designed to measure the apparent powers and time consumption of other modules to complete the predictive models. Considering the factors affecting the prediction accuracy, additional experiments are designed to test the related parameters, such as the actual speed of axis movement, actual amount of material feeding and actual material density.

The hybrid modelling based on the different working states of the modules is one of the main contributions of this research. An AM machine is divided into five types of modules, with different working states based on the functions of the components. This method provides a clear, general and customised environment to model the time, energy and material consumptions of each module. The physics-based modelling fully uses the manufacturing information of the G-code, since this code provides the accurate coordinates, speed of axis movement and amount of material feeding. Plus, G-code also provides the running sequences of the five modules. This information helps to clearly identify the time consumption and power profile of each module, which significantly simplifies the modelling process and reduces the workload of experiments in data-driven modelling. The data-driven modelling and additional experiments fully consider the characteristics of machine and material. This has been shown to achieve an effective prediction in subsequent experimental validations.

To validate the effectiveness of proposed prediction method, two case studies of fused deposition modelling (FDM) 3D printers are presented in **Chapter 7**. But first, in **Chapter 6**, three predictive models are used as objective functions in the loop of the optimisation algorithm.

CHAPTER 6   MULTI-OBJECTIVE OPTIMISATION TO REDUCE TIME, ENERGY AND MATERIAL CONSUMPTIONS OF ADDITIVE MANUFACTURING TECHNOLOGIES

6.1. Introduction

This chapter introduces the details of multi-objective optimisation, which aims to obtain the most feasible solution set of process parameters to minimise the time, energy and material consumptions of an AM process. The improvement and application of meta-heuristic algorithms in this optimisation problem is an innovative approach. Due to the wide range of applications in sophisticated optimisation problems, one of meta-heuristic algorithms is selected as the optimisation tool. Since non-dominated sorting genetic algorithm II (NSGA-II) has been widely used to solve optimisation problems with two or three objectives in industrial manufacturing, it is improved and applied in this study to determine the most appropriate solution of process parameters. On the basis of the original algorithm, the prediction process – from inputting the process parameters into CAM to the generation of G-code – is embedded into the process of objective function calculation. The reason for this is that each solution of process parameters generates a unique G-code file. The information in G-code is fully used by the consumption modelling and thus the predicted consumptions are also unique.

This chapter explains in detail each optimisation step that was improved and applied in the problem. The steps include population initialisation, non-dominated sorting, crowding distance ranking, elitism, selection, crossover operator, mutation operator and recombination. Experiments are designed to produce Pareto fronts under different combinations of optimisation parameters, including population size, number of generations, crossover probability and mutation probability. hypervolume (HV) indicator is used to evaluate all

obtained Pareto fronts and determine the optimum front that has the maximum HV value. The solutions in the optimum Pareto front can be used as a reference, which aids the decision making of the most feasible solution of process parameters for consumption reduction.

6.2. Application of NSGA-II in the multi-objective optimisation problem

In this study, the original NSGA-II is improved to be adaptable in this optimisation problem. **Figure 6.1** presents the flowchart of the improved algorithm. To start, the optimisation problem has been defined in **Section 4.4**. The three objectives (i.e. $M = 3$) refer to the total time, energy and material consumptions in an AM task. The population size N refers to the number of individuals in the initialised population. Each individual represents one candidate solution of process parameters. The innovative improvement based on the original NSGA-II is described as follows.

In physics-based modelling, since each combination of process parameters will produce a unique G-code file, the parameters calculated from G-code will have unique values. As a result, the predictive models of different process parameters will also be different. Thus, the process of objective function calculation in the original NSGA-II needs to be adjusted in this study. As shown in **Figure 6.1**, the entire prediction process is embedded in the process of objective function calculation. In more detail, the process parameters of each solution in the current population are input into the slicer software to generate the corresponding G-code. After that, the data in G-code is processed to calculate the time of axis movement with actual displacements and the amount of material feeding. The calculated parameters are imported into the predictive models, while other parameters have already been obtained through experiments. Once the predictive models are formulated, the consumptions are predicted and used as the fitness values of each solution for the subsequent step of non-dominated sorting. Although the above process needs to be performed for every new-born individual of the offspring generation, it can achieve high-precision predictions and the final optimum solutions will be more convincing.
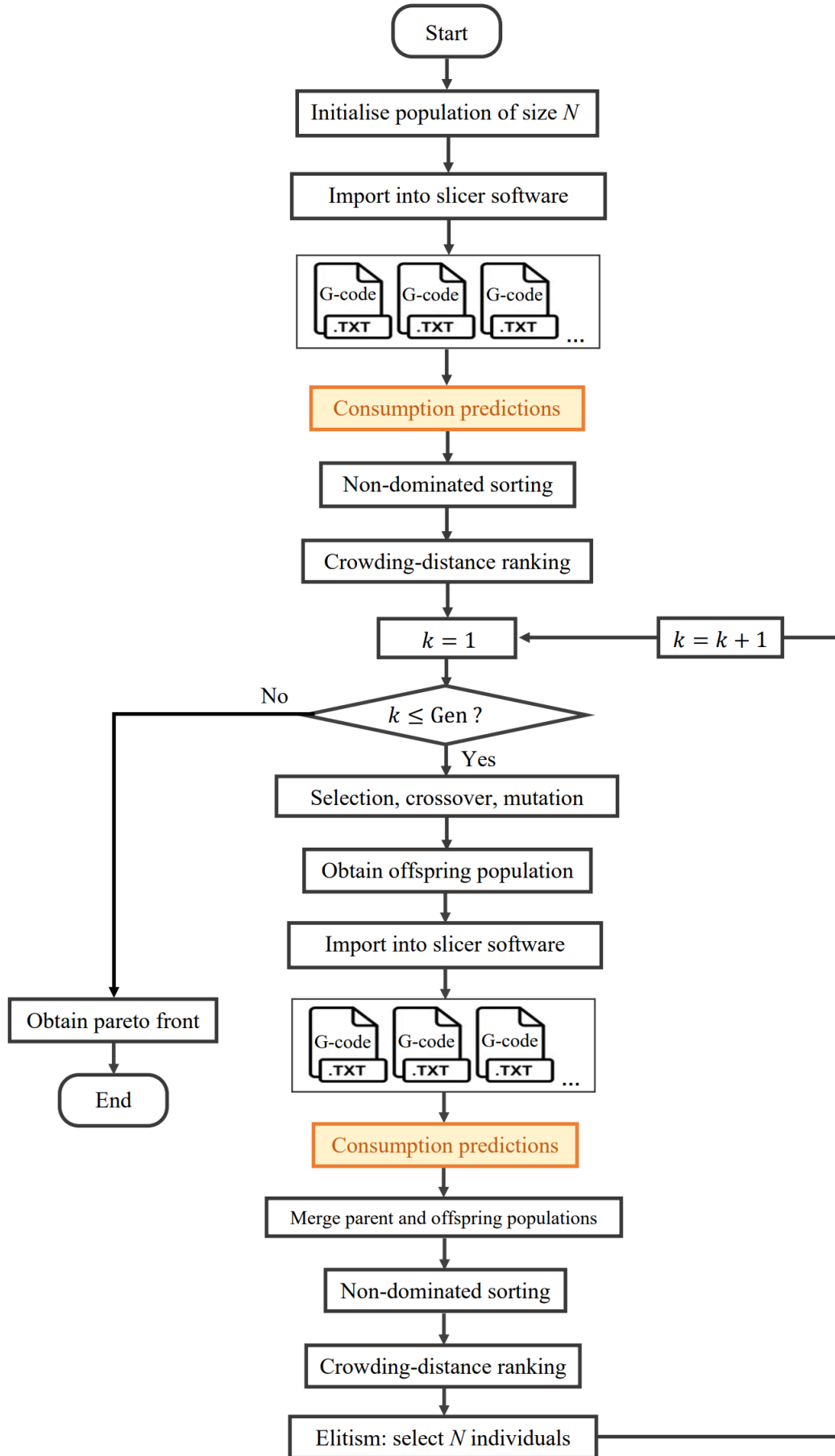
Figure 6.1: Flowchart of NSGA-II algorithm applied to the multi-objective optimisation problem in this study

In the following sections, the details of each optimisation step applied in this study will be discussed.

6.2.1. Encoding scheme of population initialisation

A random population is first initialised based on the problem constraints and ranges. Learning from the natural selection and genetic mechanism of Darwin's theory of evolution, all candidate solutions in the population are converted into chromosomes and the process parameters are encoded as genotypes distributed on the chromosomes (Whitley, 1994; Mitchell, 1998). In this study, the population size is defined as N. It indicates that there are N numbers of individuals randomly created as chromosomes. Each individual represents a solution containing n numbers of decision variables, which are encoded as n genes distributed along the chromosome. As shown in **Figure 6.2**, I_r^N denotes the rth gene among the n genes on the Nth chromosome. Each gene is assigned a random value within its variable range $[I_r^{\ L}, \ I_r^{\ U}]$. The definition of the variable range is discussed as follow.

Process parameters	Symbols	Parameter ranges		Granularity
		Lower bound	Upper bound	
Layer thickness	LT	0.030mm	0.400mm	0.001mm
Infill density	ID	1%	100%	5%
Target temperature of material processing module	T_{mp}^1	190℃	270℃	1℃
Speed of axis movement in X, Y directions	F_{xy}	5mm/s	140mm/s	1mm/s
Speed of axis movement in Z directions	F_z	5mm/s	30mm/s	1mm/s
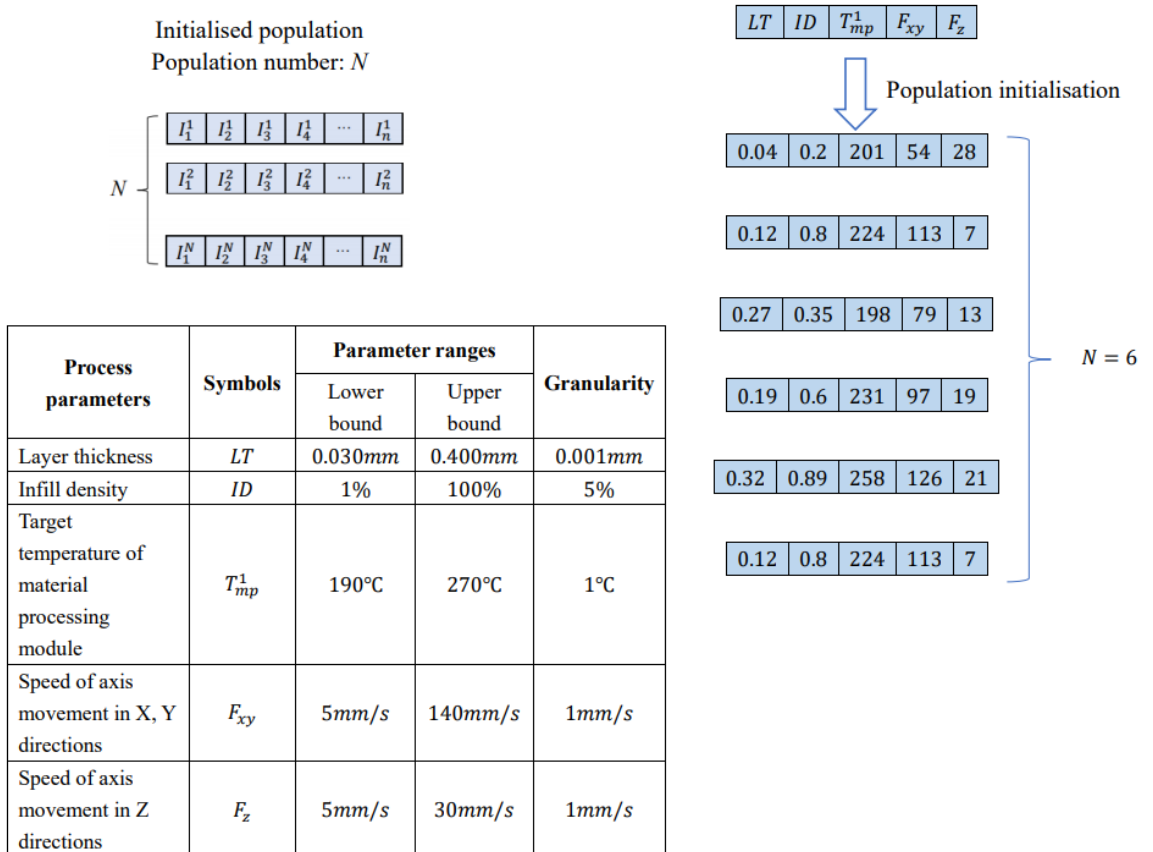
Figure 6.2: Example of population initialisation using real-coded genetic operations

The process parameters to be optimised contain integers, decimals and percentages. Therefore, according to the number of types of process parameters, this study uses the real-coded genetic algorithm (GA) to encode the decision variables. The variables are represented directly by the process parameters, where the ranges from lower bounds $I_r{}^L$ to upper bounds $I_r{}^U$ are determined by the machine characteristics. **Figure 6.2** presents an example of the population initialisation process. In this example, assume that there are six (i.e. $N = 6$) populations to be initialised, while five types of process parameters (i.e. $n = 5$) are considered in this three-objective problem, namely layer thickness LT, infill density ID, target temperature T_{mp}^1 of the material processing module, speed F_{xy} of axis movement with or without material feeding in X, Y directions, and speed F_z of axis movement in Z direction. Therefore, six individuals are initialised as six chromosomes. Five genes (i.e. five process parameters) on each chromosome are randomly assigned within the user-defined parameter range.

The granularity of each process parameters is defined based on the coding rules of slicer software. The reason is that some slicer software may have special regulations for the digital formats of some process parameters. For example, in Cura slicer software, the granularity of target temperature is 1°C for the material processing module. It indicates that the target temperature input into the slicer software must be an integer. In order to ensure that the slicer software can generate G-code normally, the process parameter of target temperature needs to be rounded to an integer before importing into the software.

After the initialisation, the parameters in each individual case are imported into the slicer software to yield the corresponding G-code file. The data in G-code is automatically processed to calculate the time consumption of axis movement and the amount of material feeding. After this, these results are imported into three predictive models to calculate the time, energy and material consumptions. These predicted results can be used as the fitness values for the subsequent non-dominated sorting and crowding distance ranking. Once all individuals in the initialised population are formulated (i.e. $j = N$), the optimisation cycle will begin and continue to the next step.

6.2.2. Elitism based on non-dominated sorting and crowding distance ranking

Deb et al. (2002) show in detail the calculation method of non-dominated sorting. The pseudo codes are presented in **Appendix I (1)**. The basic steps of applying the method in this study are summarised as follows.

- At first, the fitness values of each individual (i.e. every solution of the process parameters) are calculated through three objective functions $\mathcal{F}_1(\mathbf{x})$, $\mathcal{F}_2(\mathbf{x})$, $\mathcal{F}_3(\mathbf{x})$, which respectively denote the total time consumption t_{total}, total energy consumption E_{total}, and total material consumption M_{total} of individual $\mathbf{x}$.

- Then, every individual needs to calculate two entities: the domination count $\mathcal{L}_{\mathbf{x}_p}$ of the individual $\mathbf{x}_p$ and the solution set $S_{\mathbf{x}_p}$ containing all individuals dominated by individual $\mathbf{x}_p$. To determine the dominance relationship, any two individuals are compared with each other based on the fitness values. For example, when all three consumptions $\mathcal{F}_{Obj}(\mathbf{x}_p)$ of individual $\mathbf{x}_p$ are less than the three consumptions $\mathcal{F}_{Obj}(\mathbf{x}_q)$ of individual $\mathbf{x}_q$, it means that individual $\mathbf{x}_p$ dominates individual $\mathbf{x}_q$.

- As the first step in finding the first non-dominated front, the individual $\mathbf{x}_p$ with zero domination count (i.e. $\mathcal{L}_{\mathbf{x}_p} = 0$) is ranked with level L_1. In other words, if the individual $\mathbf{x}_p$ is not dominated by any other individuals in current population, then it belongs to the first non-dominated front.

- The rest of the individuals $\mathbf{x}_q$ dominated by $\mathbf{x}_p$ are assigned with domination counts reduced by one. Those individuals $\mathbf{x}_q$ with new dominance values of zero (i.e. $\mathcal{L}_{\mathbf{x}_q} = 0$) are assigned with the second level L_2, which belongs to the second non-dominated

front. The remaining individuals are compared by following the same non-domination criteria until all individuals are sorted.

According to the front levels from low to high, the individuals in the current population are put into the parent population until it is filled, as shown in **Figure 6.3**. When individuals located in the same front level and yet exceeding the population size N are encountered (e.g. individuals on level L_3 in **Figure 6.3**), the density of individuals will be compared through crowding distance ranking. This is to ensure that the individuals located in lesser crowded regions are preserved and others are eliminated.
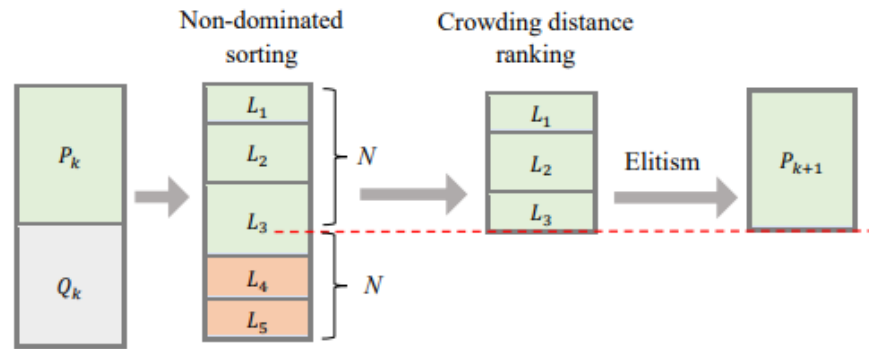
Figure 6.3: Schematic of NSGA-II non-dominated sorting and crowding distance ranking

Referring to Deb et al. (2002), the pseudo codes of crowding distance ranking are summarised in **Appendix I (2)**. The crowding distance refers to the Euclidean distance between two adjacent individuals in the same front. It is calculated to estimate the density of individuals surrounding a particular individual (Verma et al., 2021).

In this study, there are C individuals located on the same front level. The two boundary individuals $\mathbf{x}_1$ and $\mathbf{x}_C$ refer to the solution sets of process parameters that have at least one maximum or minimum consumption among the time, energy and material consumptions. This is to ensure that all intermediate individuals can participate in the comparison of crowding distance. The distance values $\mathcal{D}[\mathbf{x}_t]_{distance}$ of other intermediate individuals $\mathbf{x}_t$ are calculated as the absolute normalised differences between the objective values $\mathcal{F}_{Obj}(\mathbf{x}_{t+1})$ and $\mathcal{F}_{Obj}(\mathbf{x}_{t-1})$ of two adjacent individuals $\mathbf{x}_{t+1}$ and $\mathbf{x}_{t-1}$, as shown in

Equation (6.1). $\mathcal{F}_{Obj}{}^{max}$ and $\mathcal{F}_{Obj}{}^{min}$ denote the maximum and minimum time, energy and material consumptions of all individuals on the current front level.

$$\mathcal{D}[\mathbf{x}_t]_{distance} = \sum_{Obj=1}^{3} \frac{\mathcal{F}_{Obj}(\mathbf{x}_{t+1}) - \mathcal{F}_{Obj}(\mathbf{x}_{t-1})}{\mathcal{F}_{Obj}{}^{max} - \mathcal{F}_{Obj}{}^{min}} \qquad (6.1)$$

The elitism is performed by following two criteria: for two individuals with two different non-domination ranks, the individual with the lower or better rank will be retained; otherwise, for two individuals in the same front, the individual with a higher (i.e. lesser crowded) distance will be retained (Deb et al., 2002). After that, all retained individuals in the elite population P_{k+1} are used for the selection of parents to produce offspring Q_{k+1} through simulated binary crossover (SBX) operator and polynomial mutation (PLM) operator.

6.2.3. Binary tournament selection

Tournament selection is an efficient and robust selection mechanism commonly used in genetic algorithms (GAs) attributed to its adjustable selection pressure. Compared with other selection methods in GAs, the coding of tournament selection is simple and effective for both parallel and non-parallel architecture (Fang and Li, 2010). In NSGA-II, tournament selection is used to select individuals as parents from the elite population to a mating pool. The selected individuals are the ones whose genes will be inherited by the next generation (Miller and Goldberg, 1995). Usually, the tournaments are held between two individuals (i.e. binary tournament) (Blickle and Thiele, 1996). Therefore, this study utilises the binary tournament selection to realise the selection of parents.

The pseudo codes of binary tournament selection are summarised in **Appendix I (3)**. To ensure that the population size of selected parents is *N*, the number of tournaments is defined as *N*. In each tournament, two individuals (e.g. $\mathbf{x}_m$, $\mathbf{x}_n$) in the elite population P_{k+1} are randomly selected to participate the tournament. Based on the non-dominated levels, the individual that has the lower (or better) level is selected as a parent. When encountering two individuals on the same level, the crowded-comparison operator is used to guide the

selection, and the one that has a larger crowding distance is selected as a parent. The aim of this step is to achieve a uniformly spread-out Pareto front (Deb et al., 2002). After the selections, the parent population containing N individuals is used to produce offspring Q_{k+1} through simulated binary crossover (SBX) operator and polynomial mutation (PLM) operator.

6.2.4. Simulated binary crossover operator

This study uses real-coded genetic algorithm (GA) to encode the decision variables. It indicates that the six genes on the chromosome are directly represented by six process parameters for the AM process. Therefore, simulated binary crossover (SBX) is applied as the real-coded recombination operator to deal with real parameters, which simulates the single-point crossover on binary strings of decision variables (Beyer and Deb, 2001; Deb and Agrawal, 1995, Raghuwanshi and Kakde, 2004; Deb et al., 2007). Note that each individual in parent population has a pre-defined probability pc to participate in the crossover process. It indicates that the individuals not participating in the crossover process will be replicated as offspring.
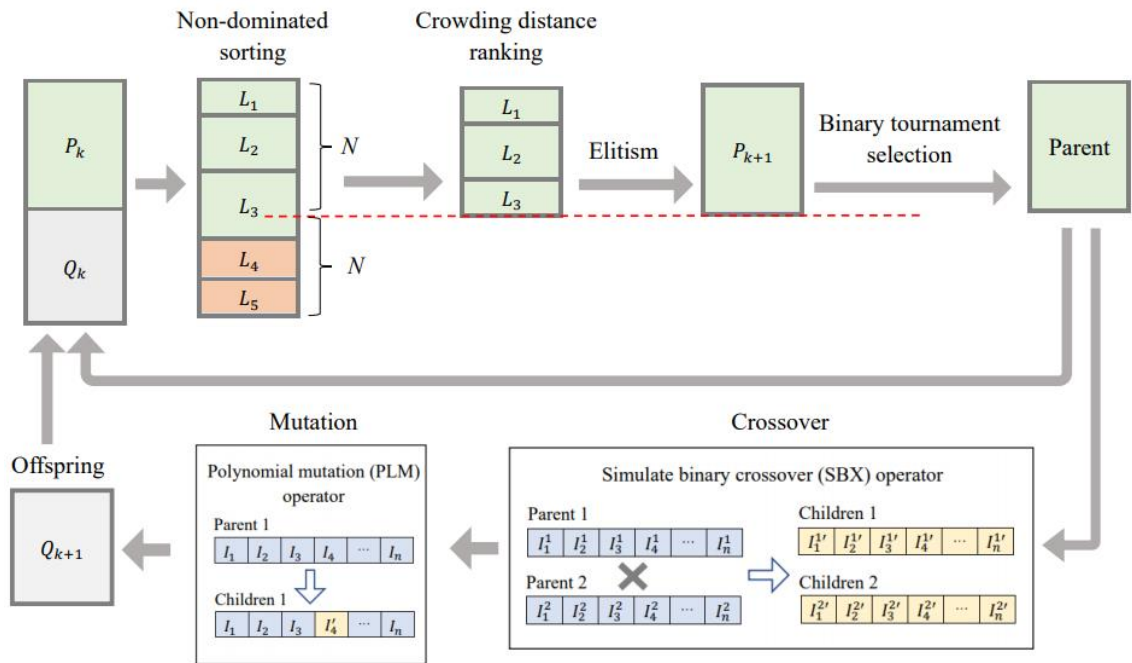
Figure 6.4: Schematic of NSGA-II optimisation process using simulated binary crossover (SBX) operator and polynomial mutation (PLM) operator

The working principles of binary crossover are summarised into four attributes: 1) the total gene value of offspring is the same as the total gene value of the parent; 2) each point on the coded strings has the same probability to be the crossover point; 3) offspring have a higher probability to be close to the parent; and 4) the crossover point in the lower bit of a coded string leads to a smaller change in the gene value (Deb et al., 2007).

SBX is applied by using the probability density function to simulate the above working principles of binary crossover. As shown in **Figure 6.4**, the process parameters located on the same locus of two parent chromosomes are p_1 and p_2, and their offspring are c_1 and c_2. By following the above principles, the sum of the gene values of the parent is equal to the sum of gene values of the offspring, as expressed in **Equation (6.2)**. A spread factor β_c is used to indicate the ratio of the absolute difference between offspring and parent, as expressed in **Equation (6.3)**. When $\beta_c < 1$, the offspring are enclosed by the parent; when $\beta_c = 1$, the offspring are the same as the parent; and when $\beta_c > 1$, the offspring enclose the parent (Deb and Agrawal, 1995). By substituting β_c into **Equation (6.2)**, two offspring can be expressed as **Equation (6.4)** and **Equation (6.5)**.

$$p_1 + p_2 = c_1 + c_2 \tag{6.2}$$

$$\beta_c = \frac{|c_2 - c_1|}{|p_2 - p_1|} \tag{6.3}$$

$$c_1 = \frac{(p_1 + p_2)}{2} - \frac{\beta_c(p_2 - p_1)}{2} \tag{6.4}$$

$$c_2 = \frac{(p_1 + p_2)}{2} + \frac{\beta_c(p_2 - p_1)}{2} \tag{6.5}$$

Referring to Deb and Agrawal (1995), Deb et al., (2007), the probability distribution of spread factor β_c is defined as a specified probability density function $c(\beta_c)$ in **Equation (6.6)**. As shown in **Figure 6.5**, a larger distribution index η_c gives a higher probability for creating the offspring closer to the parent. Additionally, a random number u_c between 0 and 1 is defined, which indicates the cumulative distribution function of $c(\beta_c)$ in **Equation**

(6.7). In **Figure 6.5**, u_c refers to the area under the probability curve from zero to an arbitrary point β_c^0. The closer that the value of u_c is to 0.5, the higher the probability that offspring are close to parents. Based on **Equation (6.6)** and **Equation (6.7)**, the spread factor β_c can be expressed as **Equation (6.8)**.

$$c(\beta_c) = \begin{cases} 0.5(\eta_c + 1)\beta_c{}^{\eta_c} & \beta_c \leq 1 \\ 0.5(\eta_c + 1)\frac{1}{\beta_c{}^{\eta_c+2}} & \beta_c > 1 \end{cases} \tag{6.6}$$

$$u_c = \int_0^{\beta_c^0} c(\beta_c)d\beta_c \tag{6.7}$$

$$\beta_c = \begin{cases} (2u_c)^{\frac{1}{\eta_c+1}} & 0 < u_c \leq 0.5 \\ \left(\frac{1}{2-2u_c}\right)^{\frac{1}{\eta_c+1}} & 0.5 < u_c \leq 1 \end{cases} \tag{6.8}$$
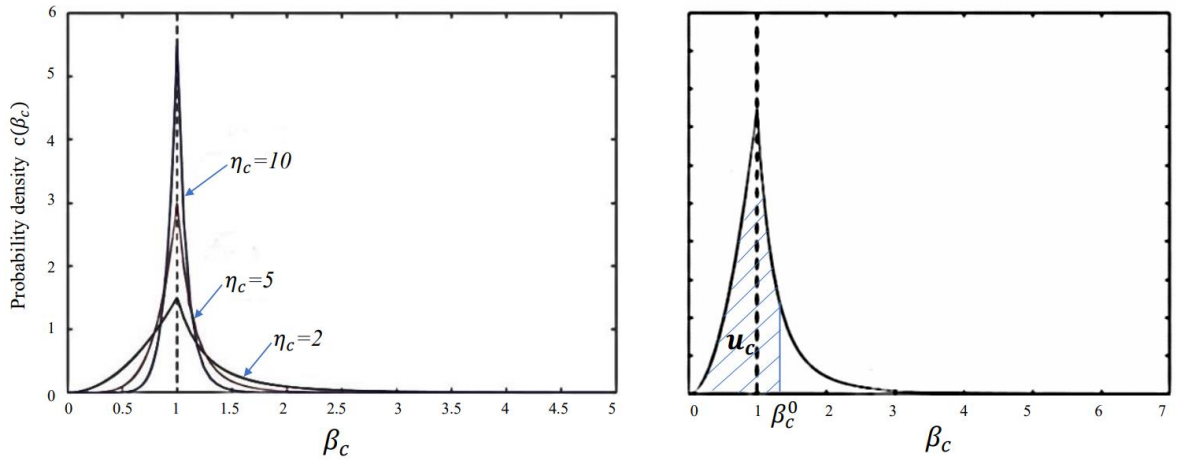
Figure 6.5: Probability density function of the spread factor β_c for SBX operator (Deb et al., 2002)

In this study, η_c is a non-negative real number defined by users, which decides the probability density of the offspring process parameter being close to the parent process parameter, while u_c is randomly assigned a value between 0 and 1 to determine the value of β_c at each crossover operation. Referring to **Equation (6.4)** and **Equation (6.5)**, **Equation (6.9)** and **Equation (6.10)** present examples of SBX crossover on the process parameter of layer thickness LT. LT_1 and LT_2 denote the layer thickness on two parent chromosomes, while LT_1' and LT_2' denote the offspring after the SBX crossover. The

parameter values of the two offspring are determined by the user-defined value of η_c and the random value of u_c.

$$LT_1' = \frac{(LT_1 + LT_2)}{2} - \frac{\beta_c(LT_2 - LT_1)}{2} \qquad (6.9)$$

$$LT_2' = \frac{(LT_1 + LT_2)}{2} + \frac{\beta_c(LT_2 - LT_1)}{2} \qquad (6.10)$$

6.2.5. Polynomial mutation operator

The polynomial mutation (PLM) operator evolved from Deb and Agrawal. (1995) prevents the premature convergence of sub-optimal solutions by using a polynomial probability distribution to mutate a gene on a parent chromosome to a neighbouring value (Subashini and Bhuvaneswari, 2012; Deb and Deb, 2014; Zeng et al., 2016). As shown in **Figure 6.6**, the PLM in real-coded genetic algorithm (GA) has an adjustable probability to create a solution close to the parent, or ensure the candidate solutions reaching the entire search space (Subashini and Bhuvaneswari, 2012). Here we define each individual in parent population has a pre-defined probability *pm* to participate in the mutation process. It indicates that the individuals not participating in the mutation process will be replicated as offspring.

In this study, the parent gene of a variable I_r is p_3 and its offspring is c_3. c_3 can be expressed as a value distributed around the parent p_3, as expressed in **Equation (6.11)**. A spread factor β_m is defined to determine the distance from offspring to parent in **Equation (6.12)**. Similarly, the user-defined index η_m can be any non-negative real number to determine the probability density of the offspring distribution, while u_m is a random number between 0 and 1 to determine the value of β_m at each mutation operation. Furthermore, $p_3 - I_r^{(L)}$ and $I_r^{(U)} - p_3$ refer to the distances from the parent p_3 to the lower bound $I_r^{(L)}$ and upper bound $I_r^{(U)}$ of the variable I_r. This is to ensure the diverse distribution of new individuals in the range of each process parameter.

$$c_3 = \begin{cases} p_3 + \beta_m\big(p_3 - I_r{}^{(L)}\big) & 0 < u_m < 0.5 \\ p_3 + \beta_m\big(I_r{}^{(U)} - p_3\big) & 0.5 \le u_m < 1 \end{cases} \tag{6.11}$$

$$\beta_m = \begin{cases} \left((2u_m)^{\frac{1}{\eta_m+1}} - 1\right) & 0 < u_m < 0.5 \\ \left(1 - [2(1-u_m)]^{\frac{1}{\eta_m+1}}\right) & 0.5 \le u_m < 1 \end{cases} \tag{6.12}$$

In this study, the lower and upper bounds are determined by the range of the process parameter. **Equation (6.13)** presents an example of PLM mutation on the process parameter of layer thickness, assuming that the range of layer thickness is $LT \in [0.045mm, 0.35mm]$. Thus, the lower bound $LT^{(L)}$ and upper bound $LT^{(U)}$ are 0.045 and 0.35. Referring to **Equation (6.11)**, the offspring $LT_3{}'$ mutated from the parent LT_3 is calculated as **Equation (6.13)**, where η_m is an arbitrary non-negative real number and u_m is a random number between 0 and 1.

$$LT_3{}' = \begin{cases} LT_3 + \beta_m(LT_3 - 0.045) & 0 < u_m < 0.5 \\ LT_3 + \beta_m(0.35 - LT_3) & 0.5 \le u_m < 1 \end{cases} \tag{6.13}$$
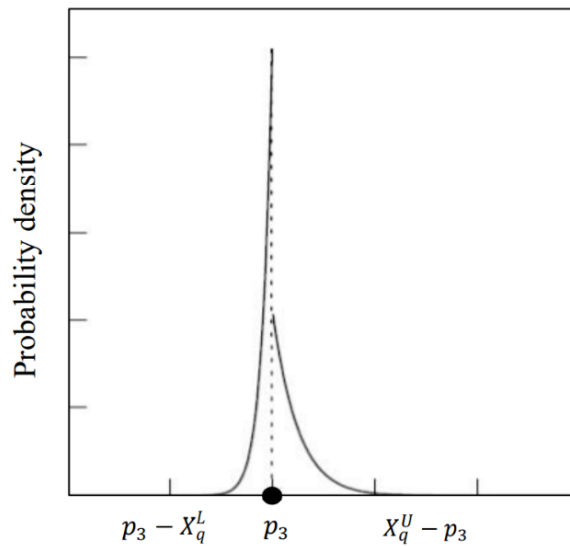
Figure 6.6: Probability density function of producing a mutated offspring using a PLM operator (Deb et al., 2002)

6.2.6. Recombination

After the SBX crossover and PLM mutation, all created individuals form the offspring population Q_{k+1}. According to **Figure 6.1** and **Figure 6.3**, the offspring Q_{k+1} and the parent P_{k+1} are recombined as the next generation, whose population is of size *2N*. All *2N* individuals are looped back into the slicer software, their G-code files are produced, and their consumptions are obtained through the predictive models. Based on the predicted results, all individuals continue to be ranked through non-dominated sorting and crowding distance ranking. Then the elite individuals are retained for the tournament selection of parent population. The selected parents continue to produce offspring for the next iteration of optimisation. This iteration continues until it reaches the maximum number of iterations (i.e. $k = Gen$). Finally, a near-optimal approximate Pareto front is obtained. The front contains all non-dominated solutions of process parameters on the first front level L_1.

Above sections present the details of each NSGA-II optimisation step. The selection of optimisation algorithm is based on the number of objectives and overall complexity. Considering the $O(MN^2)$ complexity and the superior performance in solving optimisation problems with two or three objectives, NSGA-II is found to be the feasible optimisation tool in this study. In the following case studies, the population size in optimisation tests is set within the range from 10 to 40 due to the limitation of our computing resources. Thus, it is not expected that NSGA-II applied in this study is able to rapidly find the global optimal solutions. However, even at the vicinity of a local Pareto-optimal front, NSGA-II is able to find a set of well-spread solutions as a guide for the manufacturers, since the crowded comparison can promote the diversified distribution of individuals in the objective space (Deb et al., 2002).

Despite the advantages of NSGA-II, this optimisation algorithm still faces a few weaknesses, especially in the high-dimensional optimisation problems. As the number of objectives increases, the feasibility of sorting through the dominance relationship will be reduced, and the complexity of crowding distance calculation will be increased. Thus, in

future work, if the optimisation problem is extended to more than three objectives, it is recommended to select another appropriate optimisation algorithm from meta-heuristics.

6.3. Design of experiments for NSGA-II optimisation

The methodology of Taguchi design of experiments for NSGA-II optimisation test has been discussed in **Section 4.6.2**. This study uses the $L_{16}(4^4)$ orthogonal table, in which four factors represent four optimisation parameters: population size N, number of generations Gen, crossover probability pc and mutation probability pm. Each optimisation parameter is configured with four levels, as listed in **Table 6. 1**. Considering the scale of experiments and the computational capabilities of our existing computing resources, the levels of population size N is set within the range from 10 to 40, and the number of generations Gen is set within the range from 50 to 200. Referring to Nebro et al. (2007), the crossover probability pc and mutation probability pm are set within the ranges of values commonly used in NSGA-II optimisation.

Table 6. 1: Specification of NSGA-II optimisation parameters

Factor		Symbol	Levels			
1	Population size	N	10	20	30	40
2	Number of generations	Gen	50	100	150	200
3	Crossover probability	pc	0.85	0.9	0.95	1.00
4	Mutation probability	pm	0.15	0.20	0.25	0.30

Based on the above, there are 16 optimisation tests to be performed under different combinations of optimisation parameters before an AM process. Each test will produce one Pareto front. The response of each test is the hypervolume (HV) indicator $I_H(A)$ used to compare the qualities of all obtained fronts. The calculation of HV indicator has been discussed in the methodology in **Section 4.6.3**.

Table 6. 2: Experiments of NSGA-II optimisation tests under different combinations of optimisation parameters

Test No.	Factor levels			
	Population size	Number of generations	Probability of crossover	Probability of mutation
	N	*Gen*	*pc*	*pm*
1	10	50	0.85	0.15
2	10	100	0.9	0.20
3	10	150	0.95	0.25
4	10	200	1.00	0.30
5	20	50	0.9	0.25
6	20	100	0.85	0.30
7	20	150	1.00	0.15
8	20	200	0.95	0.20
9	30	50	0.95	0.30
10	30	100	1.00	0.25
11	30	150	0.85	0.20
12	30	200	0.9	0.15
13	40	50	1.00	0.20
14	40	100	0.95	0.15
15	40	150	0.9	0.30
16	40	200	0.85	0.25

6.4. Application indication of NSGA-II optimisation

The previous sections present the details of NSGA-II optimisation to minimise AM time, energy and material consumptions. This section summarises and provides an indication of applying the proposed optimisation method to real-world AM systems.

Preparation for NSGA-II optimisation

- Define the predictive models of time, energy and material consumptions as objective functions.
- Prepare the CAD design to be printed.
- Configure the process parameters to be optimised and the value range of each process parameter

Perform NSGA-II optimisation tests

- Perform NSGA-II optimisation under different combinations of optimisation parameters.
- Record the optimal solutions of process parameters and the corresponding predicted consumptions after each test.

Calculate hypervolume indicator

- Calculate the hypervolume of each solution set on the near-optimal approximate Pareto front.
- Compare the hypervolumes of 16 near-optimal approximate Pareto fronts, and select the front with the maximum hypervolume as a guide for the manufacturers.

Figure 6.7: Basic workflow of multi-objective optimisation using NSGA-II

The basic workflow of optimising resource consumptions before printing the CAD design is shown in **Figure 6.7**. The first step is to obtain the predictive models for the AM machine through the prediction modelling method discussed in last chapter. The predictive models are used to represent the objective functions to be minimised. Besides, the CAD design in Standard triangle language (STL) format needs to be prepared as the input of NSGA-II algorithm. According to the machine characteristics and customer demands, the process parameters to be optimised and their value ranges also need to be configured in the algorithm.

The second step is to perform the NSGA-II algorithm under 16 different combinations of optimisation parameters. By the end of each test, the optimal solutions of process parameters should be recorded. The corresponding predicted consumptions of each solution should also be recorded.

The final step is to calculate the hypervolume (HV) indicator of each obtained front. Through comparison, the solutions on the front that has the maximum HV indicator will be taken as the suggestion for the process parameter setting of current AM task.

6.5. Summary

This chapter introduces the optimisation steps of the improved non-dominated sorting genetic algorithm II (NSGA-II) to search for the most feasible solution sets of process parameters with the minimum time, energy and material consumptions. Simulated binary crossover (SBX) and polynomial mutation (PLM) are used as the crossover operator and mutation operator to perform the real-coded recombination of process parameters. Taguchi design of experiments is applied to perform the optimisation under different combinations of optimisation parameters, including population size, number of generations, crossover probability and mutation probability. In each test, the HV indicator is applied to quantify the quality of the obtained non-dominated solution set on the first front level. The larger the HV indicator, the better the performance of the solution.

The improvement of original NSGA-II is one of the contributions of this research. Since different process parameters produce different G-code, the prediction process – from inputting the process parameters into CAM to the generation of G-code – is embedded into the process of objective function calculation. This method results in more convincing optimisation results. In the following chapters, the proposed optimisation method will be applied to two fused deposition modelling (FDM) printers to validate its feasibility in a practical manufacturing context, and the results and analyses will be discussed.

CHAPTER 7   APPLICATION OF PREDICTION METHOD IN REAL-WORLD AM SYSTEMS

7.1. Introduction

This chapter aims to validate the feasibility of the prediction method. The proposed methodology has been applied to two different types of fused deposition modelling (FDM) 3D printers: ANYCUBIC i3 Mega 3D printer and Monoprice Mini Delta three-linear slider 3D printer. The former uses the Cartesian system to realise the axis movement, while the latter uses three parallel stepper motors with a three-linear slider to realise the axis movement.

The components of each machine are first classified into five modules, namely axis movement, material feeding, material processing, component heating and auxiliary components. Then, a Gantt chart is created based on the coding rules of each machine to illustrate the running sequences and working states of all modules. Next, consumption modelling is performed on each module. In physics-based modelling, the time, distance of axis movement with actual displacements and amount of material feeding are modelled from the processing of G-code. In data-driven modelling, experiments are performed to measure the component heating time and the apparent powers of each module under different process parameters. Based on the experimental results, the functional relationships between the measured parameters and process parameters are derived by using polynomial regression method. Referring to Jenkins and Quintana-Ascencio (2020), it is originally planned that the number of data points for one regression model is 25. However, due to the impact of the COVID19 epidemic starting from 2019, we reduce the number of experiments in the limited time and use the existing collected data for the prediction modelling.

Due to the unique operating mechanisms of different AM machines, the modelling of power and time consumptions of certain modules need to be customised and adjusted

according to the machine characteristics. In the following sections, details of the predictive models of two AM machines are described.

7.2. Experimental setup

This section introduces the experimental setup for the prediction of time, energy and material consumptions in the AM process. Two fused deposition modelling (FDM) printers are tested to validate the feasibility of the proposed prediction method. A power meter is applied to measure the apparent power and time consumptions of the components in two FDM printers. A density meter is applied to measure the actual density of the polylactic acid (PLA) material filament. The curve-fitting tool in MATLAB is used to analyse the functional relationships between the measured parameters and process parameters. Polynomial regression method is applied to calculate the coefficients in the functions. Details of each experimental device are described as follows.

7.2.1. Fused deposition modelling 3D printers

Fused deposition modelling (FDM) technology is one of the trendiest and foundational rapid prototyping technologies developed by Stratasys (Carneiro et al., 2015). It not only satisfies the functional requirements of specific structures but also enables the sufficient reproducibility and control of the desired microstructure and porosity of 3D objects (Too et al., 2002; Chua et al., 2010). In a typical FDM process, a physical object is created from the CAD design via computer numerical control (CNC) robotic extrusion of PLA filament material layer by layer (Agarwala et al., 1996). The toolpaths defined by G-code are used to instruct the material deposition are generated from the supporting slicer software, such as Cura, Slic3r, Simplify3D, etc. Since most of slicer software for FDM technologies is available for free to provide open-source code for developing third-party plug-ins, this study has chosen the FDM technology as the case study to verify the feasibility of the proposed modelling method. Two different types of FDM 3D printers have been used to compare the prediction accuracies of predictive models.

The first FDM machine to be considered is the ANYCUBIC i3 Mega 3D printer. The printer fabricates by using $1.75\,mm$ diameter PLA filament as raw material and Cura developed by Ultimaker as the slicer software. **Table 7.1** lists the specifications of this printer. As shown in **Figure 7.1**, three stepper motors of the Cartesian system are responsible for axis movement in X, Y, Z directions. The wire feeder/extruder driven by the fourth stepper motor is used to load the PLA filament from the spool to the machine nozzle. The hotend inside the extruder is used to melt the filament from solid to liquid. To assist the AM process, the heating of the build platform is synchronous with material deposition, which aims to ensure that the printed object is firmly attached to the platform. Additionally, the display unit, temperature sensor, and user interface and connectivity also participate in the AM process to monitor and control the machine status.
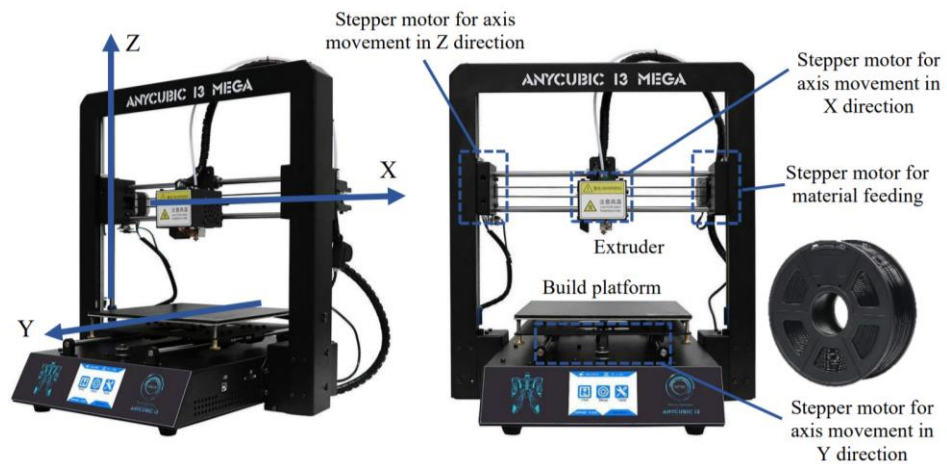
Figure 7.1: Consumption-related components of ANYCUBIC 3D printer (i3 Mega S, 2020)

Table 7.1: Specifications of ANYCUBIC i3 Mega 3D printer (i3 Mega S, 2020)

Technology	Fused deposition modelling	**Supported material**	PLA, ABS, HIPS, wood
Build size	$210\times210\times205\,mm^3$	**Printer dimensions**	$405\times410\times453\,mm^3$
Layer resolution	0.04–$0.3\,mm$	**Infill density**	0–100%
Extruder quantity	Single	**Nozzle diameter**	$0.4\,mm$
Bed temperature	0–$80°C$	**Extruder temperature**	170–$250°C$
Filament diameter	$1.75\,mm$	**PLA temperature**	150–$220°C$
Print speed	10–$150\,mm/s$	**Cooling fans**	Enable/Unable
Travel speed in X, Y axes	10–$300\,mm/s$	**Slicer software**	Cura
Travel speed in Z axis	$5\,mm/s$	**Input rating**	110V/220V AC, 50/60Hz

The second FDM machine to be considered is the Monoprice Mini Delta three-linear slider 3D printer. **Table 7.2** lists the specifications of this printer. The same as in the first case, the Monoprice printer also uses $1.75mm$ diameter PLA filament as raw material and Cura as the slicer software. The difference is that the axis movement on the Monoprice machine is driven by the Delta system, in which the three-linear slider consists of three stepper motors. As shown in **Figure 7.2**, the three stepper motors achieve axis movement through the linkage motion instead of each being responsible for a single direction. In addition, the other components play the same roles as in the first case during the AM process, including the wire feeder/extruder, fourth stepper motor for material loading, nozzle hotend, build platform/bed, display unit, temperature sensor, and user interface and connectivity.
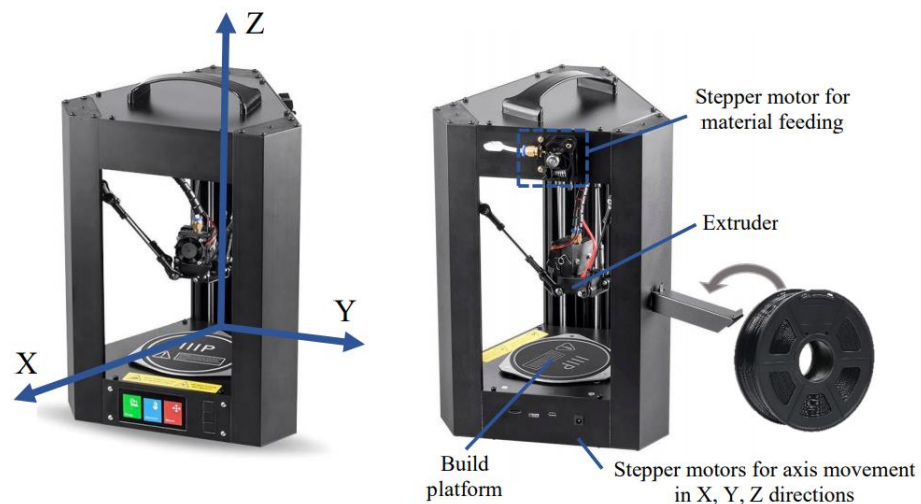
Figure 7.2: Consumption-related components of Monoprice 3D printer (Monoprice, 2020)

Table 7.2: Specifications of Monoprice MP Mini Delta 3D printer (Monoprice, 2020)

Technology	Fused filament fabrication	Supported material	ABS, PLA, wood fill, copper fill, steel fill, bronze fill
Build size	$110{\times}120{\times}180mm^3$	**Printer dimensions**	$360{\times}440{\times}480mm^3$
Layer resolution	0.05–0.2mm	**Infill density**	0–100%
Extruder quantity	Single	**Nozzle diameter**	0.4mm
Bed temperature	0–60℃	**Extruder temperature**	100–260℃
Filament diameter	1.75mm	**PLA temperature**	150–220℃
Print speed	10–150mm/s	**Cooling fans**	Enable/Unable
Travel speed in X, Y axes	10–150mm/s	**Slicer software**	Cura
Travel speed in Z axis	10–150mm/s	**Input rating**	100–240VAC, 50/60 Hz, 4A

7.2.2. Slicer software

Cura is the official slicer software for both ANYCUBIC 3D printer and Monoprice 3D printer. The setting of the process parameters of both machines can be completed in Cura, and the running sequences of modules and path planning are determined by Cura's coding rules for the machine in question. In the definition of NSGA-II optimisation decision variables, the process parameters to be optimised can be selected by manufacturers, while all other process parameters are set as defaults. In order to demonstrate how the proposed method works in real-world AM system, we selected six important process parameters as examples, including layer thickness LT, speeds F_{xy}, F_z of axis movement in X, Y, Z directions, extruder temperature T_{mp}^a, bed temperature T_h^b and infill density ID.

7.2.3. Yokogawa CW500 power quality analyser

A power meter is required to measure the apparent power and time consumptions of machine components. In this study, the Yokogawa CW500 power quality analyser and the supporting software CW500 Viewer are used to measure and analyse the recorded data in the form of scatter plots. **Table 7.3** lists the specifications of the CW500 analyser, of which the maximum voltage and maximum current are $600V$ and $50A$ respectively. The sampling rate of $24\mu s$ indicates that the analyser enables the testing of an average of 41,666 samples per second. The range of record interval indicates that the granularity of the power plot extends from one point per second to one point per 10 minutes.

The circuit connection of the power measurement is presented in **Figure 7.3**. A circuit box has been designed to separate the neutral, live and earth wires inside the power cord of an AM machine into three wires. This is to assist in the taking of power and time measurements from only the power cord instead of disassembling the AM machine. Then, two voltage probes and a current clamp-on probe are used to measure the voltage and current, respectively, of the AM machine.
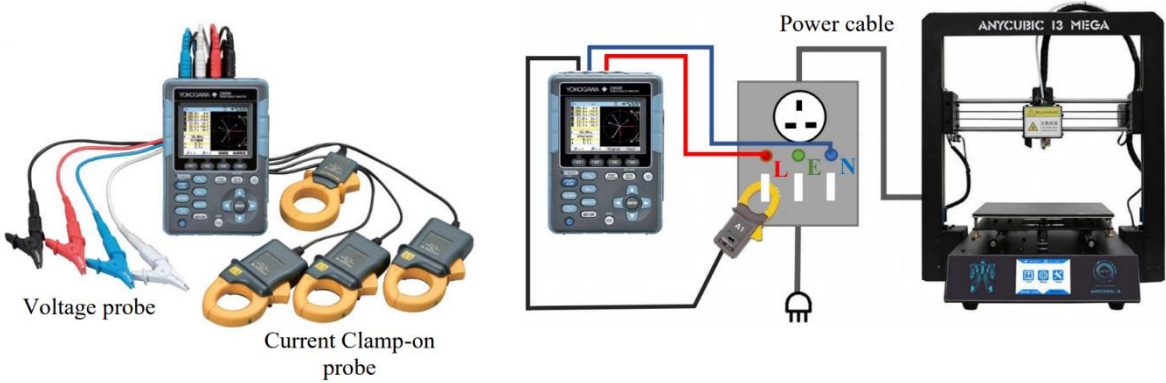
Figure 7.3: Circuit connection of power and time measurements by using Yokogawa CW500 power quality analyser (CW500, 2020)

Table 7.3: Specifications of Yokogawa CW500 power quality analyser (CW500, 2020).

Sampling rate	$24\mu s$
Voltage range	$600V$
Current clamp range	$50A$
Record interval range	$1s–10mins$

7.2.4. Sartorius Practum313-1S Milligram Balance

A density meter is required to test the actual density of the polylactic acid (PLA) material during additional experiments. As shown in **Figure 7.4**, this study uses a Sartorius Practum313-1S Milligram Balance as the density meter to measure the masses of PLA filament samples in both air and water environments. Specifications of the density meter are listed in **Table 7.4**.

Figure 7.4: Sartorius Practum313-1S Milligram Balance (Sartorius YDK03, 2020)

Table 7.4: Specifications of Sartorius Practum313-1S Milligram Balance (Sartorius, 2020)

Capacity	$310g$
Readability	$0.001g$
Repeatability (standard deviation)	$0.001g$
Typical stabilisation time (seconds)	3s
Weighing pan size diameter	$120mm$
Weighing chamber height	$209mm$
Dimensions	$360\times216\times320mm$

The actual density ρ_{act} is calculated as shown in **Equation (7.1)**, in which W_{air} denotes the mass of a PLA sample measured in air, W_{water} denotes the mass of a sample measured in water and ρ_{H_2O} denotes the density of water at the current room temperature. The value of ρ_{H_2O} is provided by Sartorius YDK03 (2020).

$$\rho_{act} = \frac{W_{air} \cdot \rho_{H_2O}}{W_{air} - W_{water}} \tag{7.1}$$

7.3. Predictive models of ANYCUBIC i3 Mega 3D printer

This section presents the modelling of time, energy and material consumptions of the ANYCUBIC i3 Mega fused deposition modelling (FDM) 3D printer. The modelling procedure follows the application indication in Chapter 5. Each step is described as follow.

1) **Module classification**

At first, the components are classified into five modules, namely axis movement, material feeding, material processing, component heating and auxiliary components. The axis movement module refers to the Cartesian system driven by three stepper motors in X, Y, Z directions. The material feeding module refers to the extruder. The material processing module refers to the nozzle hotend. The component heating module refers to the build

platform/bed. The auxiliary components module refers to the display unit, temperature sensor, and user interface and connectivity.

2) Power and time tests of AM system

Figure 7.5 presents the Gannt chart of five modules' cooperation to print a general AM task manufactured by the ANYCUBIC printer. The first plot in the grey box indicates the total apparent power of all five modules throughout the entire task. Other sub-plots indicate the apparent power of each module operating independently. Note that the powers of the axis movement module and material feeding module are combined, because the four stepper motors of these two modules can only run synchronously. Thus, the powers of these two modules are measured together in this case study. Based on the power profiles, the working states of five modules are defined as follows.

- The two modules of material processing (i.e., nozzle hotend) and component heating (i.e., build platform/bed) both have two working states: the initial heating state and the heat preservation state.

- The axis movement module has two working states: the axis movement state with actual displacements and the standby state waiting for completion of other modules' operations. Since there is no interruption during the material deposition, the axis movement module remains in the state of axis movement with actual displacements.

- The material feeding module has two working states: the material feeding state with an actual feeding amount and the standby state waiting for the next operation of material feeding. When the heated modules reach their target temperatures, the axis movement and material feeding modules start to deposit material on each layer until the end of the AM process.

- The auxiliary components module remains in the state of continuous monitoring and control of the machine status throughout the entire process.
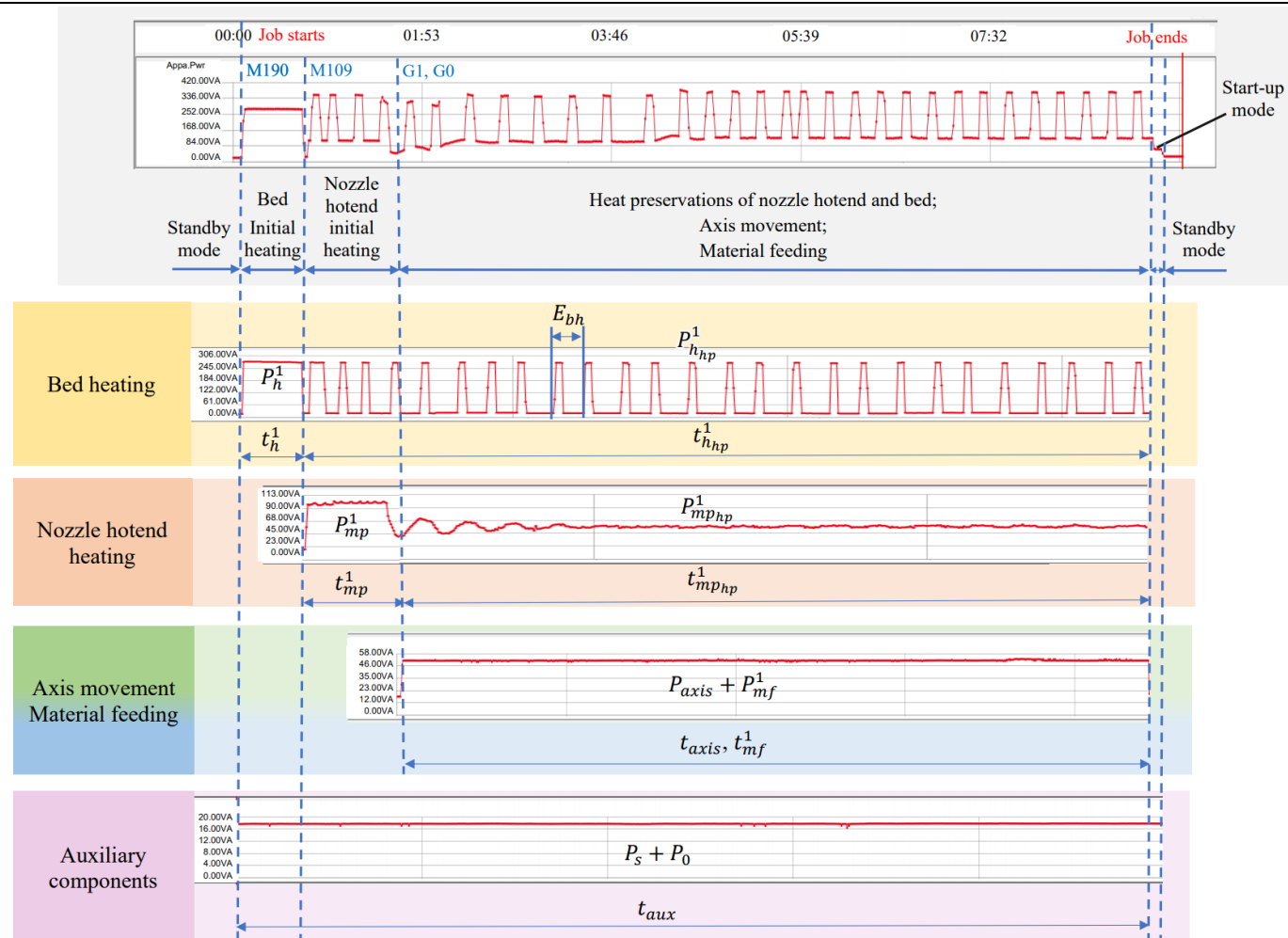
Figure 7.5: Power profiles of ANYCUBIC i3 Mega FDM 3D printer and consumption-related component

3) Generate prototypes of predictive models

Based on the Gannt chart, the prototypes of predictive models can be formulated. The total time consumption is modelled as the union of time consumption of each module, as expressed in **Equation (7.2)**. t_{axis} denotes the time consumption of axis movement module. t_{mp}^1 and $t_{mp_{hp}}^1$ denote the time consumptions of initial heating state and heat preservation state of material processing module (i.e. nozzle hotend). t_h^1 and $t_{h_{hp}}^1$ denote the time consumptions of initial heating state and heat preservation state of component heating module (i.e. build platform / bed). t_{mf}^1 denotes the time consumption of material feeding module. t_{aux} denotes the time consumption of auxiliary components.

$$t_{total} = t_{axis} \cup t_{mp}^1 \cup t_h^1 \cup t_{mp_{hp}}^1 \cup t_{h_{hp}}^1 \cup t_{mf}^1 \cup t_{aux} \qquad (7.2)$$

The total energy consumption is modelled as the sum of energy consumption of five modules, as expressed in **Equation (7.3)**. E_{axis}, E_{mp}, E_h, E_{mf} and E_{aux} respectively denote the energy consumption of axis movement module, material processing module (i.e. nozzle hotend), component heating module (i.e. build platform / bed), material feeding module and auxiliary components.

$$E_{total} = E_{axis} + E_{mp} + E_h + E_{mf} + E_{aux} \qquad (7.3)$$

The total material consumption is modelled as the product of the material density ρ and the cumulative volume $\sum V_{unit}$ of material feeding, as expressed in **Equation (7.4)**.

$$M_{total} = \rho \cdot \sum V_{unit} \qquad (7.4)$$

4) Hybrid modelling to obtain model parameters

In the final step, the predictive models of resource consumptions of each module will be defined on the basis of the above prototypes. The parameters that formulate the models will be obtained in three ways: calculating from G-code, measuring through experiments, and

modelling based on the running sequences of the five modules. The hybrid modelling method applied to obtain the model parameters will be presented in the following sections.

7.3.1. Predictive model of time consumption

This section describes the time consumption modelling for each module in the ANYCUBIC i3 Mega fused deposition modelling (FDM) 3D printer. The predictive models of above time consumptions for five modules are described in the following sub-sections.

7.3.1.1. Time consumption of axis movement

The time spent on axis movement only includes the time spent on actual displacements with or without material feeding, since there is no interruption during the process of material deposition. Thus, there is no interval time t_{xyz}^0 during axis movement and thus t_{xyz}^0 is equal to zero. The total time consumption t_{axis} of axis movement is modelled as **Equation (7.5)**. t_{xyz} can be directly calculated from the coordinates and speeds of axis movement provided by G-code.

$$t_{axis} = t_{xyz} = \sum \frac{\sqrt{\Delta X^2 + \Delta Y^2}}{F_{xy}} + \sum \frac{\Delta Z}{F_z} \tag{7.5}$$

7.3.1.2. Time consumption of material processing

This section models the time consumption of the material processing module. In the initial heating state, the time consumption t_{mp}^1 is modelled as a function of the temperature difference ΔT_{mp}^1 between the current temperature $T_{mp_0}^1$ and target temperature T_{mp}^1. To obtain the functional relationship, experiments are conducted to test the time t_{mp}^1 spent on initial heating under random temperature differences ΔT_{mp}^1. In **Table 7.5**, the target temperature T_{mp}^1 in the G-code commands "M104 ST_{mp}^1" and "M109 ST_{mp}^1" can be manually assigned. The value of T_{mp}^1 is set within the range from the minimum to the

maximum temperature that the nozzle hotend can be heated to. The value of the current temperature $T_{mp_0}^1$ is set within the range from the current room temperature to the maximum temperature of the nozzle hotend.

Table 7.5: Information for measuring the time consumptions of the material processing module under different process parameters for the ANYCUBIC 3D printer

Time consumption	Related parameters	Parameter ranges			
		Lower bound		Upper bound	
t_{mp}^1	Current temperature $T_{mp_0}^1$	Current room temperature	23°C	Maximum temperature of nozzle hotend	250°C
	Target temperature T_{mp}^1	Minimum temperature of nozzle hotend	170°C	Maximum temperature of nozzle hotend	250°C
G-code commands	M104 S(T_{mp}^1) : Set the target temperature T_{mp}^1 of nozzle hotend				
	M109 S(T_{mp}^1): Heat the nozzle hotend to the target temperature T_{mp}^1				

To ensure the diversity and dispersion of data points in the value space, the current temperatures $T_{mp_0}^1$ and target temperatures T_{mp}^1 are randomly assigned within the pre-defined ranges to ensure that the temperature differences ΔT_{mp}^1 are evenly dispersed in the coordinate system used for regression analysis. The experimental results are presented in **Appendix II (1–9)** and summarised in **Table 7.6**. By using the polynomial regression tool in MATLAB, the regression model of t_{mp}^1 is shown in **Figure 7.6** and expressed as **Equation (7.6)**. The R^2 to evaluate the goodness-of-fit is calculated as 0.9920.

$$t_{mp}^1 = 0.2834\Delta T_{mp}^1 + 10.29 \tag{7.6}$$

$$\Delta T_{mp}^1 = T_{mp}^1 - T_{mp_0}^1 \tag{7.7}$$

Table 7.6: Experimental results of the initial heating time under random temperature differences of the material processing module in the ANYCUBIC 3D printer

Test No.	Current temperature	Target temperature	Temperature difference	Time consumption
	$T_{mp_0}^1$	T_{mp}^1	ΔT_{mp}^1	t_{mp}^1
	(°C)	(°C)	(°C)	(s)
1	131	180	49	24
2	86	180	94	36
3	84	180	96	37
4	146	200	54	26
5	72	200	128	47
6	26	200	174	57
7	78	220	142	53
8	34	220	186	63
9	30	220	190	65
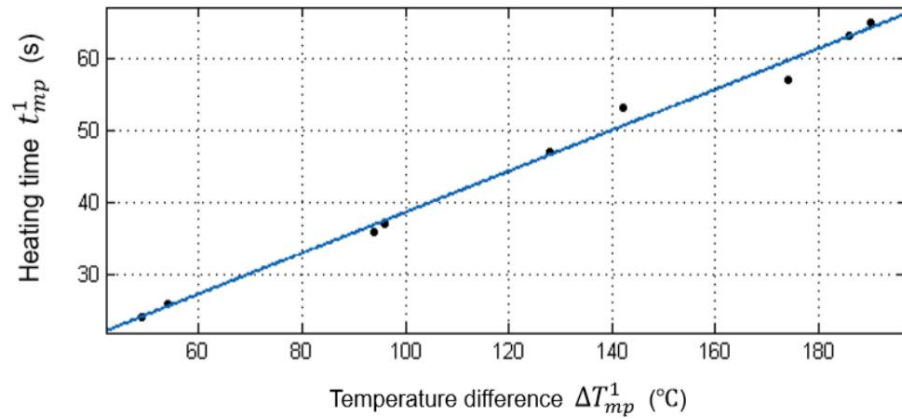
Figure 7.6: Regression model of initial heating time and temperature difference of the material processing module in the ANYCUBIC 3D printer

The heat preservation of the material processing module is synchronous with the modules of axis movement and material feeding, according to the Gannt chart of the five modules in **Figure 7.5**. Therefore, the time $t_{mp_{hp}}^1$ spent in the heat preservation state is equal to the time t_{axis} spent on axis movement, as expressed in **Equation (7.8)**.

$$t_{mp_{hp}}^1 = t_{axis} \tag{7.8}$$

7.3.1.3. Time consumption of component heating

This section models the time consumption of component heating module. In the initial heating state, the time consumption t_h^1 is modelled as a function of the temperature difference ΔT_h^1 between the current temperature $T_{h_0}^1$ and the target temperature T_h^1. Experiments are conducted to test the time t_h^1 spent on initial heating under random temperature differences ΔT_h^1. In **Table 7.7**, the target temperature T_h^1 in the G-code commands "M140 ST_h^1" and "M190 ST_h^1" is manually assigned. The values of $T_{h_0}^1$ and T_h^1 are both randomly set within the range from the current room temperature to the maximum temperature of the build platform/bed.

Table 7.7: Information for measuring the time consumptions of component heating under different process parameters for the ANYCUBIC 3D printer

Time consumption	Related parameters	Parameter ranges			
		Lower bound		**Upper bound**	
t_h^1	Current temperature $T_{h_0}^1$	Current room temperature	23°C	Maximum temperature of build platform/bed	80°C
	Target temperature T_h^1	Current room temperature	23°C	Maximum temperature of build platform/bed	80°C
G-code commands	M140 S(T_h^1) : Set the target temperature T_h^1 of build platform/bed				
	M190 S(T_h^1) : Heat the build platform/bed to the target temperature T_h^1				

The experimental results are presented in **Appendix II (10–22)** and summarised in **Table 7.8**. The results prove that the time consumption t_h^1 is functionally related to the temperature difference ΔT_h^1. With the assistance of the polynomial regression method, the regression model of t_h^1 is shown in **Figure 7.7** and expressed as **Equation (7.9)**. The R^2 is calculated as 0.9624.

$$t_h^1 = 4.778\Delta T_h^1 - 10.4 \tag{7.9}$$

$$\Delta T_h^1 = T_h^1 - T_{h_0}^1 \tag{7.10}$$

Table 7.8: Experimental results of the initial heating time under random temperature differences of the component heating module in the ANYCUBIC 3D printer

Test No.	Current temperature $T_{h_0}^1$ (°C)	Target temperature T_h^1 (°C)	Temperature difference ΔT_h^1 (°C)	Time consumption t_h^1 (s)
10	40.0	45	5	15
11	36.0	45	9	31
12	34.0	45	11	40
13	29.0	50	21	94.5
14	27.0	50	23	108
15	26.0	50	24	118
16	21.5	50	28.5	101
17	47.0	60	13	46
18	43.0	60	17	73
19	29.0	60	31	128
20	40.0	70	30	138
21	35.0	70	35	159
22	34.0	70	36	168
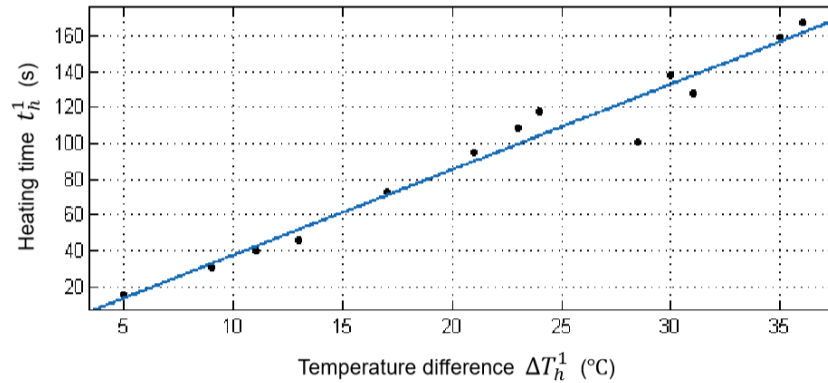
Figure 7.7: Regression model of initial heating time and temperature difference of the component heating module in the ANYCUBIC 3D printer

According to the Gannt chart of five modules in **Figure 7.5**, the heat preservation of the component heating module begins at the same time as the initial heating of the material processing module. Therefore, the time consumption $t_{h_{hp}}^1$ of heat preservation consists of two parts: the time t_{mp}^1 spent during initial heating of the material processing module and the time t_{axis} spent on axis movement, as expressed in **Equation (7.11)**.

$$t_{h_{hp}}^1 = t_{mp}^1 + t_{axis} \qquad (7.11)$$

7.3.1.4. Time consumption of material feeding

The material feeding is synchronous with axis movement during the processing of material deposition. Therefore, the time consumption t_{mf}^1 of material feeding is the same as the time consumption t_{axis} of axis movement, as expressed in **Equation (7.12)**.

$$t_{mf}^1 = t_{axis} \tag{7.12}$$

7.3.1.5. Time consumption of auxiliary components

The auxiliary modules, namely the display unit, temperature sensor, and user interface and connectivity, remain in operating status throughout the entire AM process. Therefore, the time consumption t_{aux} is equal to the total time consumption t_{total}, as expressed in **Equation (7.13)**.

$$t_{aux} = t_{total} \tag{7.13}$$

7.3.1.6. Total time consumption of all modules

Based on the above models, the total time consumption t_{total} of an AM process is the union of time consumed by the five modules. According to the Gannt chart of the five modules in **Figure 7.5**, the total time consumption t_{total} of ANYCUBIC i3 Mega FDM 3D printer is modelled as the sum of time consumptions of three modules: material processing, component heating and axis movement, as expressed in **Equation (7.14)**.

$$t_{total} = t_h^1 + t_{mp}^1 + t_{axis} \tag{7.14}$$

7.3.2. Predictive model of energy consumption

This section describes the energy consumption modelling for each module in the ANYCUBIC i3 Mega FDM 3D printer. The predictive models of above energy consumptions for five modules are described in the following sub-sections.

7.3.2.1. Energy consumptions of axis movement and material feeding

This section models the energy consumptions of the axis movement module and the material feeding module. Due to the unique manufacturing mechanism of this AM machine, the four stepper motors used to drive the two modules always run synchronously to deposit material. Thus, experiments are conducted to measure the total apparent powers of two modules together.

Initially, the apparent power P_{axis} of the axis movement module is modelled as a function of speeds F_{xy} and F_z in X, Y, Z directions. The apparent power P_{mf}^c of material feeding is modelled as a function of the feeding rate F_{xy} in X, Y directions. To calculate the functional relationships, experiments are conducted to measure the apparent powers under different axis movement speeds and material feeding rates. When the two modules run together to deposit material on a specific toolpath, the speed of axis movement is the same as the rate of material feeding.

Note that the axis movement and material feeding are driven by four stepper motors. Three stepper motors are responsible for the axis movement in X, Y, Z directions. One stepper motor is responsible for loading the material filament from spool to nozzle. Therefore, experiments are conducted to measure the apparent powers of all combinations of the four stepper motors. As shown in **Table 7.9**, the G-code commands are manually defined to instruct the modules to move for a sufficient displacement or to feed a sufficient amount of material filament. The value of each axis movement speed or feeding rate is set within the range from the lowest to the highest speed or feeding rate that the modules can achieve.

Table 7.9: Information for measuring the apparent powers of the axis movement module and material feeding module in X, Y, Z directions under different process parameters for the ANYCUBIC 3D printer (G-Code – Reprap, 2020)

Apparent power	Related parameters		Parameter ranges			
			Lower bound		Upper bound	
P_{axis}	Speed of axis movement in X, Y directions	F_{xy}	Lowest speed of axis movement in X, Y directions	$600mm$ /min	Highest speed of axis movement in X, Y directions	$9000mm$ /min
	Speed of axis movement in Z direction	F_z	Fixed speed of axis movement in Z direction		$300mm/min$	
P_{mf}^1	Rate of material feeding in X, Y directions	F_{xy}	Lowest rate of material feeding in X, Y directions	$600mm$ /min	Highest rate of material feeding in X, Y directions	$9000mm$ /min
G-code commands	G1 F_{xy} Xnnn Ynnn : Nozzle moves to the target coordinate (Xnnn, Ynnn) at a speed of F_{xy} G1 F_z Znnn : Nozzle moves to the target coordinate (Znnn) at a speed of F_z G1 F_{xy} Xnnn Ynnn Emmm : Nozzle moves to the target coordinate (Xnnn, Ynnn) with material feeding; the total amount of material feeding is mmm					

Table 7.10 presents the speeds of axis movement or rates of material feeding in each test. To ensure the diversity and dispersion of data points in the value space, each test contains six different speeds or feeding rates whose values are randomly assigned within the pre-defined ranges, except for the speed in Z direction. Note that the speed in Z direction has only one level (i.e. $F_z = 300 \, mm/min$), since the speed of axis movement in Z direction is a fixed constant due to the machine characteristics. The experimental results are listed in **Appendix II (23–31)** and summarised in **Table 7.10**.

Table 7.10: Experimental results of apparent powers of axis movement and material feeding at different speeds in X, Y, Z directions for the ANYCUBIC 3D printer

Test No.	Stepper motors	Speeds F_{xy}, F_z (mm/min)	Avg. power P_{axis}, P_{mf}^1 (VA)
23	X	900, 2400, 3600, 5400, 7200, 9000	7.96363
24	Y	900, 2400, 3600, 5400, 7200, 9000	16.18841
25	Z	300	15.31416
26	Material feeding	900, 2400, 3600, 5400, 7200, 9000	41.34308
27	X, Y	900, 2400, 3600, 5400, 7200, 9000	31.00807
28	X, Z	900, 2400, 3600, 5400, 7200, 9000	22.452603
29	Y, Z	900, 2400, 3600, 5400, 7200, 9000	24.016157
30	X, Y, Z	900, 2400, 3600, 5400, 7200, 9000	31.53707
31	X, Y, Z, material feeding	900, 2400, 3600, 5400, 7200, 9000	42.47047

Through observations from the power profiles, the power of each test is distributed as a constant regardless of the speed variation. However, the total power of axis movement and material feeding driven by the four stepper motors is not the sum of the power of each individual motor. For instance, if the G-code file only has G-code commands for axis movement in X, Z directions, then the total power P_{axis} would be $22.452603VA$. If the G-code file has the commands for axis movement in three directions, then the total power P_{axis} would be $31.53707VA$. Thus, it can be concluded that the modules operate at different power levels for different combinations of the stepper motors. In a general AM process, it is certain that the G-code file contains all types of commands for the axis movement in three directions with material feeding, which means that all the stepper motors participate in material deposition. Thus, the total power of axis movement and material feeding would be $42.47047VA$, as expressed in **Equation (7.15)**.

$$P_{axis} + P_{mf}^1 = 42.47047(VA) \tag{7.15}$$

Based on the above, the total energy consumption of axis movement E_{axis} and material feeding E_{mf} can be modelled as **Equation (7.16)**. According to the prediction models of time consumptions in **Section 7.3.1.4**, the two modules run synchronous during the material

deposition process, and thus the time t_{axis} spent on axis movement represents the time t^1_{mf} spent on material feeding.

$$E_{axis} + E_{mf} = P_{axis}t_{axis} + P^1_{mf}t^1_{mf} = 42.47047t_{axis} \qquad (7.16)$$

7.3.2.2. Energy consumption of material processing

This section models the energy consumption of the material processing module. The apparent powers of P^1_{mp} initial heating state and $P^1_{mp_{hp}}$ heat preservation state are both modelled as functions of the target temperature T^1_{mp}. Experiments are conducted to measure the apparent powers P^1_{mp}, $P^1_{mp_{hp}}$ under different target temperatures T^1_{mp}. As shown in **Table 7.11**, the target temperature T^1_{mp} in the G-code commands "M104 ST^1_{mp}" and "M109 S T^1_{mp}" is randomly assigned within the range from the minimum to the maximum temperature that the module can be heated to.

Table 7.11: Information for measuring the apparent powers of the material processing module under different process parameters for the ANYCUBIC 3D printer

Apparent power		Related parameters		Parameter ranges			
				Lower bound		Upper bound	
Initial heating	P^1_{mp}	Target temperature	T^1_{mp}	Minimum temperature of nozzle hotend	170 °C	Maximum temperature of nozzle hotend	250 °C
Heat preservation	$P^1_{mp_{hp}}$						
G-code commands		M104 S(T^1_{mp}) : Set the target temperature T^1_{mp} of nozzle hotend					
		M109 S(T^1_{mp}) : Heat the nozzle hotend to the target temperature T^1_{mp}					

The experimental results are listed in **Appendix II (1–9)** and summarised in **Table 7.12**. It has been found that the apparent power P^1_{mp} of initial heating remains constant and is unrelated to the target temperature T^1_{mp} in this case study. The average power is calculated as **Equation (7.17)**.

$$P^1_{mp} = 82.23392(VA) \qquad (7.17)$$

Table 7.12: Experimental results of apparent powers of material processing at different target temperatures for the ANYCUBIC 3D printer

Test No.	Target temperature T_{mp}^1 (°C)	Apparent power of initial heating P_{mp}^1 (VA)	Apparent power of heat preservation	
			$P_{mp_{hp}}^1$ (VA)	Avg. (VA)
1	180	80.09757	29.73025	
2	180	84.61051	33.22233	32.19572
3	180	84.98951	33.63458	
4	200	83.81399	36.78407	
5	200	79.60137	34.27343	35.23348
6	200	79.03716	34.64294	
7	220	79.70132	39.09674	
8	220	83.61147	42.08892	41.27564
9	220	84.64236	42.64125	
Avg. (VA)		82.23392		

Different from initial heating, the apparent power $P_{mp_{hp}}^1$ of heat preservation gradually tends to be stabilised as a constant, and is proved to be correlated to the target temperature T_{mp}^1 according to the results in **Table 7.12**. Polynomial regression method is applied to calculate the coefficient between the apparent power $P_{mp_{hp}}^1$ and the target temperature T_{mp}^1. The regression model is presented in **Figure 7.8** and **Equation (7.18)**. The R^2 to evaluate the goodness-of-fit is calculated as 0.8337.

$$P_{mp_{hp}}^1 = 0.227T_{mp}^1 - 9.165 \tag{7.18}$$
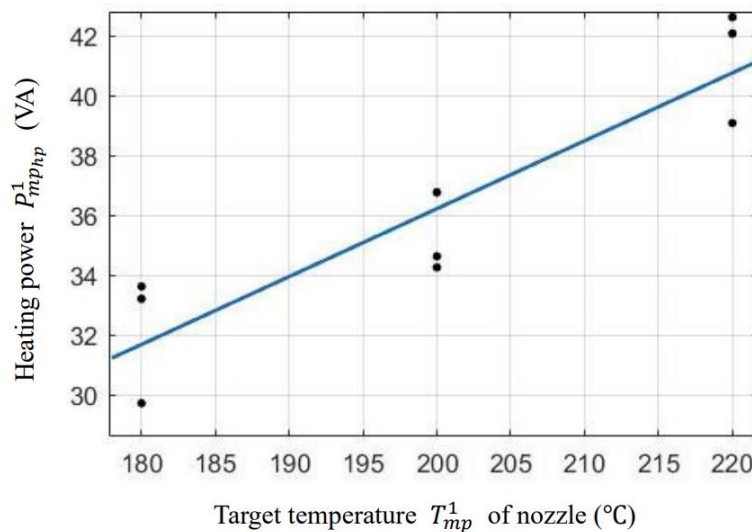
Figure 7.8: Regression model of apparent power and target temperature for heat preservation in the material processing module in the ANYCUBIC 3D printer

Based on the above, the total energy consumption E_{mp} of material processing module is modelled as the sum of the time-integral of power in the above two working states, as expressed in **Equation (7.19)**.

$$E_{mp} = P_{mp}^1 t_{mp}^1 + P_{mp_{hp}}^1 t_{mp_{hp}}^1 \qquad (7.19)$$

7.3.2.3. Energy consumption of component heating

This section models the energy consumption of component heating module. The apparent powers of P_h^1 initial heating state and $P_{h_{hp}}^1$ heat preservation state are modelled as functions of the target temperature T_h^1. Then, experiments are conducted to measure the apparent powers P_h^1, $P_{h_{hp}}^1$ under different target temperatures T_h^1. In **Table 7.13**, the target temperature T_h^1 in the G-code commands "M140 ST_h^1" and "M190 S T_h^1" is randomly assigned within the range from the current room temperature to the maximum temperature that the build platform/bed can be heated to.

Table 7.13: Information for measuring the apparent powers of component heating under different process parameters for the ANYCUBIC 3D printer

Apparent power		Related parameters		Parameter ranges			
				Lower bound		Upper bound	
Initial heating	P_h^1	Target temperature	T_h^1	Current room temperature	23°C	Maximum temperature of build platform/bed	80°C
Heat preservation	$P_{h_{hp}}^1$						
G-code commands		M140 S(T_h^1) : Set the target temperature T_h^1 of build platform/bed					
		M190 S(T_h^1)　 : Heat the build platform/bed to the target temperature T_h^1					

The experimental results of initial heating are listed in **Appendix II (10–22)** and summarised in **Table 7.14**. It has been found that the initial heating power P_h^1 of the build

platform/bed is stabilised as a constant, as shown in **Figure 7.5,** and is unrelated to the target temperature T_h^1. The average power of P_h^1 is calculated as **Equation (7.20)**.

$$P_h^1 = 262.07253(VA) \tag{7.20}$$

Table 7.14: Experimental results of apparent powers of component initial heating at different target temperatures for the ANYCUBIC 3D printer

Test No.	Target temperature	Apparent power of initial heating
	T_h^1 (°C)	P_h^1 (VA)
10	45	264.51378
11	45	263.45253
12	45	268.94294
15	50	263.22263
16	50	265.86281
17	50	274.71643
18	50	257.56893
13	60	258.98627
14	60	257.47102
20	60	255.56478
19	70	264.10028
21	70	251.13458
22	70	261.40596
Avg. (VA)		262.07253

The apparent power of component heating in the heat preservation state is different from other modules, which is distributed in the form of periodic pulses with a certain cycle time and constant amplitude until the end of the AM task. Due to the machine characteristics, this intermittent heating is to ensure that the bed temperature remains at the target value. To simplify the modelling process, the power profile is divided based on the heating cycles. The average time consumption t_{cycle}^1 and the average energy consumption E_{cycle}^1 per cycle are measured at different target temperatures T_h^1.

The results are obtained from the above experiments, as listed in **Appendix II (10–22)** and summarised in **Table 7.15**. It has been found that the energy consumption E_{cycle}^1 per cycle is stabilised as a constant and is unrelated to the target temperature T_h^1. Thus, the average value of E_{cycle}^1 is calculated as **Equation (7.21)**. Time consumption t_{cycle}^1 per

cycle is correlated to the target temperature T_h^1. Thus, polynomial regression method is applied to calculate the coefficient between t_{cycle}^1 and T_h^1. The regression model is presented in **Figure 7.9** and **Equation (7.22)**. The R^2 to evaluate the goodness-of-fit is calculated as 0.9982.

$$E_{cycle}^1 = 1331.00922(J) \tag{7.21}$$

$$t_{cycle}^1 = 0.03306{T_h^1}^2 - 4.839T_h^1 + 193 \tag{7.22}$$

Table 7.15: Experimental results of energy and time consumptions per cycle of heat preservation at different target temperatures for the ANYCUBIC 3D printer

Test No.	Target temperature T_h^1 (°C)	Energy per cycle E_{cycle}^1 (VAs)	Time per cycle t_{cycle}^1 (s)	Avg. (s)
10	45	1337.38441	42.16667	
11	45	1308.61239	42.84615	42.19475
12	45	1405.04383	41.57143	
13	60	1440.15482	21.43750	
14	60	1365.08439	22.33333	21.68750
20	60	1299.66810	21.29167	
19	70	1281.65498	16.41860	
21	70	1267.45592	16.72500	16.28120
22	70	1274.02414	15.70000	
Avg. (VAs)		1331.00922		
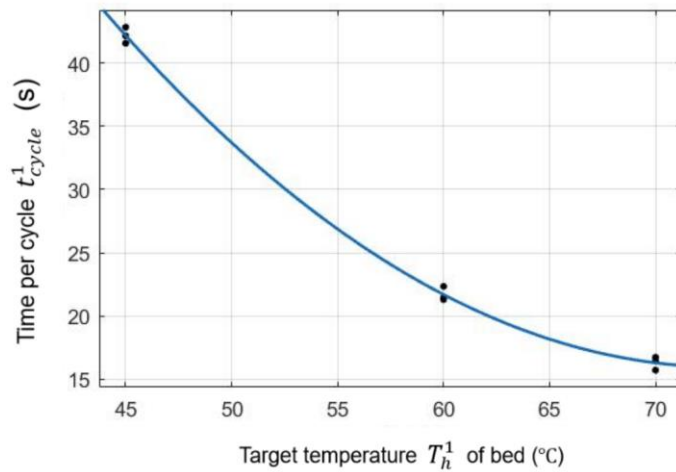
Figure 7.9: Regression model of time per cycle and target temperature for the heat preservation of component heating in the ANYCUBIC 3D printer

Based on the above, the energy consumption in the heat preservation state is modelled based on the energy E_{cycle}^1 per cycle and the total number of cycles. The number of cycles is calculated as the total time $t_{h_{hp}}^1$ of heat preservation divided by the cycle time t_{cycle}^1. The total energy consumption E_h of bed heating is the sum of energy consumed by the two working states, as expressed in **Equation (7.23)**.

$$E_h = P_h^1 t_h^1 + E_{cycle}^1 \frac{t_{h_{hp}}^1}{t_{cycle}^1} \tag{7.23}$$

7.3.2.4. Energy consumption of auxiliary components

This section models the energy consumption of auxiliary components, namely the display unit, temperature sensor, and user interface and connectivity. Before an AM task, the AM machine remains in standby mode with a stable power P_s. When the task begins, the apparent power rises by P_0 to start up the machine until the end of the task. Experiments are conducted to measure the standby power P_s and the start-up power P_0. The results are listed in **Appendix II (32, 33)**, and expressed as **Equation (7.24)** and **Equation (7.25)**. The total energy consumption E_{aux} of the auxiliary components is modelled as **Equation (7.26)**.

$$P_s = 18.47357 (VA) \tag{7.24}$$

$$P_0 = 9.58706 (VA) \tag{7.25}$$

$$E_{aux} = (P_s + P_0) t_{total} \tag{7.26}$$

7.3.2.5. Total energy consumption of all modules

Based on the above models, the total energy consumption E_{total} of the entire AM process is the sum of the energy consumed by the five modules, as expressed in **Equation (7.27)**.

$$E_{total} = E_h + E_{mp} + E_{axis} + E_{mf} + E_{aux} \tag{7.27}$$

7.3.3. Predictive model of material consumption

The modelling of material consumption is evolved from the initial conceptual model proposed in **Section 4.3.3**. For fused deposition modelling (FDM) technology, the amount of material feeding provided by G-code is in units of filament length. Therefore, the total mass M_{total} is modelled as the product of material density ρ and the total volume of material usage, as expressed in **Equation (7.30)**. Note that r denotes the diameter of the polylactic acid (PLA) filament material and l_e denotes the cumulative extruded length of material. The value of l_e is obtained from G-code commands beginning with the letter "E".

$$\rho = 1.24g/cm^3 \tag{7.28}$$

$$r = 1.75mm \tag{7.29}$$

$$M_{total} = \rho l_e \pi (\frac{r}{2})^2 \tag{7.30}$$

7.3.4. Additional experiments to improve the predictive models

Two factors that affect the prediction accuracy of the predictive models are considered in this case study, namely the occurrence of motor out-of-step during axis movement, and the deviation between the quoted material density and actual material density. Furthermore, the stepper motor responsible for material feeding also faces the problem of motor out-of-step. However, the reasons for this are complicated. On one hand, the motor loses step due to the high load of a high feeding rate and insufficient torques. On the other hand, when the material is supplied at a high feeding rate, it cannot be sufficiently melted in time, causing the material to become stuck in the nozzle and fail to be extruded onto the build platform. Therefore, in order to obtain the relationship between the actual and expected amounts of extruded material, a large number of additional experiments is needed for further modelling and analysis. This factor will be continued as future work to improve the predictive model of material consumption.

7.3.4.1. Actual speeds of axis movement

This section presents the additional experiments to obtain the functional relationships between the actual and expected speeds of axis movement in X, Y, Z directions. In X, Y directions, the G-code commands are manually defined to instruct the AM machine to move the nozzle for a sufficient displacement at different expected speeds. To ensure the diversity and dispersion of data points in the value space, there are 7 sets of experiments set up for the speed measurements in each direction. The expected speeds F_x, F_y in X, Y directions are randomly assigned within the pre-defined ranges. In Z direction, the nozzle moves at only one fixed speed due to the machine characteristics. There is only one actual speed to be tested at the expected speed of $5mm/s$. During the experiments, the total time of axis movement is recorded by the CW500 power meter to calculate the average speed.

The experimental results are presented in **Table 7.16** to **Table 7.18**. The functional relationships between the actual speeds $F_{x_{act}}$, $F_{y_{act}}$ and expected speeds F_x, F_y are obtained by using the polynomial regression method, as shown in **Figure 7.10** and **Figure 7.11**. The regression models are expressed as **Equation (7.31)** and **Equation (7.32)**, where R^2 to evaluate the goodness of fit are 1.0000 and 0.9999. The actual speed $F_{z_{act}}$ is measured as **Equation (7.33)**.

$$F_{x_{act}} = -0.001106F_x{}^2 + 1.058F_x - 0.6637 \tag{7.31}$$

$$F_{y_{act}} = -0.0017F_y{}^2 + 1.108F_y - 1.647 \tag{7.32}$$

$$F_{z_{act}} = 5.94827 (mm/s) \tag{7.33}$$

Table 7.16: Experimental results of actual speeds of axis movement in X direction for the ANYCUBIC 3D printer

Displacement (*mm*)	G-code command	Predicted time consumption (*s*)	Actual time consumption (*s*)	Expected speed F_x (*mm/s*)	Actual speed $F_{x_{act}}$ (*mm/s*)
6600	F900	440.00	440.00	15	15.00000
	F1800	220.00	221.00	30	29.86425
	F3000	132.00	133.00	50	49.62406
	F3600	110.00	112.00	60	58.92857
	F6000	66.00	70.00	100	94.28571
	F7200	55.00	60.00	120	110.00000
	F9600	41.25	47.00	160	140.42553

Table 7.17: Experimental results of actual speeds of axis movement in Y direction for the ANYCUBIC 3D printer

Displacement (*mm*)	G-code command	Predicted time consumption (*s*)	Actual time consumption (*s*)	Expected speed F_y (*mm/s*)	Actual speed $F_{y_{act}}$ (*mm/s*)
6600	F900	440.00	440.00	15	15.00000
	F1800	220.00	222.00	30	29.72973
	F3000	132.00	134.00	50	49.25373
	F3600	110.00	113.00	60	58.40708
	F6000	66.00	71.00	100	92.95775
	F7200	55.00	62.00	120	106.45161
	F9600	41.25	50.00	160	132.00000

Table 7.18: Experimental result of actual speed of axis movement in Z direction for the ANYCUBIC 3D printer

Displacement (*mm*)	G-code command	Expected time consumption (*s*)	Actual time consumption (*s*)	Expected speed F_z (*mm/s*)	Actual speed $F_{z_{act}}$ (*mm/s*)
4640	F300	928	780.00	5	5.94827
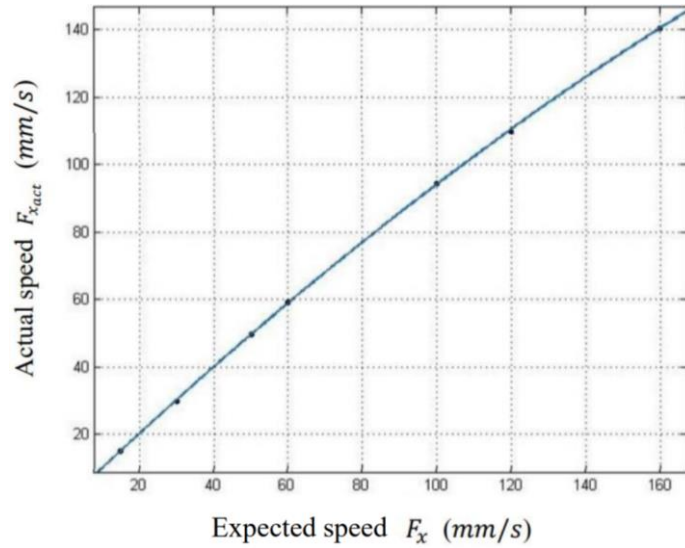
Figure 7.10: Regression model of actual and expected speeds of axis movement in X direction for the ANYCUBIC 3D printer
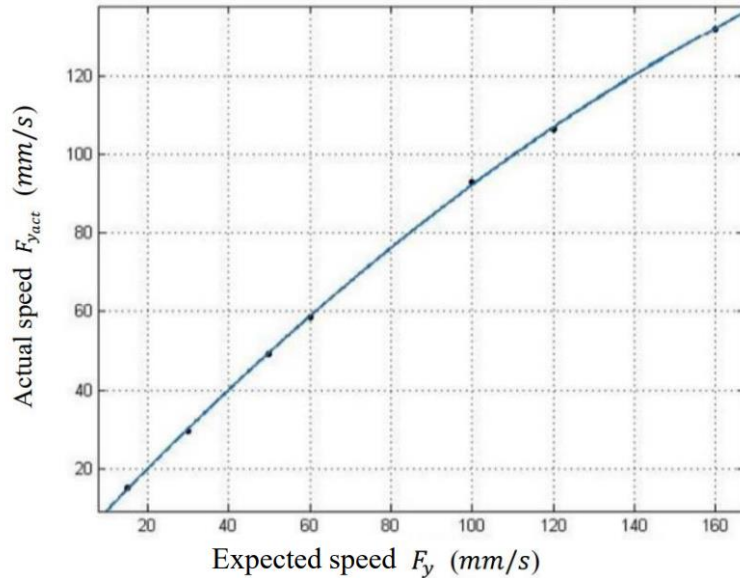
Figure 7.11: Regression model of actual and expected speeds of axis movement in Y direction for the ANYCUBIC 3D printer

7.3.4.2. Actual material density

The actual density of the polylactic acid (PLA) filament material is measured by using the Sartorius Practum313-1S Milligram Balance. Five samples are prepared for measurement of the masses W_{air}, W_{water} in air and water. Since the room temperature T during the experiment is 22.5°C, the corresponding water density ρ_{H_2O} is $0.99771 g/cm^3$ according

to Sartorius (2020). The experimental results are listed in **Table 7.19** and the average value ρ_{act} of material density is calculated as **Equation (7.34)**.

$$\rho_{act} = 1.23559 g/cm^3 \qquad (7.34)$$

Table 7.19: Experimental results of the actual density of PLA filament material

Mass in air	Mass in water	Density of material
W_{air} (g)	W_{water} (g)	ρ_{act} (g/cm^3)
0.160	0.031	1.23747
0.124	0.024	1.23716
0.097	0.019	1.24074
0.117	0.023	1.24183
0.104	0.019	1.22073
Avg. (g/cm^3)		1.23559

Based on the above, the parameters $F_{xy_{act}}$, $F_{z_{act}}$, ρ_{act} measured through additional experiments are used to replace the original parameters F_{xy}, F_z, ρ in the predictive models. To validate the accuracies of the predictive models with and without additional experiments, two AM tasks have been printed by the AM machine and the actual consumptions have been recorded. The prediction results and the result analyses will be discussed in the next chapter.

7.4. Predictive models of Monoprice MP Mini Delta 3D printer

This section presents the prediction of time, energy and material consumptions of the Monoprice MP Mini Delta fused deposition modelling (FDM) 3D printer. Same as the first case study, the modelling procedure follows the application indication in Chapter 5.

1) Module classification

At first, the components in the Monoprice printer are classified into five modules, namely axis movement, material feeding, material processing, component' heating and auxiliary components. The axis movement module refers to the Delta system driven by three linked stepper motors in X, Y, Z directions. The material feeding module refers to the extruder. The material processing module refers to the nozzle hotend. The component heating module refers to the build platform. The auxiliary components module refers to the display unit, temperature sensor, and user interface and connectivity.

2) Power and time tests of AM system

Figure 7.12 and **Figure 7.13** show the power profiles of a general AM task, for which the G-code is also generated by Cura. Note that the powers of the axis movement module and material feeding module are also combined, since the four stepper motors of these two modules can only run synchronously. Due to the unique coding rules of Cura, the running sequences of the modules are different from the first case study. Based on the power profiles, the working states of five modules are defined as follows.

- The material feeding module has two working states: the material feeding state with an actual feeding amount and the standby state.

- The axis movement module has two working states: the state of axis movement with actual displacements and the standby state. Based on the coding rules, the machine needs to calibrate the origin coordinates and initialise the material feeding amount at the beginning of each AM task. Therefore, the modules of axis movement and material

feeding driven by four stepper motors remain in operation throughout the entire task. The calibration is to move the nozzle from the final coordinates in the last AM process back to the platform origin. However, since the last coordinate is not provided in the current G-code file, the time consumption of this calibration process is unknown and not fixed. Thus, the calibration is temporarily not considered in this case study, and the modelling starts only from the initial heating of the nozzle hotend. For the continuous printing of multiple AM jobs, the consumptions of calibration process can be added into the predictive models when the last coordinate in the previous AM process is known.

- According to the power profile, the material processing module (i.e., nozzle hotend) has three working states: the initial heating state, the transition state and the heat preservation state. When an AM task begins, the initial heating starts at a temperature 5°C higher than the target temperature. This coding rule is to ensure that the polylactic acid (PLA) material can be melted at a sufficient temperature to prepare for material deposition. Once the module reaches the specified temperature, the material deposition starts, and the heating stops for a period of time without a power supply. Here, we define this period as the transition time t_{trans}. Then, the material processing module switches to the heat preservation stage until the end of the AM task. Due to the unique coding rules, when the deposition of first layer is completed, the temperature of the nozzle hotend is restored to the target temperature T_{mp}^1 in the heat preservation state.

- The module of component heating (i.e., build platform/bed) has two working states: the initial heating state and the heat preservation state. The initial heating begins when the first layer is completed. When reaching the target temperature, the module is switched to the state of heat preservation till the end of the AM process.

- The auxiliary components module remains in the state of continuous monitoring and control of the machine status throughout the entire process.
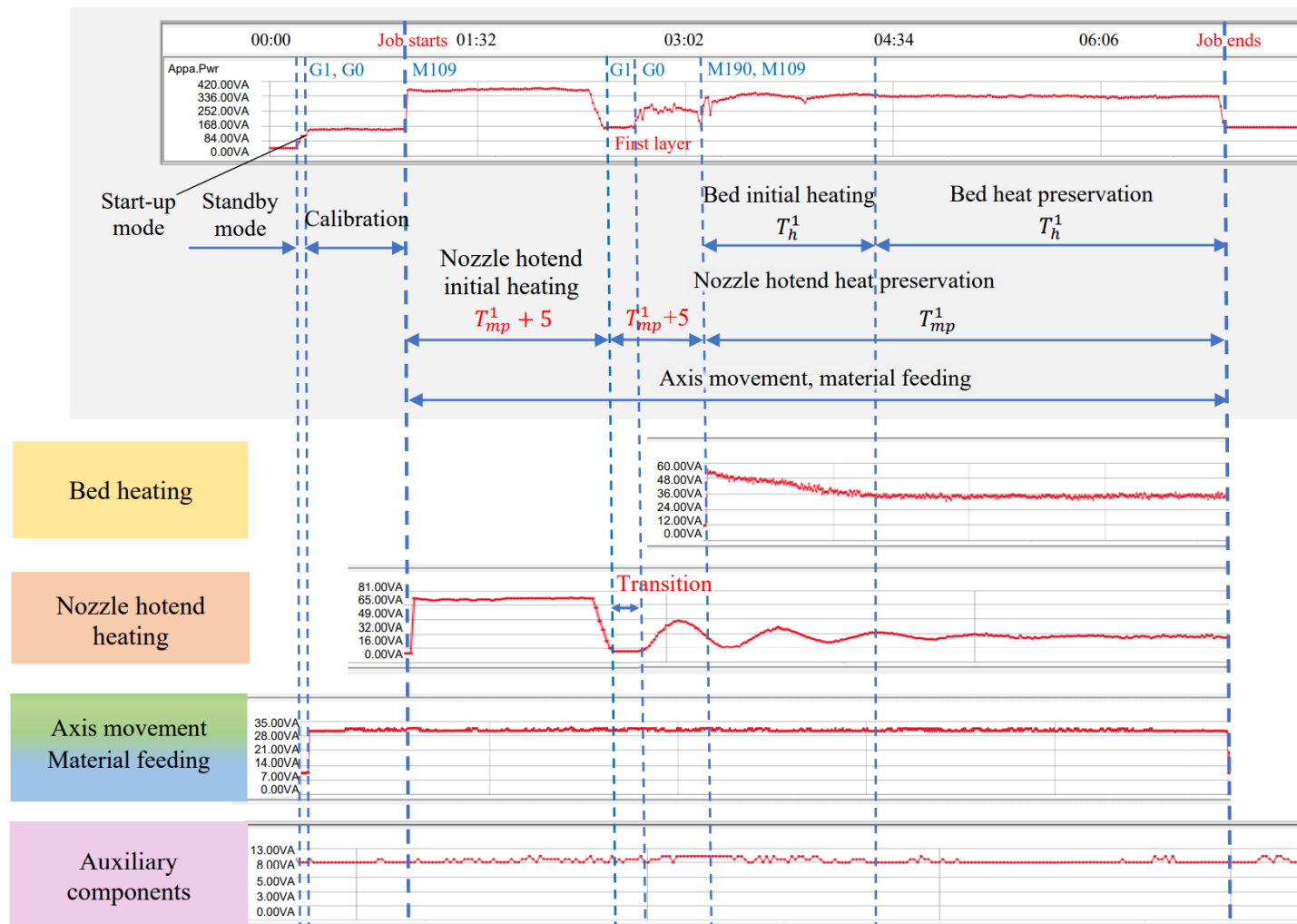
Figure 7.12: Power profiles of Monoprice MP Mini Delta FDM 3D printer and consumption-related components
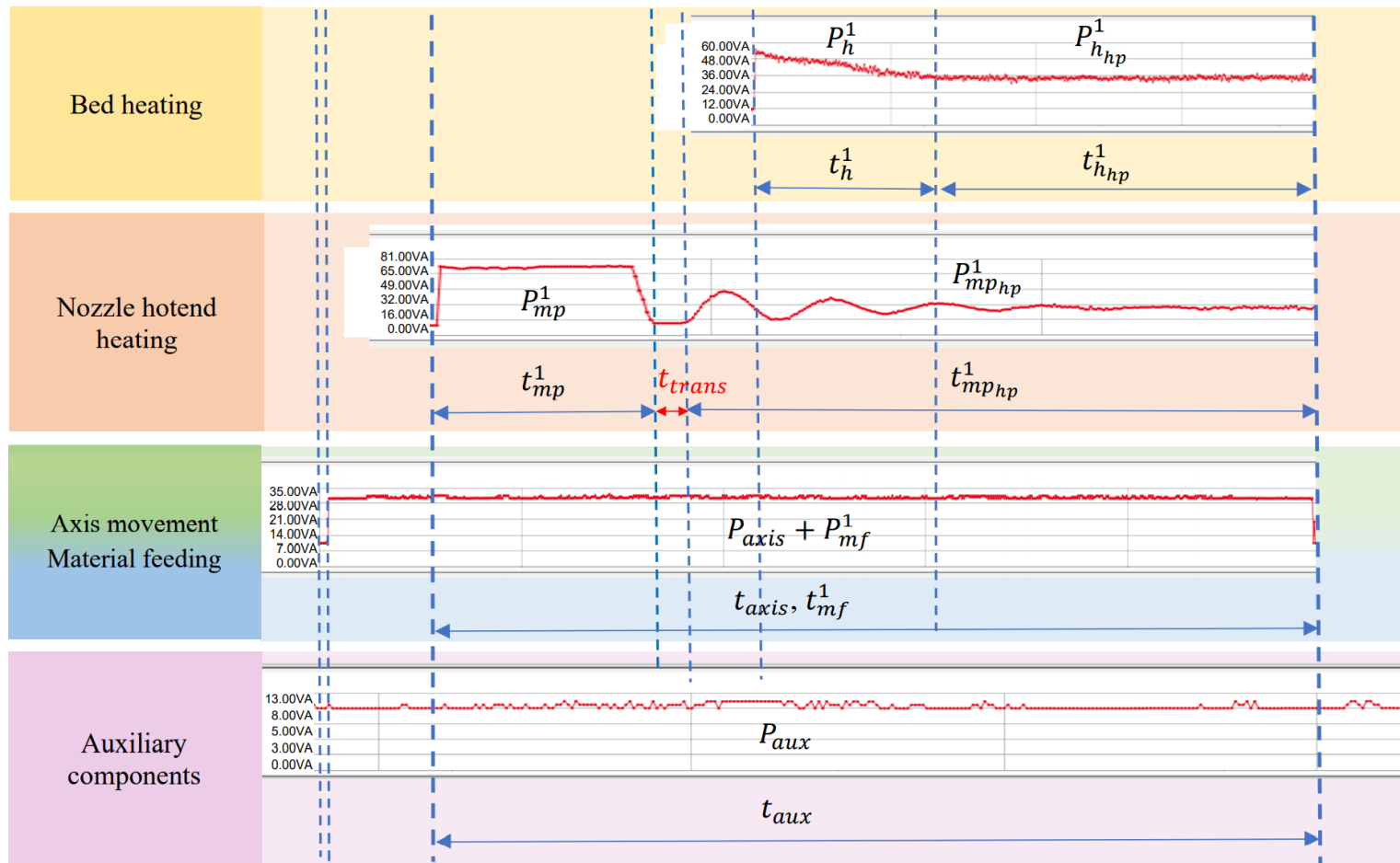
Figure 7.13: Power profiles of five types of modules in Monoprice MP Mini Delta FDM 3D printer

3) Generate prototypes of predictive models

According to the Gannt chart, the total time consumption is modelled as the union of time consumption of each module, as expressed in **Equation (7.35)**. t_{axis} denotes the time consumption of axis movement module. t_{mp}^1 , t_{trans} and $t_{mp_{hp}}^1$ denote the time consumptions of initial heating state, transition state and heat preservation state of material processing module (i.e. nozzle hotend). t_h^1 and $t_{h_{hp}}^1$ denote the time consumptions of initial heating state and heat preservation state of component heating module (i.e. build platform / bed). t_{mf}^1 denotes the time consumption of material feeding module. t_{aux} denotes the time consumption of auxiliary components.

$$t_{total} = t_{axis} \cup t_{mp}^1 \cup t_h^1 \cup t_{trans} \cup t_{mp_{hp}}^1 \cup t_{h_{hp}}^1 \cup t_{mf}^1 \cup t_{aux} \qquad (7.35)$$

Same as the first case study, the total energy consumption is modelled as the sum of energy consumption of five modules, as expressed in **Equation (7.36)**. E_{axis}, E_{mp}, E_h, E_{mf} and E_{aux} respectively denote the energy consumption of axis movement module, material processing module (i.e. nozzle hotend), component heating module (i.e. build platform / bed), material feeding module and auxiliary components.

$$E_{total} = E_{axis} + E_{mp} + E_h + E_{mf} + E_{aux} \qquad (7.36)$$

The total material consumption is also modelled as the product of the material density ρ and the cumulative volume $\sum V_{unit}$ of material feeding, as expressed in **Equation (7.37)**.

$$M_{total} = \rho \cdot \sum V_{unit} \qquad (7.37)$$

4) Hybrid modelling to obtain model parameters

The final step is to obtain the predictive models of each module on the basis of the above prototypes. The model parameters will be obtained through the hybrid modelling method. Details will be presented in the following sections.

7.4.1. Predictive model of time consumption

This section describes the time consumption modelling for each module in the Monoprice MP Mini Delta fused deposition modelling (FDM) 3D printer. The predictive models are described in the following sub-sections.

7.4.1.1. Time consumption of axis movement

As shown in **Figure 7.12**, the axis movement module starts running at the beginning of an AM task. When the initial heating of the material processing module begins, the axis movement module is in the standby state to wait for completion of the component heating. Therefore, there is an interruption during axis movement. The interval time t_{xyz}^0 of this interruption represents the initial heating time t_{mp}^1 of the material processing module (i.e. nozzle hotend). In **Equation (7.38)**, the total time consumption t_{axis} of axis movement includes two parts: the time t_{xyz} spent on axis movement with actual displacements and the initial heating time t_{mp}^1 of the material processing module. The former is directly calculated from G-code and the latter is modelled in the following sections.

$$t_{axis} = t_{xyz} + t_{mp}^1 \tag{7.38}$$

7.4.1.2. Time consumption of material processing

This section models the time consumption of the material processing module. In the initial heating state, due to the unique coding rules of the Monoprice 3D printer, the nozzle hotend is heated to a temperature that is 5°C higher than the target temperature T_{mp}^1. Thus, the time consumption t_{mp}^1 is modelled as a function of the temperature difference $\Delta T_{mp}^1 + 5$ between the current temperature $T_{mp_0}^1$ and the temperature $T_{mp}^1 + 5$. Experiments are conducted to test the time t_{mp}^1 spent on initial heating under random temperature differences ΔT_{mp}^1. As shown in **Table 7.20**, the target temperature T_{mp}^1 in the G-code commands "M104 ST_{mp}^1" and "M109 ST_{mp}^1" is randomly assigned with different values. The

value of T_{mp}^1 is set within the range from the melting point of the material to the maximum temperature that the nozzle hotend can be heated to. The value of the current temperature $T_{mp_0}^1$ is set within the range from the current room temperature to the maximum temperature of the nozzle hotend.

Table 7.20: Information for measuring the time consumptions of the material processing module under different process parameters for the Monoprice 3D printer

Time consumption	Related parameters		Parameter ranges			
			Lower bound		Upper bound	
t_{mp}^1	Current temperature	$T_{mp_0}^1$	Current room temperature	23°C	Maximum temperature of nozzle hotend	260°C
t_{trans}	Target temperature	T_{mp}^1	Melting point of material	150°C	Maximum temperature of nozzle hotend	260°C
G-code commands	M104 S(T_{mp}^1) : Set the target temperature T_{mp}^1 of nozzle hotend					
	M109 S(T_{mp}^1) : Heat the nozzle hotend to the target temperature T_{mp}^1					

The experimental results are presented in **Appendix III (1–4)** and summarised in **Table 7.21**. The results prove that the time consumption t_{mp}^1 is functionally related to the temperature difference ΔT_{mp}^1. By using the polynomial regression method, the regression model is shown in **Figure 7.14** and expressed as **Equation (7.39)**. Note that in a practical AM task, the temperature of initial heating is 5°C higher than the predefined target temperature T_{mp}^1. The R^2 to evaluate the goodness-of-fit is calculated as 0.9920.

$$t_{mp}^1 = 0.4401(\Delta T_{mp}^1 + 5) + 1.934 \tag{7.39}$$

Table 7.21: Experimental results of initial heating time under random temperature differences and transition time at different target temperatures of the material processing module in the Monoprice 3D printer

Test No.	Current temperature $T_{mp_0}^1$ (°C)	Target temperature T_{mp}^1 (°C)	Temperature difference ΔT_{mp}^1 (°C)	Initial heating time t_{mp}^1 (s)	Transition time t_{trans} (s)
1	32	150	118	50	29
2	71	170	99	47	23
3	63	190	127	60	20
4	49	210	161	73	14
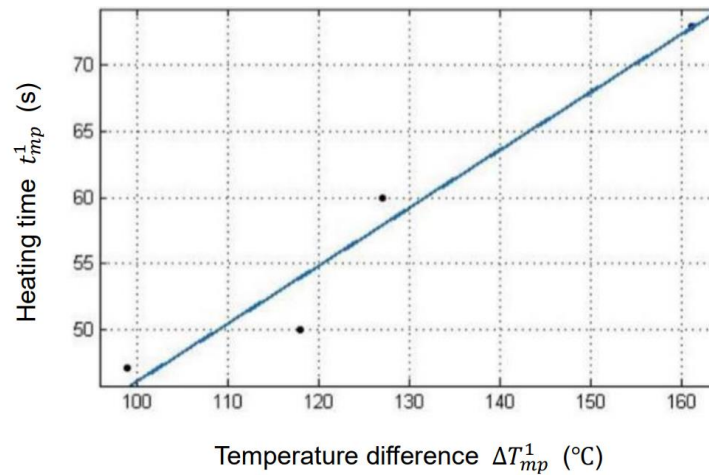
Figure 7.14: Regression model of initial heating time and temperature difference of the material processing module in the Monoprice 3D printer

After the initial heating, the material processing module experiences a period of transition time t_{trans} without a power supply. Time measurements are also performed. The results in **Table 7.21** prove that the transition time t_{trans} is related to the target temperature T_{mp}^1. By using the polynomial regression method, the regression model of the transition time t_{trans} and target temperature T_{mp}^1 is presented in **Figure 7.15** and **Equation (7.40)**. In this process, the temperature of the material processing module is still 5°C higher than the predefined target temperature T_{mp}^1. The R^2 to evaluate the goodness-of-fit is 0.9487.

$$t_{trans} = -0.24(T_{mp}^1 + 5) + 64.7 \tag{7.40}$$
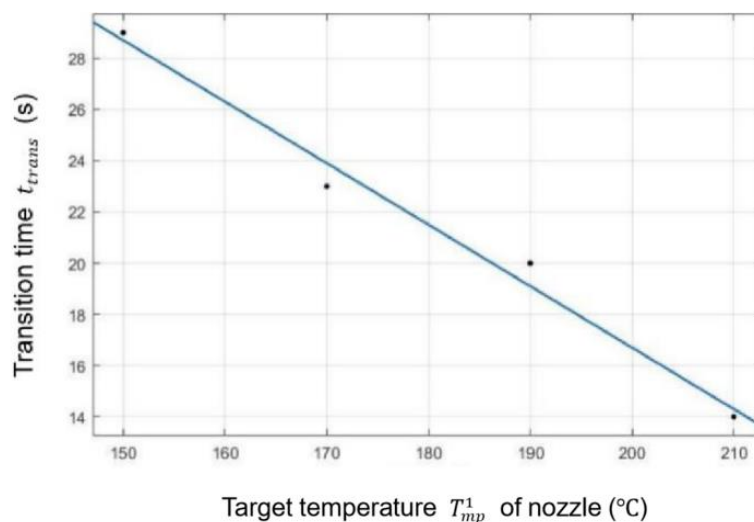
Figure 7.15: Regression model of transition time and target temperature of the material processing module in the Monoprice 3D printer

After the initial heating, the module is switched to the heat preservation state and the material deposition starts to construct the 3D object. When the first layer is completed, the temperature of the material processing module is restored to the target temperature T_{mp}^1 and the heat preservation continues. Therefore, the time spent on heat preservation consists of two parts: the heat preservation time $t_{mp_{hp\_first}}^1$ for the first layer at temperature $T_{mp}^1 +5$, and the heat preservation time $t_{mp_{hp\_rest}}^1$ for the remaining layers at the target temperature T_{mp}^1, as expressed in **Equation (7.41)**.

$$t_{mp_{hp}}^1 = t_{mp_{hp\_first}}^1 + t_{mp_{hp\_rest}}^1 \qquad (7.41)$$

According to the Gannt chart in **Figure 7.12**, the heat preservation time $t_{mp_{hp\_first}}^1$ refers to the time spent on material disposition of the first layer excluding the transition time t_{trans}, as expressed in **Equation (7.42)**. Note that q denotes the total number of G-code command lines used to print the first layer in X, Y directions. The heating time $t_{mp_{hp\_rest}}^1$ refers to the time spent on depositing the remaining layers, as expressed in **Equation (7.43)**.

$$t_{mp_{hp\_first}}^1 = \sum_{g=1}^{q} \frac{\sqrt{\Delta X^2 + \Delta Y^2}}{F_{xy}} - t_{trans} \qquad (7.42)$$

$$t_{mp_{hp\_rest}}^1 = t_{xyz} - \sum_{g=1}^{q} \frac{\sqrt{\Delta X^2 + \Delta Y^2}}{F_{xy}} \qquad (7.43)$$

7.4.1.3. Time consumption of component heating

This section models the time consumption of component heating module. According to the power profile in **Figure 7.12**, the power P_h^1 of initial heating state gradually decreases from the maximum heating power $P_{h_{max}}^1$ to the heat preservation power $P_{h_{hp}}^1$. Once the module reaches the target temperature, the power of heat preservation state become stable. **Figure 7.16** presents the downward trend of the initial heating power P_h^1 with unstable fluctuations. To simplify the consumption modelling, the relationship between the heating power P_h^1 and the heating time t_h^1 is simplified to a polynomial function with a fixed slope.
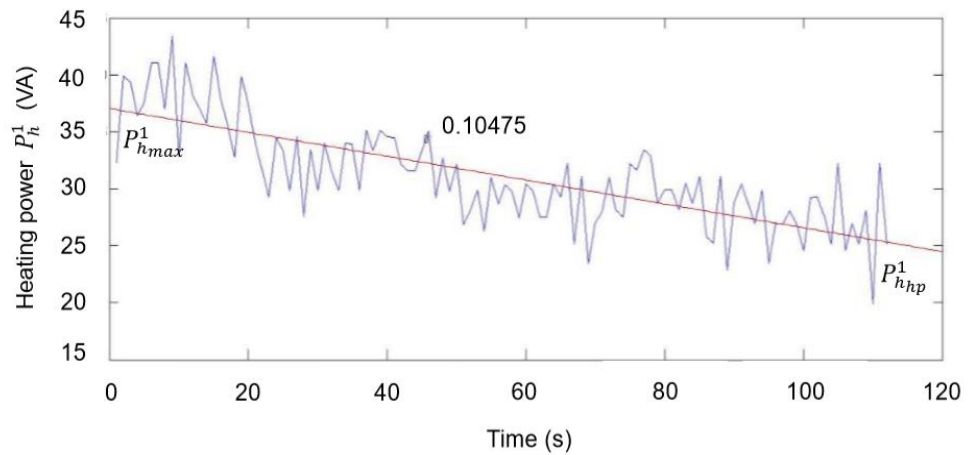
Figure 7.16: Experimental result of the initial heating power of the build platform/bed in the Monoprice 3D printer

Due to the unique heating method of this AM machine, it is necessary to understand the relationships between the maximum heating power $P^1_{h_{max}}$, the heat preservation power $P^1_{h_{hp}}$, the initial heating time t^1_h and the target temperature T^1_h of the build platform/bed. Thus, experiments are conducted to test the time t^1_h spent on initial heating under random temperature differences ΔT^1_h. As shown in **Table 7.22**, the current temperature $T^1_{h_0}$ and the target temperature T^1_h are both randomly set within the range from the current room temperature to the maximum temperature of the build platform/bed. During the experiments, the CW500 power meter is used to record the initial heating time t^1_h, the maximum heating power $P^1_{h_{max}}$ and the heat preservation power $P^1_{h_{hp}}$.

Table 7.22: Information for measuring the time consumptions of component heating under different process parameters for Monoprice 3D Printer

Time consumption; apparent powers	Related parameters		Parameter ranges			
			Lower bound		Upper bound	
t^1_h $P^1_{h_{max}}$ $P^1_{h_{hp}}$	Current temperature	$T^1_{h_0}$	Current room temperature	23°C	Maximum temperature of build platform/bed	60°C
	Target temperature	T^1_h	Current room temperature	23°C	Maximum temperature of build platform/bed	60°C
G-code commands	M140 S(T^1_h) : Set the target temperature T^1_h of build platform/bed M190 S(T^1_h) : Heat the build platform/bed to the target temperature T^1_h					

The experimental results are presented in **Appendix III (5–9)** and **Table 7.23**. It has been found that the maximum heating power $P_{h_{max}}^1$ and the heat preservation power $P_{h_{hp}}^1$ are both related to the target temperature T_h^1. The initial heating time t_h^1 is unrelated to the target temperature T_h^1 or temperature difference ΔT_h^1, while the decreasing slope remains around a stable value. The average slope is calculated as 0.10475.

Table 7.23: Experimental results of heating powers under five random temperature differences and five different target temperatures of the component heating module in the Monoprice 3D printer

Test No.	$T_{h_0}^1$ (°C)	T_h^1 (°C)	ΔT_h^1 (°C)	$P_{h_{max}}^1$	$P_{h_{hp}}^1$	t_h^1 (s)	Slope
5	30	40	10	26.32867	11.58044	112	0.131681
6	30	45	15	28.50403	14.16599	147	0.097538
7	23	50	27	32.65663	17.28068	162	0.094913
8	33	55	22	38.49048	19.76008	187	0.100163
9	31	60	29	41.07333	22.77295	184	0.099459
Avg. slope							0.10475

Based on the above, the time consumption t_h^1 of initial heating is modelled as a function of $P_{h_{max}}^1$, $P_{h_{hp}}^1$ and the average slope, as shown in **Equation (7.44)**. The modelling of powers $P_{h_{max}}^1$ and $P_{h_{hp}}^1$ will be discussed in **Section 7.4.2.3**. Based on the Gannt chart of five modules, the time consumption $t_{h_{hp}}^1$ of the heat preservation is modelled as the time t_{xyz} spent on material deposition, excluding the time of the first layer's construction and the initial heating time t_h^1, as shown in **Equation (7.45)**.

$$t_h^1 = \frac{P_{h_{max}}^1 - P_{h_{hp}}^1}{0.10475} \tag{7.44}$$

$$t_{h_{hp}}^1 = t_{xyz} - \sum_{g=1}^{q} \frac{\sqrt{\Delta X^2 + \Delta Y^2}}{F_{xy}} - t_h^1 \tag{7.45}$$

7.4.1.4. Time consumption of material feeding

This section models the time consumption of material feeding module, which has two working states: the material feeding state with an actual feeding amount and the standby state. Since the material feeding is synchronous with axis movement, the time consumption t_{axis} of axis movement represents time consumption t_{mf}^1 of material feeding, as expressed in **Equation (7.46)**.

$$t_{mf}^1 = t_{axis} \tag{7.46}$$

7.4.1.5. Time consumption of auxiliary components

This auxiliary components, namely the display unit, temperature sensor, and user interface and connectivity, remain in an operating status throughout the entire AM process. Therefore, the time consumption t_{aux} is the same as the total time consumption t_{total}, as expressed in **Equation (7.47)**.

$$t_{aux} = t_{total} \tag{7.47}$$

7.4.1.6. Total time consumption of all modules

Based on the above models, the total time consumption t_{total} is the union of time consumed by all five modules. According to the running sequences of the five modules in **Figure 7.12**, t_{total} refers to the sum of time consumptions of two modules – material processing and axis movement – as expressed in **Equation (7.48)**.

$$t_{total} = t_{mp}^1 + t_{xyz} \tag{7.48}$$

7.4.2. Predictive model of energy consumption

This section models the energy consumption of each module in the Monoprice MP Mini Delta FDM 3D printer. The predictive models are described in the following sub-sections.

7.4.2.1. Energy consumptions of axis movement and material feeding

Based on the power profiles of axis movement module and material feeding module, it has been found that both modules have stable powers during material deposition process. Thus, the apparent power P_{axis} of the axis movement module is modelled as a function of speeds F_{xy} and F_z in X, Y, Z directions. The apparent power P_{mf}^c of material feeding is modelled as a function of the feeding rate F_{xy} in X, Y directions. To calculate the functional relationships, experiments are conducted to measure the apparent powers under different axis movement speeds and material feeding rates.

Table 7.24: Information for measuring the apparent powers of the axis movement module and material feeding module in X, Y, Z directions under different process parameters for the Monoprice 3D printer (G-Code – Reprap, 2020)

Apparent powers	Related parameters		Parameter ranges			
			Lower bound		Upper bound	
P_{axis}	Speed of axis movement in X, Y, Z directions	F_{xy}, F_z	Lowest speed of axis movement in X, Y directions	$600mm$ $/min$	Highest speed of axis movement in X, Y directions	$9000mm$ $/min$
P_{mf}^1	Rate of material feeding in X, Y directions	F_{xy}	Lowest rate of material feeding in X, Y directions	$600mm$ $/min$	Highest rate of material feeding in X, Y directions	$9000mm$ $/min$
G-code commands	G1 F_{xy} Xnnn Ynnn : Nozzle moves to the target coordinate (Xnnn, Ynnn) at a speed of F_{xy} G1 F_z Znnn : Nozzle moves to the target coordinate (Znnn) at a speed of F_z G1 F_{xy} Xnnn Ynnn Emmm : Nozzle moves to the target coordinate (Xnnn, Ynnn) with material feeding; the total amount of material feeding is mmm					

The axis movement and material feeding are driven by four stepper motors. Similar to the first case study, experiments are conducted to measure the apparent powers of all combinations of the four stepper motors. As shown in **Table 7.24**, the speed or feeding rate F_{xy} in X, Y directions and the speed F_z in Z direction are assigned within the range from the lowest to the highest speed or feeding rate. The coordinates in G-code commands are defined to instruct (a) the axis movement module to move for a sufficient displacement and (b) the material feeding module to feed a sufficient amount of material filament.

The experimental results are listed in **Appendix III (10–18)** and **Table 7.25**. The same as in the first case study, the power of axis movement is distributed as a constant regardless of the speed variation. Also, the modules operate at different power levels for different combinations of the four stepper motors. Since all stepper motors are involved in a general AM process, the total power of two modules is expressed as **Equation (7.49)**.

$$P_{axis} + P_{mf}^1 = 28.25414 (VA) \tag{7.49}$$

Table 7.25: Experimental results of apparent powers of axis movement and material feeding at different speeds in different directions for the Monoprice 3D printer

Test No.	Stepper motors	Speeds F_{xy}, F_z (mm/min)	Avg. power P_{axis}, P_{mf}^1 (VA)
10	X	1200, 3600, 5400, 9000	19.26776
11	Y	1200, 3600, 5400, 9000	19.90313
12	Z	1200, 3600, 5400, 9000	21.07183
13	Material feeding	1200, 3600, 5400, 9000	28.55376
14	X, Y	1200, 3600, 5400, 9000	18.72511
15	X, Z	1200, 3600, 5400, 9000	20.30556
16	Y, Z	1200, 3600, 5400, 9000	20.40393
17	X, Y, Z	1200, 3600, 5400, 9000	20.29855
18	X, Y, Z, material feeding	1200, 3600, 5400, 9000	28.25414

Based on the above, the total energy consumption of axis movement E_{axis} and material feeding E_{axis} is modelled as the product of total power and time consumption t_{axis}, as expressed in **Equation (7.50)**.

$$E_{axis} + E_{mf} = \left(P_{axis} + P_{mf}^1 \right) t_{axis} = 28.25414 t_{axis} \tag{7.50}$$

7.4.2.2. Energy consumption of material processing

This section models the energy consumption of the material processing module. The apparent powers P_{mp}^1 of initial heating and $P_{mp_{hp}}^1$ of heat preservation are modelled as functions of the target temperature T_{mp}^1. Experiments are conducted to measure the apparent powers P_{mp}^1, $P_{mp_{hp}}^1$ under different target temperatures T_{mp}^1. In **Table 7.26**, the target temperature T_{mp}^1 in the G-code commands "M104 ST_{mp}^1" and "M109 S T_{mp}^1" is manually assigned with within the range from the melting point of the material to the maximum temperature that the module can be heated to.

Table 7.26: Information for measuring the apparent powers of the material processing module under different process parameters for the Monoprice 3D printer

Apparent power		Related parameter		Parameter ranges			
				Lower bound		Upper bound	
Initial heating	P_{mp}^1	Target temperature	T_{mp}^1	Melting point of material	150℃	Maximum temperature of nozzle hotend	250℃
Heat preservation	$P_{mp_{hp}}^1$						
G-code commands		M104 S(T_{mp}^1) : Set the target temperature T_{mp}^1 of nozzle hotend M109 S(T_{mp}^1) : Heat the nozzle hotend to the target temperature T_{mp}^1					

The experimental results are presented in **Appendix III (1–4)** and **Table 7.27**. It has been found that the apparent power P_{mp}^1 of initial heating remains constant and is unrelated to the target temperature T_{mp}^1. The average power is calculated as **Equation (7.51)**.

$$P_{mp}^1 = 58.96088(VA) \tag{7.51}$$

Table 7.27: Experimental results of apparent powers of material processing at different target temperatures for the Monoprice 3D printer

Test No.	Target temperature	Apparent power of initial heating	Apparent power of heat preservation
	T_{mp}^1 (℃)	P_{mp}^1 (VA)	$P_{mp_{hp}}^1$ (VA)
1	150	59.78204	16.72852
2	170	60.24474	19.22486
3	190	58.73848	21.20641
4	210	57.07825	23.46649
Avg. (VA)		58.96088	

After the initial heating and transition processes, the power $P^1_{mp_{hp}}$ of heat preservation gradually tends to be stabilised as a constant and is found to be related to the target temperature T^1_{mp}. Polynomial regression method is applied to calculate the coefficient between the apparent power $P^1_{mp_{hp}}$ and the target temperature T^1_{mp}. The regression model is presented in **Figure 7.17** and **Equation (7.52)**. The R^2 to evaluate the goodness-of-fit is calculated as 0.9982.

$$P^1_{mp_{hp}} = 0.111T^1_{mp} + 0.1807 \tag{7.52}$$

Figure 7.17: Regression model of apparent power and target temperature for the heat preservation of the material processing module

Due to the unique coding rules in Cura, the temperature of heat preservation during the construction of the first layer is 5°C higher than the target temperature T^1_{mp}. Thus, the apparent power $P^1_{mp_{hp\_first}}$ of heat preservation for the first layer is improved from **Equation (7.52)** to **Equation (7.53)**. For the remaining layers, the temperature of the material processing module is restored back to the target temperature T^1_{mp}. The apparent power $P^1_{mp_{hp}}$ of heat preservation for the remaining layers is expressed as **Equation (7.52)**.

$$P^1_{mp_{hp\_first}} = 0.111\left(T^1_{mp} + 5\right) + 0.1807 \tag{7.53}$$

Based on the above, the total energy consumption E_{mp} of the material processing module is the sum of energy consumed by three states: the initial heating, the heat preservation during the construction of the first layer and the heat preservation during the construction of the remaining layers. It is expressed as **Equation (7.54)**.

$$E_{mp} = P^1_{mp} t^1_{mp} + P^1_{mp_{hp\_first}} t^1_{mp_{hp\_first}} + P^1_{mp_{hp}} t^1_{mp_{hp\_rest}} \tag{7.54}$$

7.4.2.3. Energy consumption of component heating

This section models the energy consumption of component heating module. According to the previous discussion, the relationship between the initial heating power P^1_h and the initial heating time t^1_h has been simplified to a polynomial function with a fixed slope. The experimental results of the maximum heating powers $P^1_{h_{max}}$ and the heat preservation powers $P^1_{h_{hp}}$ at different target temperatures T^1_h have been listed in **Appendix III (5–9)** and **Table 7.23** in **Section 7.4.1.3**.

According to the experimental results, it has been found that the maximum heating powers $P^1_{h_{max}}$ and the heat preservation powers $P^1_{h_{hp}}$ are both related to the target temperature T^1_h. Polynomial method is applied to calculate the coefficients between the apparent powers $P^1_{h_{max}}$, $P^1_{h_{hp}}$ and the target temperature T^1_h. As shown in **Figure 7.18** and **Figure 7.19**, the regression models of the apparent powers at the two heating stages are expressed as **Equation (7.55)** and **Equation (7.56)**. The values of R^2 to evaluate the goodness-of-fit are calculated as 0.9781 and 0.999, respectively.

$$P^1_{h_{max}} = 0.7895T^1_h - 6.065 \tag{7.55}$$

$$P^1_{h_{hp}} = 0.56T^1_h - 10.88 \tag{7.56}$$
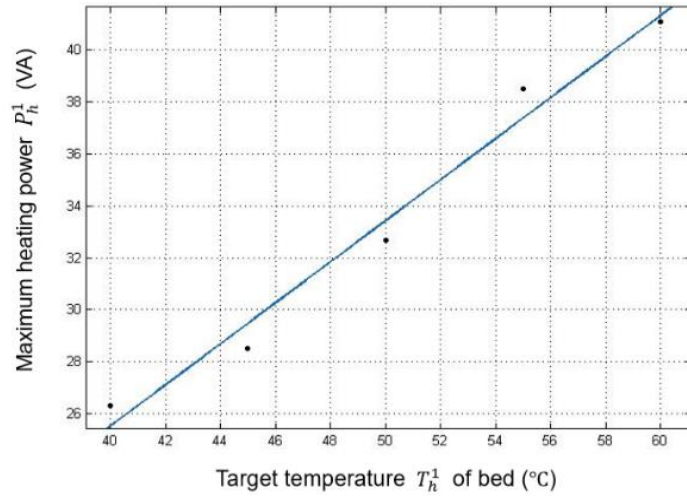
Figure 7.18: Regression model of the maximum heating power and target temperature for the initial heating of the component heating module in the Monoprice 3D printer
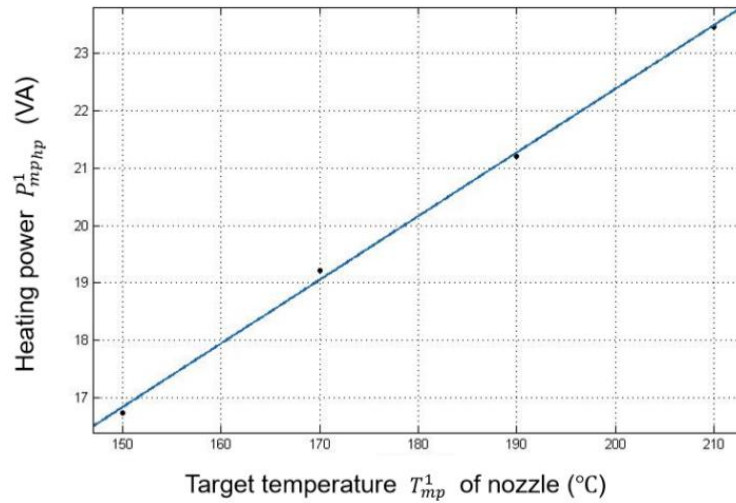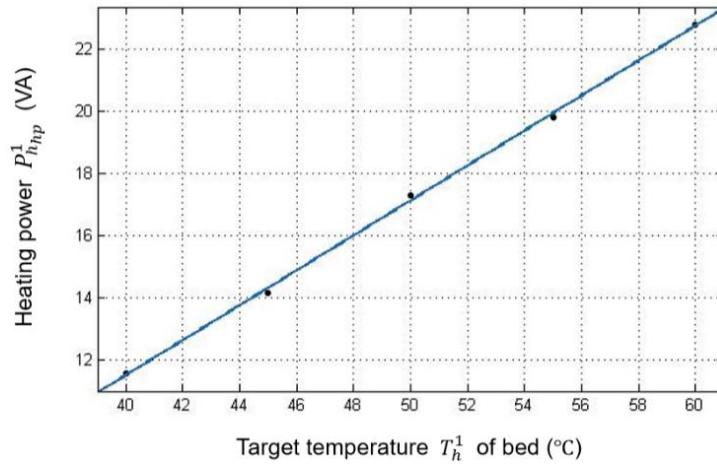

Figure 7.19: Regression model of apparent power and target temperature for the heat preservation of the component heating module in the Monoprice 3D printer

Based on the above models, the total energy consumption E_h of the component heating module is the sum of the time-integral of power in the two working states, as expressed in **Equation (7.57)**.

$$E_h = \int_o^{t_h^1} P_h^1 dt + \int_o^{t_{h_{hp}}^1} P_{h_{hp}}^1 dt = \frac{(P_{h_{max}}^1 + P_{h_{hp}}^1)}{2} t_h^1 + P_{h_{hp}}^1 t_{h_{hp}}^1 \qquad (7.57)$$

7.4.2.4. Energy consumption of auxiliary components

The auxiliary component, namely the display unit, temperature sensor, and user interface and connectivity, remain using stable power throughout the entire AM process. The total

time consumption t_{aux} of auxiliary components is the same as the total time consumption t_{total} of the entire AM task. Similar to the first case study, experiments are conducted to measure the standby power P_s and the start-up power P_0. The results are listed in **Appendix III (19, 20)** and the models are expressed as **Equation (7.58)** and **Equation (7.59)**. The total energy consumption E_{aux} of the auxiliary components is modelled as the sum of the time-integral of power, as expressed in **Equation (7.60)**.

$$P_s = 10.77589(VA) \qquad (7.58)$$

$$P_0 = 1.65420(VA) \qquad (7.59)$$

$$E_{aux} = (P_s + P_0)t_{total} \qquad (7.60)$$

7.4.2.5. Total energy consumption of five modules

Based on the above models, the total energy consumption E_{total} is the sum of energy consumed by all five modules, as expressed in **Equation (7.61)**.

$$E_{total} = E_h + E_{mp} + E_{axis} + E_{mf} + E_{aux} \qquad (7.61)$$

7.4.3. Predictive model of material consumption

The Monoprice 3D printer uses the same polylactic acid (PLA) filament material as in the first case study. Thus, the modelling of material consumption is the same as the modelling from **Equation (7.28)** to **Equation (7.30)** in **Section 7.3.3**. The total length l_e of extruded material is calculated from G-code commands.

7.4.4. Additional experiments to improve predictive models

The factors that affect the accuracy of the predictive models are the same as in the first case study, namely the occurrence of motor out-of-step of the axis movement, and the deviation between the quoted and actual material densities. Additional experiments on testing the actual speeds of axis movement and the actual material density are presented as follows.

7.4.4.1. Actual speeds of axis movement

Additional experiments are conducted to obtain the functional relationships between the actual and expected speeds of axis movement in X, Y, Z directions. In each direction, the G-code commands are manually defined to instruct the AM machine to move the nozzle for a sufficient displacement at different expected speeds. The expected speeds F_x, F_y, F_z in X, Y, Z directions are randomly assigned within the pre-defined ranges. In each test, the total time of axis movement is recorded by the CW500 power meter to calculate the average speed. Experimental results are presented in **Table 7.28** to **Table 7.30.**

Table 7.28: Experimental results of actual speeds of axis movement in X direction for the Monoprice 3D printer

Displacement (mm)	G-code command	Predicted time consumption (s)	Actual time consumption (s)	Expected speed	Actual speed
				F_x (mm/s)	$F_{x_{act}}$ (mm/s)
14130	F900	942.0000	828	15	17.06522
	F1800	471.0000	418	30	33.80383
	F3000	282.6000	324	50	43.61111
	F3600	235.5000	289	60	48.89273
	F6000	141.3000	225	100	62.80000
	F7200	117.7500	208	120	67.93269
	F9600	88.3125	186	160	75.96774

Table 7.29: Experimental results of actual speeds of axis movement in Y direction for the Monoprice 3D printer

Displacement (*mm*)	G-code command	Predicted time consumption (*s*)	Actual time consumption (*s*)	Expected speed F_y (*mm/s*)	Actual speed $F_{y_{act}}$ (*mm/s*)
	F900	942.0000	826	15	17.10654
	F1800	471.0000	418	30	33.80383
	F3000	282.6000	305	50	46.32787
14130	F3600	235.5000	284	60	49.75352
	F6000	141.3000	218	100	64.81651
	F7200	117.7500	201	120	70.29851
	F9600	88.3125	179	160	78.93855

Table 7.30: Experimental results of actual speeds of axis movement in Z direction for the Monoprice 3D printer

Displacement (*mm*)	G-code command	Predicted time consumption (*s*)	Actual time consumption (*s*)	Expected speed F_z (*mm/s*)	Actual speed $F_{z_{act}}$ (*mm/s*)
	F900	714.6700	1270	15	8.44094
	F1800	357.3300	637	30	16.82889
	F3000	214.4000	384	50	27.91667
10720	F3600	178.6700	321	60	33.39564
	F6000	107.2000	199	100	53.86935
	F7200	89.3300	180	120	59.55556
	F9600	67.0000	162	160	66.17284

Based on the experimental results, the functional relationships between the actual speeds $F_{x_{act}}$, $F_{y_{act}}$, $F_{z_{act}}$ and the expected speeds F_x, F_y, F_z of axis movement in X, Y, Z directions are obtained by using the polynomial regression method. The regression models are shown in **Figure 7.20** to **Figure 7.22** and expressed in **Equation (7.62)** to **Equation (7.64)**, for which the R^2 to evaluate the goodness-of-fit are 0.9882, 0.9881 and 0.9971, respectively.

$$F_{x_{act}} = -0.002364 F_x{}^2 + 0.7888 F_x + 9.048 \tag{7.62}$$

$$F_{y_{act}} = -0.002477 F_y{}^2 + 0.8274 F_y + 8.593 \tag{7.63}$$

$$F_{z_{act}} = -0.001985 F_z{}^2 + 0.7597 F_z - 3.809 \tag{7.64}$$
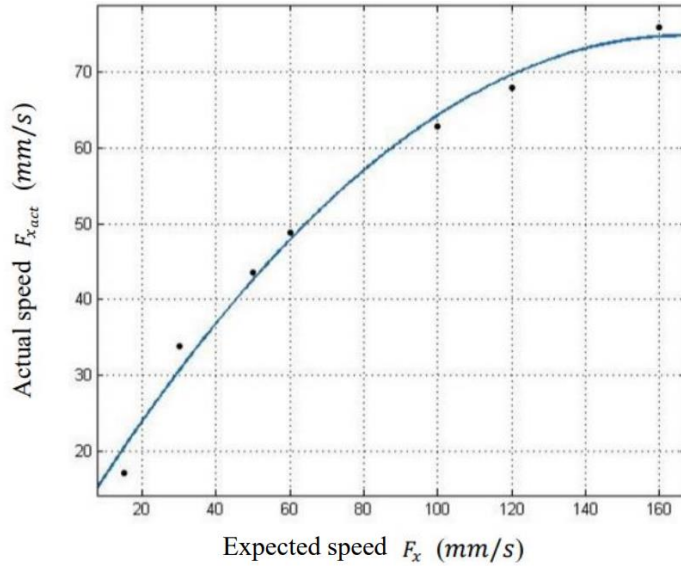
Figure 7.20: Regression model of actual and expected axis movement speeds in X direction for the Monoprice 3D printer
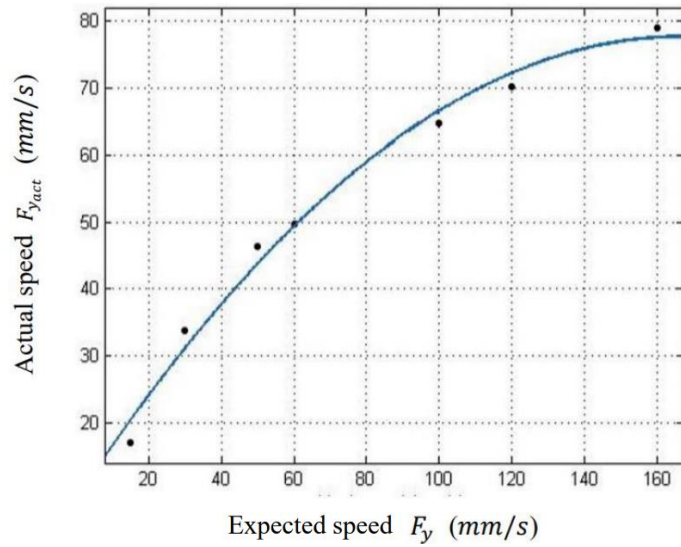
Figure 7.21: Regression model of actual and expected axis movement speeds in Y direction for the Monoprice 3D printer
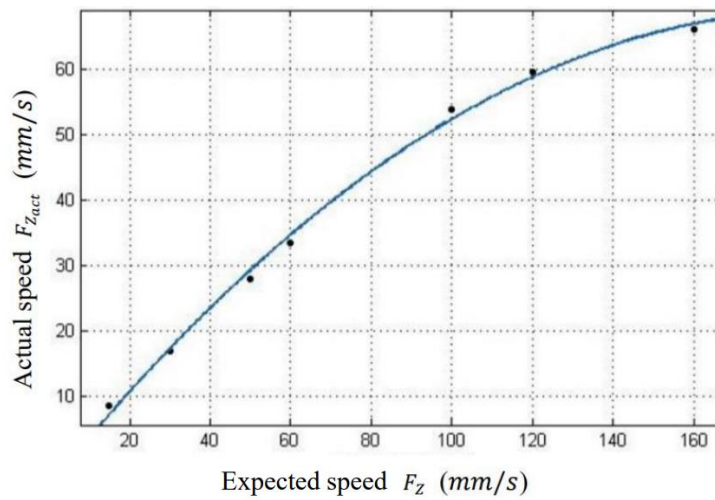
Figure 7.22:Regression model of actual and expected axis movement speeds in Z direction for the Monoprice 3D printer

7.4.4.2. Actual material density

The polylactic acid (PLA) filament material of the Monoprice 3D printer is the same as in the first case study. Therefore, the actual material density ρ_{act} is also measured as **Equation (7.34)** in **Section 7.3.4.2**.

7.5. Summary

The case studies of two different FDM 3D printers are presented to build up the predictive models by following the proposed prediction methodology. To begin, the consumption-related components in each machine are classified into five types of modules, namely axis movement, material processing, component heating, material feeding and auxiliary components. The different working states of each module are also defined. Then, the hybrid modelling method is applied to model the time, energy and material consumptions of each working state in each module. Physics-based modelling is applied to calculate three parameters based on G-code, namely the time, distance of axis movement with actual displacements and the amount of material feeding. For other parameters, data-driven modelling is applied to conduct experiments to measure the time consumptions and apparent powers of each working state under different values of the related process parameters. The functional relationships between the measured results and process parameters are derived through polynomial regression. Furthermore, factors affecting the prediction accuracy are also considered in both machines, namely the occurrence of motor out-of-step and the actual material density. Additional experiments are conducted to test the actual speeds of axis movement and the actual density of the polylactic acid (PLA) filament material. Those actual parameters are used to replace the original parameters in the predictive models.

In the following chapter, the predictive models will be used to predict the resource consumptions of real-world AM processes. To validate the effectiveness of the prediction method, the predicted results will be compared with the actual consumptions to calculate the prediction accuracy.

CHAPTER 8   VALIDATION OF PREDICTIVE MODELS AND MULTI-OBJECTIVE OPTIMISATION

8.1. Introduction

This chapter validates the effectiveness of predictive models of the aforementioned two case studies in Chapter 7. Firstly, each fused deposition modelling (FDM) printer has been assigned two AM tasks under different process parameters. The consumptions with and without considering the impact of machine characteristics have been both predicted and compared with the actual consumptions. The prediction accuracy is calculated by using the mean absolute per cent error (MAPE), since MAPE is an effective statistical measure commonly used to calculate the prediction accuracy of a forecasting method (De Myttenaere et al., 2016). According to the results, it has been proved that the prediction method achieves acceptable prediction accuracy, and the additional experiments deliver an improvement of the prediction accuracy for both AM machines.

In addition, the effectiveness of NSGA-II optimisation has been also validated in this chapter. The predictive models have been used as three objective functions in NSGA-II. It aims to search for the near-optimal approximate Pareto fronts of process parameters for a CAD design printed by two FDM printers. 16 optimisation tests have been performed on each printer under different optimisation parameters. Each test has produced one Pareto front. The hypervolume (HV) indicator of each front has been calculated and compared with each other to obtain the front that has the maximum HV indicator. The solutions of process parameters in the front can be used as a reference to aid the decision making of process parameter setting in the prefabrication stage.

The analyses of optimisation results obtained from Taguchi experiments are commonly conducted through two methods: range analysis and analysis of variance (ANOVA) (Dar and Anuradha. 2018; Khanna and Davim, 2015; Hwang et al., 2008; Cox and Reid, 2000). The range analysis aims to compare and rank the main effects of four optimisation parameters on the quality of obtained Pareto front (i.e. HV indicator of Pareto front). The ANOVA aims to further quantify the significant contributions of optimisation parameters on the HV indicator. The analysis results can provide guidance for manufacturers to personalise the most feasible optimisation parameters for optimisation testing of other CAD designs.

According to the prediction results and optimisation results, the proposed method has been proved to be effective in predicting and optimising the resource consumptions for real-world AM systems. Details of the results analyses are presented in the following sections.

8.2. Experimental validations of predictive models of two fused deposition modelling 3D printers

This section presents and discusses the prediction results of four AM tasks printed by the ANYCUBIC i3 Mega 3D printer and the Monoprice MP Mini Delta 3D printer. The aim is to validate the effectiveness of proposed prediction method in real-world AM systems. At first, each AM machine has been instructed to print two different components under random combinations of process parameters. By using the predictive models defined in last chapter, the time, energy and material consumptions of each AM task are predicted. Then, the predicted consumptions are compared with the actual consumptions to calculate the prediction accuracies (i.e. mean absolute percent error (MAPE)) of the predictive models.

8.2.1. Prediction results of ANYCUBIC i3 Mega 3D printer

This section presents the prediction results of task 01 and task 02 printed by the ANYCIBIC 3D printer. The orthographic views of two components are shown in **Figure 8.1**. After

importing the CAD designs in standard triangle language (STL) format into Cura slicer software, the process parameters in **Table 8.1** are selected for demonstration and randomly assigned within the parameter ranges. Other process parameters are set to default values.
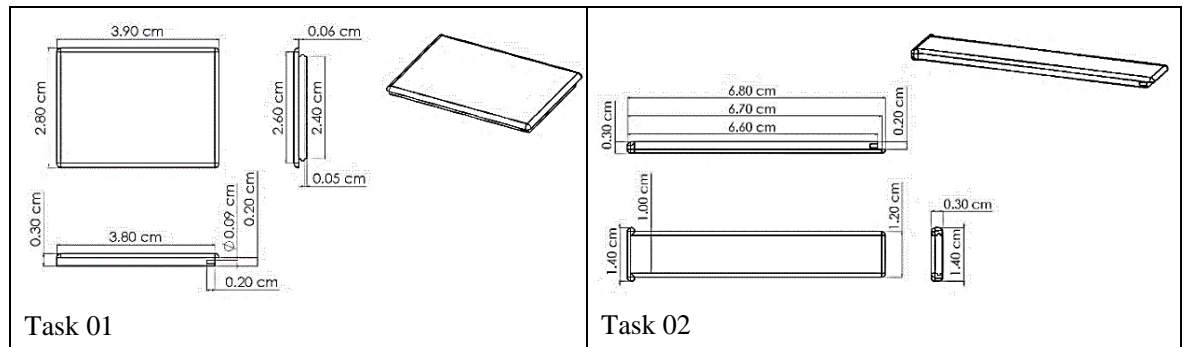
Figure 8.1: Orthographic views of two components printed by the ANYCUBIC 3D printer

Table 8.1. Ranges and assigned values of related parameters input in the predictive models of task 01 and task 02 printed by the ANYCUBIC 3D printer

Parameters of predictive models	Symbols	Units	Parameter ranges	Parameter values	
				Task 01	Task 02
Current temperature of build platform	$T_{h_0}^1$	°C	None	22	23
Current temperature of nozzle hotend	$T_{mp_0}^1$	°C	None	22	22
Target temperature of build platform	T_h^1	°C	[23, 80]	60	53
Target temperature of nozzle hotend	T_{mp}^1	°C	[180, 250]	200	180
Speed of axis movement in X, Y directions with material feeding	F_{xy_m}	mm/s	[10, 150]	60	72
Speed of axis movement in X, Y directions without material feeding	F_{xy_n}	mm/s	[10, 300]	120	130
Speed of axis movement in Z direction	F_z	mm/s	5.94872	5.94872	5.94872
Layer thickness	LT	mm	[0.04, 0.3]	0.04	0.04
Infill density	ID	%	[0, 5, 10, 15, …,100]	20	20

After the setting of process parameters, the G-code files used to print two components are generated. Then, three types of parameters are input into the models, including the process parameters defined in **Table 8.1**, the time of axis movement and the amount of material feeding calculated from G-code. Finally, the consumptions with and without the additional experiments on testing the actual speed of axis movement and the actual material density are both predicted, as listed in **Table 8.2** and **Table 8.3**. To calculate the prediction accuracy, the

actual consumptions are measured by using the CW500 power meter and Sartorius density meter. The measured results are also presented in two tables and **Appendix II (34–35)**.

Table 8.2. Prediction results of time, energy and material consumptions of task 01 printed by the ANYCUBIC 3D printer

Consumptions	Experiment result (*ER*)	Prediction results (*PR*)			
		Predictive model	Accuracy (percent error)	Improved predictive model	Accuracy (percent error)
Time (*s*)	3149.00000	3040.77213	3.43690%	3049.40426	3.16277%
Energy (VAS)	579979.80000	530024.65949	8.61326%	531469.98655	8.36405%
Material (*g*)	2.42200	2.61691	−8.04745%	2.60761	−7.66350%

Table 8.3. Prediction results of time, energy and material consumptions of task 02 printed by the ANYCUBIC 3D printer

Consumptions	Experiment result (*ER*)	Prediction results (*PR*)			
		Predictive model	Accuracy (percent error)	Improved predictive model	Accuracy (percent error)
Time (*s*)	2245.00000	2112.53469	5.90046%	2121.32766	5.50879%
Energy (VAS)	364326.57000	332160.03772	8.82904%	333463.41855	8.47129%
Material (*g*)	1.99300	2.20535	−10.65479%	2.19750	−10.26091%

Referring to the method (i.e. $\text{MAPE} = \frac{1}{n_{test}} \sum_{i=1}^{n_{test}} \left| \frac{ER_i - PR_i}{ER_i} \right|$) to calculate the mean absolute percent error (MAPE) in **Section 4.7.1**, the MAPE of each predictive model is calculated as the average percent error of two tests. **Table 8.4** presents the prediction accuracies of the predictive models.

Table 8.4. Prediction accuracies of time, energy and material consumptions of task 01 and task 02 printed by the ANYCUBIC 3D printer

Consumptions	Prediction accuracies					
	Predictive model			Improved predictive model		
	Task 01	Task 02	MAPE	Task 01	Task 02	MAPE
Time (*s*)	3.43690%	5.90046%	4.66868%	3.16277%	5.50879%	4.33578%
Energy (VAS)	8.61326%	8.82904%	8.72115%	8.36405%	8.47129%	8.41767%
Material (*g*)	−8.04745%	−10.65479%	9.35112%	−7.66350%	−10.26091%	8.96221%

According to the results in **Table 8.4**, the accuracies of time, energy and material consumptions for printing both components are all improved after the additional experiments on testing the actual speed of axis movement and the actual material density. Due to the unique G-code for each AM task, the corresponding predictive models are different, resulting in the different prediction accuracies and accuracy improvements. This result not only confirms the effectiveness of the proposed prediction modelling method, and also verifies the impacts of machine characteristics and G-code on the resource consumptions. The reasons for the deviation between the predicted consumptions and the actual consumptions are discussed as follows.

With respect to the accuracy of time consumption, this study has simplified the modelling by regarding the speed of axis movement as a constant. In a practical AM process, the axis movement on a displacement experiences three phases: the acceleration to target speed, the axis movement at a constant speed, and the deceleration from target speed to zero. Nevertheless, the measurements and calculations of acceleration and deceleration of axis movement are disturbed by the motor out-of-step, since the actual speed of axis movement is unknown when considering the phases of acceleration and deceleration. Therefore, this study has mainly focused on the additional experiments that test the actual speed of axis movement by treating the speed as a constant. The mean absolute percent error (MAPE) of time consumption is mainly due to the neglects of the acceleration and deceleration phases. To further improve the prediction accuracy, the measurements of acceleration and deceleration for axis movement will continue to be researched as future work.

With respect to the accuracy of energy consumption, since the modelling is based on the apparent power and time consumption of each module, the MAPE of energy consumption is mainly due to the MAPE of time consumption. Another reason is that the apparent powers with fluctuations measured from five modules have been simplified in order to reduce the workload of modelling process. As discussed in **Section 7.3.2.2**, the apparent power of material processing module (i.e. nozzle hotend) at the state of heat preservation is gradually

stabilised from fluctuation. Thus, this study has simplified the apparent power to a constant whose value is related to the target temperature. In addition, as discussed in **Section 7.3.2.3**, the apparent power of component heating module (i.e. build platform) at the state of heat preservation is distributed in the form of periodic pulses. To simplify the modelling, this study has divided the apparent power based on the heating cycles and has modelled the energy consumption based on the average time consumption and average energy consumption per cycle.

With respect to the accuracy of material consumption, the motor out-of-step is the main reason that effect the prediction accuracy. This study has implemented additional experiments to test the actual speed of axis movement. However, the stepper motor responsible for material feeding faces the same problem of motor out-of-step. Compared with axis movement, the reasons causing this problem in material feeding are more complicated, as discussed in **Section 7.3.4**. On one hand, the motor loses step due to the high load of a high feeding rate and insufficient torques. On the other hand, the material supplied at a high feeding rate cannot be sufficiently melted in time, causing the material to become stuck in the nozzle and fail to be extruded. Both of above two reasons result in the material supply being less than expected. To obtain the relationship between the actual and expected amounts of material feeding, additional experiments are needed to test the characteristics of the material and the stepper motor for material feeding. This work will continue to be researched as future work.

8.2.2. Prediction results of Monoprice MP Mini Delta 3D printer

This section presents the prediction results of task 03 and task 04 printed by the Monoprice 3D printer. The orthographic views of two components are shown in **Fig 8.2**. According to the machine specification in **Section 7.2.1**, the process parameters of each component are randomly assigned within the parameter ranges, as shown in **Table 8.5**. Similar to the first

case study, this case study assigns values to the same process parameters in **Table 8.5**, while other process parameters are set to default values.
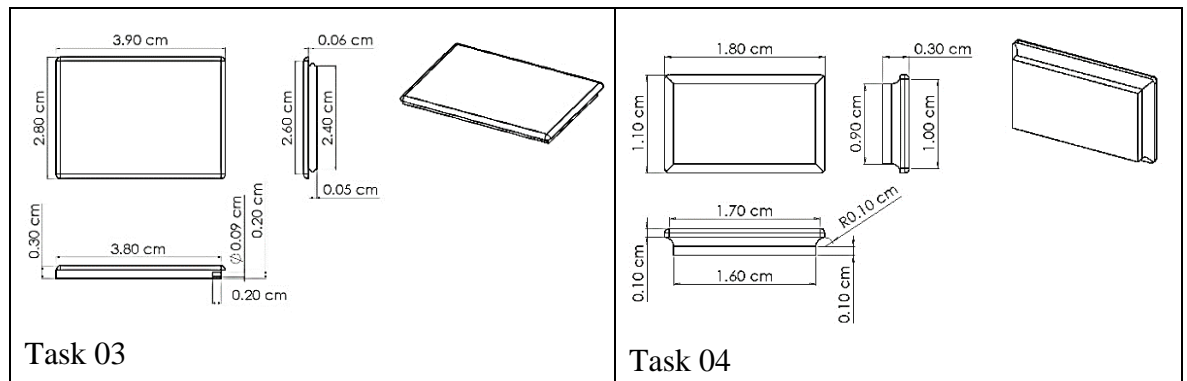
Fig 8.2: Orthographic views of task 03 and task 04 printed by the Monoprice 3D printer

Table 8.5. Ranges and assigned values of related parameters input in the predictive models of task 03 and task 04 printed by the Monoprice 3D printer

Parameters of predictive models	Symbols	Unit	Parameter ranges	Parameter values	
				Task 03	Task 04
Current temperature of build platform	$T_{h_0}^1$	℃	None	24	25
Current temperature of nozzle hotend	$T_{mp_0}^1$	℃	None	20	32
Target temperature of build platform	T_h^1	℃	[23, 60]	47	60
Target temperature of nozzle hotend	T_{mp}^1	℃	[180, 260]	182	200
Speed of axis movement in X, Y directions with material feeding	F_{xy_m}	mm/s	[10, 150]	63	50
Speed of axis movement in X, Y, Z directions without material feeding	F_{xy_n}, F_z	mm/s	[10, 150]	98	150
Layer thickness	LT	mm	[0.05, 0.2]	0.15	0.15
Infill density	ID	%	[0, 5, 10, 15, …,100]	20	20

By importing the CAD designs and the pre-defined process parameters into the slicer software, the G-code files used to print two components are generated. By using the predictive models established in **Section 7.3.4**, the predicted time, energy and material consumptions with and without the additional experiments are calculated and presented in **Table 8.6** and **Table 8.7**. In addition, the actual consumptions are measured to calculate the prediction accuracy, which are also presented in two tables and **Appendix II (34–35)**.

Table 8.6. Prediction results of time, energy and material consumptions of task 03 printed by the Monoprice 3D printer

Consumptions	Experiment result (*ER*)	Prediction results (*PR*)			
		Predictive model	Accuracy (percent error)	Improved predictive model	Accuracy (percent error)
Time (*s*)	1176	1280.16282	−8.85738%	1147.92052	2.38771%
Energy (VAS)	88043.65	98282.34109	−11.62911%	88331.74660	−0.32722%
Material (*g*)	2.23500	2.81922	−26.13960%	2.80920	−25.69128%

Table 8.7. Prediction results of time, energy and material consumptions of task 04 printed by the Monoprice 3D printer

Consumptions	Experiment result (*ER*)	Prediction results (*PR*)			
		Predictive model	Accuracy (percent error)	Improved predictive model	Accuracy (percent error)
Time (*s*)	358.00000	357.99159	0.23492%	329.49882	7.96122%
Energy (VAS)	31059.93000	32065.28409	−3.23682%	29664.35516	4.49317%
Material (*g*)	0.50900	0.65299	−28.28880%	0.65067	−27.83301%

Based on the above results, the mean absolute percent error (MAPE) of each predictive model is calculated as the average percent error of two tests. **Table 8.8** presents the prediction accuracies of the predictive models. The reasons for the deviation between the predicted consumptions and the actual consumptions are discussed as follows.

Table 8.8. Prediction accuracies of time, energy and material consumptions of task 03 and task 04 printed by the Monoprice 3D printer

Consumptions	Prediction accuracies					
	Predictive model			Improved predictive model		
	Task 03	Task 04	MAPE	Task 03	Task 04	MAPE
Time (*s*)	−8.85738%	0.23492%	4.31123%	2.38771%	7.96122%	5.17447%
Energy (VAS)	−11.62911%	−3.23682%	7.43297%	−0.32722%	4.49317%	2.08298%
Material (*g*)	−26.13960%	−28.28880%	27.21420%	−25.69128%	−27.83301%	26.76215%

From the time consumption perspective in task 03, note that the mean absolute percent error (MAPE) of the improved predictive model is increased from 0.23492% to 7.96122%. The reason is that although the impact of motor out-of-step for axis movement has been considered, the deviation of the initial heating time of the material processing module (i.e. nozzle hotend) still accounts for a certain percentage of MAPE. Since the volume of the printed object (i.e. $0.41195 cm^3$) in task 03 is small, the time spent on component heating takes a high proportion of total time consumption, so that the deviation of time spent on components heating has a higher impact on the final prediction accuracy. According to the experiment result in **Appendix III (21)**, the time spent on axis movement with material feeding takes 75.98% of total time consumption. While the time spent on the initial heating of nozzle hotend takes 24.02% of total time consumption. Compared with task 03, the volume of printed object (i.e. $1.80885 cm^3$) in task 04 is 4.39 times the volume in task 03. Therefore, according to the experiment results of task 04 in **Appendix III (22)**, the time spent on axis movement with material feeding takes 94.37% of total time consumption, while the initial heating time of nozzle hotend 04 takes 6.63% of total time consumption. Based on the above, it is concluded that the deviation between the predicted time and actual time of component heating has a more significant impact on the prediction accuracy for the small-volume printing. The higher the volume of printed object, the lower the MAPE will be.

Moreover, the consumption modelling has also simplified the speed of axis movement as a constant. Similar to the first case study, the impact of acceleration and deceleration on the prediction accuracy are not considered in this study. To further improve the prediction accuracy, the acceleration and deceleration of axis movement will continue to be researched as future work.

From the energy consumption perspective, the consumption modelling has simplified the measured apparent powers with fluctuations to constant and regular values. For example, the apparent power of component heating module (i.e. build platform) at the state of heat preservation is gradually stabilised from fluctuation. Thus, this study has simplified the

apparent power to a constant whose value is related to the target temperature. This method can achieve the rapid modelling with an acceptable prediction accuracy.

From the material consumption perspective, the motor out-of-step is also the main reason that effect the prediction accuracy. Details have been discussed in **Section 8.2.1**. To address this issue, additional modelling, experiments and result analyses are needed to improve the prediction accuracy of material consumption. This will be continued as future work.

8.2.3. Comparison and discussion of the predictive models of two fused deposition modelling 3D printers

According to the prediction results, the effectiveness of proposed prediction modelling method has been validated in two fused deposition modelling (FDM) printers. The mean absolute percent errors (MAPEs) prove that the predictive models can achieve acceptable prediction accuracies. In particular, the consideration of machine characteristics in different AM machines is found to achieve different degrees of improvement in prediction accuracy. The reason is explained as follow.

As shown in **Table 8.9**, note that the prediction accuracies of time consumptions in Task 01 and Task 02 printed by the ANYCUBIC 3D printer have been improved by 0.27413% and 0.39167%, respectively. While the prediction accuracies of Task 03 and Task 04 printed by the Monoprice 3D printer have been improved by 11.24509% and 7.72630%. By comparing the accuracy improvements of two machines, it is found that the improvement of the Monoprice 3D printer is much higher than that of the ANYCUBIC 3D printer. The reason is due to the motor out-of-step of the axis movement module driven by three stepper motors, as discussed in Chapter 7. Through the observation of additional experiments on testing the actual speed of axis movement, the deviation between actual speed and expected speed of the ANYCUBIC 3D printer is smaller than that of the Monoprice 3D printer. In other words, the ANYCUBIC 3D printer performs better than the Monoprice 3D printer in terms of axis

movement. In the same way, the different improvement in the prediction accuracy of energy consumption between the two machines is also due to the above reason.

Table 8.9. Improved prediction accuracies of predictive models after the additional experiments on two FDM 3D printers

Consumptions	Improvement of prediction accuracy after additional experiments			
	ANYCUBIC 3D printer		Monoprice 3D printer	
	Task 01	Task 02	Task 03	Task 04
Time (s)	0.27413%	0.39167%	11.24509%	7.72630%
Energy (VAS)	0.24921%	0.35775%	11.30189%	7.72999%
Material (g)	0.38395%	0.39388%	0.44832%	0.45579%

Based on the above, it can be concluded that the degree of improvement in prediction accuracy is determined by the machine performance. For machines with superior performance, or in the case of limited experimental equipment and time, it is optional to use the proposed prediction method without spending extra time on additional experiments.

8.3. Experimental validations of NSGA-II optimisation applied to two fused deposition modelling 3D printers

This section presents and analyses the optimisation results (i.e. hypervolume (HV) indicator) of an AM task to be printed by the ANYCUBIC i3 Mega 3D printer and the Monoprice MP Mini Delta 3D printer. The component in **Fig 8.3** is used as the input of the NSGA-II algorithm.
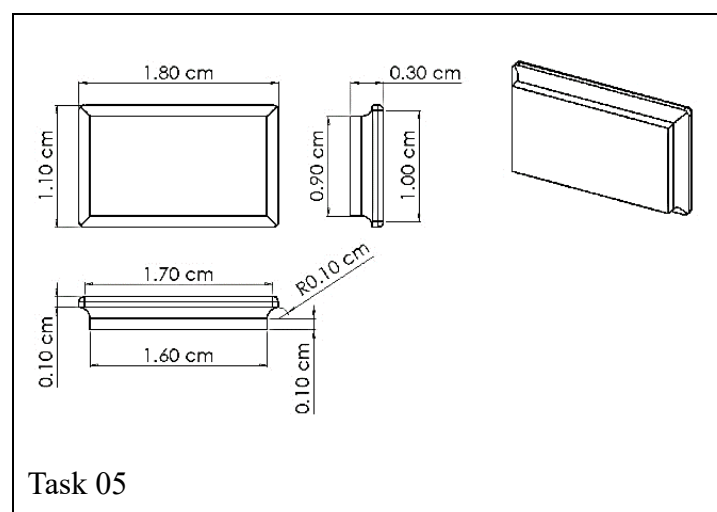
Fig 8.3: Orthographic views of the component in task 05

This study has used Python 3.8.2 to realise the programming and running of NSGA-II optimisation algorithm. In order to reduce the time cost of optimisation process, three computing devices have been allocated to run the optimisation algorithm under different optimisation parameters. The configurations of three devices are listed in **Table 8.10**.

Table 8.10. Computing devices used for the NSGA-II optimisation tests

Computing devices	Configuration
Dell Precision 5820 Workstation (WS)	Intel(R) Xeon(R) W2155 CPU 3.30GHz 3.31GHz
Dell Optiplex 7040 personal computer (D-PC)	Intel(R) Core(TM) i7-6700 CPU 3.40GHz 3.41GHz
High-performance computing cluster (HPC)	1 × Intel Xeon X3363 CPU 2.83GHz
Programming language	Python 3.8.2

Referring to the methodology in **Section 4.6.2**, the $L_{16}(4^4)$ orthogonal table has been used. It indicates that 16 optimisation tests should be performed under different combinations of optimisation parameters, namely population size *N*, number of generations *Gen*, crossover probability pc and mutation probability pm. Each test produces one Pareto front, whose hypervolume (HV) indicators are calculated and compared with other fronts to obtain the optimum front with the maximum HV indicator. Through the range analysis and analysis of variance (ANOVA), the optimisation parameters that mainly effect the value of HV indicator are obtained. Details of the optimisation results and results analyses are presented in the following sections.

8.3.1. Optimisation result analyses of ANYCUBIC i3 Mega 3D printer

This section presents and analyses the optimisation results for printing the component in **Fig 8.3** by the ANYCUBIC i3 Mega FDM 3D printer. The process parameters to be optimised and the constraints of each parameter are based on customer demands and machine characteristics. As a demonstration, six process parameters are selected to be optimised in this case study, including layer thickness *LT*, infill density *ID*, target temperature T_{mp}^1 of material processing module (i.e. nozzle hotend), target temperature T_h^1 of component heating module (i.e. build platform), speed F_{xy_m} of axis movement in X, Y directions with material feeding, and speed F_{xy_n} of axis movement in X, Y directions without material feeding. As shown in **Table 8.11**, the constraints of process parameters are defined based on the machine characteristic in **Section 7.2.1**. The aim is to find the optimum solution of process parameters within the constraints for this AM task.

Table 8.11. Process parameters to be optimised for printing task 05 by the ANYCUBIC 3D printer

Process parameters	Symbols	Units	Parameter ranges		Granularity
			Lower bound	Upper bound	
Layer thickness	LT	mm	0.040	0.300	0.001
Infill density	ID	%	0	100	5
Target temperature of nozzle hotend	T_{mp}^1	°C	180	250	1
Target temperature of build platform	T_h^1	°C	23	80	1
Speed of axis movement in X, Y directions with material feeding	F_{xy_m}	mm/s	10	150	1
Speed of axis movement in X, Y directions without material feeding	F_{xy_n}	mm/s	10	300	1

The optimisation results of 16 tests are presented in **Table 8.12**, which lists the non-dominated solutions of process parameters on each Pareto front. Note that there are total 30 non-dominated solutions (i.e. $n_{ns} = 30$) obtained from 16 optimisation tests. Therefore, according to the coordinate calculation method of reference point (i.e. $r_R = 1 + \frac{1}{n_{ns}-1}$) in **Section 4.6.3**, the coordinates of the reference point R should be (1.03448, 1.03448, 1.03448) in the normalised objective space. By following the methodology in **Section 4.6.3**, the HV indicator of each Pareto front is calculated and also listed in this table.

Table 8.12: Optimisation results of HV indicators for printing task 05 by the ANYCUBIC 3D printer

Test No.	Number of optimal solutions	Hypervolume indicator	Optimal process parameter						Consumptions		
			Target temperature of build platform	Target temperature of nozzle hotend	Speed of axis movement in X, Y directions with material feeding	Speed of axis movement in X, Y directions without material feeding	Layer thickness	Infill density	Material	Time	Energy
		$I_H(A)$	T_h^1	T_{mp}^1	F_{xy_m}	F_{xy_n}	LT	ID	M_{total}	T_{total}	E_{total}
1	2	0.205503	26	197	113	122	0.267	0	0.64680	128.41105	16701.79999
			26	212	86	128	0.232	0	0.62730	141.85412	18656.68471
2	1	0.681671	23	212	109	157	0.226	0	0.61570	126.03740	14174.29752
3	2	0.104885	27	205	99	235	0.241	5	0.63442	144.89938	19714.49318
			32	217	92	140	0.226	0	0.61570	171.52166	27619.49927
4	2	0.898252	23	185	84	210	0.262	0	0.64490	111.22985	11918.82293
			23	182	100	182	0.226	0	0.61570	117.90507	12665.07925
5	2	0.815477	23	194	88	184	0.267	0	0.64680	113.45856	12299.97947
			23	193	102	200	0.226	0	0.61570	120.89312	13162.44822
6	2	0.671497	23	180	132	193	0.242	0	0.62824	112.37906	12001.78999
			23	180	136	196	0.241	0	0.62655	112.42780	12007.46269
7	1	0.853262	23	188	120	151	0.226	0	0.61570	119.09979	12877.14671

			23	180	124	190	0.264	0	0.64681	108.51476	11552.08691
8	3	0.917371	23	180	114	227	0.227	0	0.61796	116.76729	12512.46431
			23	180	130	255	0.226	0	0.61570	116.82823	12519.55623
			23	198	113	130	0.226	0	0.61570	122.14354	13397.49473
9	3	0.875220	23	188	112	184	0.223	0	0.62283	119.28379	12898.71929
			23	186	105	230	0.243	0	0.63586	114.43276	12304.95944
			23	**181**	**108**	**184**	**0.262**	**0**	**0.64490**	**108.98000**	**11615.30731**
10	**3**	**0.930460**	**23**	**180**	**144**	**200**	**0.229**	**0**	**0.62195**	**116.64550**	**12498.29170**
			23	**180**	**135**	**204**	**0.226**	**0**	**0.61570**	**116.65654**	**12499.57594**
11	1	0.101774	23	181	130	202	0.262	0	0.64490	108.88348	11604.06674
12	1	0.102479	23	180	129	199	0.262	0	0.64490	108.59982	11561.98672
			23	181	114	209	0.262	0	0.64490	108.93327	11609.86493
13	3	0.922440	23	182	135	233	0.226	0	0.61570	117.27987	12592.13633
			23	181	117	195	0.248	0	0.64310	112.71215	12049.93825
14	2	0.372949	23	180	113	193	0.267	0	0.64680	108.83823	11589.73092
			23	180	128	189	0.264	0	0.64681	108.51037	11551.57611
15	1	0.670841	23	180	132	198	0.241	0	0.62655	112.42463	12007.09274
16	1	0.618453	23	180	134	198	0.242	0	0.62824	112.37858	12001.73446

According to the above results, it is found that the solutions of process parameters in Test 10 achieves the maximum HV indicator. Compared with other solutions, this solution achieves a better diversity of alternative solutions and consumes less time, energy and material. To validate the effectiveness of NSGA-II optimisation, the optimal solutions in **Table 8.12** are compared with the default setting of process parameters for the ANYCUBIC 3D printer. The predicted consumptions are listed in **Table 8.13**. The improvements of resource savings are also calculated. It is found that compared with the default settings, the time, energy and material consumptions of the recommended settings are all reduced. The reductions in time and energy consumptions are particularly obvious. Within the parameter ranges, the lower component heating temperatures and infill density, and the higher print speed and layer thickness can consume less time, energy and material. This results not only verifies the effectiveness of the proposed optimisation method in real-world AM systems, and also confirm the impacts of process parameters on the resource consumptions.

Table 8.13: Comparison of predicted consumptions between the default setting and recommended setting of process parameters for printing task 05 by the ANYCUBIC 3D printer

	Process parameters						Consumptions		
	T_h^1	T_{mp}^1	F_{xy_m}	F_{xy_n}	LT	ID	M_{total}	T_{total}	E_{total}
Defaults	60	200	60	120	0.15	10	0.65845	213.16305	20688.83035
Recommendation	23	181	108	184	0.262	0	0.64490	108.98000	11615.30731
	Resource saving percentages						*2.05786%*	*48.87482%*	*43.85711%*
	23	180	144	200	0.229	0	0.62195	116.64550	12498.29170
	Resource saving percentages						*5.54332%*	*45.27874%*	*39.58918%*
	23	180	135	204	0.226	0	0.61570	116.65654	12499.57594
	Resource saving percentages						*6.49252%*	*45.27356%*	*39.58297%*

Based on the optimisation results, the main effects or the significant contributions of optimisation parameters on the HV indicator are analysed through two methods: range

analysis and ANOVA. Referring to the methodology in **Section 4.7.2**, the analysis results are listed in **Table 8.14** and **Table 8.15**.

Table 8.14: Main effects of optimisation parameters on the HV indicator for printing task 05 by the ANYCUBIC 3D printer

Levels	Calculation methods	Factors			
		PS	*Gen*	*pc*	*pm*
1	$\sum \overline{I_H^1(A)}$	0.472578	0.70466	0.399307	0.299635
2	$\sum \overline{I_H^2(A)}$	0.814402	0.580231	0.567617	0.655814
3	$\sum \overline{I_H^3(A)}$	0.502483	0.432691	0.483693	0.617319
4	$\sum \overline{I_H^4(A)}$	0.562257	0.634139	0.901104	0.778953
Delta	$\overline{\sum I_H(A)}_{max} - \overline{\sum I_H(A)}_{min}$	0.341824	0.27197	0.501797	0.479318
Rank		3	4	1	2

Table 8.15: ANOVA for evaluating the significances of factors on HV indicator for printing task 05 by the ANYCUBIC 3D printer

Factors	Degree of freedom	Sums of squares	Mean squares	F-Value	P-Value
	DF	SS_p	MS_p		
PS	3	0.29022	0.09674	1.01	0.497
Gen	3	0.15969	0.05323	0.56	0.679
Pm	3	0.57975	0.19325	2.02	0.289
Pc	3	0.50031	0.16677	1.74	0.330
Error	3	SS_e	MS_e		
		0.28719	0.09573		
Total	15	SS_t 1.8171			

According to the Delta values in **Table 8.14**, the main effects that each optimisation parameter has can be directly observed from **Fig 8.4**. The sequence of optimisation parameters based on their significances on the HV indicator $I_H(A)$ is the probability of crossover *pc*, probability of mutation *pm*, population size *N*, and number of generation *Gen*. However, the effect trend of each factor is not obvious. The ANOVA results in **Table 8.15**

further prove this result, since the P-values of four factors for the response of HV indicator are all higher than 0.05. The reason for the above result is explained as follows.
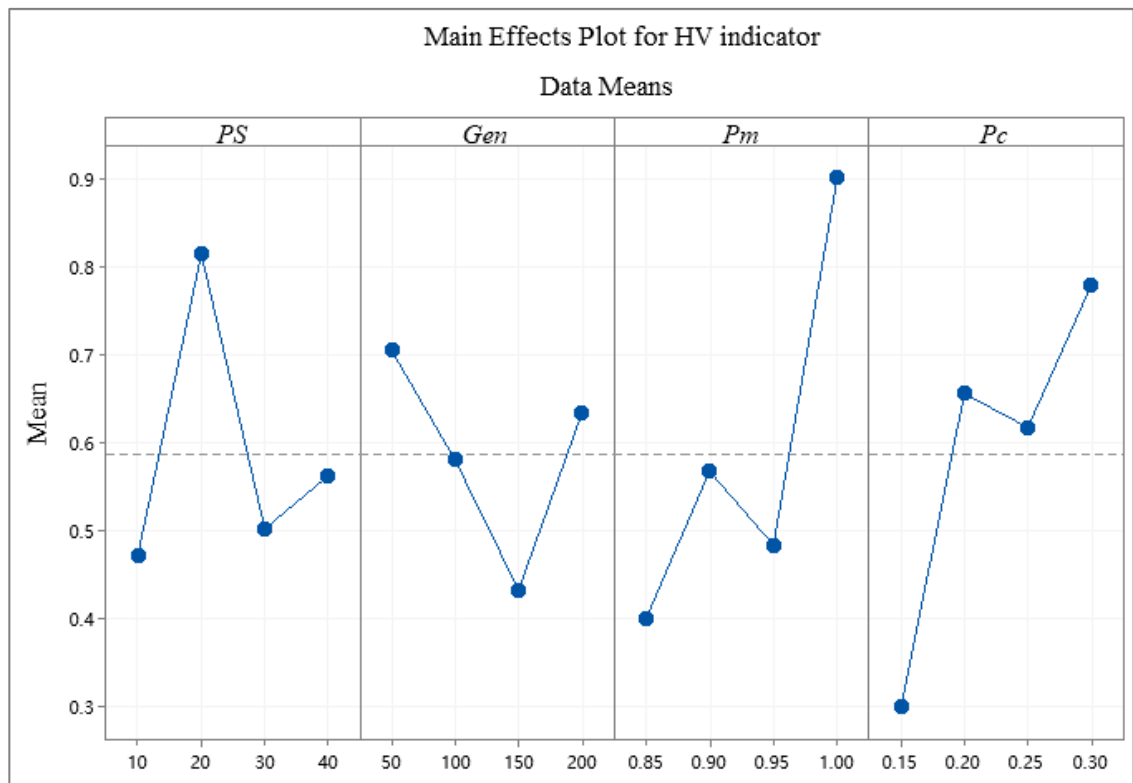

Fig 8.4: Main effects of optimisation parameters for HV indicator for printing task 05 by the ANYCUBIC 3D printer

Due to limited computing resources, the range of possible values for the optimisation parameters is limited. Therefore, the initial population randomly generated at the initial stage of NSGA-II optimisation has an impact on the optimisation result (i.e. the non-dominated solutions on the final Pareto front). In general optimisation problems using NSGA-II, the larger values of population size N and number of generations Gen are supposed to produce a better Pareto front with a higher HV indicator. Therefore, in future studies, larger value ranges will be assigned to the optimisation parameters to confirm this hypothesis.

8.3.2. Optimisation result analyses of Monoprice MP Mini Delta 3D printer

This section presents and analyses the optimisation results for printing the component in **Fig 8.3** by the Monoprice MP mini Delta 3D printer. The process parameters to be optimised are same as the first case study. In **Table 8.16**, the constraints of each process parameter are defined based on the machine characteristic in **Section 7.2.1**.

Table 8.16. Process parameters to be optimised for printing task 05 by the Monoprice 3D printer

Process parameters	Symbols	Units	Parameter ranges		Granularity
			Lower bound	Upper bound	
Layer thickness	LT	mm	0.050	0.200	0.001
Infill density	ID	%	0	100	5
Nozzle temperature	T_{mp}^1	°C	180	260	1
Bed temperature	T_h^1	°C	23	60	1
Speed of axis movement in X, Y directions with material feeding	F_{xy_m}	mm/s	10	150	1
Speed of axis movement in X, Y, Z directions without material feeding	F_{xy_n}, F_z	mm/s	10	150	1

The non-dominated solutions of process parameters on the obtained Pareto fronts are presented in **Table 8.17**. Note that there are total 41 non-dominated solutions (i.e. $n_{ns} = 41$) obtained from the optimisation tests. Thus, according to the coordinate calculation method of reference point in **Section 4.6.3**, the coordinates of the reference point R are calculated as (1.025, 1. 025, 1.025) in the normalised objective space. The HV indicator of each test is calculated and listed in this table.

Table 8.17: Optimisation results of HV indicators for printing task 05 by the Monoprice 3D printer

Test No.	Number of optimal solutions	Hypervolume indicator	Optimal process parameter						Consumptions		
			Target temperature of build platform	Target temperature of nozzle hotend	Speed of axis movement in X, Y directions with material feeding	Speed of axis movement in X, Y, Z directions without material feeding	Layer thickness	Infill density	Material	Time	Energy
		$I_H(A)$	T_h^1	T_{mp}^1	F_{xy_m}	F_{xy_n}, F_z	LT	ID	M_{total}	T_{total}	E_{total}
1	2	0.05679	36	200	74	63	0.164	5	0.63860	196.69652	16902.73072
			26	194	114	68	0.171	5	0.65016	189.12148	15278.91421
2	2	0.12790	38	193	100	94	0.156	0	0.63840	181.90703	15702.93931
			35	180	131	84	0.197	0	0.67799	156.34604	13347.27410
3	4	0.45198	36	184	105	72	0.183	0	0.65463	164.28251	14090.58844
			34	184	117	68	0.172	0	0.65075	168.69108	14251.91848
			26	190	106	117	0.164	0	0.64337	174.83718	14246.62660
			33	184	106	96	0.184	0	0.65610	163.32866	13810.45252
4	1	0.36930	25	185	108	116	0.164	0	0.64337	172.52367	13878.91086
5	2	0.26227	48	183	129	110	0.156	0	0.63840	175.41236	15837.23351
			31	180	95	100	0.182	0	0.65775	172.82683	14195.95456
6	3	0.50090	24	180	128	118	0.183	0	0.65463	160.13160	12876.73090
			30	180	138	133	0.187	0	0.65611	159.80122	13261.23145

			28	180	129	128	0.183	0	0.65463	159.94442	13133.31088
7	4	0.79757	23	180	136	148	0.184	0	0.65610	159.63029	12779.58175
			28	182	131	139	0.2	5	0.63922	163.07337	13394.39098
			24	180	136	68	0.195	0	0.66264	157.03996	12680.32587
			32	181	124	139	0.2	5	0.63922	162.63787	13619.84224
8	4	0.69859	23	181	128	123	0.155	5	0.63753	185.73613	14449.41341
			24	180	142	133	0.183	0	0.65463	159.83483	12858.14309
			23	181	136	115	0.172	0	0.65075	165.20622	13158.55101
			23	181	138	133	0.156	0	0.63840	173.86006	13702.48929
9	**3**	**1.03459**	**39**	**180**	**133**	**144**	**0.156**	**0**	**0.63840**	**173.43093**	**14870.85264**
			23	**180**	**132**	**145**	**0.2**	**0**	**0.63967**	**154.35298**	**12448.33403**
			29	**180**	**137**	**146**	**0.2**	**5**	**0.63922**	**162.10246**	**13345.12478**
10	4	0.66706	23	180	132	145	0.184	0	0.65610	159.66328	12781.64813
			23	180	133	138	0.183	0	0.65463	159.76684	12788.11809
			30	180	130	135	0.155	5	0.63753	184.93259	14931.91430
			30	180	145	138	0.156	0	0.63840	173.20790	14152.22691
11	1	0.75998	23	180	129	149	0.2	5	0.63922	162.04564	12931.43157
12	1	0.49560	23	180	142	129	0.164	0	0.64337	168.76029	13352.77241
13	5	0.64876	33	181	136	131	0.183	0	0.65463	160.29110	13530.15764
			26	181	129	105	0.184	0	0.65610	160.75934	13078.30336
			26	181	118	105	0.164	0	0.64337	170.42813	13700.15757

			35	180	122	134	0.198	0	0.66323	155.35691	13305.34380
			38	180	133	135	0.196	0	0.65924	155.23012	13506.31625
14	2	0.76798	23	180	149	148	0.155	0	0.63753	184.30277	14328.84180
			23	180	129	149	0.2	5	0.63922	162.04564	12931.43157
15	2	0.76792	23	180	129	149	0.2	5	0.63922	162.04564	12931.43157
			23	180	147	145	0.155	5	0.63753	184.37444	14333.27794
16	1	0.75998	23	180	129	149	0.2	5	0.63922	162.04564	12931.43157

According to the above results, the solutions of process parameters in Test 09 achieves the maximum HV indicator and consumes the optimum combination of time, energy and material consumptions. The optimal solutions are compared with the default setting of process parameters for the Monoprice 3D printer. As shown in **Table 8.18**, the time, energy and material consumptions of the recommended settings are less than the default settings. Similar to the first case study, the lower component heating temperatures and infill density, and the higher print speed and layer thickness can consume less time, energy and material. This result also verifies the effectiveness of the proposed optimisation method and the impacts of process parameters on the resource consumptions.

Table 8.18: Comparison of predicted consumptions between the default setting and recommended setting of process parameters for printing task 05 by the Monoprice 3D printer

	Process parameters						Consumptions		
	T_h^1	T_{mp}^1	F_{xy_m}	F_{xy_n}	LT	ID	M_{total}	T_{total}	E_{total}
Defaults	60	200	50	100	0.2	25	0.67166	338.19389	76946.36341
Recommendation	39	180	133	144	0.156	0	0.63840	173.43093	14870.85264
	Resource saving percentages						*4.95191%*	*48.71849%*	*80.67374%*
	23	180	132	145	0.2	0	0.63967	154.35298	12448.33403
	Resource saving percentages						*4.76283%*	*54.35962%*	*83.82206%*
	29	180	137	146	0.2	5	0.63922	162.10246	13345.12478
	Resource saving percentages						*4.82982%*	*52.06819%*	*82.65659%*

Furthermore, the main effects of optimisation parameters on the value of HV indicator are analysed through two methods: range analysis and ANOVA. Referring to the methodology in **Section 4.7.2**, the results are listed in **Table 8.19** and **Table 8.20**.

Table 8.19: Range analysis of the effect of each factor on HV indicator for printing task 05 by the Monoprice 3D printer

Levels	Calculation methods	Factors			
		PS	Gen	pc	pm
1	$\overline{\sum I_H^1(A)}$	0.251493	0.500603	0.519413	0.529485
2	$\overline{\sum I_H^2(A)}$	0.564833	0.51596	0.413423	0.558808
3	$\overline{\sum I_H^3(A)}$	0.739308	0.694363	0.738285	0.535323
4	$\overline{\sum I_H^4(A)}$	0.73616	0.580868	0.620673	0.668178
Delta	$\overline{\sum I_H(A)}_{max} - \overline{\sum I_H(A)}_{min}$	0.487815	0.19376	0.324863	0.138693
Rank		1	3	2	4

Table 8.20: ANOVA for evaluating the significances of factors on HV indicator for printing task 05 by the Monoprice 3D printer

Factors	Degree of freedom	Sums of squares		Mean squares	F-Value	P-Value
	DF	SS_p		MS_p		
PS	3	0.63085		0.21028	10.13	0.044
Gen	3	0.09314		0.03105	1.50	0.374
Pm	3	0.23171		0.07724	3.72	0.155
Pc	3	0.05029		0.01676	0.81	0.568
Error	3	SS_e		MS_e		
		0.06226		0.02075		
Total	15	SS_t	1.06826			

According to the Delta values in **Table 8.19**, the main effects of each optimisation parameter can be observed from **Fig 8.5**. The sequence of optimisation parameters based on their significances on the HV indicator $I_H(A)$ is the population size N, probability of crossover pc, number of generation Gen, and probability of mutation pm. The main effect of population size N is relatively significant compared with other parameters. The ANOVA results in **Table 8.20** further prove the range analysis result, since P-values of population

size N is less than the significant level 0.05 for the response of HV indicator in this case study.
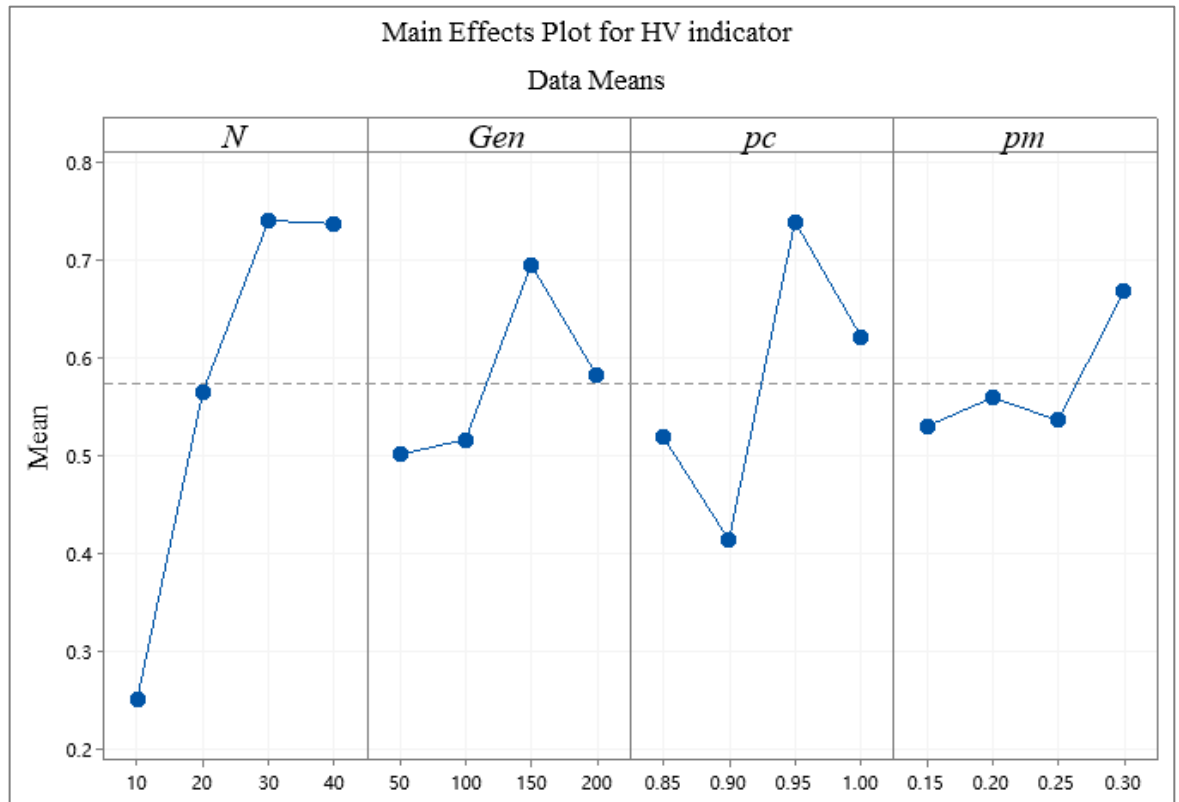
Fig 8.5: Main effects of optimisation parameters for HV indicator for printing task 05 by the Monoprice 3D printer

The reason for the above result is similar to the first case study. The value range of optimisation parameters is limited due to the limited computing resources. This leads to the optimisation result being overly dependent on the randomly generated initial population. Therefore, the contribution of the optimisation parameters on the optimal solutions is not significant in both case studies.

8.3.3. Comparison and discussion of the optimisation results of two fused deposition modelling 3D printer

From the comparison of the two case studies, the recommended values of the process parameters used to print the same component are different for the two AM machines. One of

the reasons is that the process parameters of the two machines have different value ranges. The other reason can be drawn that the optimisation result is determined by the machine characteristics. Since the predictive models are customised, the fitness values for the same solution on two machines will be different, leading to the different optimal solutions. Therefore, there is no universal rule to guide the specific value setting of process parameters for general AM technologies. However, from two case studies, the results can provide a trend to guide the parameter settings, for example, the lower component heating temperatures and infill density, and the higher print speed and layer thickness that consume less time, energy and material.

In addition, in the first case study, the effect trend of optimisation parameters for hypervolume (HV) indicator is not obvious. In the second case study, the main effect of population size is significant compared with other parameters. A larger population size is found to produce a better Pareto front with a higher HV indicator. The reason for this result has been discussed in previous sections. The limited population size and number of generations may lead to the optimisation result being overly dependent on the randomly generated initial population. Therefore, future research needs to perform optimisation tests by assigning a larger value range to the optimisation parameters.

Furthermore, the case studies have also recorded the computational time of each optimisation test. The experimental results are presented in **Appendix IV** and **Appendix V**. Through the observation from results, it is found that the larger values of population size and number of generations result in a longer computational time. To perform optimisation tests under larger optimisation parameters, the high-performance computing equipment is needed to speed up the computation.

8.4. Summary

This chapter validates the effectiveness of the predictive models in two case studies. Each FDM printer has been assigned two different AM tasks, and each AM task is printed under

a random combination of process parameters. The prediction accuracies of the predictive models with and without considering the impact of machine characteristics are both obtained, including the actual speed of axis movement and the actual density of thermoplastic material. The mean absolute percent errors (MAPEs) of the predictive models are mainly resulted from three reasons.

First, the axis movement speed has been simplified to a constant without considering the acceleration and deceleration phases. The purpose is to facilitate the measurement of actual axis movement speed when the stepper motors are in out-of-step conditions. Second, some apparent powers with fluctuations measured from five modules have been simplified to constant and regular values. The purpose is to achieve the rapid prediction with an acceptable prediction accuracy. Third, the motor for material feeding loses step due to the high load, insufficient torques, and the insufficient melting of material at a high feeding rate. To address above issue, additional work is needed to test the characteristics of machine and material in future. Except for the impact of machine performance, the proposed prediction method has been proved to be effective for real-world AM systems. The consideration of machine characteristic has also been proved to further improve the prediction accuracies on the basis of original predictive models.

The feasibility of the multi-objective optimisation method is also verified in two case studies. The non-dominated sorting genetic algorithm II (NSGA-II) has been applied to search for the optimal Pareto fronts of process parameters for a component printed by two FDM printers. Three objectives to be minimised are respectively represented by the time, energy and material consumptions. The Taguchi robust design method has been applied to design the experiments of optimisation process. Four optimisation parameters are considered as four factors in the experiments, including population size, number of generations, crossover probability and mutation probability. Each factor is defined with four levels, whose values are within the range commonly used in NSGA-II optimisation. Therefore, the $L_{16}(4^4)$ orthogonal table has been used, which indicates that 16 optimisation tests have been performed on each printer. Each test has produced one Pareto front.

To evaluate and compare the qualities of obtained Pareto fronts, the hypervolume (HV) indicator is used as the response of each optimisation test. The solutions of process parameters that have the maximum HV indicator is the optimum solution for the AM task. This result can provide guidance for setting a feasible combination of process parameters in the prefabrication stage. Furthermore, the significances of optimisation parameters on the HV indicator are analysed by using the range analysis and analysis of variance (ANOVA) methods. In the first case study of ANYCUBIC i3 Mega FDM 3D printer, the main effects of optimisation parameters on the HV indicator are not significant. In the second case study of Monoprice MP Mini Delta FDM 3D printer, the main effect of population size on the HV indicator is significant. The higher value of population size produces a better Pareto front with a higher HV indicator.

Based on the above, the proposed prediction and optimisation methods have been proved to be effective for real-world AM systems. The consideration of machine characteristics has been verified to have a significant improvement of the prediction accuracy. The optimum solution of process parameters provides guidance for setting the feasible process parameters in prefabrication stage. Moreover, based on the analyses of optimisation results, it is concluded that the optimal solution of process parameters is determined by the machine characteristics. Due to the unique predictive models, there is no universal guidance regarding the most feasible setting of process parameters and optimisation parameters for general AM technologies. This conclusion further confirms the significance of proposed prediction and multi-objective optimisation method in this research work.

CHAPTER 9   CONCLUSION AND FUTURE WORK

This chapter concludes the research work in this thesis and proposes the future research directions. To begin, the method of prediction and multi-objective optimisation is summarised. Based on the prediction results and optimisation results in previous chapter, a conclusion is made that proposed method is effective for the prediction and optimisation of time, energy and material consumptions in AM process. Then, the contribution of this PhD research is re-emphasised. At last, future work based on the finding of this research are discussed.

9.1. Summary of research work and conclusion

The prediction and multi-objective optimisation of time, energy, material consumptions for AM technologies have not been well explored. In this thesis, a general prediction modelling and optimisation method is proposed, aiming to achieve an accurate prediction and high-efficient optimisation of three consumptions.

A hybrid data-driven and physics-based modelling scheme is proposed to build up the predictive models of time, energy and material consumptions based on machine characteristics. Through the investigation of the existing AM technologies on the market, all consumption-related components are classified into five types of modules: axis movement, material processing, material feeding, component heating and auxiliary components. Then, the consumptions of each module are modelled as functions of process parameters. To obtain the functional relationships, hybrid modelling is performed to obtain the coefficients between the consumptions and process parameters. In physics-based modelling, the time of axis movement and the amount of material usage are calculated from G-code. In data-driven modelling, the parameters that cannot be calculated from G-code are measured through experiments. The apparent power and time of each module is measured under different process parameters by using a power meter. Based on the experimental results, the functional

relationships (i.e. the coefficients between the power, time and process parameters) are derived through regression analysis methods. On the basis of predictive models, additional experiments are carried out to test the actual values of some parameters in the predictive models. The reason is that the values of those parameters are affected by the characteristics of machine and material in a practical manufacturing context, for example, the occurrence of motor out-of-step caused by the high loads of stepper motors during high-speed printing, the actual density of material, etc. To improve the prediction accuracy, additional experiments are conducted to test the actual speed of axis movement and the actual density of material. The measured results are used to replace the original values of parameters in the predictive models.

Based on the predictive models, meta-heuristics are developed to approximate the Pareto front of process parameters to minimise the time, energy and material consumptions. The predictive models of three consumptions are used as three objective functions to be minimised. This study applies non-dominated sorting genetic algorithm II (NSGA-II) to this optimisation problem. Experiments are designed by using Taguchi robust design method to perform optimisation under different combinations of optimisation parameters (i.e. population size, number of generations, crossover probability and mutation probability). Each optimisation test can produce one Pareto front with non-dominated solutions of process parameters. Then, the hypervolume (HV) indicator is used to compare and evaluate the quality of Pareto fronts obtained from all tests. The front with the maximum HV indicator is the final optimum front, which provides guidance or a trend for setting the feasible process parameters in the prefabrication stage.

The effectiveness of the prediction method and the multi-objective optimisation method has been validated on two different fused deposition modelling (FDM) 3D printers. Referring to the proposed prediction method, the predictive models of time, energy and material consumptions for each printer have been built up. By considering the impact of machine characteristics, additional experiments have been carried out to test the actual speed of axis movement and the actual density of thermoplastic material. Each printer has printed two AM tasks. The predicted consumptions with and without additional experiments are

both compared with the actual consumptions to calculate the prediction accuracies. In addition, NSGA-II has been applied to an AM task to be printed by two printers, aiming to seek for the optimum solutions of process parameters. Referring to the proposed optimisation method, experiments of NSGA-II optimisation have been performed on each printer under different combinations of optimisation parameters. Each optimisation test has produced one Pareto front. The non-dominated solutions on the Pareto front that has the maximum HV indicator are the optimum solutions for current AM task. Furthermore, the significant contributions of optimisation parameters on the response have been analysed through range analysis and analysis of variance (ANOVA) methods.

According to the prediction and optimisation results of two case studies, the proposed method has been proved to achieve an effective prediction and optimisation of AM's time, energy and material consumptions. The improved prediction accuracy after the additional experiments is determined by the machine performance. The optimum solutions of process parameters provide a reference for the setting of feasible process parameters in prefabrication stage. Since the predictive models are customised, there is no general rule to guide the setting of process parameters and optimisation parameters for general AM technologies.

To the author's best knowledge, the methods provide the basis for predicting and optimising above three consumptions for general AM technologies, and are also expected to be extended to any other manufacturing technologies that manufactures by using numerical control (NC) programming. The prediction method creates a modular, customisable and flexible interface to build up the predictive models with a consideration of machine and material characteristics, production environment, and customer demands. Details of each contribution are summarised as follows.

- The module classification summarises and divides all consumption-related components of the existing AM technologies into five modules: axis movement, material processing, component heating, material feeding and auxiliary components. This method provides

a general, clear and concise modelling framework to realise the consumption modelling of each module based on its functions.

- The physics-based modelling based on the manufacturing information in G-code largely reduces the workload of experiments in data-driven modelling. This method is unlimited to any AM machine and complex structure of CAD design, and is also adoptable to any other manufacturing technologies working with numerical control (NC) programming.

- Since the power profiles and running sequences of all modules are related and determined by the G-code commands, their relationship is displayed in the form of a Gantt chart. This step clearly reflects the running sequences, working states and time consumptions of five modules, and also provides clear guidance for the consumption modelling of each module.

- The impact of the machine characteristics on prediction accuracy has been considered in this study; for example, the occurrence of motor out-of-step during high-speed axis movement and high-rate material feeding, the actual density of material, etc. To improve the prediction accuracy, additional experiments can be carried out to test the actual values of affected parameters in terms of machine characteristics and customer demands.

Meta-heuristics have been applied to search for the most feasible solutions of process parameters related to the near-optimal approximate Pareto front. The improved optimisation algorithm provides a customisable and flexible framework to personalise the optimisation objectives and the process parameter to be optimised. Details of the contribution are summarised as follows.

- During the optimisation process, every new solution of process parameters is imported into computer-aided manufacturing (CAM) and produces its unique G-code file, whose manufacturing information determines the predictive models and the predicted

consumptions. Therefore, the process from inputting process parameters into slicer software to consumption prediction is embedded in the fitness calculation process. Instead of using a fixed predictive model, the above step fully uses the manufacturing information in G-code of each AM task, which makes the optimisation results to be more convincing.

9.2. Future work

This PhD research has proposed a foundational method for predicting and optimising the time, energy and material consumptions of AM technologies. However, there are some limitations and possible extensions that continue to be developed. The limitations are summarised as follows.

- Firstly, in order to build up the predictive models, it is inevitable to perform experiments on the AM machine to obtain the relationships between the process parameters and some parameters in the models. This requires a certain time cost and necessary equipment.

- Secondly, due to the unique characteristics of the machine components, the predictive models of some modules need to be customised according to the power profiles and coding rules. This study only provides a general modelling framework to guide how to divide machine components into different modules and how to model based on power profiles and G-code. However, it cannot provide a detailed modelling method for a single component that can be universally applied.

- Thirdly, the proposed foundational method requires the manufacturer to have an understanding of the components and functions of the AM machine being used at the beginning. In order to apply the method to industrial manufacturing, the entire process from module classification to prediction modelling, and then to multi-objective optimisation needs to be integrated as a complete system that is convenient for manufacturers to use.

On the basis of the research work in this paper, future work to further improve the proposed method will be presented in the following sections.

9.2.1. Improvement of the predictive model of material consumption

The stepper motor out-of-step during material feeding in the fused deposition modelling (FDM) process is still a problem to be addressed. There are two factors that are causing step losses. Firstly, a high feeding rate causes the overloading of the operation, which means that the stepper motor is incapable of transporting the material to the target coordinates at the specified speed, resulting in insufficient material supply. The relationship between the material feeding amount and the feeding rate is still unknown. Besides, during the experiments, the material needs to be heated while being supplied. A high feeding rate or an insufficient heating temperature both might lead to the insufficient melting of the material, which hinders the supply of it. This is the second factor causing step losses. Therefore, there are three more factors that affect the prediction accuracy of material consumption, namely the heating temperature, material melting speed and material melting point. The impact of these factors on the material feeding amount is still a problem to be solved.

9.2.2. Acceleration and deceleration of axis movement

This study temporally builds up the time model of the axis movement module by assuming that the printer follows the G-code instructions at a constant speed under ideal conditions. In a practical AM process, the axis movement on each displacement comprises three phases: accelerated motion, uniform motion and decelerated motion. In order to further refine the model, the measurement of acceleration requires a high-precision time-measuring instrument and additional experiments to be designed. The research on the acceleration calculation will be continued as future work.

9.2.3. Multi-task parallel manufacturing

The case studies in the thesis focused on the prediction and parameter optimisation of a single AM task. The parallel printing of multiple 3D objects can further verify the practicability of the proposed method. When an AM machine fabricates more than two parts at the same time, the parameters of these parts are usually the same. If the multi-objective optimisation is applied to these tasks at the same time, it can avoid repeated optimisation processes and thereby efficiently obtain the optimal solution set. Therefore, more case studies of multi-task parallel manufacturing will be conducted as future work.

9.2.4. Experimental validations on identical additive manufacturing machines

This study has applied the proposed methodology to two different fused deposition modelling (FDM) machines. Further experimental validations will be conducted on multiple identical AM machines to verify whether the predictive models can be commonly used in identical AM machines using the same components.

9.2.5. Experimental validations on other additive manufacturing technologies

This study has applied the proposed methodology to two fused deposition modelling (FDM) machines. Further experimental validations will be conducted on other AM technologies to verify the feasibility of this method. Although the consumption-related modules on other AM technologies are different, their operations follow the same coding principles. Also, some AM technologies provide the multi-axis movement module; for instance, the five-axis movement in direct energy deposition (DED) technology. It realises the use of X_A and Y_B axes in addition to the three linear axes in X, Y, Z directions, as shown in **Figure 9.1**. The two extra axes not only eliminate the support structures but also achieve the rapid

prototyping of non-planar surfaces with a higher quality of surface finish. The programming of G-code is similar to "G61.223 X123.105 Y21.017 Z8.126 A30 B90", where A and B represent the rotary angle and tilt angle of the printer nozzle, respectively. Therefore, in future work, the predictive models need to add new modules to quantify the extra axes.
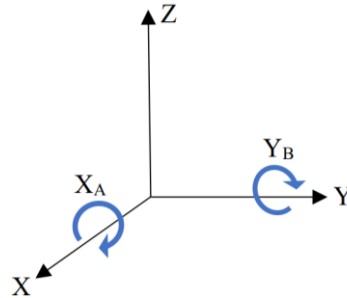
Figure 9.1: Five-axis movement of AM technology

9.2.6. Optimisation tests under large optimisation parameters

The case studies in this thesis have implemented non-dominated sorting genetic algorithm II (NSGA-II) optimisation tests under different combination of optimisation parameters. However, the values ranges of population size and number of generations are limited due to the limited computing resources. In future work, additional optimisation tests will be performed under higher values of optimisation parameters.

9.2.7. Predictions and optimisations of additional objectives

Three parameters for prediction and optimisation are considered in this study, namely time, energy and material consumptions. In future work, new objectives can be defined to expand the model in terms of customer demands; for example, the printing capability (e.g. printing space, printing orientation) of the AM machine, the mechanical performance (e.g. tensile strength), surface roughness and hardness of the printed objects, etc.

9.2.8. Real-time consumption modelling and updating of predictive models

The proposed prediction method performs the hybrid modelling for an AM machine with a number of experiments. To improve the adoptability of this method, the real-time consumption modelling during practical AM process should be continued as future work. A platform can be developed to collect and process the data of power, time, temperature in real-time. Besides, the platform can automatically classify the components into different modules with different working states, and build up the predictive models based on the collected data. This can avoid the manufacturers from spending time and cost on the consumption modelling before using the machine to work.

In addition, the long-term use of an AM machine can produce mechanical losses. These losses mainly depend on seven factors: duration of use, intensity and load of use, quality and wear resistance of the mechanical equipment, accuracy or precision of the installation and assembly of the mechanical equipment, external influences during use, maintenance and repair, and the proficiency of users. Those factors not only affect the machine performance but also reduce the prediction accuracy (Aramcharoen and Mativenga, 2014; Hu et al., 2012). Therefore, in future work, the important parameters (e.g. apparent power, axis movement speed and time consumption) can be measured in real-time during the AM process. The predictive models can also be updated in real-time according to changes in the machine characteristics.

BIBLIOGRAPHY

Abdel-Basset, M., Abdel-Fatah, L. and Kumar Sangaiah, A. 2018. "Metaheuristic Algorithms: A Comprehensive Review". *Computational Intelligence For Multimedia Big Data On The Cloud With Engineering Applications*, Academic Press, pp. 185-231.

Agarwala, M.K., Jamalabad, V.R., Langrana, N.A., Safari, A., Whalen, P.J. and Danforth, S.C. 1996. "Structural quality of parts processed by fused deposition", *Rapid Prototyping Journal*, **2**(4), pp. 4-19.

Ahsan, A., Habib, M. and Khoda, B. 2015. "Resource based process planning for additive manufacturing", *Computer-Aided Design*, **69**, pp. 112-125.

Aramcharoen, A. and Mativenga, P. 2014. "Critical factors in energy demand modelling for CNC milling and impact of toolpath strategy", *Journal of Cleaner Production*, **78**, pp. 63-74.

Arora, P., Arora, R., Haleem, A. and Kumar, H. 2020. "Application of additive manufacturing in challenges posed by COVID-19", *Materials Today: Proceedings*.

Auger, A., Bader, J., Brockhoff, D. and Zitzler, E. 2009. "Theory of the hypervolume indicator: optimal µ-distributions and the choice of the reference point", *Proceedings of the tenth ACM SIGEVO workshop on Foundations of genetic algorithms*, pp. 87-102.

Avram, O. and Xirouchakis, P. 2011. "Evaluating the use phase energy requirements of a machine tool system", *Journal of Cleaner Production*, **19**(6-7), pp. 699-711.

Balabokhin, A. and Tarbutton, J. 2017. "Iso-scallop tool path building algorithm 'based on tool performance metric' for generalized cutter and arbitrary milling zones in 3-axis CNC milling of free-form triangular meshed surfaces", *Journal of Manufacturing Processes*, 28, pp. 565-572.

Balogun, V.A., Kirkwood, N.D. and Mativenga, P.T. 2014. "Direct electrical energy demand in fused deposition modelling", *Procedia Cirp*, **15**, pp. 38-43.

Bartolo, P.J. 2007. "Photo-Curing Modeling: Direct Irradiation", *The International Journal of Advanced Manufacturing Technology*, **32**(5-6), pp. 480-491.

Bartolo, P.J. and Lenz, E. 2006. "Computer Simulation of Stereolithographic Curing Reactions: Phenomenological Versus Mechanistic Approaches", *CIRP Annals-Manufacturing Technology*, **55**(1), pp. 221-225.

Barzegari, M. R. and Rodrigue, D. 2009. "The effect of injection molding conditions on the morphology of polymer structural foams". *Polymer Engineering & Science*, **49**(5), pp. 949-959.

Baumers, M., Tuck, C., Bourell, D.L., Sreenivasan, R. and Hague, R. 2011. "Sustainability of additive manufacturing: measuring the energy consumption of the laser sintering process", *Proceedings of the Institution of Mechanical Engineers, Part B: Journal of Engineering Manufacture*, **225**(12), pp. 2228-2239.

Baumers, M., Tuck, C., Wildman, R., Ashcroft, I., Rosamond, E. and Hague, R. 2012. "Transparency Built-in", *Journal of Industrial Ecology*, **17**(3), pp. 418-431.

Baumung, W. and Fomin, V. 2018. "Optimization Model to Extend Existing Production Planning and Control Systems for the Use of Additive Manufacturing Technologies in the Industrial Production", *Procedia Manufacturing*, **24**, pp. 222-228.

Bayraktar, Ö., Uzun, G., Çakiroğlu, R., Guldas, A. 2016. "Experimental Study On The 3D-Printed Plastic Parts And Predicting The Mechanical Properties Using Artificial Neural Networks", *Polymers For Advanced Technologies*, **28** (8), pp. 1044-1051.

Behandish, M., Nelaturi, S. and de Kleer, J. 2018. "Automated process planning for hybrid manufacturing", *Computer-Aided Design*, **102**, pp. 115-127.

Beyer, H. G. and Deb, K. 2001. "On self-adaptive features in real-parameter evolutionary algorithms", *IEEE Transactions on evolutionary computation*, **5**(3), pp. 250-270.

Bhuvanesh Kumar, M. and Sathiya, P. 2020. "Methods and materials for additive manufacturing: A critical review on advancements and challenges", *Thin-Walled Structures*, p. 107228.

Blickle, T. and Thiele, L. 1996. "A comparison of selection schemes used in evolutionary algorithms", *Evolutionary Computation*, **4**(4), pp. 361-394.

Bower, K.M. 2007. "Analysis of Variance (ANOVA) using MINITAB", *Scientific Computing & Instrumentation*, **17**, pp. 64-65.

Brockhoff. D., Friedrich, T. and Neumann, F. 2008. "Analyzing hypervolume indicator based algorithms", *International Conference on Parallel Problem Solving from Nature*, Springer, Berlin, Heidelberg, pp. 651-660.

Brockhoff. D., Bader. J., Thiele. L. and Zitzler E. 2013. "Directed Multiobjective Optimization Based on the Weighted Hypervolume Indicator", *Journal Of Multi-Criteria Decision Analysis*, **20**(5-6), pp. 291-317.

Bui, H., Pierson, H.A., Nurre, S.G. and Sullivan, K.M. 2019. "Tool path planning optimization for multi-tool additive manufacturing", *Procedia Manufacturing*, **39**, pp. 457-464.

Burwell, J. 1957. "Survey of possible wear mechanisms", *Wear*, 1(2), pp. 119-141.

Cai, Y. and Choi, S. 2019. "Deposition Group-based Toolpath Planning for Additive Manufacturing with Multiple Robotic Actuators", *Procedia Manuf*, **34**, pp. 584-593.

Carlson, R. 2001. "Design of Experiments, Principles and Applications, L. Eriksson, E. Johansson, N. Kettaneh-Wold, C. Wikström and S. Wold, Umetrics AB, Umeå Learnways AB, Stockholm, 2000, ISBN 91-973730-0-1, xii+ 329 pp", *Journal of Chemometrics: A Journal of the Chemometrics Society*, **15**(5), pp. 495-496.

Calvanese, M.L., Albertelli, P., Matta, A. and Taisch, M. 2013. "Analysis Of Energy Consumption In CNC Machining Centers And Determination Of Optimal Cutting Conditions", *Re-Engineering Manufacturing For Sustainability*, pp. 227-232.

Carneiro, O., Silva, A. and Gomes, R. 2015. "Fused deposition modeling with polypropylene", *Materials & Design*, **83**, pp. 768-776.

Campbell, I., Combrinck, J., de Beer, D. and Barnard, L. 2008. "Stereolithography build time estimation based on volumetric calculations", *Rapid Prototyping Journal*, **14**(5), pp. 271-279.

Chen, D., Heyer, S., Ibbotson, S., Salonitis, K., Steingrímsson, J.G. and Thiede, S. 2015. "Direct digital manufacturing: definition, evolution, and sustainability implications", *Journal of Cleaner Production*, **107**, pp. 615-625.

Chergui, A., Hadj-Hamou, K. and Vignat, F. 2018. "Production scheduling and nesting in additive manufacturing", *Computers & Industrial Engineering*, **126**, pp. 292-301.

Chiandussi, G., Codegone, M., Ferrero, S. and Varesio, F.E. 2012. "Comparison of multi-objective optimization methodologies for engineering applications", *Computers & Mathematics with Applications*, **63**(5), pp. 912-942.

Choi, S. and Zhu, W. 2010. "A dynamic priority-based approach to concurrent toolpath planning for multi-material layered manufacturing", *Computer-Aided Design*, **42**(12), pp. 1095-1107.

Chua, C.K. and Leong, K.F. 2014. "3D Printing and Additive Manufacturing: Principles and Applications (with Companion Media Pack) of Rapid Prototyping Fourth Edition[M]", *World Scientific Publishing Company*, pp. vii-ix.

Chua, C., Leong, K. and Lim, C. 2010. "Rapid prototyping: principles and applications (with companion CD-ROM)", *World Scientific Publishing Company*, pp. 137-147.

Coelho, R.T., de Souza, A.F., Roger, A.R., Rigatti, A.M.Y. and de Lima Ribeiro, A.A. 2010. "Mechanistic approach to predict real machining time for milling free-form geometries applying high feed rate", *The International Journal of Advanced Manufacturing Technology*, **46**(9-12), pp. 1103-1111.

Corduan, N., Himbart, T., Poulachon, G., Dessoly, M., Lambertin, M., Vigneau, J. and Payoux, B. 2003. "Wear Mechanisms of New Tool Materials for Ti-6AI-4V High Performance Machining", *CIRP Annals*, **52**(1), pp. 73-76.

Coupek, D., Friedrich, J., Battran, D. and Riedel, O. 2018. "Reduction of Support Structures and Building Time by Optimized Path Planning Algorithms in Multi-axis Additive Manufacturing", *Procedia CIRP*, **67**, pp. 221-226.

Cox, D. R. and Reid, N. 2000. "The theory of the design of experiments", *CRC Press*, pp. 165-170.

Crespo-Cano, R., Cuenca-Asensi, S., Fernández, E. and Martínez-Álvarez, A. 2019. "Metaheuristic Optimisation Algorithms for Tuning a Bioinspired Retinal Model", *Sensors*, **19**(22), 4834.

Curry, D. and Dagli, C. 2014. "Computational Complexity Measures for Many-objective Optimization Problems", *Procedia Computer Science*, **36**, pp. 185-191.

Curve Fitting Toolbox. 2020. *Uk.Mathworks.com*. [Online]. [Accessed: 29 October 2020]. Available from: https://uk.mathworks.com/products/curvefitting.

CW500 Power Quality Analyzer, Yokogawa Test & Measurement Corporation. 2020. *Tmi.Yokogawa.com*. [Online]. [Accessed: 27 October 2020]. Available from: https://tmi.yokogawa.com/solutions/products/power-analyzers/cw500-power-quality-analyzer/.

Dar, A. and Anuradha, N. 2018. "Use of orthogonal arrays and design of experiment via Taguchi L9 method in probability of default", *Accounting*, **4**(3), pp. 113-122.

De Myttenaere, A., Golden, B., Le Grand, B. and Rossi, F. 2016. "Mean absolute percentage error for regression models", *Neurocomputing*, **192**, pp. 38-48.

Deb, K. and Agrawal, R.B. 1995. "Simulated binary crossover for continuous search space", *Complex Systems*, **9**(2), pp. 115-148.

Deb, K. and Deb, D. 2014. "Analysing mutation schemes for real-parameter genetic algorithms", *International Journal of Artificial Intelligence and Soft Computing*, **4**(1), pp. 1-28.

Deb, K. and Goyal, M. 1996. "A combined genetic adaptive search (GeneAS) for engineering design", *Computer Science and Informatics*, **26**, pp. 30-45.

Deb, K., Miettinen, K. and Sharma, D. 2009. "A hybrid integrated multi-objective optimization procedure for estimating nadir point", *International conference on evolutionary multi-criterion optimization*, Springer, Berlin, Heidelberg, pp. 569-583.

Deb, K., Pratap, A., Agarwal, S. and Meyarivan, T. 2002. "A fast and elitist multiobjective genetic algorithm: NSGA-II", *IEEE transactions on evolutionary computation*, **6**(2), pp. 182-197.

Deb, K., Sindhya, K and Okabe, T. 2007. "Self-adaptive simulated binary crossover for real-parameter optimization", *Proceedings of the 9th annual conference on Genetic and evolutionary computation*, pp. 1187-1194.

Deng, Z., Lv, L., Huang, W., Wan, L. and Li, S. 2020. "Modelling of carbon utilisation efficiency and its application in milling parameters optimisation", *International Journal of Production Research*, **58**(8), pp. 2406-2420.

Dewes, R. and Aspinwall, D. 1997. "A review of ultra high speed milling of hardened steels", *Journal of Materials Processing Technology*, **69**(1-3), pp. 1-17.

Di Angelo, L. and Di Stefano, P. 2011. "A neural network-based build time estimator for layer manufactured objects", *The International Journal of Advanced Manufacturing Technology*, **57**(1-4), pp. 215-224.

Diaz, N., Redelsheimer, E. and Dornfeld, D. 2011. "Energy Consumption Characterization and Reduction Strategies for Milling Machine Tool Use", *Glocalized Solutions for Sustainability in Manufacturing*, pp. 263-267.

Dietmair, A. and Verl, A. 2009a. "Energy consumption forecasting and optimisation for tool machines", *Energy*, **62**, pp. 62-67.

Dietmair, A. and Verl, A. 2009b. "A generic energy consumption model for decision making and energy efficiency optimisation in manufacturing", *International Journal of Sustainable Engineering*, **2**(2), pp. 123-133.

Draper, N.R. and Smith, H. 1998. "Applied regression analysis", *John Wiley & Sons*, **326**, pp. 15-44.

Elbestawi, M., Chen, L., Becze, C. and El-Wardany, T. 1997. "High-Speed Milling of Dies and Molds in Their Hardened State", *CIRP Annals*, **46**(1), pp. 57-62.

El-Habrouk, M., Darwish, M. and Mehta, P. 2000. "Active power filters: A review", *IEE Proceedings – Electric Power Applications*, **147**(5), pp. 403-413.

Faassen, R.P.H., Van de Wouw, N., Oosterling, J.A.J. and Nijmeijer, H. 2003. "Prediction of regenerative chatter by modelling and analysis of high-speed milling", *International Journal of Machine Tools and Manufacture*, **43**(14), pp. 1437-1446.

Fang, Y. and Li, J. 2010. "A Review of Tournament Selection in Genetic Programming", *Advances In Computation And Intelligence*, pp. 181-192.

F-Distribution Tables. 2020. *Socr.ucla.edu*. [Online]. [Accessed: 28 December 2020]. Available from: http://www.socr.ucla.edu/Applets.dir/F_Table.html.

Fera, M., Fruggiero, F., Lambiase, A., Macchiaroli, R. and Todisco, V. 2018. "A modified genetic algorithm for time and cost optimization of an additive manufacturing single-machine scheduling", *International Journal of Industrial Engineering Computations*, **9**(4), pp. 423-438.

Fleming, C., Walker, S., Branyan, C., Nicolai, A., Hollinger, G. and Mengüç, Y. 2017. "Toolpath Planning for Continuous Extrusion Additive Manufacturing", *Technical Report. Oregon State University*.

Fok, K.Y., Cheng, C.T., Chi, K.T. and Ganganath, N. 2016. "A Relaxation Scheme for TSP-Based 3D Printing Path Optimizer", *2016 International Conference on Cyber-Enabled Distributed Computing and Knowledge Discovery (CyberC)*, Chengdu, pp. 382-385.

Ford, S. and Despeisse, M. 2016. "Additive manufacturing and sustainability: an exploratory study of the advantages and challenges", *Journal of Cleaner Production*, **137**, pp. 1573-1587.

Frazier, W.E. 2014. "Metal additive manufacturing: a review", *Journal of Materials Engineering and Performance*, **23**(6), pp. 1917-1928.

Gandhi, P., Murthy, Z. and Pati, R. 2011. "Optimization of process parameters by Taguchi robust design method for the development of nano-crystals of sirolimus using sonication based crystallization", *Crystal Research and Technology*, **47**(1), pp. 53-72.

Ganganath, N., Cheng, C.T., Fok, K.Y. and Chi, K.T. 2016. "Trajectory planning for 3D printing: A revisit to traveling salesman problem", *2016 2nd International Conference on Control, Automation and Robotics (ICCAR)*, Hong Kong, 2016, pp. 287-290.

G-Code – Reprap. 2020. *Reprap.Org*. [Online]. [Accessed: 27 October 2020]. Available from: https://reprap.org/wiki/G-code.

Gregorec Jr, J.L., Hines, D. and Harju, R.P. 2006. *U.S. Patent Application.* No. 29/199,945.

Griffiths, C.A., Howarth, J., De Almeida-Rowbotham, G., Rees, A. and Kerton, R. 2016. "A design of experiments approach for the optimisation of energy and waste during the production of parts manufactured by 3D printing", *Journal of Cleaner Production*, **139**, pp. 74-85.

Gunst, R.F. and Mason, R.L. 2009. "Fractional factorial design", *Wiley Interdisciplinary Reviews: Computational Statistics*, **1**(2), pp. 234-244.

Gutowski, T., Dahmus, J. and Thiriez, A. 2006. "Electrical energy requirements for manufacturing processes", *13th CIRP international conference on life cycle engineering*. CIRP International Leuven, Belgium, **31**(1), pp. 623-638.

Hao, J. and Wang, B. 2014. "Parameter Sensitivity Analysis on Deformation of Composite Soil-Nailed Wall Using Artificial Neural Networks and Orthogonal Experiment", *Mathematical Problems in Engineering*, **2014**, pp. 1-8.

Hao, L., Raymond, D., Strano, G. and Dadbakhsh, S. 2010. "Enhancing the sustainability of additive manufacturing", *5th International Conference on Responsive Manufacturing – Green Manufacturing (ICRM 2010)*, pp. 390-395.

Hbaieb, M., Othmani, R. and Bouzid, W. 2011. "Time modeling in high-speed machining of mold pocket", *The International Journal of Advanced Manufacturing Technology*, **53**(1-4), pp. 113-120.

He, Y., Liu, F., Wu, T., Zhong, F.P. and Peng, B. 2012. "Analysis and estimation of energy consumption for numerical control machining", *Proceedings of the Institution of Mechanical Engineers, Part B: Journal of Engineering Manufacture*, **226**(2), pp. 255-266.

Hu, S., Liu, F., He, Y. and Hu, T. 2012. "An on-line approach for energy efficiency monitoring of machine tools", *Journal of Cleaner Production*, **27**, pp. 133-140.

Huang, R., Riddle, M., Graziano, D., Warren, J., Das, S., Nimbalkar, S., Cresko, J. and Masanet, E. 2016. "Energy and emissions saving potential of additive manufacturing: the case of lightweight aircraft components", *Journal of Cleaner Production*, **135**, pp. 1559-1570.

Hwang, C. C., Lyu, L. Y., Liu, C. T. and Li, P. L. 2008. "Optimal design of an SPM motor using genetic algorithms and Taguchi method", *IEEE Transactions on Magnetics*, **44**(11), pp. 4325-4328.

i3 Mega S. 2020. *ANYCUBIC 3D Printing*. [Online]. [Accessed: 27 October 2020]. Available from: https://www.anycubic.com/products/anycubic-i3-mega-s.

Ishibuchi, H., Imada. R., Setoguchi, Y. and Nojima, Y. 2017. "Reference point specification in hypervolume calculation for fair comparison and efficient search", *Proceedings of the Genetic and Evolutionary Computation Conference*, pp. 585-592.

Jenkins, D.G. and Quintana-Ascencio, P.F. 2020. "A solution to minimum sample size for regressions", *PLOS ONE*, **15**(2), e0229345.

Jeswiet, J. and Kara, S. 2008. "Carbon emissions and CES™ in manufacturing", *CIRP Annals*, **57**(1), pp. 17-20.

Jiang, J. and Ma, Y. 2020. "Path planning strategies to optimize accuracy, quality, build time and material use in additive manufacturing: a review". *Micromachines*, **11**(7), p. 633.

Jiang, L., Ye, H., Zhou, C. and Chen, S., 2019. "Parametric topology optimization toward rational design and efficient prefabrication for additive manufacturing", *Journal of Manufacturing Science and Engineering*, **141**(4), p. 041007.

Jin, Y., Du, J. and He, Y. 2017. "Optimization of process planning for reducing material consumption in additive manufacturing", *Journal of Manufacturing Systems*, **44**, pp. 65-78.

Jin, G.Q., Li, W.D. and Gao, L. 2013. "An adaptive process planning approach of rapid prototyping and manufacturing", *Robotics and Computer-Integrated Manufacturing*, **29**(1), pp. 23-38.

Jin, G., Li, W., Tsai, C. and Wang, L. 2011. "Adaptive tool-path generation of rapid prototyping for complex product models", *Journal of Manufacturing Systems*, **30**(3), pp. 154-164.

Jung, J.Y. 2002. "Manufacturing cost estimation for machined parts based on manufacturing features", *Journal of Intelligent Manufacturing*, **13**(4), pp. 227-238.

Kellens, K., Baumers, M., Gutowski, T.G., Flanagan, W., Lifset, R. and Duflou, J.R. 2017. "Environmental dimensions of additive manufacturing: Mapping application domains and their environmental implications", *Journal of Industrial Ecology*, **21**(S1), pp. 49-68.

Khan, A. and Baig, A. R. 2015. "Multi-objective feature subset selection using non-dominated sorting genetic algorithm", *Journal of applied research and technology*, **13**(1), pp. 145-159.

Khanna, N. and Davim, J. P. 2015. "Design-of-experiments application in machining titanium alloys for aerospace structural components", *Measurement*, **61**, pp. 280-290.

Kong, D., Choi, S., Yasui, Y., Pavanaskar, S., Dornfeld, D. and Wright, P. 2011. "Software-based tool path evaluation for environmental sustainability", *Journal of Manufacturing Systems*, 30(4), pp. 241-247.

Kordonowy, D.N. 2002. "A power assessment of machining tools", *Massachusetts Institute of Technology*, pp. 15-21.

Kraaikamp, F. D. C. and Meester, H. L. L. 2005. "A Modern Introduction to Probability and Statistics", pp. 329-350.

Kruth, J.P., Mercelis, P., Vaerenbergh, J.V., Froyen, L. and Rombouts, M. 2005. "Binding mechanisms in selective laser sintering and selective laser melting", *Rapid Prototyping Journal*, **11**(1), pp. 26-36.

Kruth, J.P., Wang, X., Laoui, T. and Froyen, L. 2003. "Lasers and materials in selective laser sintering", *Assembly Automation*, **23**(4), pp. 357-371.

Kumar, S., Mani, V. and Devraj, N. 2014. "Production Planning and Process Improvement in an Impeller Manufacturing Using Scheduling and OEE Techniques", *Procedia Materials Science*, **5**, pp. 1710-1715.

Le, V. T., Paris, H. and Mandil, G. 2017. "Process planning for combined additive and subtractive manufacturing technologies in a remanufacturing context", *Journal of Manufacturing Systems*, **44**, pp. 243-254.

Lee, Y., Filliben, J.J., Micheals, R.J. and Phillips, P.J. 2013. "Sensitivity analysis for biometric systems: A methodology based on orthogonal experiment designs", *Computer Vision and Image Understanding*, **117**(5), pp. 532-550.

Li, C., Xiao, Q., Tang, Y. and Li, L. 2016. "A method integrating Taguchi, RSM and MOPSO to CNC machining parameters optimization for energy saving", *Journal of Cleaner Production*, **135**, pp. 263-275.

Li, Q., Kucukkoc, I. and Zhang, D.Z. 2017. "Production planning in additive manufacturing and 3D printing", *Computers & Operations Research*, **83**, pp. 157-172.

Liang, K.Y. and Zeger, S.L. 1993. "Regression analysis for correlated data", *Annual review of public health*, **14**(1), pp. 43-68.

Lin, F., Yang, Y., Wang, S., Xu, Y., Ma, H. and Yu, R. 2019. "Urban public bicycle dispatching optimization method", *PeerJ Computer Science*, **5**, p. e224.

Liu, C., Li, Y., Wang, W. and Shen, W. 2013. "A feature-based method for NC machining time estimation", *Robotics and Computer-Integrated Manufacturing*, **29**(4), pp. 8-14.

Liu, N., Zhang, Y. and Lu, W. 2015. "A hybrid approach to energy consumption modelling based on cutting power: a milling case", *Journal of Cleaner Production*, **104**, pp. 264-272.

Luo, Y., Ji, Z., Leu, M.C. and Caudill, R. 1999. "Environmental performance analysis of solid freedom fabrication processes", *Proceedings of the 1999 IEEE international symposium on electronics and the environment (Cat. No. 99CH36357)*, IEEE, pp. 1-6.

Matias, J.M., Bartolo, P.J. and Pontes, A.V. 2009. "Modeling and simulation of photofabrication processes using unsaturated polyester resins", *Journal of Applied Polymer Science*, **114**(6), pp. 3673-3685.

Meteyer, S., Xu, X., Perry, N. and Zhao, Y.F. 2014. "Energy and Material Flow Analysis of Binder-jetting Additive Manufacturing Processes", *Procedia CIRP*, **15**, pp. 19-25.

Miller, B. and Goldberg, D. 1995. "Genetic Algorithms, Tournament Selection, and the Effects of Noise", *Complex systems*, **9**(3), pp. 193-212.

MINI+, O. 2020. *Original Prusa MINI+ - Prusa Research*. [Accessed: 27 October 2020]. Available from: https://shop.prusa3d.com/en/3d-printers/994-original-prusa-mini.html.

Mitchell, M. 1998. "An introduction to genetic algorithms", *MIT Press*, pp. 1-15.

Monoprice, M. 2020. *MP Mini Delta 3D Printer*. [Online]. [Accessed: 27 October 2020]. Available from: https://www.monoprice.uk/products/monoprice-mp-mini-delta-3d-printer?_pos=12&_sid=48820a43e&_ss=r.

Mueller, B. 2012. "Additive manufacturing technologies – Rapid prototyping to direct digital manufacturing", *Assembly Automation*, **32**(2).

Mueller, B. and Kochan, D. 1999. "Laminated object manufacturing for rapid tooling and patternmaking in foundry industry", *Computers in Industry*, **39**(1), pp. 47-53.

Munguía, J., Ciurana, J. and Riba, C. 2009. "Neural-network-based model for build-time estimation in selective laser sintering", *Proceedings of the Institution of Mechanical Engineers, Part B: Journal of Engineering Manufacture*, **223**(8), pp. 995-1003.

Nebro, A.J., Alba, E., Molina, G., Chicano, F., Luna, F. and Durillo, J.J. 2007. "Optimal antenna placement using a new multi-objective CHC algorithm", *Proceedings of the 9th annual conference on Genetic and evolutionary computation*, pp. 876-883.

Newman, S.T., Zhu, Z., Dhokia, V. and Shokrani, A. 2015. "Process planning for additive and subtractive manufacturing technologies", *CIRP Annals*, **64**(1), pp. 467-470.

Osyczka, A. and Kundu, S. 1995. "A new method to solve generalized multicriteria optimization problems using the simple genetic algorithm", *Structural Optimization*, **10**(2), pp. 94-99.

Ou-Yang, C. and Lin, T.S. 1997. "Developing an integrated framework for feature-based early manufacturing cost estimation", *The International Journal of Advanced Manufacturing Technology*, **13**(9), pp. 618-629.

Pattanaika, A., Adarsha, H., Prashanthakumar, H.G. and Kaushik, V. 2018. "Tribological behaviour of epoxy-marble powder composite with taguchi optimization technique", *Composites*, **8**, pp. 110-117.

Pei, J., Liu, X., Pardalos, P.M., Fan, W., Yang, S. and Wang, L. 2013. "Application of an effective modified gravitational search algorithm for the coordinated scheduling

problem in a two-stage supply chain", *The International Journal of Advanced Manufacturing Technology*, **70**(1-4), pp. 335-348.

Peng, T. 2016. "Analysis of Energy Utilization in 3D Printing Processes", *Procedia CIRP*, **40**, pp. 62-67.

Peng, T. and Sun, W. 2017. "Energy modelling for FDM 3D printing from a life cycle perspective", *International Journal of Manufacturing Research*, **12**(1), pp. 83-98.

Polynomial Curve Fitting. 2020. *uk.mathworks.com* [Online]. [Accessed: 27 October 2020]. Available from: https://uk.mathworks.com/help/curvefit/polynomial-curve-fitting.html.

Qin, J., Ying, L. and Roger G. 2017. "A Framework Of Energy Consumption Modelling For Additive Manufacturing Using Internet Of Things", *Procedia CIRP*, **63**, pp. 307-312.

Qin, J., Ying, L. and Roger G. 2018. "Multi-Source Data Analytics For AM Energy Consumption Prediction". *Advanced Engineering Informatics*, **38**, pp. 840-850.

Qin, J., Liu, Y., Grosvenor, R., Lacan, F. and Jiang, Z. 2020. "Deep learning-driven particle swarm optimisation for additive manufacturing energy optimisation", *Journal of Cleaner Production*, **245**, p. 118702.

Raghuwanshi, M.M. and Kakde, O.G. 2004. "Survey on multiobjective evolutionary and real coded genetic algorithms", *Proceedings of the 8th Asia Pacific symposium on intelligent and evolutionary systems*, pp. 150-161.

Rajemi, M.F. and Mativenga, P.T. 2010. *Energy analysis in turning and milling.* Ph.D. thesis, University of Manchester.

Rajemi, M., Mativenga, P. and Aramcharoen, A. 2010. "Sustainable machining: selection of optimum turning conditions based on minimum energy considerations", *Journal of Cleaner Production*, **18**(10-11), pp. 1059-1065.

Ren, L., Sparks, T., Ruan, J. and Liou, F. 2010. "Integrated process planning for a multiaxis hybrid manufacturing system", *Journal of Manufacturing Science and Engineering*, **132**(2), p. 021006.

Sandra, L. A. 1994. "PHB Practical Handbook of Curve Fitting." *ed: CRC Press: Boca Raton, FL, USA*.

Sartorius Practum313-1S Analytical Balance. 2020. *Scalesgalore.com.* [Online]. [Accessed: 27 October 2020]. Available from: *https://www.scalesgalore.com/product/Sartorius-Practum3131S-Milligram-Balance-310-g-x-1-mg-px32945.cfm.*

Sartorius YDK03. 2020. *Sartorius.com.* [Online]. [Accessed: 27 October 2020]. Available from: https://www.sartorius.com/shop/medias/-usermanual-en-Manual-YDK03-WYD6150ck.pdf?context=bWFzdGVyfGRvY3VtZW50c3wzNDQzNDA3fGFwcGx pY2F0aW9uL3BkZnxkb2N1bWVudHMvaDk1L2g4Zi84OTQzMTM3OTE0OTEwL nBkZnxlZmZiOTU5MmIwMDJmZGI0OTIwNGVlMzhkMTQyZTNiZmY5MDQ3N ThlY2NjMmYzZGM1ZjM2MDNkNzg5MDZmMjcw.

Shembekar, A.V., Yoon, Y.J., Kanyuck, A. and Gupta, S.K. 2018. "Trajectory planning for conformal 3d printing using non-planar layers", *International Design Engineering Technical Conferences and Computers and Information in Engineering Conference*, American Society of Mechanical Engineers, **51722**, p. V01AT02A026.

Smid, P. 2003. "CNC programming handbook: a comprehensive guide to practical CNC programming", *Industrial Press Inc.*, pp. 47-92.

Smid, P. 2010. "CNC control setup for milling and turning: mastering CNC control systems", *Industrial Press Inc.*, pp. 261-263.

Sreenivasan, R. and Bourell, D. 2010. "Sustainability Study in Selective Laser Sintering – An Energy Perspective", *Minerals, Metals and Materials Society/AIME, 420 Commonwealth Dr., P. O. Box 430 Warrendale PA 15086 USA.[np]*.

Subashini, G. and Bhuvaneswari, M.C. 2012. "Comparison of multi-objective evolutionary approaches for task scheduling in distributed computing systems", *Sadhana*, **37**(6), pp. 675-694.

Swamidass. P.M. and Winch, G.W. 2002. "Exploratory study of the adoption of manufacturing technology innovations in the USA and the UK", *International Journal of Production Research*, **40**(12), pp. 2677-2703.

Too, M.H., Leong, K.F., Chua, C.K., Du, Z.H., Yang, S.F., Cheah, C.M. and Ho, S.L. 2002. "Investigation of 3D non-random porous structures by fused deposition modelling", *The International Journal of Advanced Manufacturing Technology*, **19**(3), pp. 217-223.

Treatstock. 2020. "Guides What Is Material Jetting?". *Treatstock.co.uk*. [Online]. [Accessed: 27 October 2020]. Available from: https://www.treatstock.co.uk/guide/article/126-what-is-material-jetting.

Tymrak, B.M., Kreiger, M. and Pearce, J.M. 2014. "Mechanical properties of components fabricated with open-source 3-D printers under realistic environmental conditions", *Materials & Design*, **58**, pp. 242-246.

Verma, S., Pant M. and Snasel, V. 2021. "A Comprehensive Review on NSGA-II for Multi-Objective Combinatorial Optimization Problems", *IEEE Access*, **9**, pp. 57757-57791.

Volpato, N., Galvão, L.C., Nunes, L.F., Souza, R.I. and Oguido, K. 2020. "Combining heuristics for tool-path optimisation in material extrusion additive manufacturing", *Journal of the Operational Research Society*, **71**(6), pp. 867-877.

Walter, M., Holmström, J., Tuomi, H. and Yrjölä, H. 2004. "Rapid manufacturing and its impact on supply chain management", *Proceedings of the logistics research network annual conference*, pp. 9-10.

Wang, H., Xu, X., Zhang, C. and Hu, T. 2018. "A hybrid approach to energy-efficient machining for milled components via STEP-NC", *International Journal of Computer Integrated Manufacturing*, **31**(4-5), pp. 442-456.

Watson, J. and Taminger, K. 2018. "A decision-support model for selecting additive manufacturing versus subtractive manufacturing based on energy consumption", *Journal of Cleaner Production*, **176**, pp. 1316-1322.

Wdowik, R., Magdziak, M., Ratnayake, R.C. and Borsellino, C. 2018. "Application of process parameters in planning and technological documentation: CNC machine tools and CMMs programming perspective", *Procedia CIRP*, **78**, pp. 43-48.

Whitley, D. 1994. "A genetic algorithm tutorial", *Statistics and Computing*, **4**(2), pp. 65-85.

Wu, H., Fahy, W., Kim, S., Kim, H., Zhao, N., Pilato, L., Kafi, A., Bateman, S. and Koo, J. 2020. "Recent developments in polymers/polymer nanocomposites for additive manufacturing", *Progress in Materials Science*, **111**, p. 100638.

Yang, J., Chen, Y., Huang, W. and Li, Y. 2017. "Survey on artificial intelligence for additive manufacturing", *2017 23rd International Conference on Automation and Computing (ICAC)*, IEEE, **2017**, pp. 1-6.

Yang, J. and Liu, Y. 2020. "Energy, time and material consumption modelling for fused deposition modelling process", *Procedia CIRP*, **90**, pp. 510-515.

Yap, Y.L., Wang, C., Sing, S.L., Dikshit, V., Yeong, W.Y. and Wei, J. 2017. "Material jetting additive manufacturing: An experimental study using designed metrological benchmarks", *Precision Engineering*, **50**, pp. 275-285.

Yılmaz, Ö. 2020. "Examining additive manufacturing in supply chain context through an optimization model", *Computers & Industrial Engineering*, **142**, p. 106335.

Yoon, H., Lee, J., Kim, H., Kim, M., Kim, E., Shin, Y., Chu, W. and Ahn, S. 2014. "A comparison of energy consumption in bulk forming, subtractive, and additive processes: Review and case study", *International Journal of Precision Engineering and Manufacturing-Green Technology*, **1**(3), pp. 261-279.

Yusoff, Y., Ngadiman, M. and Zain, A. 2011. "Overview of NSGA-II for Optimizing Machining Process Parameters", *Procedia Engineering*, **15**, pp. 3978-3983.

Zeng, G., Chen, J., Li, L., Chen, M., Wu, L., Dai, Y. and Zheng, C. 2016. "An improved multi-objective population-based extremal optimization algorithm with polynomial mutation", *Information Sciences*, **330**, pp. 49-73.

Zhang, D., Li, M., Ji, X., Wu, J. and Dong, Y. 2019. "Revealing potential of energy-saving behind emission reduction", *Management of Environmental Quality: An International Journal*, **30**(4), pp. 714-730.

Zhang, Y. and Bernard, A. 2013. "Generic build time estimation model for parts produced by SLS", *High value manufacturing: Advanced research in virtual and rapid prototyping. Proceedings of the 6th International Conference on Advanced Research in Virtual and Rapid Prototyping*, pp. 43-48.

Zhang, Y., Bernard, A., Valenzuela, J.M. and Karunakaran, K. 2015. "Fast adaptive modeling method for build time estimation in Additive Manufacturing", *CIRP Journal of Manufacturing Science and Technology*, **10**, pp. 49-60.

Zhang, Y., Bernard, A., Harik, R. and Karunakaran, K.P. 2017. "Build orientation optimization for multi-part production in additive manufacturing", *Journal of Intelligent Manufacturing*, **28**, pp. 1393-1407.

Zhou, J., Herscovici, D. and Chen, C. 2000. "Parametric process optimization to improve the accuracy of rapid prototyped stereolithography parts", *International Journal of Machine Tools and Manufacture*, **40**(3), pp. 363-379.

Zhu, Z., Dhokia, V.G., Nassehi, A. and Newman, S.T. 2013a. "A review of hybrid manufacturing processes – State of the art and future perspectives", *International Journal of Computer Integrated Manufacturing*, **26**(7), pp. 596-615.

Zhu, Z., Dhokia, V. and Newman, S. 2013b. "The development of a novel process planning algorithm for an unconstrained hybrid manufacturing process", *Journal of Manufacturing Processes*, **15**(4), pp. 404-413.

Zitzler, E., Brockhoff, D. and Thiele, L. 2007. "The Hypervolume Indicator Revisited: On the Design of Pareto-compliant Indicators Via Weighted Integration", *International Conference on Evolutionary Multi-Criterion Optimization*. Springer: Berlin, Heidelberg, pp. 862-876.

Zitzler, E. and Thiele, L. 1998. "Multiobjective optimization using evolutionary algorithms—a comparative case study", *International conference on parallel problem solving from nature.* Springer: Berlin, Heidelberg, pp. 292-301.

Z Table and Z Score Calculation. 2020. *Z Score Table*. [Online]. [Accessed: 27 October 2020]. Available from: http://www.z-table.com/.

APPENDIX I PSEUDO CODES OF NSGA-II ALGORITHM

1.   Pseudo code of non-dominated sorting in NSGA-II algorithm (Deb et al., 2002)

for each $\mathbf{x}_p \in X^n$ $\quad S_{\mathbf{x}_p} = \phi$ $\quad \mathcal{L}_{\mathbf{x}_p} = 0$ $\quad$ for each $\mathbf{x}_q \in X^n$: $\quad\quad$ if $(\mathbf{x}_p \prec \mathbf{x}_q)$: $\quad\quad\quad S_{\mathbf{x}_p} = S_{\mathbf{x}_p} \cup \{\mathbf{x}_q\}$ $\quad\quad$ else if $(\mathbf{x}_p \succ \mathbf{x}_q)$: $\quad\quad\quad \mathcal{L}_{\mathbf{x}_p} = \mathcal{L}_{\mathbf{x}_p} + 1$ $\quad$ if $\mathcal{L}_{\mathbf{x}_p} = 0$: $\quad\quad \mathcal{R}_{\mathbf{x}_p} = 1$ $\quad\quad L_1 = L_1 \cup \{\mathbf{x}_p\}$	**Find the non-dominated individuals on the first level** There are three objectives in this MO problem (i.e. $M = 3$, $Obj = 1, 2, 3$) $\quad \mathcal{F}_1(\mathbf{x}_p)$: Total time consumption of solution $\mathbf{x}_p$ $\quad \mathcal{F}_2(\mathbf{x}_p)$: Total energy consumption of solution $\mathbf{x}_p$ $\quad \mathcal{F}_3(\mathbf{x}_p)$: Total material consumption of solution $\mathbf{x}_p$ If $\mathbf{x}_p$ dominates $\mathbf{x}_q$ (i.e. $\mathcal{F}_{Obj}(\mathbf{x}_p) \leq \mathcal{F}_{Obj}(\mathbf{x}_q)$), then add $\mathbf{x}_q$ to the solution set dominated by $\mathbf{x}_p$. If $\mathbf{x}_q$ dominates $\mathbf{x}_p$ (i.e. $\mathcal{F}_{Obj}(\mathbf{x}_q) \leq \mathcal{F}_{Obj}(\mathbf{x}_p)$), then increment the dominance counter of $\mathbf{x}_p$. If $\mathbf{x}_p$ is not dominated by any individual in current population, then the dominance counter $\mathcal{L}_{\mathbf{x}_p}$ of $\mathbf{x}_p$ is equal to 0, the ranking level of $\mathbf{x}_p$ is 1, $\mathbf{x}_p$ belong to the first level L_1
$\alpha = 1$ while $L_\alpha \neq \phi$: $\quad S_{\mathbf{x}_q} = \phi$ $\quad$ for each $\mathbf{x}_p \in L_\alpha$: $\quad\quad$ for each $\mathbf{x}_q \in S_{\mathbf{x}_p}$: $\quad\quad\quad \mathcal{L}_{\mathbf{x}_q} = \mathcal{L}_{\mathbf{x}_q} - 1$ $\quad\quad\quad$ if $\mathcal{L}_{\mathbf{x}_q} = 0$: $\quad\quad\quad\quad \mathcal{R}_{\mathbf{x}_q} = \alpha + 1$ $\quad\quad\quad\quad S_{\mathbf{x}_q} = S_{\mathbf{x}_q} \cup \{\mathbf{x}_q\}$ $\quad \alpha = \alpha + 1$ $\quad L_\alpha = S_{\mathbf{x}_q}$	**Sort the rest individuals on the next level** $\mathbf{x}_p$ belongs to the αth ranking level L_α $\mathbf{x}_q$ is dominated by $\mathbf{x}_p$ and belongs to solution set $S_{\mathbf{x}_p}$ If the dominance counter $\mathcal{L}_{\mathbf{x}_q}$ of $\mathbf{x}_q$ is 0, then $\mathbf{x}_q$ belongs to the next level

2. Pseudo code of crowding distance ranking in NSGA-II algorithm (Deb et al., 2002)

for each $\mathbf{x}_t \in X^n$:	For each individual $\mathbf{x}_t$, the distance is initialised at first
$\quad \mathcal{D}[\mathbf{x}_t]_{distance} = 0$	There are three objectives in this MO problem (i.e. $M = 3$, $Obj = 1, 2, 3$)
	$\quad \mathcal{F}_1(\mathbf{x}_t)$: Total time consumption of solution $\mathbf{x}_t$
	$\quad \mathcal{F}_2(\mathbf{x}_t)$: Total energy consumption of solution $\mathbf{x}_t$
	$\quad \mathcal{F}_3(\mathbf{x}_t)$: Total material consumption of solution $\mathbf{x}_t$
for each objective $Obj = 1$ to 3:	
$\quad \mathcal{D} = sort(\mathcal{D}, Obj)$	Individuals are sorted based on each objective
$\quad \mathcal{D}[\mathbf{x}_1]_{distance} = \mathcal{D}[\mathbf{x}_C]_{distance} = \infty$	Ensure the boundary points are selected
$\quad$ for $t = 2$ to $C - 1$:	
$\quad\quad \mathcal{D}[\mathbf{x}_t]_{distance} = \mathcal{D}[\mathbf{x}_t]_{distance} + \frac{\mathcal{F}_{Obj}(\mathbf{x}_{t+1}) - \mathcal{F}_{Obj}(\mathbf{x}_{t-1})}{\mathcal{F}_{Obj}{}^{max} - \mathcal{F}_{Obj}{}^{min}}$	

3. Pseudo code of binary tournament selection in NSGA-II algorithm (Blickle and Thiele, 1996)

Tournament=2	Tournament size is defined as 2.
$P_{k+1} = \{\mathbf{x}_1, \mathbf{x}_2, \dots, \mathbf{x}_N\}$	Population size is defined as N.
for each selection $i = 1$ to N:	The number of selection times is N.
$\quad$ if $\mathcal{L}_{\mathbf{x}_m} < \mathcal{L}_{\mathbf{x}_n}$:	In each tournament selection, compare two random candidates $\mathbf{x}_m$, $\mathbf{x}_n$ through non-dominated ranks and crowding distances.
$\quad\quad P'_{k+1} = P'_{k+1} \cup \{\mathcal{L}_{\mathbf{x}_m}\}$	
$\quad$ else if $\mathcal{L}_{\mathbf{x}_m} > \mathcal{L}_{\mathbf{x}_n}$:	Select the candidate belonging to the lower non-dominated level as parent.
$\quad\quad P'_{k+1} = P'_{k+1} \cup \{\mathcal{L}_{\mathbf{x}_n}\}$	
$\quad$ else if $\mathcal{L}_{\mathbf{x}_m} = \mathcal{L}_{\mathbf{x}_n}$:	If two candidates belong to the same non-dominated level, select the one that has the larger crowding distance.
$\quad\quad$ if $\mathcal{D}[\mathbf{x}_m]_{distance} > \mathcal{D}[\mathbf{x}_n]_{distance}$:	
$\quad\quad\quad P'_{k+1} = P'_{k+1} \cup \{\mathcal{L}_{\mathbf{x}_m}\}$	
$\quad\quad$ else if $\mathcal{D}[\mathbf{x}_m]_{distance} > \mathcal{D}[\mathbf{x}_n]_{distance}$:	
$\quad\quad\quad P'_{k+1} = P'_{k+1} \cup \{\mathcal{L}_{\mathbf{x}_n}\}$	
Return P'_{k+1}	

# APPENDIX II EXPERIMENTAL RESULTS OF CONSUMPTION MODELLING AND VALIDATION OF ANYCUBIC I3 MEGA 3D PRINTER

Predictive model of time and energy consumptions

Appendix II: Power profiles of material processing module at different target temperatures T_{mp}^1

1.

2.
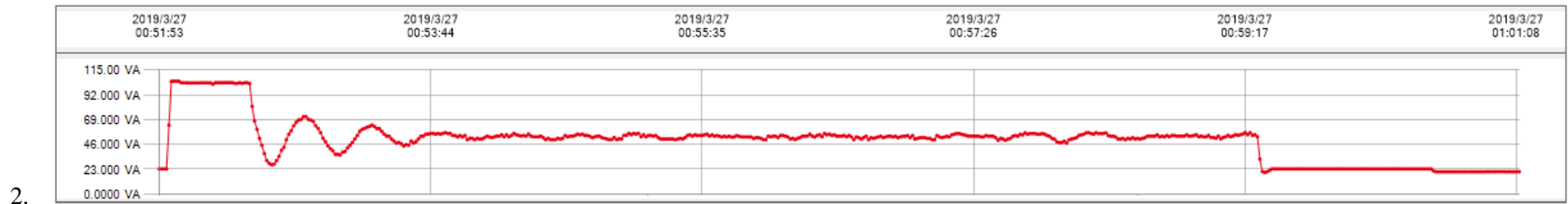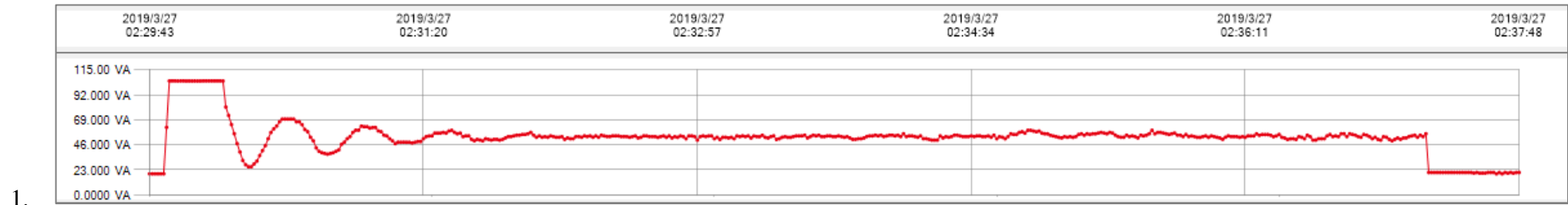
3.
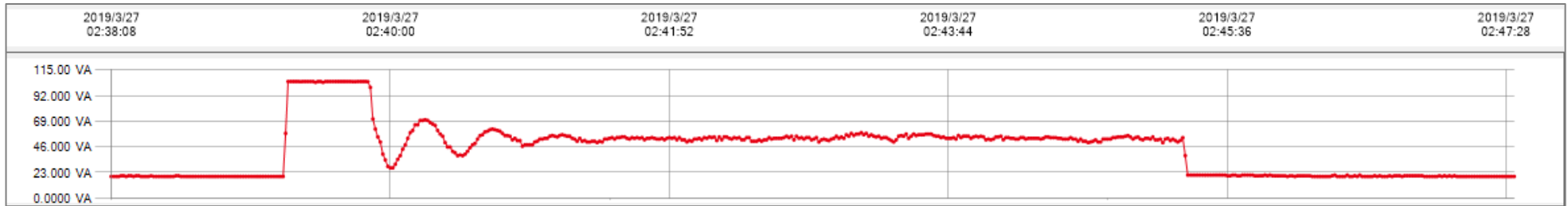
4.
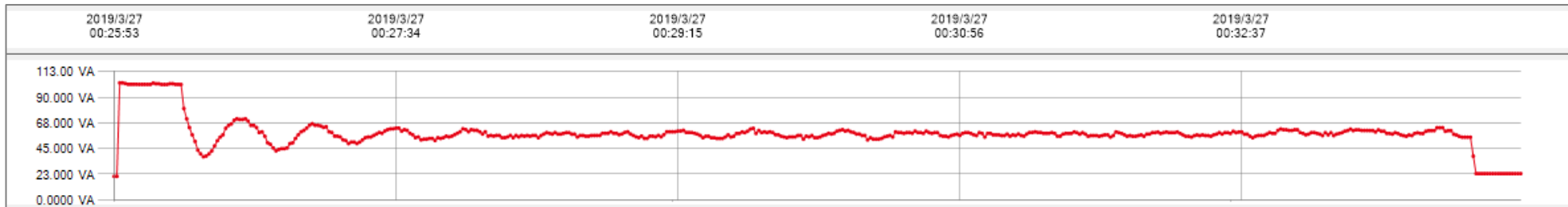
5.
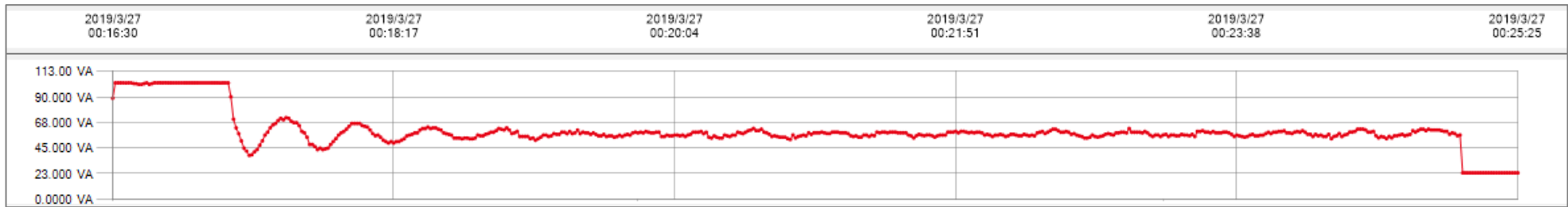
6.
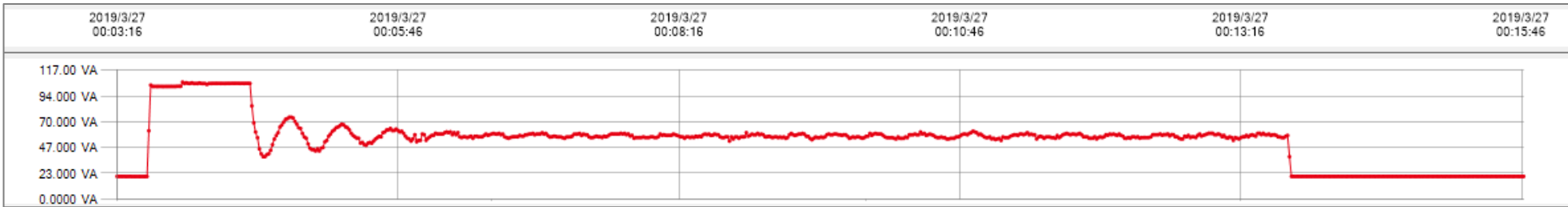
7.
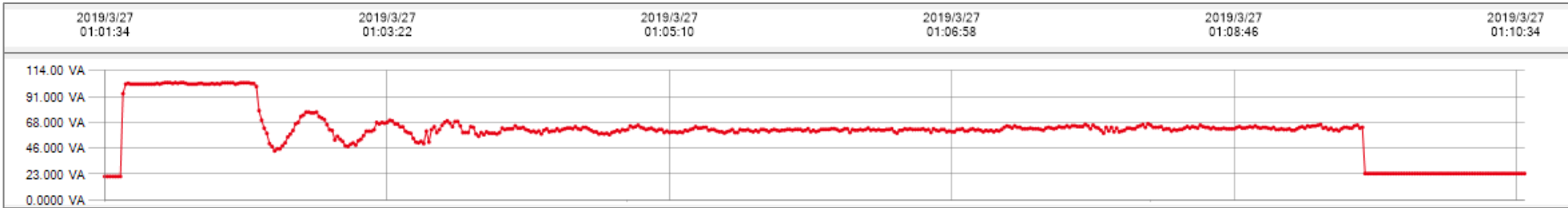
8.

9.
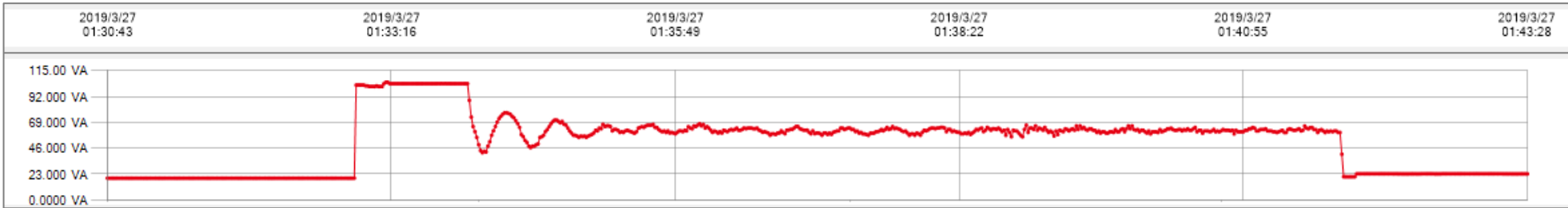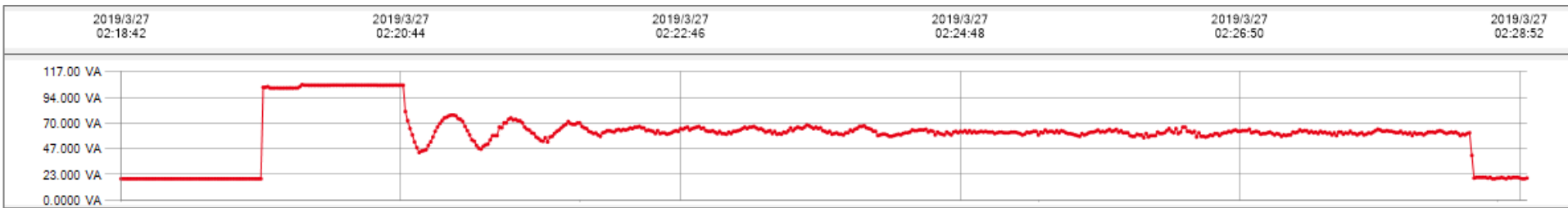
Appendix II: Power profiles of the component heating module at different target temperatures T_h^1

10.

11.

326

12.

13.

14.
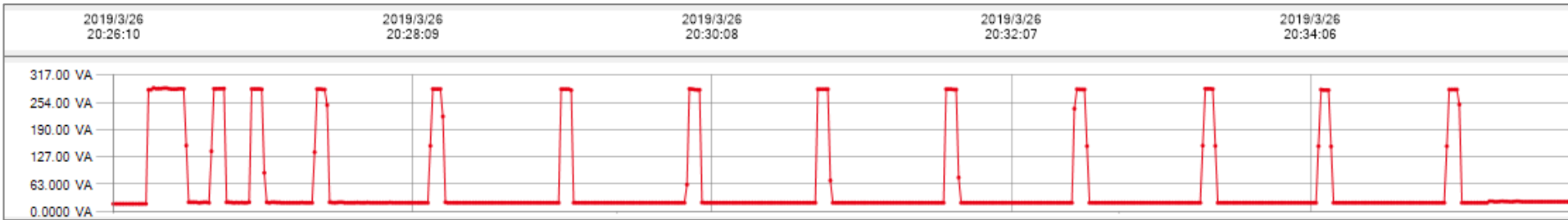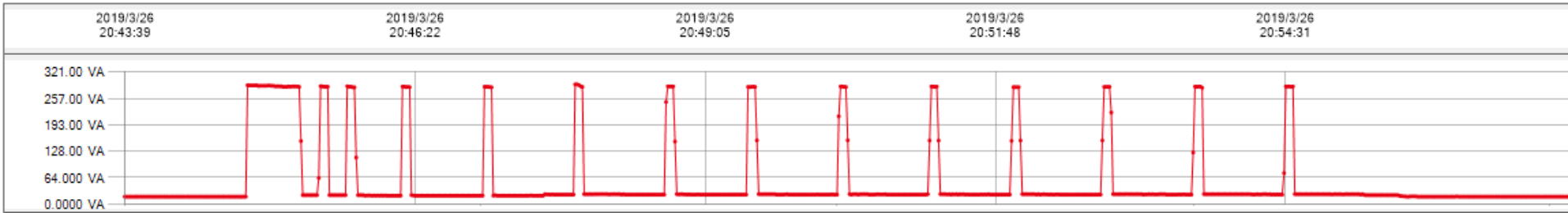
15.
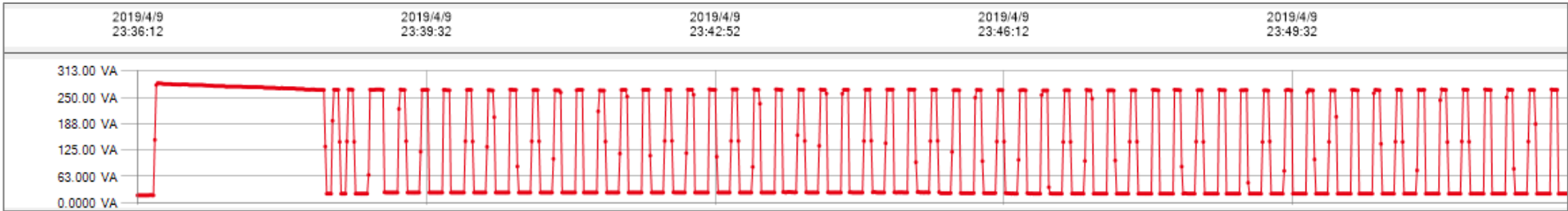
16.
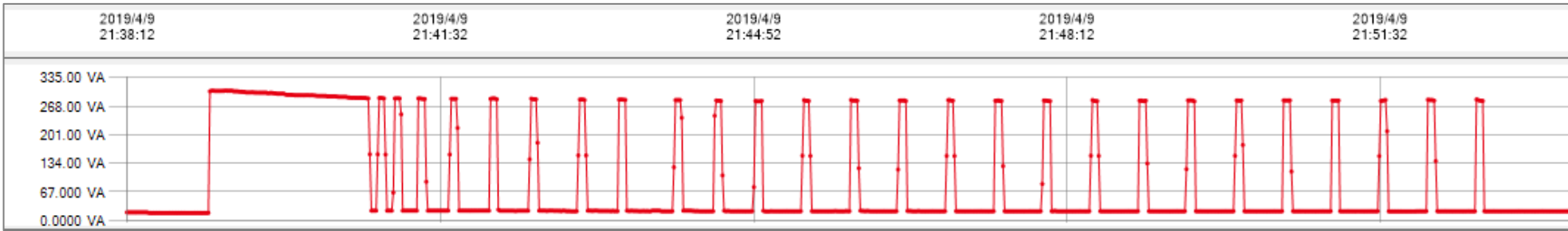
17.
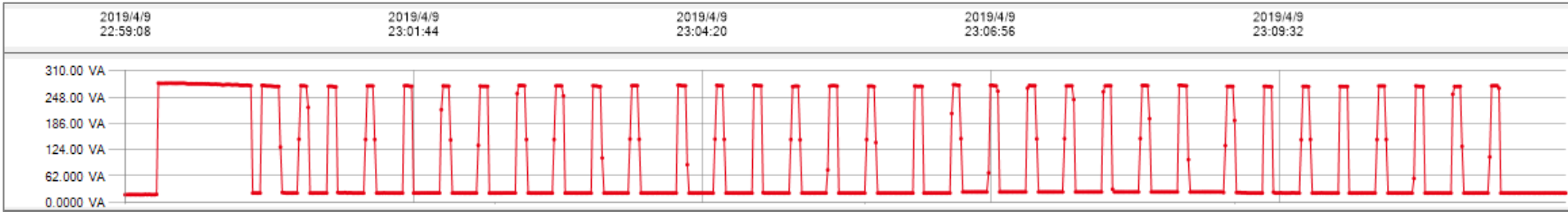
18.
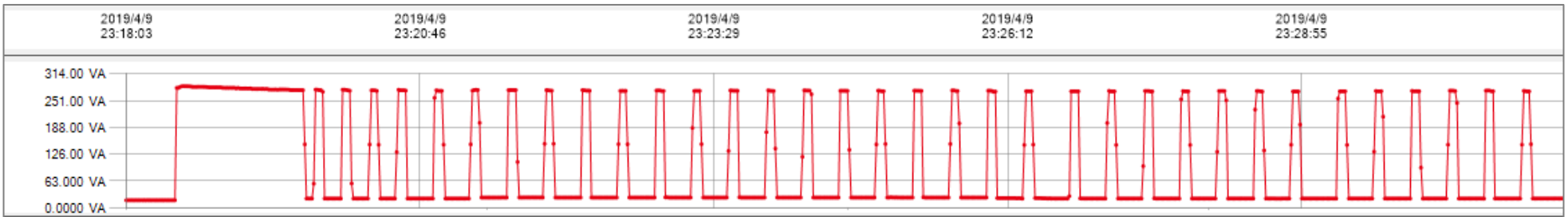
19.
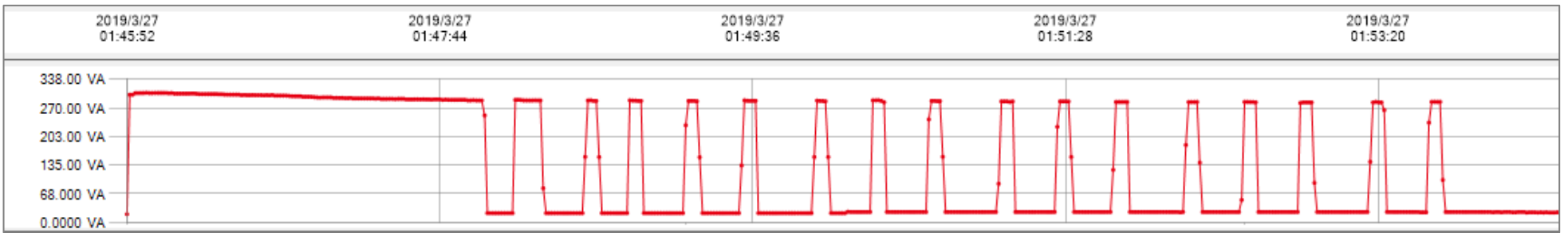
20.
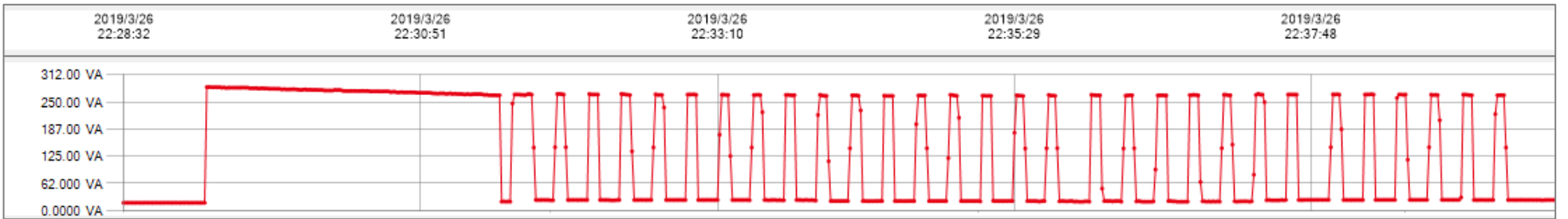
21.

22.
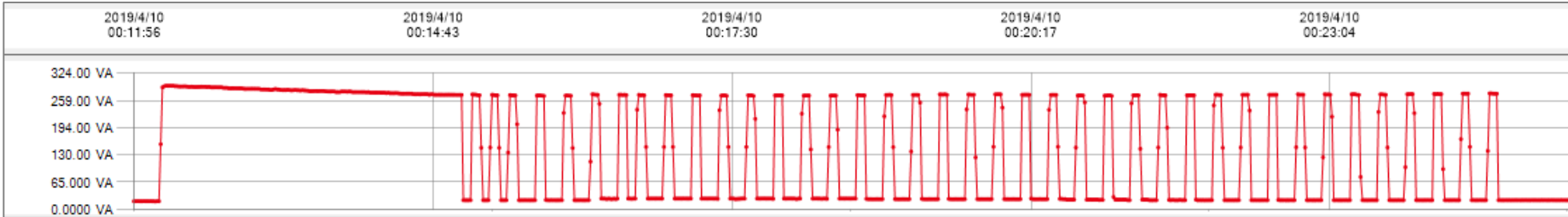
23. Appendix II: Power profile of axis movement in X direction at different speeds
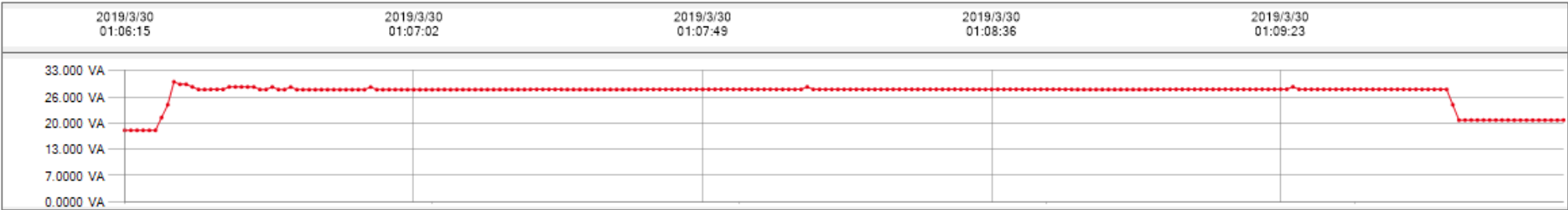
24. Appendix I: Power profile of axis movement in Y direction at different speeds

| 2019/3/30 15:13:44 | 2019/3/30 15:14:37 | 2019/3/30 15:15:30 | 2019/3/30 15:16:23 | 2019/3/30 15:17:16 | 2019/3/30 15:18:09 |

41.000 VA
33.000 VA
25.000 VA
16.000 VA
8.0000 VA
0.0000 VA
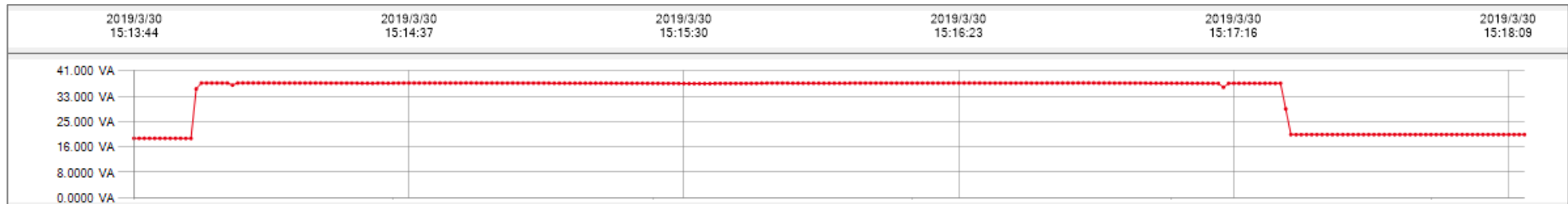
25. Appendix I: Power profile of axis movement in Z direction at the speed of $300 mm/min$

| 2019/4/8 00:43:34 | 2019/4/8 00:45:55 | 2019/4/8 00:48:16 | 2019/4/8 00:50:37 | 2019/4/8 00:52:58 | 2019/4/8 00:55:19 |

41.000 VA
33.000 VA
25.000 VA
16.000 VA
8.0000 VA
0.0000 VA
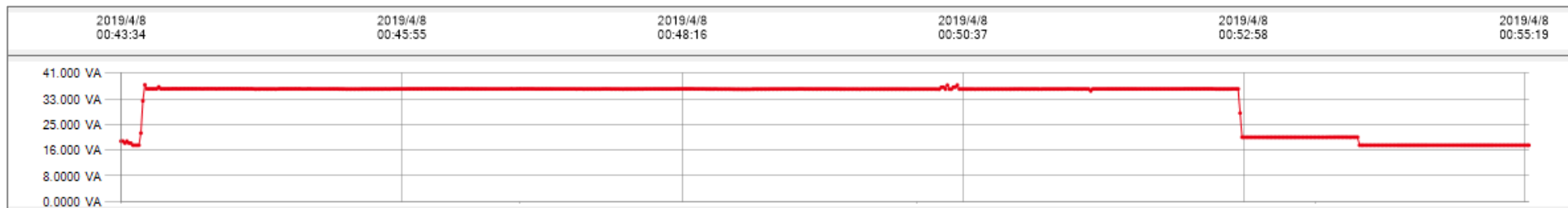
26. Appendix II: Power profile of material feeding module at different rates accompanied by material processing at the target temperature T_{mp}^1 of 200℃. (Note that the operation of material feeding is stipulated to be accompanied by material processing due to the self-protection mechanism of the ANYCUBIC 3D printer. This is to ensure that the material is extruded while being heated to prevent unmelted material from blocking the nozzle. Therefore, the power

P_{mf}^1 of material feeding is obtained by subtracting the heat preservation power $P_{mp_{hp}}^1$ at the target temperature of 200℃ from the total power of the two modules.)
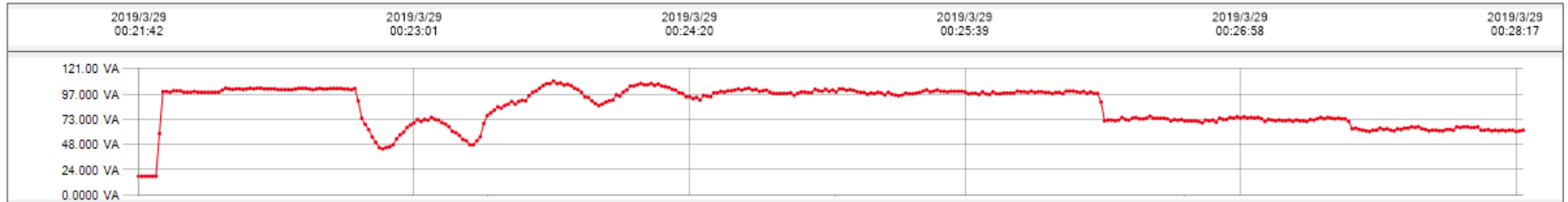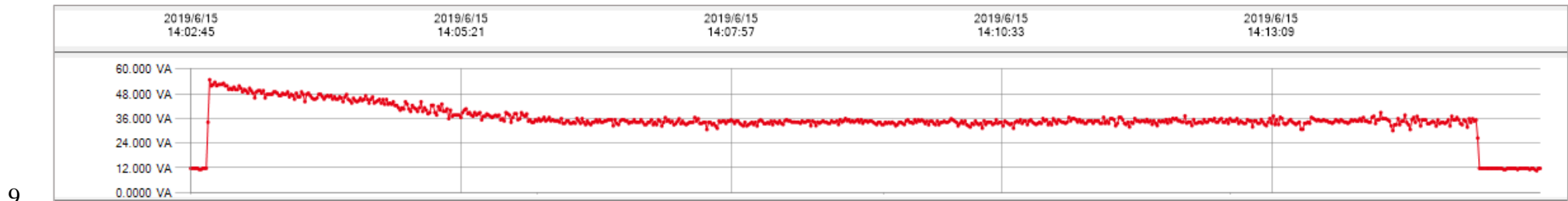
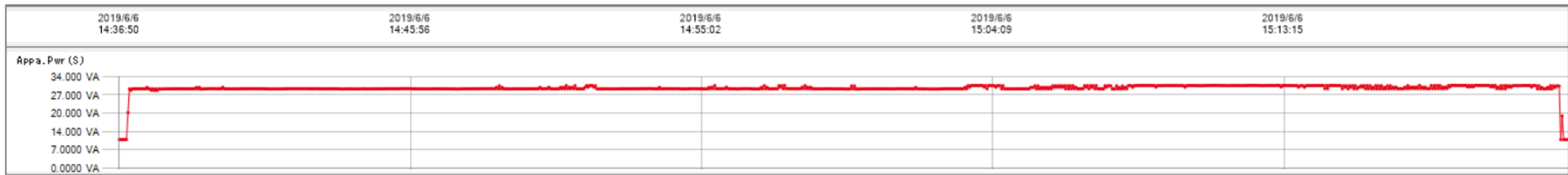27. Appendix II: Power profile of axis movement in X, Y directions at different speeds
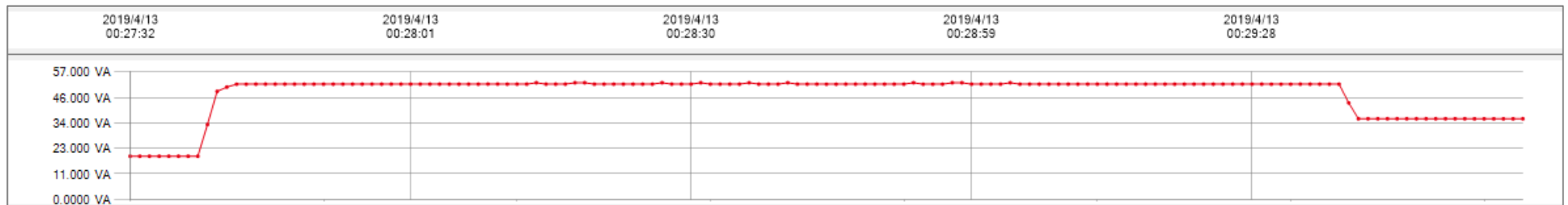
28. Appendix II: Power profile of axis movement in X, Z directions at different speeds
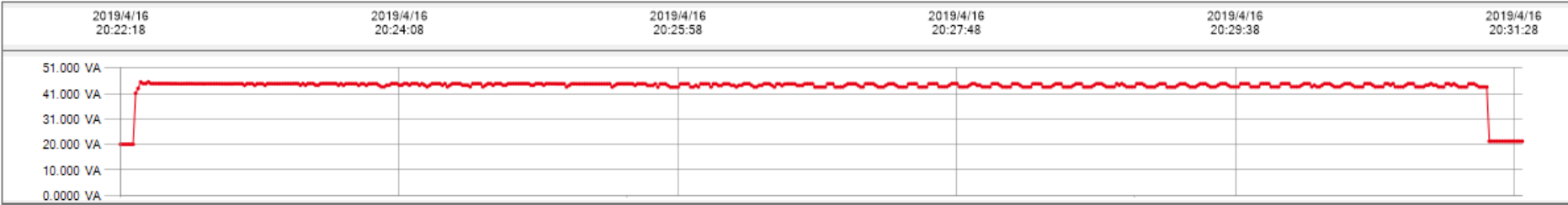
29. Appendix II: Power profile of axis movement in Y, Z directions at different speeds
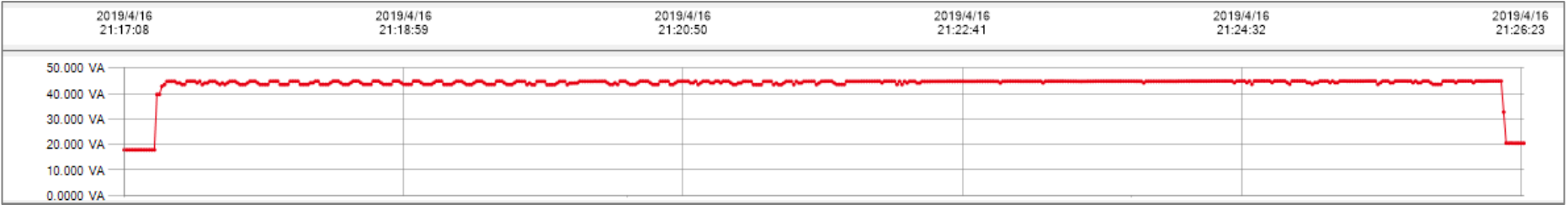
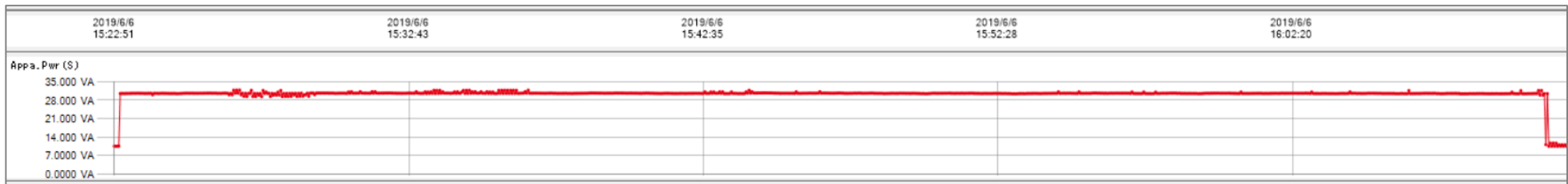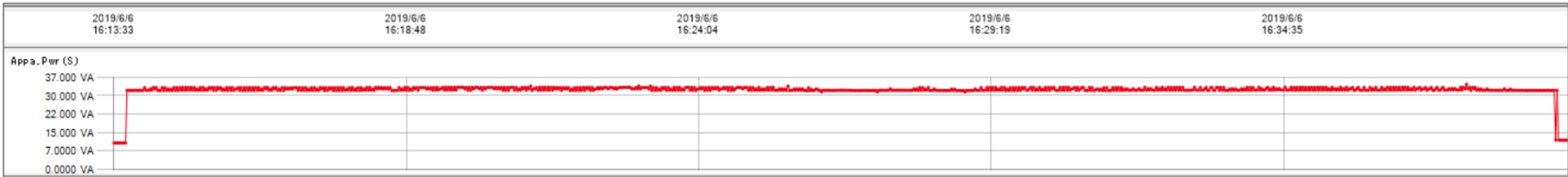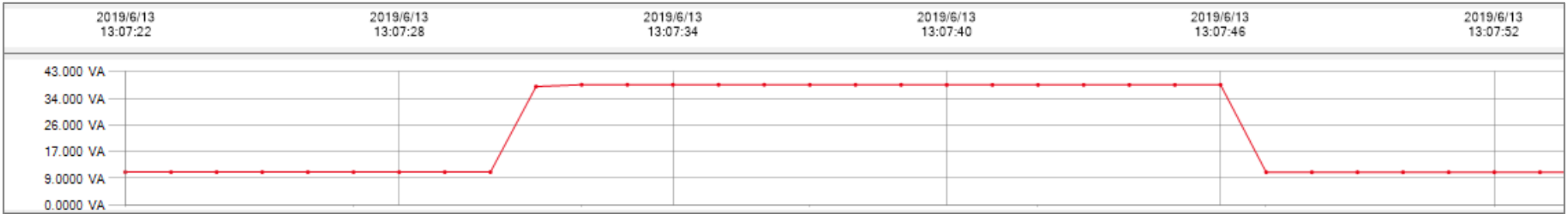## 30. Appendix II: Power profile of axis movement in X, Y, Z directions at different speeds
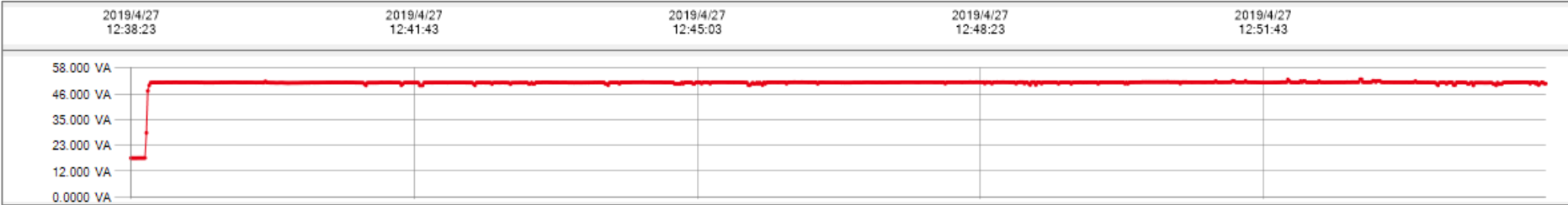
31. Appendix II: Power profile of axis movement in X, Y, Z directions with material feeding at different speeds/rates.
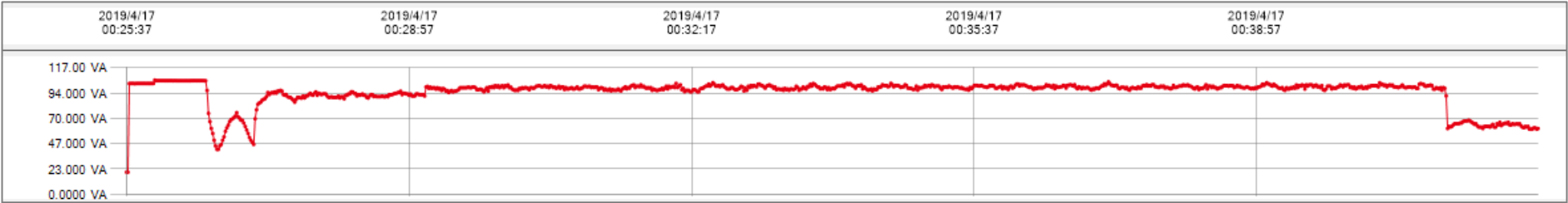
32. Appendix II: Power profile of machine standby mode
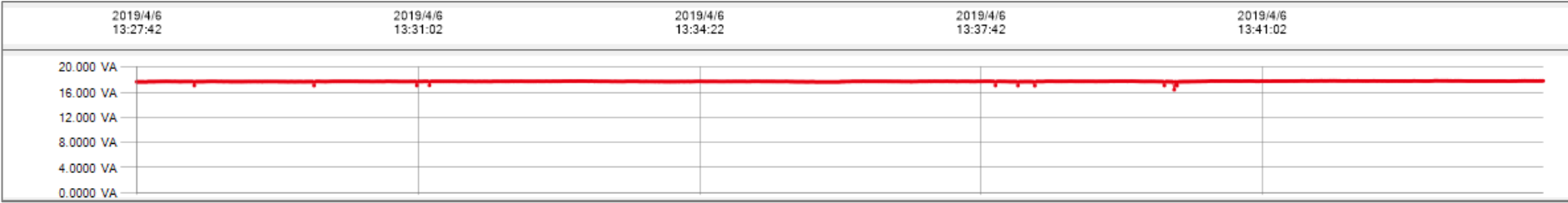
33. Appendix II: Power profile of machine start-up mode
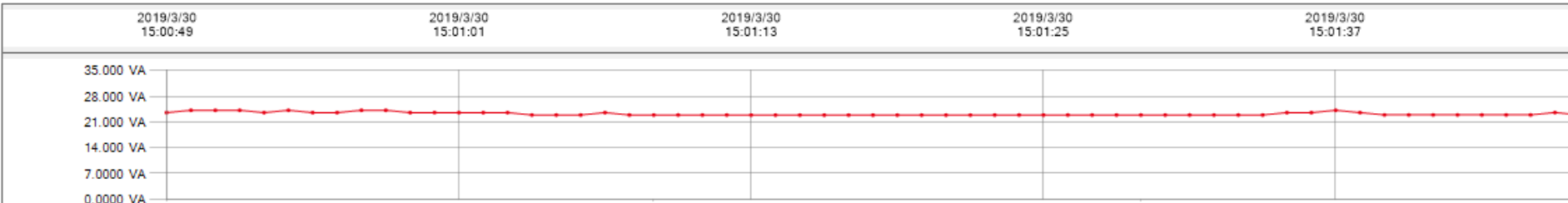
Experimental validations

34. Appendix II: Power profile of Task 01 manufactured by ANYCUBIC i3 Mega printer

35. Appendix II: Power profile of Task 02 manufactured by ANYCUBIC i3 Mega printer

APPENDIX III EXPERIMENTAL RESULTS OF CONSUMPTION MODELLING AND VALIDATION OF MONOPRICE MP MINI DELTA 3D PRINTER

Predictive model of time and energy consumptions

Appendix III: Power profiles of material processing module at different target temperatures T_{mp}^1

1.

2.
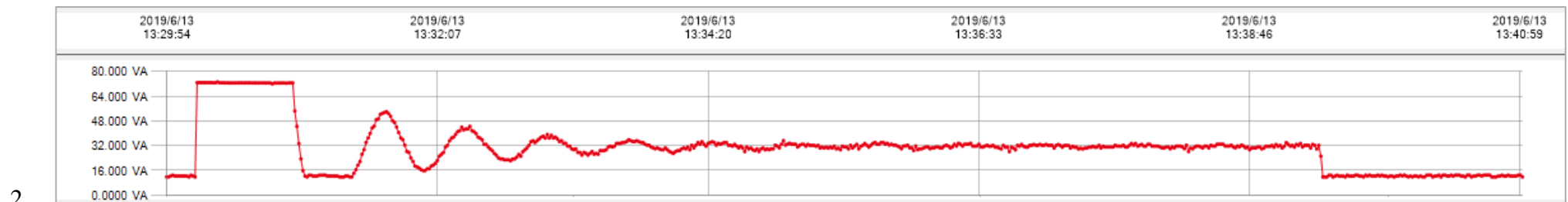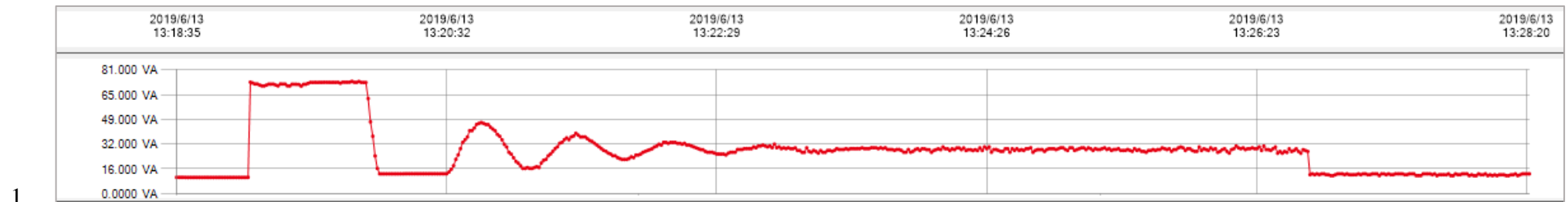
3.

4.
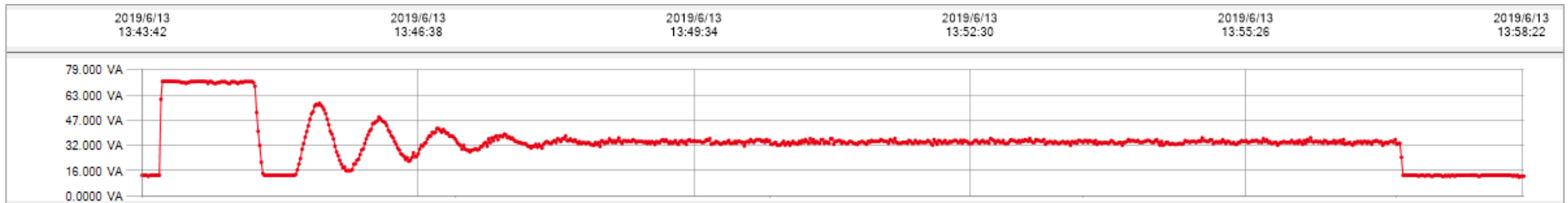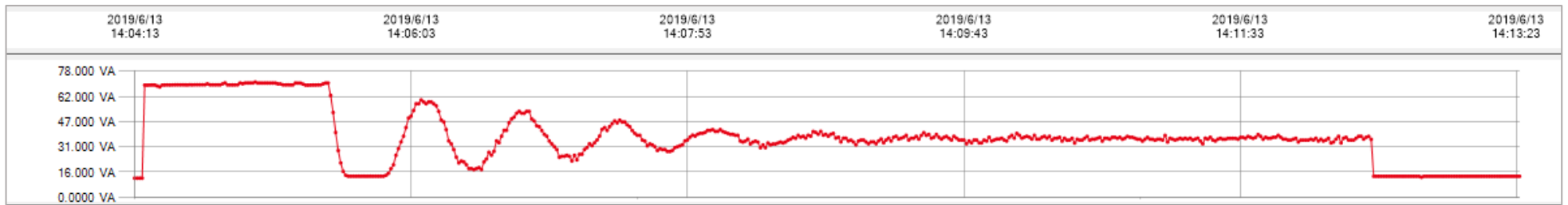
Appendix III: Power profiles of component heating module at different target temperatures T_h^1

5.

6.

7.

8.

9.
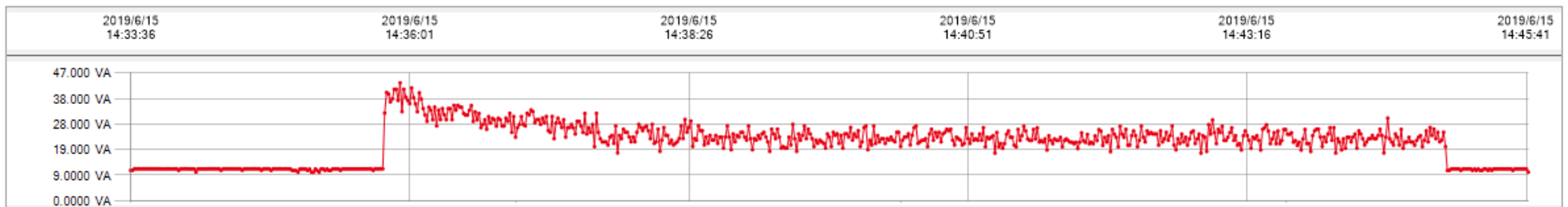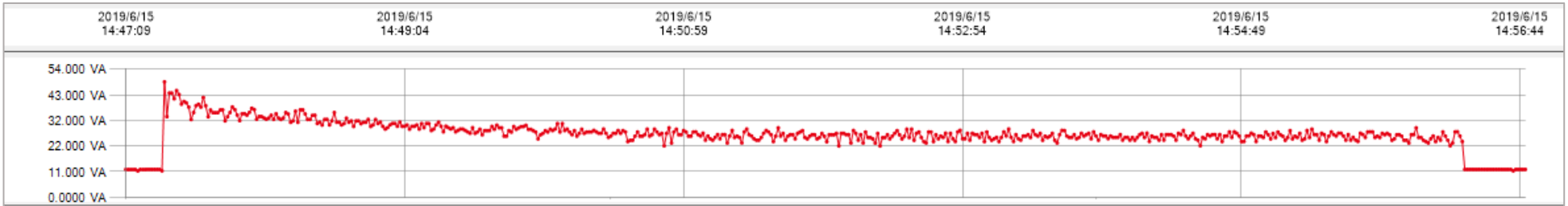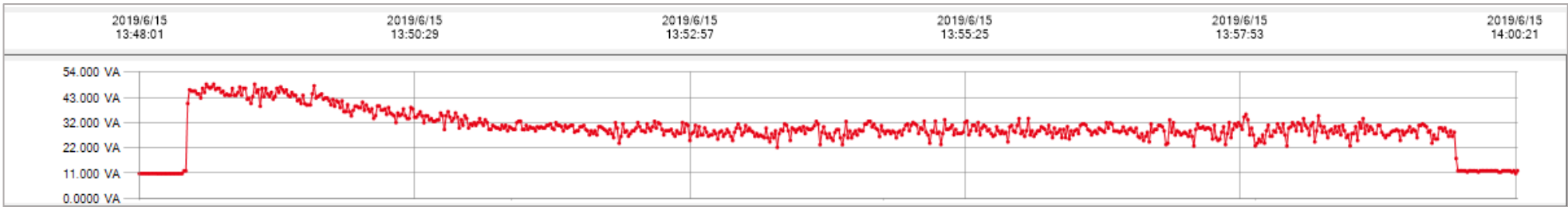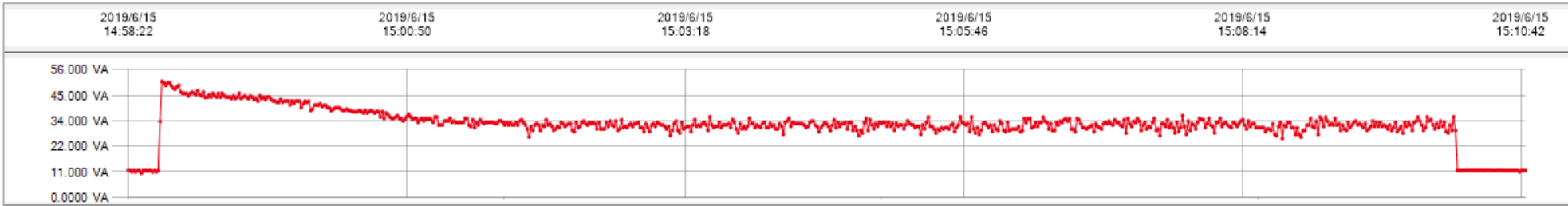
10. Appendix III: Power profile of axis movement in X direction at different speeds

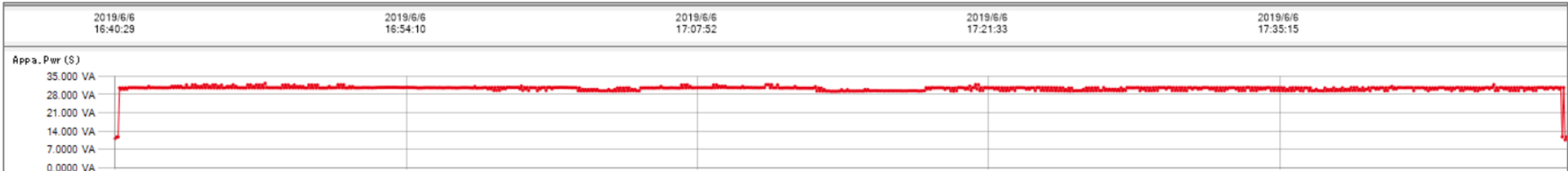11. Appendix III: Power profile of axis movement in Y direction at different speeds

12. Appendix III: Power profile of axis movement in Z direction at different speeds
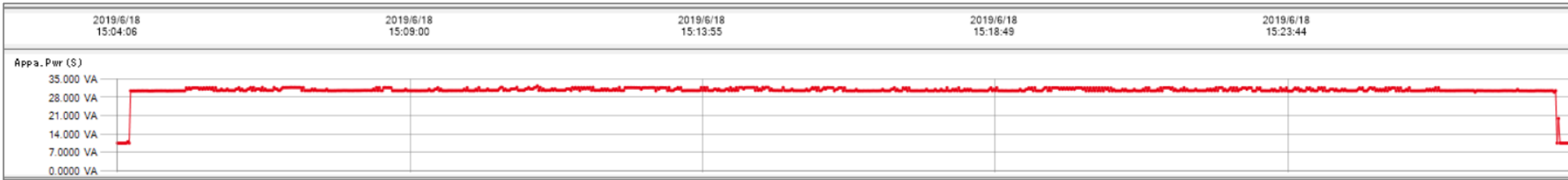

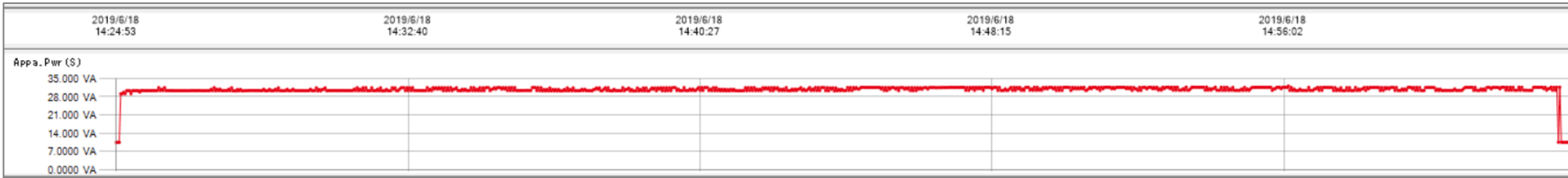13. Appendix III: Power profile of material feeding at different rates

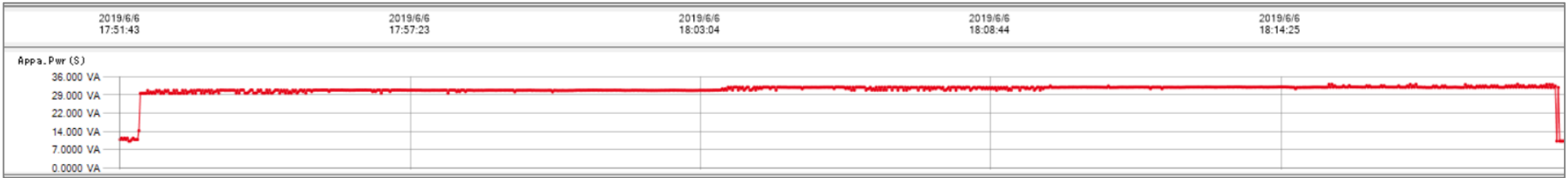14. Appendix III: Power profile of axis movement in X, Y directions at different speeds

15. Appendix III: Power profile of axis movement in X, Z directions at different speeds
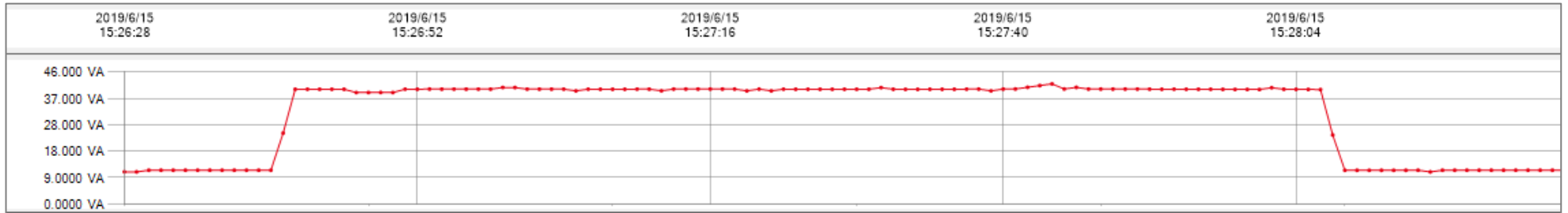

16. Appendix III: Power profile of axis movement in Y, Z directions at different speeds
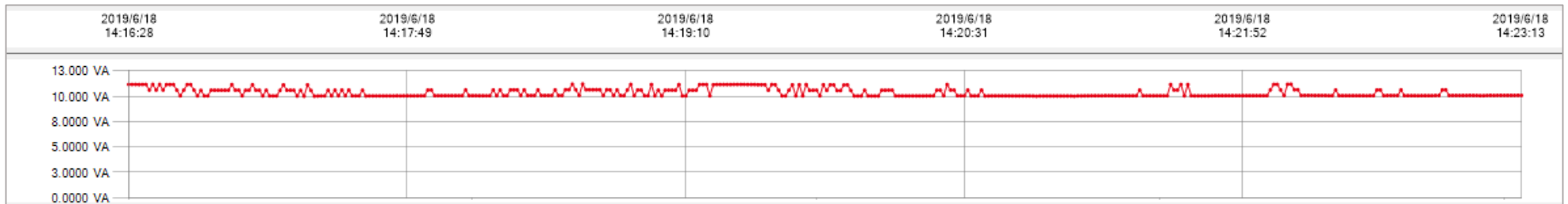

17. Appendix III: Power profile of axis movement in X, Y, Z directions at different speeds
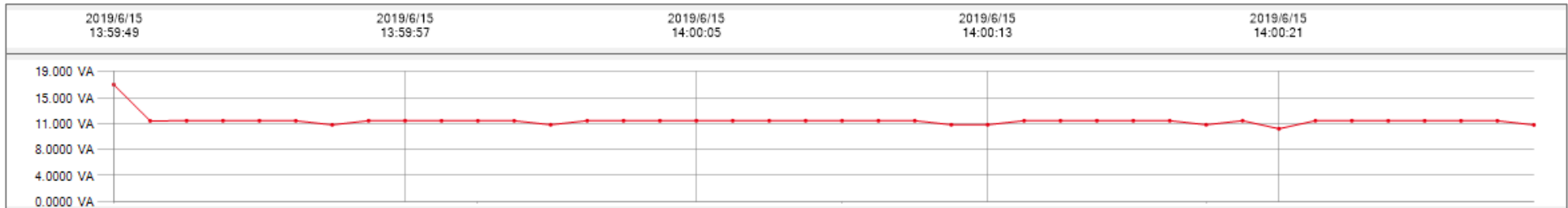
18. Appendix III: Power profile of axis movement in X, Y, Z directions with material feeding at different speeds/rates

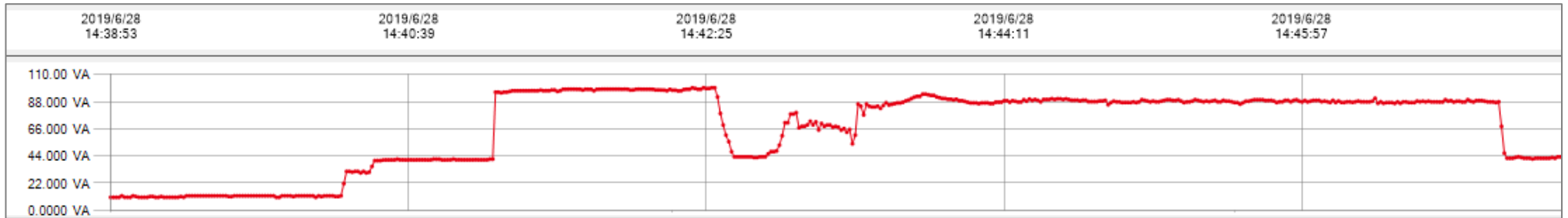19. Appendix III: Power profile of machine standby mode

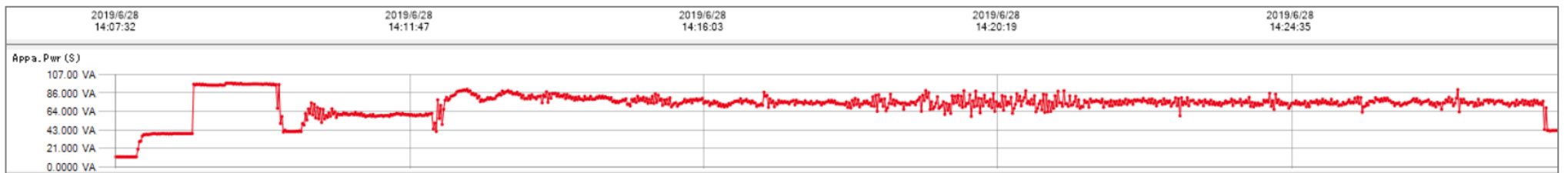20. Appendix III: Power profile of machine start-up mode

Experimental validations

21. Appendix III: Power profile of job 03 manufactured by Monoprice MP Mini Delta printer

22. Appendix III: Power profile of job 04 manufactured by Monoprice MP Mini Delta printer

APPENDIX IV NSGA-II OPTIMISATION TEST RESULTS OF COMPUTATIONAL TIME OF ANYCUBIC I3 MEGA 3D PRINTER

Test No.	Optimisation parameters				Computational time	Computing devices
	Population size	Number of generations	Probability of crossover	Probability of mutation		
	N	Gen	pc	pm	t_{com}	
1	10	50	0.85	0.15	43784.68	D-PC
2	10	100	0.90	0.20	134573.01	D-PC
3	10	150	0.95	0.25	225610.33	D-PC
4	10	200	1.00	0.30	295250.48	D-PC
5	20	50	0.90	0.25	266033.57	D-PC
6	20	100	0.85	0.30	284365.99	WS
7	20	150	1.00	0.15	405293.39	WS
8	20	200	0.95	0.20	547260.68	WS
9	30	50	0.95	0.30	345108.35	WS
10	30	100	1.00	0.25	658167.85	WS
11	30	150	0.85	0.20	1437831.02	HPC

12	30	200	0.90	0.15	1037201.50	HPC
13	40	50	1.00	0.20	1089475.40	D-PC
14	40	100	0.95	0.15	1014549.49	WS
15	40	150	0.90	0.30	1607494.47	WS
16	40	200	0.85	0.25	1946296.44	WS

APPENDIX V NSGA-II OPTIMISATION TEST RESULTS OF COMPUTATIONAL TIME OF MONOPRICE MP MINI DELTA 3D PRINTER

Test No.	Optimisation parameters				Computational time	Computing devices
	Population size	Number of generations	Probability of crossover	Probability of mutation		
	N	Gen	pc	pm	t_{com}	
1	10	50	0.85	0.15	57330.23	D-PC
2	10	100	0.90	0.20	176954.38	D-PC
3	10	150	0.95	0.25	267551.38	D-PC
4	10	200	1.00	0.30	424548.98	D-PC
5	20	50	0.90	0.25	358133.01	D-PC
6	20	100	0.85	0.30	349852.81	WS
7	20	150	1.00	0.15	538202.92	WS
8	20	200	0.95	0.20	773435.63	WS
9	30	50	0.95	0.30	1114440.52	HPC
10	30	100	1.00	0.25	1590633.02	D-PC
11	30	150	0.85	0.20	1360739.3	D-PC

12	30	200	0.90	0.15	2397155.47	D-PC
13	40	50	1.00	0.20	720718.59	WS
14	40	100	0.95	0.15	2448221.01	D-PC
15	40	150	0.90	0.30	2068115.22	WS
16	40	200	0.85	0.25	3693249.92	D-PC